SURFACE CHEMISTRY OF FLOTATION

EDITED BY: Zhiyong Gao, Przemyslaw B. Kowalczuk and Jan Zawala
PUBLISHED IN: Frontiers in Materials and Frontiers in Chemistry

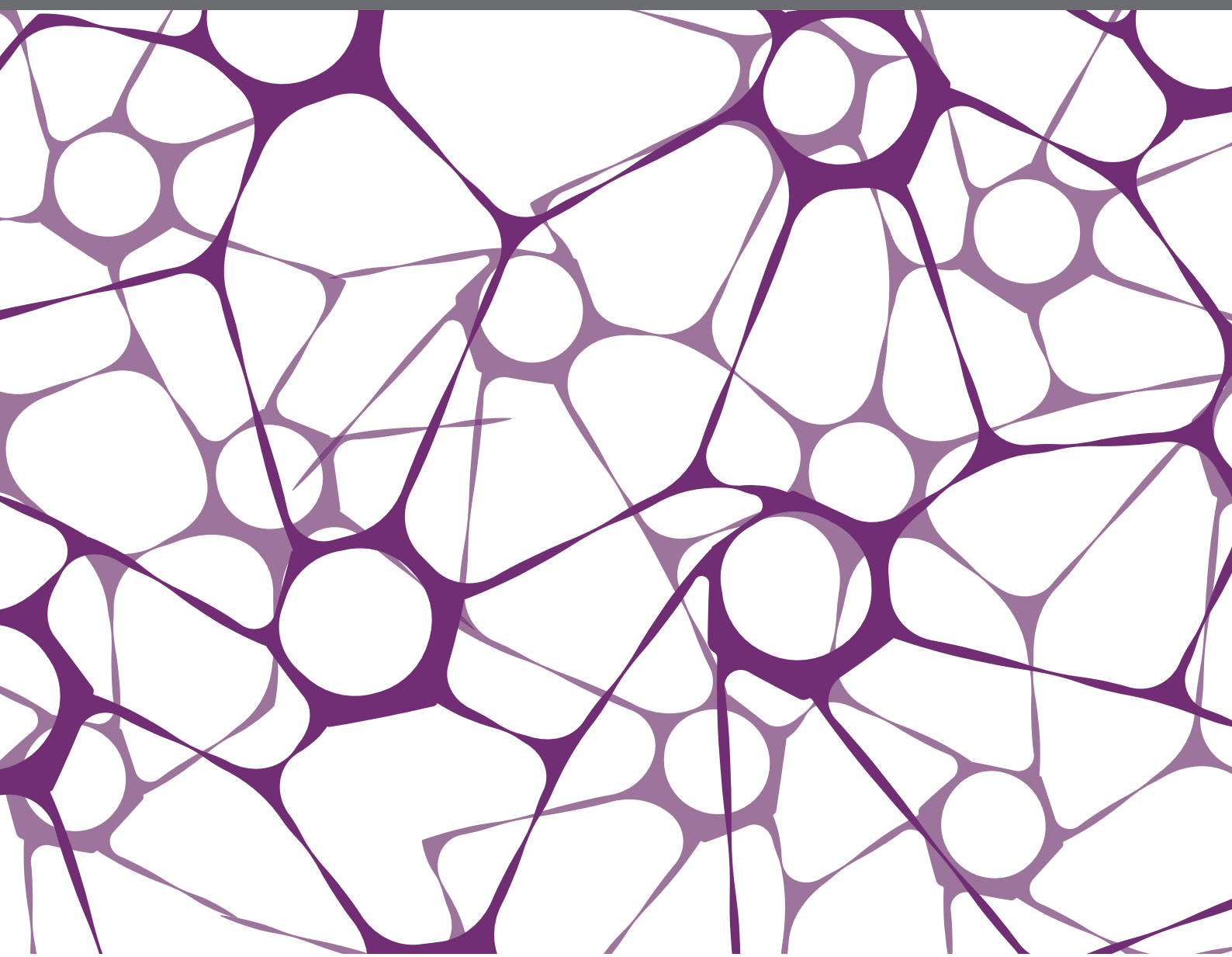

frontiers Research Topics

frontiers

ISSN 1664-8714
ISBN 978-2-88966-209-8
DOI 10.3389/978-2-88966-209-8

About Frontiers

Frontiers is more than just an open-access publisher of scholarly articles: it is a pioneering approach to the world of academia, radically improving the way scholarly research is managed. The grand vision of Frontiers is a world where all people have an equal opportunity to seek, share and generate knowledge. Frontiers provides immediate and permanent online open access to all its publications, but this alone is not enough to realize our grand goals.

Frontiers Journal Series

The Frontiers Journal Series is a multi-tier and interdisciplinary set of open-access, online journals, promising a paradigm shift from the current review, selection and dissemination processes in academic publishing. All Frontiers journals are driven by researchers for researchers; therefore, they constitute a service to the scholarly community. At the same time, the Frontiers Journal Series operates on a revolutionary invention, the tiered publishing system, initially addressing specific communities of scholars, and gradually climbing up to broader public understanding, thus serving the interests of the lay society, too.

Dedication to Quality

Each Frontiers article is a landmark of the highest quality, thanks to genuinely collaborative interactions between authors and review editors, who include some of the world's best academicians. Research must be certified by peers before entering a stream of knowledge that may eventually reach the public - and shape society; therefore, Frontiers only applies the most rigorous and unbiased reviews.
Frontiers revolutionizes research publishing by freely delivering the most outstanding research, evaluated with no bias from both the academic and social point of view. By applying the most advanced information technologies, Frontiers is catapulting scholarly publishing into a new generation.

What are Frontiers Research Topics?

Frontiers Research Topics are very popular trademarks of the Frontiers Journals Series: they are collections of at least ten articles, all centered on a particular subject. With their unique mix of varied contributions from Original Research to Review Articles, Frontiers Research Topics unify the most influential researchers, the latest key findings and historical advances in a hot research area! Find out more on how to host your own Frontiers Research Topic or contribute to one as an author by contacting the Frontiers Editorial Office: researchtopics@frontiersin.org

SURFACE CHEMISTRY OF FLOTATION

Topic Editors:
Zhiyong Gao, Central South University, China
Przemyslaw B. Kowalczuk, Norwegian University of Science and Technology, Norway
Jan Zawala, Jerzy Haber Institute of Catalysis and Surface Chemistry, Poland

Citation: Gao, Z., Kowalczuk, P. B., Zawala, J., eds. (2020). Surface Chemistry of Flotation. Lausanne: Frontiers Media SA. doi: 10.3389/978-2-88966-209-8

Table of Contents

frontiers in Materials

EDITORIAL
published: 12 October 2020
doi: 10.3389/fmats.2020.595146

Editorial: Surface Chemistry of Flotation

Zhiyong Gao[1], *Jan Zawala*[2]* *and Przemyslaw B. Kowalczuk*[3]

[1] School of Resource Processing and Bioengineering, Central South University, Changsha, Hunan Province, China, [2] Jerzy Haber Institute of Catalysis and Surface Chemistry Polish Academy of Sciences, Krakow, Poland, [3] Department of Geoscience and Petroleum, Norwegian University of Science and Technology, Trondheim, Sør-Trøndelag, Norway

Keywords: flotation, bubble, surfactant, separation, surface chemistry, adsorption

Editorial on the Research Topic

Surface Chemistry of Flotation

Flotation, separating minerals based on the interaction between air bubbles and mineral surfaces, reigns supreme in the mining field. Since the early 20th century, flotation, especially sulfide flotation, has been a well-developed industrial technology. In the meantime, tremendous efforts have been made to reveal the underlying mechanisms of flotation. A typical flotation process contains three subprocesses: a) the collision of mineral particles and air bubbles; b) the attachment in between; and c) the spreading of the three-phase contact lines. All three subprocesses must be successfully launched to achieve satisfactory flotation.

Given that surface chemistry is one of the main surface properties, it is considered to play a key role in all flotation subprocesses. In the surface chemistry of flotation, surface hydrophobicity and morphology are mainly involved, and any approach that may modify them is of great interest in this topic, including adding reagents and grinding. There is no doubt that these approaches will remain to attract attention in the future, and some novel improvements are worth making.

Flotation reagents include collector, frother, activator, depressant, pH regulator, and redox potential regulator. Many directions are promising when it comes to developing flotation reagents, including effective reagents, low-cost reagents, and environment-friendly reagents. Take the collector as an example. Mixed collectors show promise in fully making use of single collectors. A specific collector possesses unique properties: some might perform better in intensely adsorbing on the mineral surface, while others might be more selective in collecting a target mineral. And exploring the source of collectors from natural materials, such as biochemicals, is proved to lower the operating cost effectively. Besides, it is well recognized that these chemical reagents may pose a danger to the environment, and future endeavors must be aimed at avoiding this issue. Likewise, other types of flotation reagents also follow the same train of thought.

To modify the surface morphology, grinding is a practical option. An advantage of modifying the surface morphology by grinding is that it is controllable and economical by adjusting the grinding media, equipment, and duration. Numerous reports show that the surface hydrophobicity of minerals is closely related to surface roughness. Plus, the stability of liquid films between air bubbles and mineral surfaces can vary with changing surface roughness and particle size. And the liquid film stability can serve as an indicator of floatability; that is, in cases of stable films, attaching of air bubbles on the mineral surface is difficult, rendering a low flotation recovery. Furthermore, the addition of flotation reagents in the comminution stage is becoming increasingly popular in many plants, and it turns out that flotation separation can be remarkably improved.

To better understand the mechanism, many state-of-the-art technologies have been developed and utilized. Among them, atomic force microscope is a powerful tool to reveal the interaction between air bubbles and mineral surfaces with different properties. And the instruments used to characterize the liquid film present a possibility to visualize the attachment process. At the same time, simulations are employed to explain the effect of different factors, especially when the factors are

Edited and reviewed by:
Naoki Asakawa,
Gunma University, Japan

****Correspondence:***
Jan Zawala
nczawala@cyfronet.pl

Specialty section:
This article was submitted to Colloidal Materials and Interfaces, a section of the journal Frontiers in Materials

Received: *15 August 2020*
Accepted: *20 August 2020*
Published: *12 October 2020*

Citation:
Gao Z, Zawala J and Kowalczuk PB (2020) Editorial: Surface Chemistry of Flotation. Front. Mater. 7:595146. doi: 10.3389/fmats.2020.595146

extremely difficult to be investigated by conducting experiments. Besides, simulations can better calculate the involved energy change and the anisotropy of minerals with complex structures. One of the hot topics is the water–liquid layer near the mineral surfaces. On the other hand, traditional approaches, such as surface potential measurement and adsorption measurements, can still provide much useful information on mineral surface modifications and relevant interactions.

To sum up, the surface chemistry of flotation has been of primary interest in mineral processing for a long time. A deep understanding here is necessary because it not only enhances the efficient utilization of natural minerals for now but also inspires the development of novel approaches that are both sustainable and low-cost, guiding the mining industry in the right direction.

AUTHOR CONTRIBUTIONS

ZG is the main author of the article; JZ and PK contributed in the article editing and proofreading.

Conflict of Interest: The authors declare that the research was conducted in the absence of any commercial or financial relationships that could be construed as a potential conflict of interest.

frontiers in Chemistry

ORIGINAL RESEARCH
published: 24 September 2019
doi: 10.3389/fchem.2019.00645

Structures of Pb-BHA Complexes Adsorbed on Scheelite Surface

Zhao Wei[1,2†], *Wenjuan Sun*[1,2†], *Yuehua Hu*[1,2], *Haisheng Han*[1,2*], *Wei Sun*[1,2*], *Ruolin Wang*[1,2], *Yangge Zhu*[3], *Bicheng Li*[3] *and Zhenguo Song*[3]

[1] School of Minerals Processing and Bioengineering, Central South University, Changsha, China, [2] Key Laboratory of Hunan Province for Clean and Efficient Utilization of Strategic Calcium-Containing Mineral Resources, Central South University, Changsha, China, [3] B.Grimm Technology Group, Beijing, China

Previous studies have shown that Pb-BHA complexes (lead complexes of benzohydroxamic acid) have better collecting ability and can be used in flotation experiments with BHA acting as a collector and lead ions acting as activators. However, the structures of Pb-BHA complexes adsorbed on a mineral surface remain unclear. In this work, the adsorption behavior of Pb-BHA complexes on the scheelite surface was studied by flotation experiments and adsorption capacity measurements, and the structures of the adsorbed Pb-BHA complexes were determined using X-ray photoelectron spectroscopy (XPS) and time-of-flight secondary ion mass spectrometry (TOF-SIMS). The adsorption capacity results showed that more BHA was adsorbed on the scheelite surface in Pb-BHA flotation, and the XPS and TOF-SIMS analysis showed that the species of Pb-BHA complexes adsorbed on the scheelite surface were similar in activation flotation and Pb-BHA flotation. Therefore, the different contents of the complexes on the scheelite surface were responsible for the flotation behavior. XPS and TOF-SIMS showed that BHA combined with lead ions to form complexes with different structures, such as five- and four-membered ring structures. Structure fragment inference based on the measurements indicated that lead ions formed monomer complexes with two BHAs, and that lead hydroxide polymers with a certain degree of polymerization bonded with oxygen atoms in the complexes. The Pb-BHA complexes combine with oxygen atoms on the scheelite surface to form an adsorbate, rendering the surface hydrophobic.

Keywords: Pb-BHA complexes, adsorption capacity, XPS, TOF-SIMS, structure fragment

OPEN ACCESS

Edited by:
Jan Zawala,
Institute of Catalysis and Surface Chemistry (Polish Academy of Sciences), Poland

Reviewed by:
Pedro Miguel Aguiar,
Université de Montréal, Canada
Dong Chen,
Zhejiang University, China

***Correspondence:**
Haisheng Han
hanhai5086@csu.edu.cn
Wei Sun
sunmenghu@126.com

[†] These authors have contributed equally to this work

Specialty section:
This article was submitted to Physical Chemistry and Chemical Physics, a section of the journal Frontiers in Chemistry

Received: *27 June 2019*
Accepted: *09 September 2019*
Published: *24 September 2019*

Citation:
Wei Z, Sun W, Hu Y, Han H, Sun W, Wang R, Zhu Y, Li B and Song Z (2019) Structures of Pb-BHA Complexes Adsorbed on Scheelite Surface. Front. Chem. 7:645. doi: 10.3389/fchem.2019.00645

INTRODUCTION

Flotation is a widely used process for material separation, based on differences in the surface hydrophobicity and hydrophilicity of minerals. The separation of scheelite from other calcium-containing minerals such as fluorite and calcite has been difficult owing to their similar surface properties (Li and Gao, 2017; Gao et al., 2018, 2019; Jiang et al., 2018). However, previous studies have shown that Pb-BHA complexes have good collection ability and high selectivity in scheelite flotation. Their use in industrial applications solved the problem of the separation of scheelite from other calcium-bearing minerals, replacing the Petrov process to some extent (Han et al., 2017a; Wei et al., 2018; Yue et al., 2018). The better collection ability and selectivity of Pb-BHA complexes in calcium mineral flotation was attributed to be the unique molecular structure of these complexes.

However, the structure of Pb-BHA complexes adsorbed on the scheelite surface remained unclear. Previous studies have shown that the different molar ratio of Pb/BHA will influence the flotation performance of Pb-BHA complexes collector (Han et al., 2017a), indicating the structure of complexes will influence their industrial applications. Therefore, molecular-level understanding of the Pb-BHA complexes is required to improve their industrial applications.

Few research studies have focused on the formation and configuration of Pb-BHA complexes in solution or on a mineral surface (Tian et al., 2017, 2018a,b; Yue et al., 2017; He et al., 2018b; Hu et al., 2018; Cao et al., 2019). In particular, solution-chemistry-based studies of the respective components of Pb-BHA complexes in cassiterite flotation (Tian et al., 2017, 2018a,b; Cao et al., 2019) showed that lead ions and their hydroxide ions form $Pb(H_2O)$ and $Pb(OH)(H_2O)$ with water and then react with the BHA anion to produce HO-Pb-BHA complexes. He et al. (2018a,b) characterized the structure of Pb-BHA complexes in aqueous solutions through theoretical calculations and quantum chemical simulations; the results showed that the Pb-BHA complexes existed mainly in the form of $Pb\text{-}(BHA)_{n=1,2}$ at various solution pH values, and first-principles calculations indicated that $Pb(BHA)^+$ is the most stable structure. Both studies concluded that the Pb-BHA complexes in the flotation did not consist of a single structure and proposed that Pb-BHA complexes with multiple structures acted simultaneously on the mineral surface. However, these studies only analyzed the structure of Pb-BHA complexes in theory by using approaches such as solution chemistry, theoretical calculations, and simulations. Although such studies are very helpful in understanding the structure of complexes, experimental research was lacking, which is necessary to investigate the true structure of Pb-BHA complexes adsorbed on mineral surfaces. In addition, these studies usually considered the structure of Pb-BHA complexes in solution, but the structure and species composition of Pb-BHA complexes adsorbed on a mineral surface or the solid–liquid interface may be different (Rao, 2004; Bulatovic, 2015; Kupka and Rudolph, 2018), this was not studied in detail. Moreover, the differences between structures of complexes formed by lead ions and BHA in activation flotation and Pb-BHA complex flotation were not considered, although this is crucial for a better understanding of Pb-BHA complex flotation.

In this study, experimental research was conducted to investigate the structures of Pb-BHA complexes adsorbed on a scheelite surface. The adsorption behavior of Pb-BHA complexes on the scheelite surface was studied by flotation experiments and adsorption capacity measurements, and their structures were examined using X-ray photoelectron spectroscopy (XPS) and time-of-flight secondary ion mass spectrometry (TOF-SIMS), providing an in-depth understanding of the adsorption mechanism of Pb-BHA complexes on a mineral surface.

MATERIALS AND METHODS

Materials and Reagents

High-purity scheelite samples were obtained from Shizhuyuan Mine, Hunan, China. X-ray diffraction patterns and X-ray fluorescence data confirmed that the purity of the scheelite samples was >97%. A fine fraction (∼74 μm) was used for the experiments. Analytical grade BHA and lead nitrate were purchased from Tianjin Guangfu Fine Chemical Co. Ltd. (Tianjin, China), and the pH was adjusted with NaOH or HCl.

The Pb-BHA complexes used for the flotation tests and adsorption measurements were freshly prepared; solutions of lead nitrate and BHA were mixed in a beaker at the desired mole ratio, mixed evenly, and allowed to stand until use. The powdered Pb-BHA complexes precipitates used for XPS, X-Ray Diffraction (XRD), Fourier Transform Infrared Spectroscopy (FTIR), and Thermogravimetric analysis (TGA) measurements were prepared in solution and dried in a vacuum oven at 40°C, which the molar ratio of Pb/BHA in complexes were 1:1. The characterization of the Pb-BHA complexes as shown in **Supporting Information**, including XRD, FTIR, and TGA.

Flotation Test

The flotation tests were carried out in an XFG flotation machine with a 40 mL plexiglass cell at an impeller speed of 1,900 rpm. For each test, 2.0 g of the mineral sample was dispersed into 40 mL of deionized water in the cell and the flotation pulp was mixed for 1 min. The experimental procedure was as described previously (Han et al., 2017a; Wei et al., 2019). Recovery was calculated according to Equation (1), where R is the recovery, M_1 is the mass of the concentrate, and M_2 is the mass of the tailings. All the flotation experiments were conducted more than three times to ensure that the standard deviation of the experimental results was within 3%. The average value of all measurements conforming to this standard deviation was taken as the final experimental data.

$$R = \frac{M_1}{M_1 + M_2} \times 100 \quad (1)$$

Adsorption Capacity Measurements

For each test, 2.0 g of scheelite powder was mixed in desired amounts of flotation reagents in the flotation cell, and deionized water was added to make the total volume 40 mL. The process was the same as that used in the flotation experiments. Afterwards, the suspension was centrifuged for 30 min at a speed of 9,000 rpm, and the residual concentration of BHA in the supernatant was determined using a total organic carbon analyzer (TOC-L CPH/CN, Shimadzu Corporation). The amount of BHA adsorbed on the mineral surface was calculated according to Equation (2):

$$\Gamma = (C_0 - C)V/m \quad (2)$$

where Γ is the amount of lead ions or BHA adsorbed on the mineral surface (mol/g), C_0 and C are the initial and residual concentrations (mol/L) of lead ions or BHA, respectively, V is the volume of the solution (L), and m is the mass (g) of particles per sample.

X-Ray Photoelectron Spectra Measurements

XPS measurements were conducted using a Thermo Fisher Scientific K-Alpha 1063 X system. The −74 μm fractions of pure

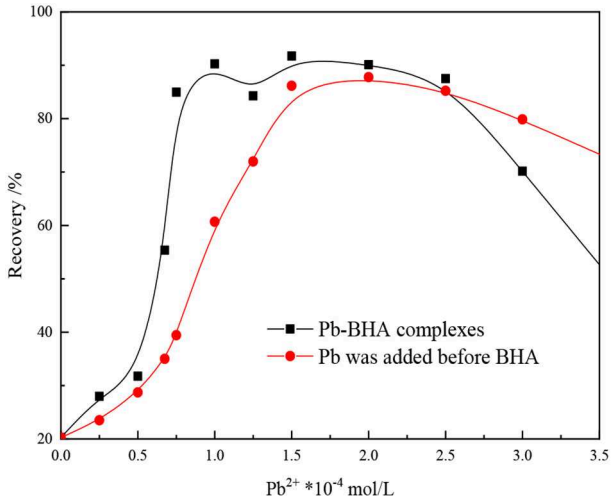

FIGURE 1 | Effect of mode of addition on flotation of scheelite (pH = 8.8 ± 0.2, C_{BHA} = 1.5 × 10^{-4} mol/L, $C_{terpineol}$ = 12.5 μL/L).

scheelite samples (2.0 g) were conditioned with the appropriate reagents using the same procedure as in the flotation tests. Finally, the samples were washed twice with 40 mL distilled water and then dried in a vacuum oven maintained below 40°C. The data were collected and processed using the Thermo Scientific Advantage software. A binding energy of 284.8 eV was adopted as the standard C(1s) binding energy.

TOF-SIMS Measurements

A crystal sample was prepared for TOF-SIMS measurements, in which the naturally cleaved crystal was polished to a smooth surface in order to meet the requirements for measurement. The sample was soaked in a Pb-BHA complex solution for 3 days before the measurements were carried out. The chemical composition of the scheelite surfaces after adsorption of different agents was determined using an ION-TOF IV instrument (Model 2100 Trift II, Physical Electronics, USA) equipped with a Ga primary ion source. The primary ion beam and acceleration voltage were 25 and 5 keV, respectively. The mass range was set to 200 × 200 μm with 1 mass unit resolution.

RESULTS AND DISCUSSION

Flotation Experiments and Adsorption Capacity Measurements

The effect of dosing mode of the reagents on the floatability of scheelite is shown in **Figure 1**. As shown in the figure, the way the reagents were added greatly influenced the flotation results, with the mixture of lead ions and BHA within a certain ratio showing a greater collection ability than the two components added sequentially. These results indicate that the Pb-BHA complexes have good collection ability for scheelite flotation and play an important part in conventional lead-activated scheelite flotation.

Figure 2 shows the adsorption amounts of lead ions and BHA on the mineral surface under activation flotation (shown as Pb^{2+}+BHA in figures) and Pb-BHA complex flotation at different pH values. The adsorption capacity was the largest in the pH range 6–10 for both lead ions and BHA. As shown in **Figure 2A**, there was no significant difference in the amount of lead ion adsorption between the activation flotation and the Pb-BHA complexes flotation, whereas in both cases, the adsorption amount was slightly lower than that of the lead ion alone. As shown in **Figure 2B**, the adsorption amount of BHA in Pb-BHA complex flotation was higher than that obtained with activation flotation, and both were significantly higher than that of BHA alone; this is consistent with the literature (Tian et al., 2017, 2018a). These results indicate that the addition of lead ions improved the adsorption of BHA on the scheelite surface, and that this improvement was more substantial for Pb-BHA complex flotation.

The adsorbed amounts of lead ions and BHA on the scheelite surface with different concentrations of lead ions and BHA were measured, as shown in **Figure 3**, with the molar concentration ratio of lead ions and BHA fixed at 1. The adsorbed amounts of lead ions and BHA on the scheelite surface increased with increasing concentration of lead ions and BHA. As shown in **Figure 3A**, there was no significant difference in the adsorption of lead ions between activation flotation and Pb-BHA complex flotation, but there was more adsorption of BHA in Pb-BHA complex flotation, consistent with the results shown in **Figure 2**. The greater amount of BHA adsorbed on the scheelite surface in Pb-BHA complex flotation resulted in a higher flotation recovery than in the case of activation flotation.

The ratio of lead ions and BHA adsorbed on the scheelite surface was calculated based on the adsorption amount results, as shown in **Figure 4**. This ratio changed with increasing concentration of lead ions and BHA, but it eventually became constant. Compared with activation flotation, there was a lower ratio of lead ions and BHA adsorbed on the scheelite surface in Pb-BHA complex flotation, indicating that there may be some difference in the structures of complexes adsorbed in the two cases. In particular, in the concentration section of scheelite flotation from **Figure 4** (usually between 1 × 10^{-4} and 3 × 10^{-4} mol/L), the ratio of Pb/BHA was between 2 and 3, which may reflect the average ratio of lead ions to BHA in the molecular structure of complexes adsorbed on the scheelite surface. However, further microscopic measurements are required to confirm this.

XPS Measurements

Some researchers confirmed that the Pb-BHA complexes existed mainly in the form of Pb-$(BHA)_{n=1,2}$ in solution (Han et al., 2017b; Yue et al., 2017; He et al., 2018a), in order to compare the species between Pb-BHA complexes and Pb-BHA complexes adsorbed on mineral surface, the XPS measurements were conducted. **Table 1** shows the electron binding energy of the different elements of BHA and Pb-BHA complexes. The binding energies of the O_{1s}, N_{1s}, and Pb_{4f} atoms underwent a large shift after the BHA interacted with lead ions, indicating that both O and N may bond to Pb to form ring complexes. When BHA

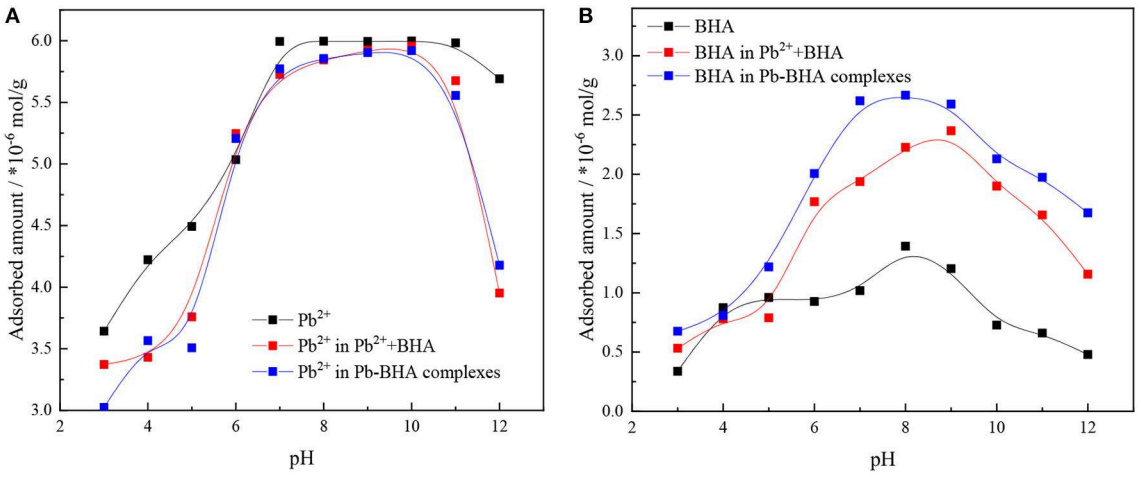

FIGURE 2 | Adsorbed amounts of **(A)** lead ions and **(B)** BHA on scheelite surface vs. pH (C_{Pb} = 1.5 × 10^{-4} mol/L, C_{BHA} = 1.5 × 10^{-4} mol/L).

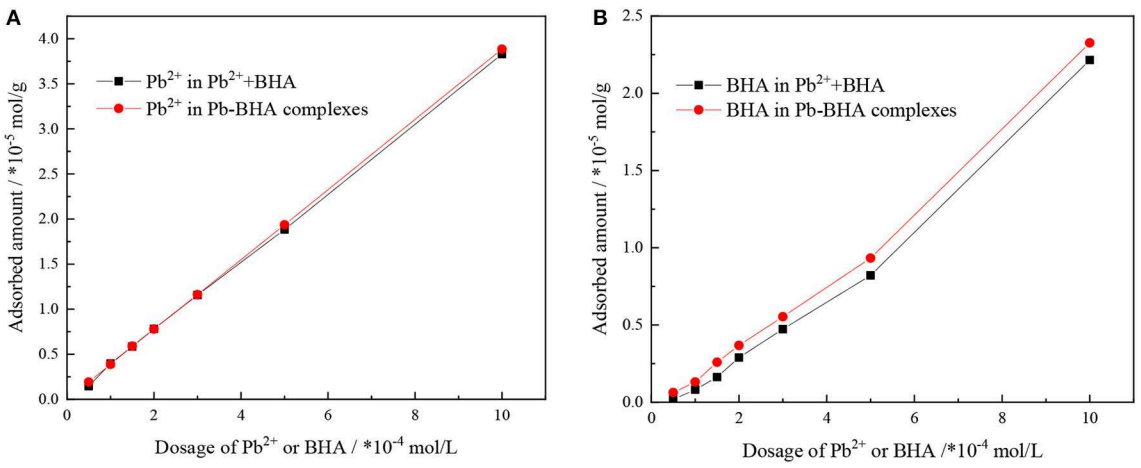

FIGURE 3 | Adsorbed amounts of **(A)** lead ions and **(B)** BHA on scheelite surface at different concentrations of lead ions and BHA (pH = 9.0 ± 0.2, C_{Pb}:C_{BHA} = 1).

is combined with lead ions, the coordination reaction occurs in two forms, as the lead ions can combine either with two oxygen atoms or with one oxygen atom and one nitrogen atom, resulting in an "O, O" five-membered ring or an "N, O" four-membered ring, respectively, and the five-membered ring complexes are the dominating configurations (Fitzpatrick and Mageswaran, 1989; Fernandes et al., 1997; Codd, 2008; Kumar et al., 2018). The significate shift in the electron binding energy of N_{1s} here indicates that the N atoms may have been able to combine with Pb to form "N, O" four-membered rings. Thus, we speculate that both configurations (four- and five-membered rings) may exist in Pb-BHA complexes, it agrees well with the reference (Dianzuo, 1982; Xia et al., 2004; Gupta and Sharma, 2013).

Figure 5 shows the N_{1s} spectra of Pb-BHA complexes. Four main chemical states of N elements were observed in the Pb-BHA complex: C-N (keto tautomer of hydroxamic acid), C=N (enol tautomer of hydroxamic acid), N-O, and a possible N-Pb coordinate bond (Fitzpatrick and Mageswaran, 1989; Brown et al., 1991, 1996). The binding energies of C-N and N-Pb were about 400 and 398 eV, respectively, but it was difficult to distinguish C=N from N-O because their binding energies were approximately 399 eV (Raole et al., 1987; Jouve et al., 1996; Yuan et al., 2009; Naumkin et al., 2012). The three peaks at 400.7, 399.1, and 398.1 eV (**Figure 5**) were assigned to C-N, N-O (or C=N), and N-Pb, respectively. The different contents of different forms of N also indicated that the Pb-BHA complexes have multiple configurations.

The different chemical states of N elements represent Pb-BHA complexes with different structures, including complexes with four- and five-membered rings formed by keto and enol tautomers of hydroxamic acid and lead ions (Fitzpatrick and Mageswaran, 1989; Kurzak et al., 1992; Codd, 2008). Three possible combinations of a single lead ion and a single BHA can be inferred from the XPS results (**Figure 5**), as shown in **Figure 6**. The -CONHO- group of BHA combines with lead ions to form complexes via coordination, resulting in "O, O" five-membered

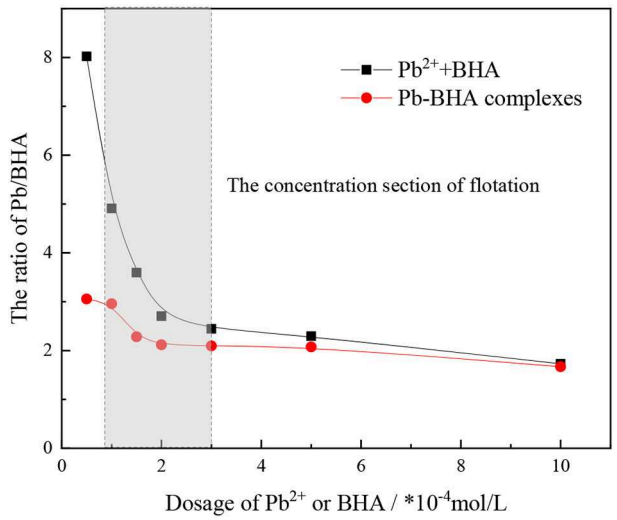

FIGURE 4 | Ratio of BHA and lead ions adsorbed on scheelite surface (pH = 9.0 ± 0.2, C_{Pb}:C_{BHA} = 1).

TABLE 1 | Electron binding energies of different elements of BHA and Pb-BHA complexes.

Elements	BHA binding energy (eV)	$Pb(OH)_2$	Pb-BHA binding energy (eV)	ΔE (eV)
O_{1s}	532.27	–	531.18	−1.19
N_{1s}	400	–	399.16	−1.05
Pb_{4f}	–	138.40	138.70	+0.30

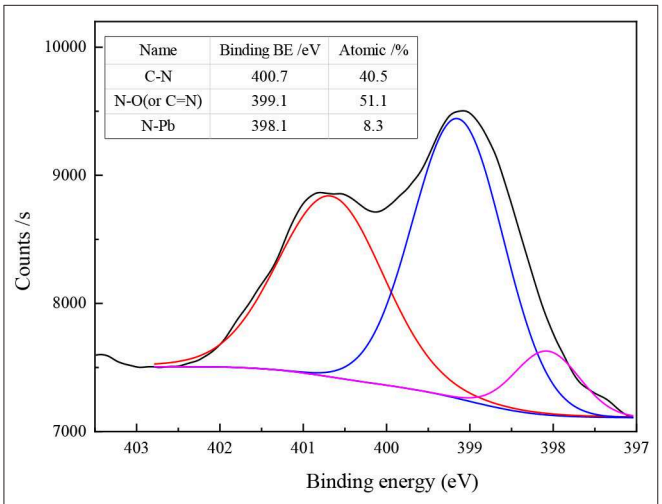

FIGURE 5 | N1s spectra of Pb-BHA complexes.

rings and "N, O" four-membered rings. In the presence of more BHA, a single lead ion can form a complex with two BHAs. Therefore, multiple components of the Pb-BHA complexes exist in the liquid phase, which may be adsorbed on the mineral surface together (Xia et al., 2004; Zhu and Zhu, 2012).

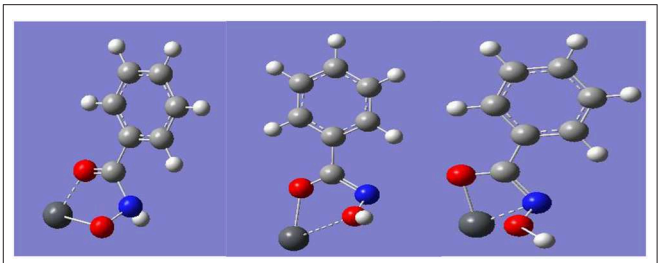

FIGURE 6 | The three possible combinations of a single lead ion and a single BHA.

TABLE 2 | The peak binding energies on the scheelite surface before and after treatment with Pb-BHA complexes.

Element	Scheelite Peak BE (eV)	Pb-BHA complexes Peak BE (eV)	Scheelite treated by Pb-BHA complexes Peak BE (eV)	ΔE (eV)
C_{1S}	284.8	284.8	284.8	0
W_{4f}	35.56	–	35.59	+0.03
O_{1s}	529.43	531.18	530.44	+1.01
Ca_{2p}	346.38	–	346.79	+0.41
Pb_{4f}	–	138.70	139.45	+0.75
N_{1s}	–	399.16	399.07	−0.09

After understanding the XPS spectra and structures of Pb-BHA complexes, we studied the structures of complexes adsorbed on the mineral surface. **Table 2** shows the peak binding energies on the scheelite surface before and after treatment with Pb-BHA complexes. The results show that the binding energies of Ca, O, and Pb on the scheelite surface have large positive shifts, the N_{1s} peak have a little negatively shifted, indicating that chemical adsorption plays an important role in the adsorption of Pb-BHA complexes on the surface of scheelite. The large shifts of the O_{1s}, Pb_{4f}, peaks binding energies indicate that they are active sites for the adsorption process, while the almost negligible shift of the binding energy of N_{1s} indicates that the chemical states of N elements in the complex and on the mineral surface are consistent.

Figure 7 shows the N_{1s} spectra of scheelite after treatment with different dosing modes of the reagents. The results show that the N elements on the scheelite surface also mainly existed in the form of C-N, N-O (or C=N), and N-Pb groups after treatment with Pb^{2+}, BHA, and Pb-BHA complexes. This indicates that the species of the component structures of complexes adsorbed on the scheelite surface were similar in two ways. As shown in **Figure 7A**, when lead ions and BHA were successively adsorbed on the scheelite surface, the relative contents of C-N, N-O (or C=N), and N-Pb groups were 45.0, 44.4, and 10.6%, respectively, compared with 23.4, 51.6, and 25.0%, respectively, for the scheelite surface treated with Pb-BHA complexes (**Figure 7B**). When lead ions and BHA were successively adsorbed on scheelite surface, there were more component structures with C-N and

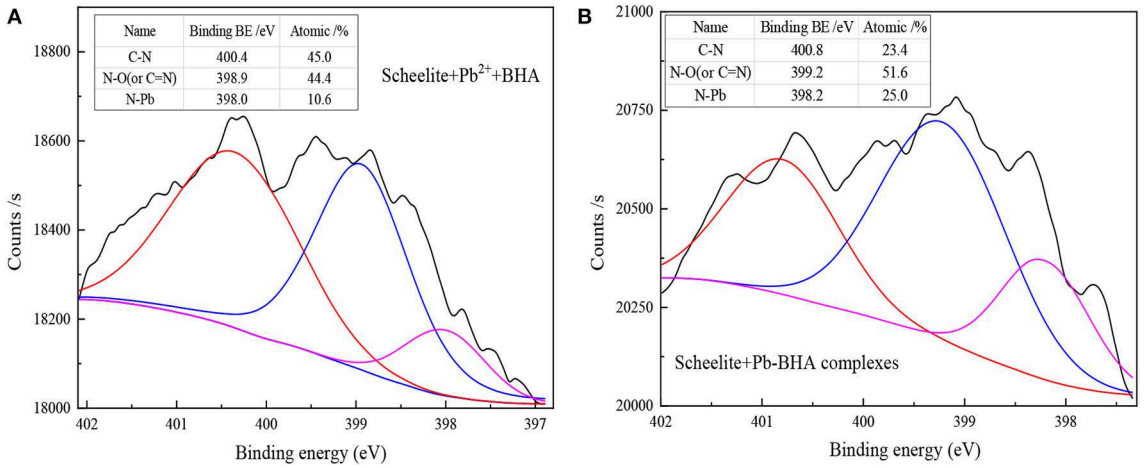

FIGURE 7 | N_{1s} spectra of scheelite after treatment with different reagents: **(A)** lead ions and BHA successively adsorbed on scheelite surface; **(B)** Pb-BHA complexes adsorbed on scheelite surface.

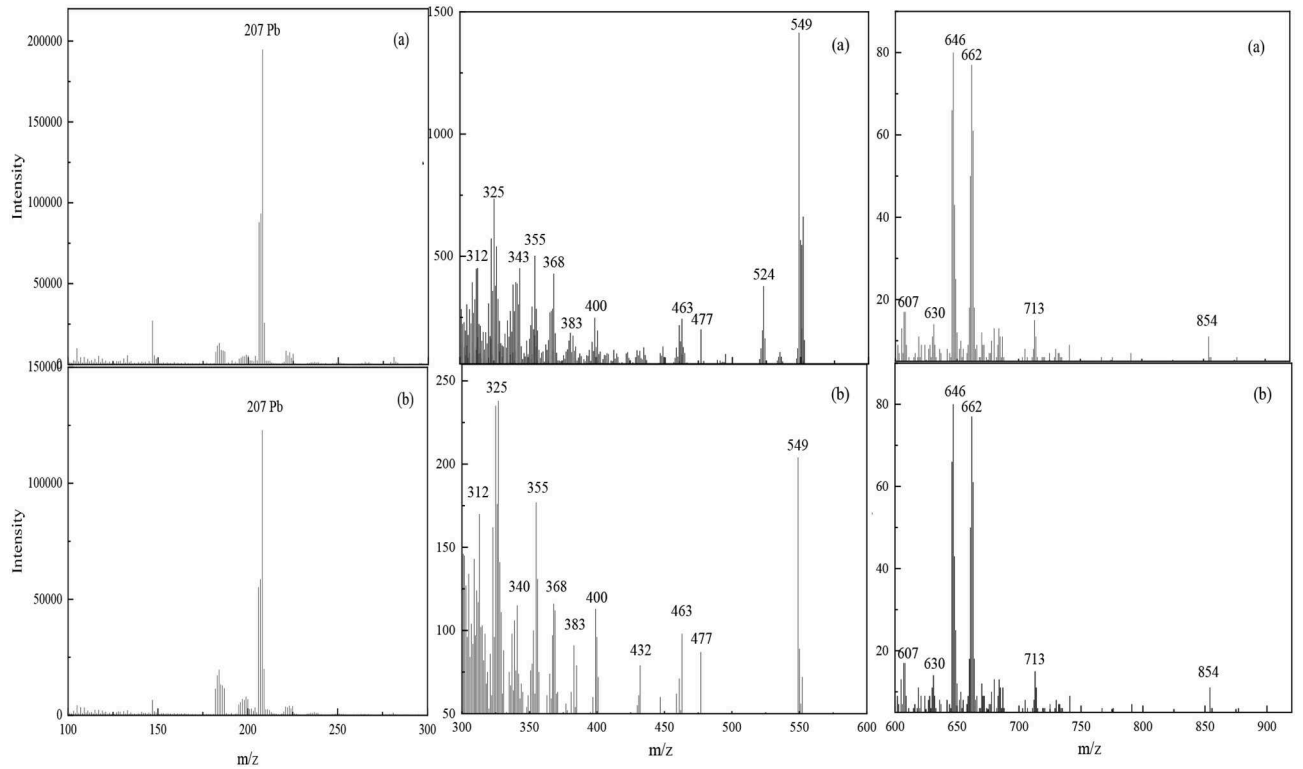

FIGURE 8 | TOF results for Pb-BHA complexes adsorbed on scheelite surface. **(a)** Scheelite treated with Pb^{2+} and BHA sequentially; **(b)** scheelite treated with Pb-BHA complexes.

N-O (or C=N) bonds, whereas more N-O (or C=N) and N-Pb bonds appeared when the scheelite surface was treated with Pb-BHA complexes. This indicated that complexes adsorbed on the scheelite surface had different contents of the various structural components. Overall, according to the XPS results, the components of complexes adsorbed on the scheelite surface had similar species in activation flotation and Pb-BHA complex flotation, but different contents of these species.

TOF-SIMS Measurements

TOF-SIMS is a highly sensitive analytical technique that can provide chemical characterization of the surfaces of materials

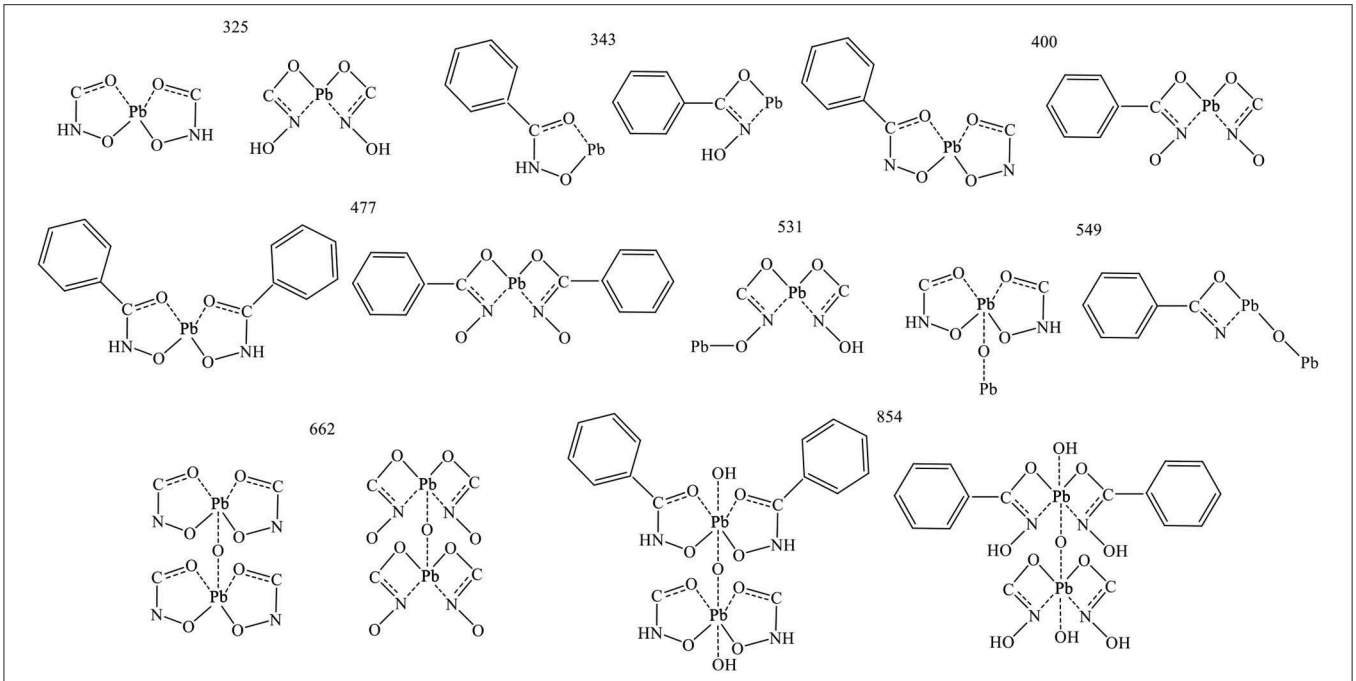

FIGURE 9 | The detected fragments of Pb-BHA complexes adsorbed on scheelite surface.

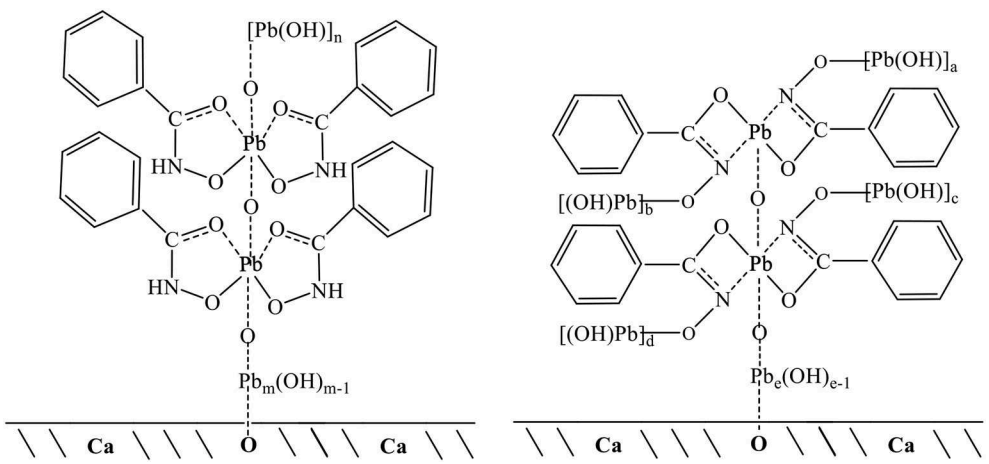

FIGURE 10 | Possible structures of Pb-BHA complexes adsorbed on scheelite surface.

(Chehreh Chelgani and Hart, 2014; Xia et al., 2015; Chenakin and Kruse, 2018). TOF-SIMS measurements were obtained to analyze the composition and structure of complexes adsorbed on the scheelite surface in activation flotation and Pb-BHA flotation. **Figure 8** shows the TOF-SIMS of a scheelite surface treated with Pb^{2+} and BHA sequentially and scheelite treated with Pb-BHA complexes. High-intensity fragments of all elements were recorded to elucidate the composition and structure of Pb-BHA complexes on the scheelite surface. The peaks detected in the two cases were essentially the same (**Figures 8a,b**). This was consistent with the XPS results, that is, the species composing the structure of Pb-BHA complexes were similar in activation flotation and Pb-BHA flotation. Thus, the different component contents of complexes adsorbed on scheelite surface were responsible for their different adsorption capacity and flotation behavior.

The composition and structure of the Pb-BHA complexes can be inferred according to the peaks in the detection region, including two forms in which the –CO–NHOH groups bind to lead ions in five- and four-membered rings, respectively. Deduced structure segments detected in the m/z range 100–900 are given in **Figure 9** (the five-membered rings of the keto

and enol tautomers of BHA are presented in one form). A lead ion could combine with one or two BHA to form monomer complexes; this was the dominant monomer of the complex formed by lead ions and BHA. Furthermore, the two complexes may have been bonded to lead atoms via oxygen atoms, as these two atom types easily combine (Breza and Manová, 1999b; Perera et al., 2001).

Solution chemical analysis of lead ions has shown that $PbOH^+$ and $Pb(OH)_{2(aq)}$ are the lead species in the flotation pH range 7–10 (Han et al., 2018; Tian et al., 2018b), that is, lead ions are in the form of lead hydroxide in solution. Previous research also concluded that polynuclear lead hydroxide species, such as $Pb_3(OH)_4^{2+}$, were formed in the pH range 7–10 (Breza and Manová, 1999a,b; Perera et al., 2001). Thus, lead ions could form polymers of lead hydroxyl in solution, in which lead ions were connected via oxygen atoms (Breza and Manová, 1999b). Here, the XPS and TOF-SIMS results showed that lead ions formed monomer complexes with two BHAs; these Pb-BHA complexes then combined with oxygen atoms. The measurements of adsorption amount indicated that the average ratio of lead ions to BHA in the molecular structures of complexes adsorbed on the scheelite surface was between 2 and 3. Therefore, we speculated that lead hydroxide polymers would bond with oxygen atoms in the complexes. Based on the measurement results, possible structures of Pb-BHA complexes adsorbed on the scheelite surface could be inferred (**Figure 10**; the five-membered rings of the keto and enol tautomers of BHA are presented in one form). BHA combines with lead ions to form both five- and four-membered rings; both of these configurations may exist on the scheelite surface. Lead ions could form mononuclear complexes with two BHAs, which would then combine with oxygen atoms to form polynuclear complexes. Lead hydroxide polymers with a certain degree of polymerization would bond with oxygen atoms in the complexes. The degree of polymerization of lead hydroxide depends on the pH and the concentration of lead ions in the solution. For the flotation pH and reagent concentrations used in the experiments, we speculated that m+n (or a+b+c+d+e) was 6–10 based on the adsorption amount measurements. At the solid-liquid interface, the functional group of Pb-BHA complexes was lead ions, which could combine with oxygen atoms on the scheelite surface to form an adsorbate. The adsorption of Pb-BHA complexes rendering the surface hydrophobic, and showed a strong collecting ability for scheelite flotation.

CONCLUSION

Pb-BHA complexes have good collection ability for scheelite flotation and have important roles in conventional lead-activated scheelite flotation. Adsorption capacity measurements showed that the adsorption amount of BHA in Pb-BHA complex flotation was higher than that in activation flotation, while the results for lead ions were similar. Therefore, more BHA adsorbed on the scheelite surface in Pb-BHA flotation, resulting in higher flotation recovery compared with activation flotation. XPS and TOF-SIMS measurements showed that the species of Pb-BHA complexes were similar in activation flotation and Pb-BHA flotation, but the contents of the three structures of N on the scheelite surface, as determined from the N_{1s} spectra (C-N, C=N, N-O, N-Pb), were different. This was considered to be responsible for the different flotation behaviors. XPS and TOF-SIMS measurements showed that BHA combined with lead ions to form five- and four-membered rings; both of these configurations may exist on the scheelite surface. Lead ions can form monomer complexes with two BHAs, which then combine with oxygen atoms to form polynuclear complexes. Lead hydroxide polymers with a certain degree of polymerization could bond with oxygen atoms in the complexes. The functional group of Pb-BHA complexes was lead ions, which could combine with oxygen atoms on the scheelite surface to form an adsorbate, rendering the surface hydrophobic.

DATA AVAILABILITY STATEMENT

All datasets generated for this study are included in the manuscript/**Supplementary Files**.

AUTHOR CONTRIBUTIONS

HH and WeiS initiated the research topic. ZW and WenS wrote the manuscript text. YH reviewed and edited the manuscript. RW, YZ, BL, and ZS provided experimental assistance. All authors reviewed the manuscript.

FUNDING

This work was supported by the National Natural Science Foundation of China (No. 51804340), the State Key Laboratory of Mineral Processing (No. BGRIMM-KJSKL-2019), the Innovation Driven Plan of Central South University (No. 2018CX036), National Project 111 (No. B14034), and the Collaborative Innovation Center for Clean and Efficient Utilization of Strategic Metal Mineral Resources.

SUPPLEMENTARY MATERIAL

The Supplementary Material for this article can be found online at: https://www.frontiersin.org/articles/10.3389/fchem.2019.00645/full#supplementary-material

REFERENCES

Breza, M., and Manová, A. (1999a). On the reliability of the structures of lead (II) hydroxo complexes obtained by MNDO method. *Collect. Czech. Chem. Commun.* 64, 1269–1273. doi: 10.1135/cccc19991269

Breza, M., and Manová, A. (1999b). On the structure of lead(II) complexes in aqueous solutions. II: tetranuclear clusters. *Polyhedron* 18, 2085–2090. doi: 10.1016/S0277-5387(99)00104-7

Brown, D. A., Coogan, R. A., Fitzpatrick, N. J., Glass, W. K., Abukshima, D. E., Shiels, L., et al. (1996). Conformational behaviour of hydroxamic acids: ab initio and structural studies. *J. Chem. Soc. Perkin Trans.* 2, 2673–2679. doi: 10.1039/P29960002673

Brown, D. A., Glass, W. K., Mageswaran, R., and Mohammed, S. A. (1991). 1H and 13C NMR studies of isomerism in hydroxamic acids. *Magn. Reson. Chem.* 29, 40–45. doi: 10.1002/mrc.1260290109

Bulatovic, S. M. (2015). *Handbook of Flotation Reagents: Chemistry, Theory and Practice*. Amsterdam.

Cao, M., Gao, Y., Bu, H., and Qiu, X. (2019). Study on the mechanism and application of rutile flotation with benzohydroxamic acid. *Miner. Eng.* 134, 275–280. doi: 10.1016/j.mineng.2019.02.016

Chehreh Chelgani, S., and Hart, B. (2014). TOF-SIMS studies of surface chemistry of minerals subjected to flotation separation – A review. *Miner. Eng.* 57, 1–11. doi: 10.1016/j.mineng.2013.12.001

Chenakin, S., and Kruse, N. (2018). Combining XPS and ToF-SIMS for assessing the CO oxidation activity of Au/TiO2 catalysts. *J. Catal.* 358, 224–236. doi: 10.1016/j.jcat.2017.12.010

Codd, R. (2008). Traversing the coordination chemistry and chemical biology of hydroxamic acids. *Coord. Chem. Rev.* 252, 1387–1408. doi: 10.1016/j.ccr.2007.08.001

Dianzuo, W. (1982). *Principle and Application of Flotation Agent*. Beijing: Metallurgical industry press.

Fernandes, M. C. M. M., Paniago, E. B., and Carvalho, S. (1997). Copper(II) mixed ligands complexes of hydroxamic acids with glycine, histamine and histidine. *J. Braz. Chem. Soc.* 8, 537–548. doi: 10.1590/S0103-50531997000500017

Fitzpatrick, N. J., and Mageswaran, R. (1989). Theoretical study of hydroxamic acids. *Polyhedron* 8, 2255–2263. doi: 10.1016/S0277-5387(00)81252-8

Gao, Y., Gao, Z., Sun, W., Yin, Z., Wang, J., and Hu, Y. (2018). Adsorption of a novel reagent scheme on scheelite and calcite causing an effective flotation separation. *J. Colloid Interface Sci.* 512, 39–46. doi: 10.1016/j.jcis.2017.10.045

Gao, Z., Fan, R., Ralston, J., Sun, W., and Hu, Y. (2019). Surface broken bonds: an efficient way to assess the surface behaviour of fluorite. *Miner. Eng.* 130, 15–23. doi: 10.1016/j.mineng.2018.09.024

Gupta, S. P., and Sharma, A. (2013). "The chemistry of hydroxamic acids," in *Hydroxamic Acids: A Unique Family of Chemicals with Multiple Biological Activities*, ed S. P. Gupta (Berlin; Heidelberg: Springer Berlin Heidelberg), 1–17.

Han, H., Hu, Y., Sun, W., Li, X. D., Cao, C. G., Liu, R. Q., et al. (2017a). Fatty acid flotation versus BHA flotation of tungsten minerals and their performance in flotation practice. *Int. J. Miner. Process.* 159, 22–29. doi: 10.1016/j.minpro.2016.12.006

Han, H., Hu, Y., Sun, W., Li, X. D., Chen, K. F., Zhu, Y. G., et al. (2018). Novel catalysis catalysis mechanisms of benzohydroxamic acid adsorption by lead ions and changes in the-surface of scheelite particles. *Miner. Eng.* 119, 11–22. doi: 10.1016/j.mineng.2018.01.005

Han, H., Liu, W., Hu, Y., Sun, W., and Li, X. (2017b). A novel flotation scheme: selective flotation of tungsten minerals from calcium minerals using Pb-BHA complexes in Shizhuyuan. *Rare Metals* 36, 533–540. doi: 10.1007/s12598-017-0907-8

He, J., Han, H., Zhang, C., Hu, Y., Yuan, D., Tian, M., et al. (2018a). New insights into the configurations of lead(II)-benzohydroxamic acid coordination compounds in aqueous solution: a combined experimental and computational study. *Minerals* 8:368. doi: 10.20944/preprints201806.0110.v2

He, J., Han, H., Zhang, C. Y., Xu, Z. J., Yuan, D. D., Chen, P., et al. (2018b). Novel insights into the surface microstructures of lead(II) benzohydroxamic on oxide mineral. *Appl. Surf. Sci.* 458, 405–412. doi: 10.1016/j.apsusc.2018.07.085

Hu, Y., He, J., Zhang, C., Zhang, C., Sun, W., Zhao, D., et al. (2018). Insights into the activation mechanism of calcium ions on the sericite surface: a combined experimental and computational study. *Appl. Surf. Sci.* 427, 162–168. doi: 10.1016/j.apsusc.2017.07.265

Jiang, W., Gao, Z., Khoso, S. A., Gao, J., Sun, W., Pu, W., et al. (2018). Selective adsorption of benzhydroxamic acid on fluorite rendering selective separation of fluorite/calcite. *Appl. Surf. Sci.* 435, 752–758. doi: 10.1016/j.apsusc.2017.11.093

Jouve, G., Séverac, C., and Cantacuzène, S. (1996). XPS study of NbN and (NbTi)N superconducting coatings. *Thin Solid Films* 287, 146–153. doi: 10.1016/S0040-6090(96)08776-7

Kumar, K., Siva, B., Rama Rao, N., and Suresh Babu, K. (2018). Rapid identification of limonoids from *Cipadessa baccifera* and *Xylocarpus granatum* using ESI-Q-ToF-MS/MS and their structure-fragmentation study. *J. Pharm. Biomed. Anal.* 152, 224–233. doi: 10.1016/j.jpba.2017.12.050

Kupka, N., and Rudolph, M. (2018). Froth flotation of scheelite – A review. *Int. J. Min. Sci. Technol.* 28, 373–384. doi: 10.1016/j.ijmst.2017.12.001

Kurzak, B., Kozłowski, H., Farkas, E., Kurzak, B., Kozłowski, H., and Farkas, E. (1992). Hydroxamic and aminohydroxamic acids and their complexes with metal ions. *Coord. Chem. Rev.* 114, 169–200. doi: 10.1016/0010-8545(92)85002-8

Li, C. W., and Gao, Z. Y. (2017). Effect of grinding media on the surface property and flotation behavior of scheelite particles. *Powder Technol.* 322, 386–392. doi: 10.1016/j.powtec.2017.08.066

Naumkin, A. V., Kraut-Vass, A., Gaarenstroom, S. W., and Powell, C. J. (2012). *NIST X-ray Photoelectron Spectroscopy Database*. Available online at: https://srdata.nist.gov/xps/Default.aspx

Perera, W. N., Hefter, G., and Sipos, P. M. (2001). An investigation of the lead(II)–hydroxide system. *Inorg. Chem.* 40, 3974–3978. doi: 10.1021/ic001415o

Rao, S. R. (2004). *Surface Chemistry of Froth Flotation*. Boston, MA: Plenum Press; Springer.

Raole, P. M., Prabhawalkar, P. D., Kothari, D. C., Pawar, P. S., and Gogawale, S. V. (1987). XPS studies of N + implanted aluminium. *Nucl. Instrum. Methods Phys. Res. B* 23, 329–336. doi: 10.1016/0168-583X(87)90386-7

Tian, M., Gao, Z., Sun, W., Han, H., Sun, L., and Hu, Y. (2018a). Activation role of lead ions in benzohydroxamic acid flotation of oxide minerals: New perspective and new practice. *J. Colloid Interface Sci.* 529 150–160. doi: 10.1016/j.jcis.2018.05.113

Tian, M., Hu, Y., Sun, W., and Liu, R. (2017). Study on the mechanism and application of a novel collector-complexes in cassiterite flotation. *Colloids Surf. A* 522, 635–641. doi: 10.1016/j.colsurfa.2017.02.051

Tian, M., Zhang, C., Han, H., Liu, R., Gao, Z., Chen, P., et al. (2018b). Novel insights into adsorption mechanism of benzohydroxamic acid on lead (II)-activated cassiterite surface: An integrated experimental and computational study. *Miner. Eng.* 122, 327–338. doi: 10.1016/j.mineng.2018.04.012

Wei, Z., Hu, Y., Han, H., Sun, W., Wang, R., and Wang, J. (2018). Selective flotation of scheelite from calcite using Al-Na_2SiO_3 polymer as depressant and Pb-BHA complexes as collector. *Miner. Eng.* 120, 29–34. doi: 10.1016/j.mineng.2018.01.036

Wei, Z., Hu, Y., Han, H., Sun, W., Wang, R. L., Sun, W. J., et al. (2019). Selective separation of scheelite from calcite by self-assembly of H2SiO3 polymer using Al3+ in Pb-BHA flotation. *Minerals* 9:43. doi: 10.3390/min9010043

Xia, L., Hart, B., and Loshusan, B. (2015). A Tof-SIMS analysis of the effect of lead nitrate on rare earth flotation. *Miner. Eng.* 70 119–129. doi: 10.1016/j.mineng.2014.09.008

Xia, Q., Li, Z., Qiu, X., and Dai, Z. (2004). Quantum chemical study on benzyhydroximic acid flotation agent. *Min. Metal. Eng.* 24, 30–33. doi: 10.1038/sj.cr.7290254

Yuan, G. D., Ye, Z. Z., Huang, J. Y., Zhu, Z. P., Perkins, C. L., and Zhang, S. B. (2009). X-ray photoelectron spectroscopy study of Al- and N- co-doped p-type ZnO thin films. *J. Cryst. Growth* 311, 2341–2344. doi: 10.1016/j.jcrysgro.2009.01.128

Yue, T., Han, H., Hu, Y., Wei, Z., Wang, J., Wang, L., et al. (2018). Beneficiation and purification of tungsten and cassiterite minerals using Pb–BHA complexes flotation and centrifugal separation. *Minerals* 8:566. doi: 10.3390/min8120566

Yue, T., Han, H. S., Hu, Y. H., Sun, W., Li, X. D., Liu, R. Q., et al. (2017). New insights into the role of Pb-BHA complexes in the flotation of tungsten minerals. *JOM J Miner. Metals Mater. Soc.* 69, 2345–2351. doi: 10.1007/s11837-017-2531-3

Zhu, J. G., and Zhu, Y. M. (2012). Search for new flotation collectors of cassiterite and wolframite slime according to flotation reagent isomerism principle (in Chinese). *Multipurpose Utilizat. Miner. Res.* 2, 10–13. doi: 10.3969/j.issn.1000-6532.2012.02.003

Conflict of Interest: YZ, BL, and ZS were employed by company BGRIMM Technology Group.

The remaining authors declare that the research was conducted in the absence of any commercial or financial relationships that could be construed as a potential conflict of interest.

frontiers in Chemistry

ORIGINAL RESEARCH
published: 12 December 2019
doi: 10.3389/fchem.2019.00813

Flotation Separation of Diaspore and Kaolinite by Using a Mixed Collector of Sodium Oleate-Tert Dodecyl Mercaptan

Xiaofei Man, Leming Ou, Chenliang Wang, Saizhen Jin and Xiqi Ma*

School of Minerals Processing and Bioengineering, Central South University, Changsha, China

Sodium oleate (NaOl), a collector in diaspore flotation, has been widely used for more than 30 years, while its low selectivity becomes an issue under today's process requirement. This study introduced tert dodecyl mercaptan (TDM) together with NaOl as a mixed collector to improve selectivity in diaspore flotation. We found that using the mixed collector of NaOl/TDM (total concentration 0.1 mM, the molar ratio 8:2 of NaOl: TDM) at pH = 9–10 significantly effectively separated diaspore and kaolinite. Comparing the recovery of Al_2O_3 and the ratio of Al_2O_3 to SiO_2 (A/S) treated by NaOl/TDM (pH = 9) and NaOl (pH = 10), the Al_2O_3 recovery and A/S in concentrate for NaOl/TDM are 7.5% and 2.2 higher than that for NaOl in mixed mineral flotation. Also, surface tension measurements, Zeta potential measurements and Fourier Transform Infrared (FTIR) spectra analysis were used to examine its selectivity from a flotation mechanical perspective. Surface tension measurements show that mixed collector NaOl/TDM has stronger surface activity and hydrophobic association than NaOl. The results of Zeta potential measurements and FTIR spectra analysis indicate that NaOl and TDM can selectively co-adsorb diaspore through physical adsorption. Moreover, the adsorption of TDM promotes the adsorption of NaOl on diaspore. However, when NaOl/TDM treats on kaolinite together, TDM can hardly adsorb on mineral surface, nor can it promote the adsorption of NaOl.

Keywords: flotation, diaspore, kaolinite, mixed collector, sodium oleate, tert dodecyl mercaptan

OPEN ACCESS

Edited by:
Zhiyong Gao,
Central South University, China

Reviewed by:
Thuat Thanh Trinh,
Norwegian University of Science and Technology, Norway
Shuling Gao,
Northeastern University, China

****Correspondence:***
Leming Ou
olmpaper@csu.edu.cn

Specialty section:
This article was submitted to Physical Chemistry and Chemical Physics, a section of the journal Frontiers in Chemistry

Received: *15 July 2019*
Accepted: *11 November 2019*
Published: *12 December 2019*

Citation:
Man X, Ou L, Wang C, Jin S and Ma X (2019) Flotation Separation of Diaspore and Kaolinite by Using a Mixed Collector of Sodium Oleate-Tert Dodecyl Mercaptan. Front. Chem. 7:813. doi: 10.3389/fchem.2019.00813

INTRODUCTION

Bauxite is an important raw material for industrial production of alumina (Zhang et al., 2017a, 2018a). In China, diaspore is the primary mineral in bauxite, accounting for more than 98% of the total reserves (Zhang et al., 2016). China's bauxite resources have the characteristics of high alumina, high silicon, and low mass ratio of Al_2O_3 to SiO_2 (A/S) (Liu et al., 2007; Hong et al., 2008; Jiang et al., 2012). Bauxite with A/S ratio of 4–6 accounts for about 60% of the total (Liu et al., 2007; Jiang et al., 2010a). However, through Bayer process, the principal method of producing alumina from bauxite (Zhang et al., 2019), producing alumina is that the mass ratio of A/S should be more than 8 (Jiang et al., 2010b; Gibson et al., 2017). Therefore, it is necessary to pre-desilicate bauxite to improve its mass ratio of A/S.

Kaolinite is a common layered silicate mineral (Jing et al., 2015). As one of the main gangue-bearing minerals in bauxite, the removal of kaolinite is of great significance to the desilication process of bauxite (Jiang et al., 2014; Liang et al., 2017). At present, there are many desilication methods. Currently, flotation desilication is the most effective way to separate diaspore from kaolinite (Jing et al., 2015; Zhang et al., 2017b), especially direct flotation (floating diaspore but suppressing kaolinite desilication) has been widely used in practical production (Zhang et al., 2018b). Flotation reagents play an important role in the flotation process (Jiang et al., 2010b). In recent years, various surfactants have been used as collectors for selective separation of diaspore and kaolinite in direct flotation, such as oleic acid (Huang et al., 2012), tall oil, oxidized paraffin soap (Yuehua et al., 2004; Hu et al., 2005), 733, styrene phosphate, hydroxamic acids, propyl gallate (Lyu et al., 2019) and their mixtures (Jiang et al., 2014), and novel synthetic chelates (Deng et al., 2015, 2016). The selectivity of synthetic chelating collectors is stronger than that of oleic acid collectors (Gibson et al., 2017), and their functional groups are mainly composed of one or several carboxyl groups, hydroxamic acid salts and amides (Jiang et al., 2011). However, oleic acid collectors are still widely used in bauxite flotation as the most commonly used collectors (Deng et al., 2015; Wang et al., 2017) due to their low cost, high collection capacity and low toxicity in China (Jarek et al., 2010; Chernyshova et al., 2011). But the strong collecting ability and low selectivity of oleic acid collectors may lead to low A/S ratio or low recovery of diaspore concentrate.

Thus, to enhance the selectivity of oleic acid collectors, the use of synergists has been increasingly investigated in recent years. The common synergists are mainly non-ionic surfactants (Kongolo et al., 2003). These non-ionic surfactants can promote the dissolution and emulsification of oleic acid collectors, reduce the surface tension of the solution, and strenigthen the adsorption of collectors on mineral surfaces (Cao et al., 2014). By adding synergists, the efficiency of collectors is improved and the dosage of collectors is reduced. Tert dodecyl mercaptan ($C_{12}H_{25}SH$, TDM), a novel surfactant, which has been used as a collector in sulfide ore flotation (sphalerite, arsenopyrite, and molybdenite) (Chen et al., 2010; Jiao et al., 2016), has great potential to be used as a synergist to improve the efficiency of diaspore flotation, despite the limitation of high price and complex production process (Jiao et al., 2016).

In this paper, the flotation separation of diaspore and kaolinite by mixing tert dodecyl mercaptan (TDM) with sodium oleate (NaOl) as a mixed collector is proposed for the first time. The flotation performance of diaspore and kaolinite was examined by single mineral tests. In addition, we analyzed the surface activity of the mixed collector by measuring its surface tension, and investigated the absorption mechanism between the mixed collector and mineral surfaces by analyzing Zeta potential and FTIR spectra.

MATERIALS AND METHODS

Materials

The single minerals used in the experiments were diaspore and kaolinite from Hebei Province and Suzhou Province of China respectively. They were both higher than 90% pure based on X-ray diffraction (shown in **Supplementary Material**) and chemical analysis. Through handpicking massive ores, artificial crushing and grounding in a porcelain mill, minerals of +37–74 μm were screened out for single mineral flotation tests and mixed mineral flotation tests. The screened minerals were grinded to −5 μm by an agate mortar for Zeta potential determinations and FTIR spectra analysis.

Reagents

Chemically pure sodium oleate (NaOl), chemically pure tert dodecyl mercaptan (TDM) and NaOl/TDM mixtures with different molar ratios were used as collectors. NaOl was supplied by China Pharmaceutical Group Chemical Reagent Co. Ltd. And TDM was supplied by Shanghai Macklin Biochemical Co. Ltd. All the reagents were ready-to-use to avoid drug failure. The analytical purity of hydrochloric acid (HCl) and sodium hydroxide (NaOH) were used as pH regulators of the system. Deionized (DI) water was used for all experiments.

Flotation Tests

Single mineral flotation tests and mixed binary mineral flotation tests were carried out in an XFG hitch groove flotation machine with a 40 ml plexiglass cell at a spindle speed of 1,900 rpm. The mineral suspension was prepared by 2.0 g of single or artificially mixed minerals to 35 ml of deionized water in a plexiglass cell. The mass ratio of diaspore to kaolinite in artificial mixed minerals is 3:1 and the A/S ratio of mixed minerals is 3.49. **Figure 1** is the flow chart of the flotation test. For single mineral flotation, the flotation concentrates and tails were filtered, dried, and weighed, and the recovery was calculated. For mixed binary mineral flotation, the content of Al and Si in the flotation products was analyzed and A/S was calculated.

Surface Tension Measurements

The surface tension was measured by the platinum ring detachment method with a BZY-2 automatic tensiometer. Before measurement, the platinum ring was cleaned with deionized water and alcohol and subsequently it was placed on the alcohol lamp flame to remove the remnants from the last measurement. When the surface tension of the collector was measured, equal volume solution was weighed and put into the glass dish of the surface tensiometer. The average of three tests was taken as the final test result.

Zeta Potential Determinations

Zeta potentials of pure minerals before and after adding collectors were measured by Coulter Delsa-440SX Zeta potential analyzer (Brookhaven Corporation, USA) at 25°C. The suspension consists of 30 mg single mineral particles and 40 ml KCl (0.01 M) background electrolyte. After adjusting the pulp pH with HCl or

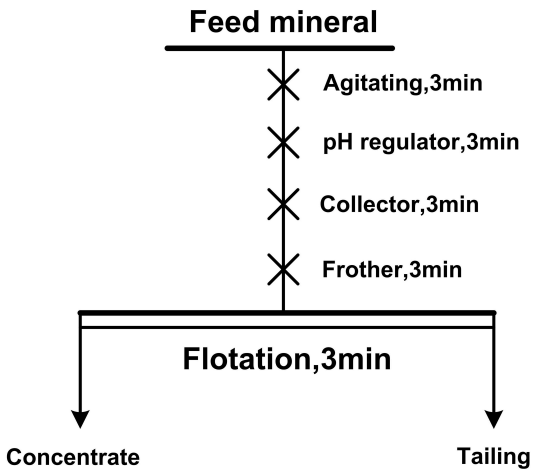

FIGURE 1 | Flowsheet of the flotation tests.

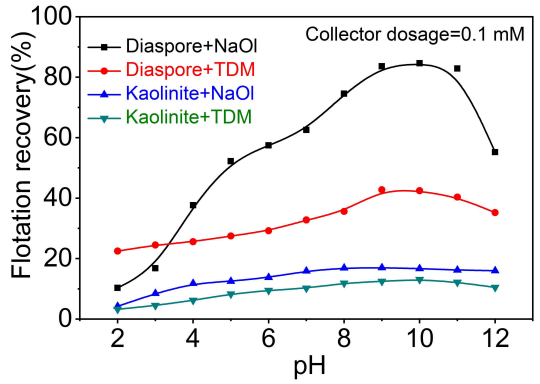

FIGURE 2 | Flotation recovery of diaspore and kaolinite with NaOl or TDM as collector (Collector dosage = 0.1 mM) as a function of pH.

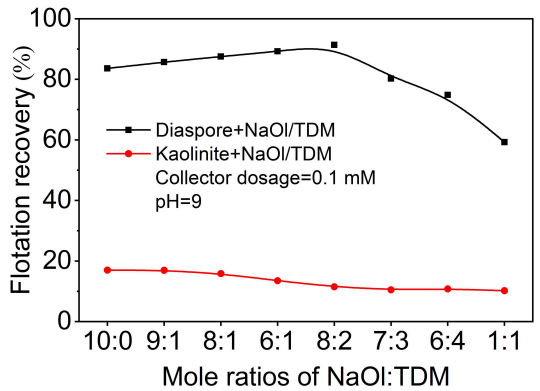

FIGURE 3 | Effect of the molar ratio of NaOl to TDM (Collector dosage = 0.1 mM, pH = 9) on the flotation recovery of diaspore and kaolinite.

NaOH, the collector was added. The suspension was agitated by a magnetic stirrer for 5 min and settled for 10 min. The supernatant was extracted by a syringe for Zeta potential measurement. The average of three tests was taken as the final result.

FTIR Spectra Analysis

Infrared spectra of reagents and minerals before and after their interaction were determined by IRAffnity-1 Fourier Transform Infrared Spectrometer (shimadzu Japan). The single mineral particles (0.5 g) were added to 35 ml deionized water. After adjusting the pulp pH and adding reagents, the sample was stirred for 40 min and filtered for 40 min subsequently. After washing three times with distilled water at the same pH, the solid samples were dried in a vacuum oven at 35°C for 24 h and analyzed by FTIR spectra analysis.

RESULTS AND DISCUSSIONS

Flotation Tests

Figure 2 shows that flotation recovery of diaspore and kaolinite varies with pH when NaOl or TDM was used as a single collector. As shown in **Figure 2**, the recovery of diaspore using NaOl increases first and then decreases with the enhancement of pH. The best pH range for the flotation by NaOl is 9–11, which is consistent with the results of other scholars (Xu et al., 2014). The recovery of NaOl to diaspore reaches the maximum of 84.6%, but at this time the recovery of NaOl to kaolinite also reaches 16.7%, so single collector NaOl cannot make an efficient separation between diaspore and kaolinite. Unlike NaOl, recovery of diaspore and kaolinite with TDM as collector alone is relatively low. The maximum recovery of diaspore by TDM at pH = 9 is only 42.8%. Obviously, neither NaOl nor TDM alone can achieve efficient flotation separation of diaspore from kaolinite. We considered further investigating the flotation of diaspore and kaolinite with NaOl/TDM mixed collector in order to obtain better separation effect.

Considering the important influence of molar ratio on mixed collector, the effects of molar ratio of NaOl and TDM on the recovery of diaspore and kaolinite were investigated. **Figure 3** shows that effects of different molar ratio of NaOl to TDM on the flotation recovery of diaspore and kaolinite. The effect of molar ratio of NaOl to TDM on the recovery of diaspore is obvious. When the molar fraction of TDM is less than 20%, the flotation recovery of diaspore with mixed collector is higher than that with NaOl. With the increase of molar fraction of TDM, the recovery of diaspore decreases sharply. When the molar ratio of NaOl to TDM is 8:2, the recovery of diaspore reaches the maximum of 91.4%. Unlike diaspore, the recovery of kaolinite does not change significantly with the molar ratio of mixed collector. The recovery of kaolinite decreases slowly with the increase of molar fraction of TDM. When the molar ratio of NaOl to TDM is 8:2, the recovery of kaolinite is 11.5%, which is 5.6% lower than that of single collector NaOl. Therefore, the optimum molar ratio of diaspore and kaolinite separated by mixed collector is about 8:2 for NaOl: TDM.

Figure 4 shows the effect of pH on the recovery of diaspore and kaolinite by flotation with NaOl/TDM mixed collector. The

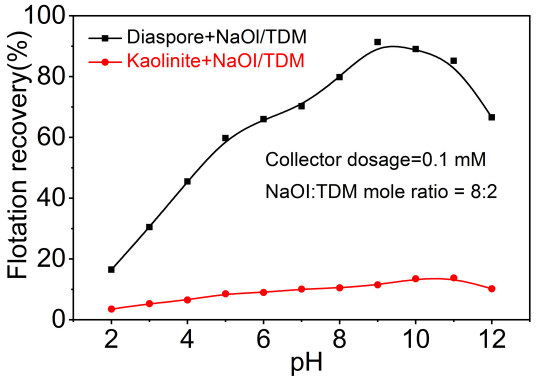

FIGURE 4 | Flotation recovery of diaspore and kaolinite with the NaOl/TDM (dosage = 0.1 mM, NaOl: TDM mole ratio = 8:2) as a function of pH.

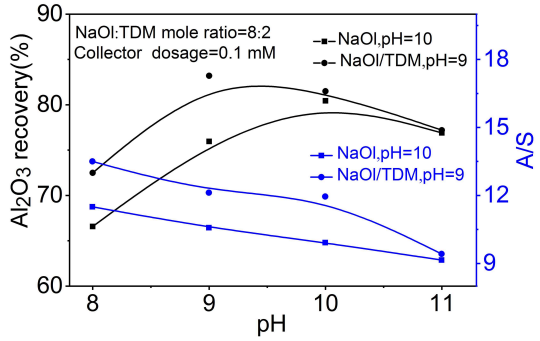

FIGURE 6 | The separation results of mixed binary minerals as a function of pH with NaOl (dosage = 0.1 mM, pH = 10) or NaOl/TDM (dosage = 0.1 mM, NaOl: TDM mole ratio = 8:2, pH = 9) as collector.

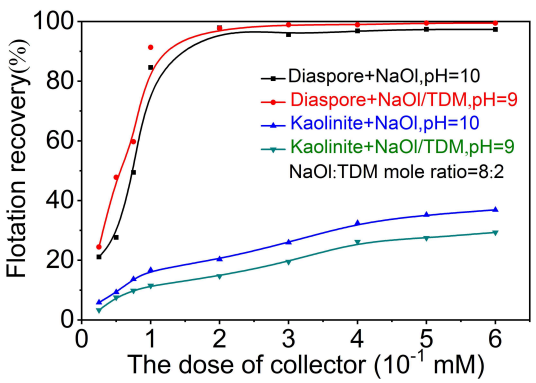

FIGURE 5 | Effect of collector dosage on the diaspore and kaolinite flotation recovery with NaOl (pH = 10) or NaOl/TDM (pH = 9, NaOl: TDM mole ratio = 8:2) as collector.

recovery of diaspore increases firstly and then decreases with the increase of pH. When the pH is 9, the recovery of diaspore reaches the maximum of 91.35%. Unlike diaspore, the recovery of kaolinite gradually increases from a minimum of 3.5% at pH 2 to a maximum of 13.8% at pH 11 and decreases with the increase until pH equals 12. Therefore, the optimal pH for the flotation separation of diaspore from kaolinite with mixed collector is 9.

The dosage influence of new collector NaOl/TDM on the flotation of diaspore and kaolinite was investigated by reference to NaOl dosage. **Figure 5** presents the effect of collector dosage on the diaspore and kaolinite flotation recovery with NaOl or NaOl/TDM as collector. As shown in **Figure 5**, the flotation recovery of diaspore increases rapidly with the increase of collector dosage when the concentration of collector is less than 0.1 mM, and then increases slowly. The recovery of diaspore by mixed collector is higher than that by NaOl single collector at various concentrations. When the concentration of the collector is 0.1 mM, the recovery of NaOl and mixed collector for diaspore are 84.62 and 91.35%, respectively. For kaolinite flotation, the recovery of kaolinite increases with the concentration of collector. When the concentrate of collector is more than 0.075 mM, the recovery of mixed collector for kaolinite is much lower than that of NaOl. The recovery of kaolinite is 16.7% when the concentrate of NaOl is 0.1 mM. At this time, the recovery of kaolinite with mixed collector is only 11.5%. Therefore, compared with the single collector of NaOl, NaOl/TDM mixed collector has better separation effect on diaspore and kaolinite. The optimum dosage range of mixed collector is from 0.1 to 0.15 mM.

In order to further verity the flotation effect of NaOl/TDM mixed collector, the flotation effect of mixed binary minerals at the special pH was studied. **Figure 6** shows the separation results of the mixed minerals as a function of pH. The A/S of the concentrate with NaOl/TDM decreases from 13.5 to 9.3 as the increase of pH. Meanwhile, the Al_2O_3 recovery increases from 73.2 to 83.6% by increasing pH from 8 to 9, and then decreases to 76.5% at pH 11. When NaOl is used as collector, the A/S decreases from 11.5 to 9.1 and the Al_2O_3 recovery increases from 67.6 to 77.2% by increasing pH from 8 to 10, and then decreases to 76.1% at pH 11. Comparing the A/S and Al_2O_3 recovery treated by NaOl/TDM (pH = 9) and NaOl (pH = 10), the A/S in concentrate is 11.9 and 9.7, respectively, and the Al_2O_3 recovery for NaOl/TDM is 7.5% higher than that for NaOl. The flotation tests of mixed binary minerals further proves that mixed NaOl/TDM collector can better separate diaspore and kaolinite.

Surface Tension Measurements

The formation of micelles in solution and the reduction of surface tension are two important properties of surfactants. The critical micelle concentration (CMC) is one of the parameters to measure collector performance in flotation. Generally, the smaller the CMC is, the larger the proportion of non-polar groups in surfactants, which means that the agents have stronger hydrophobicity and stronger collectivity. The relationship between surface tension and concentration of individual collectors NaOl, TDM, and mixed collector NaOl/TDM is shown in **Figure 7**. The order of the CMCs and the lowest surface tension of the three surfactants in **Table 1** is NaOl/TDM < NaOl << TDM. The CMC and the lowest

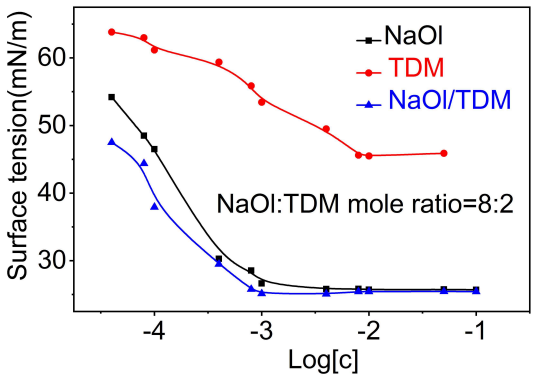

FIGURE 7 | Surface tension for the individual collectors NaOl and TDM and mixed collector NaOl/TDM (NaOl: TDM mole ratio = 8:2).

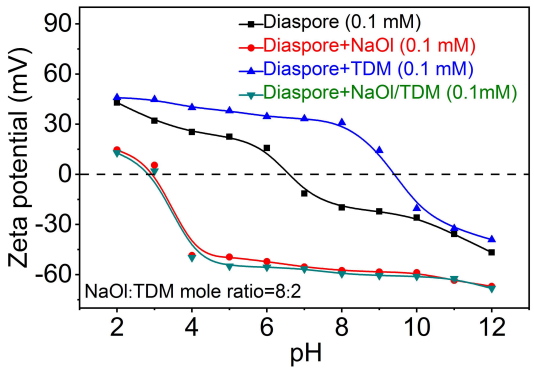

FIGURE 8 | Zeta potentials of diaspore in the presence of various flotation reagents.

TABLE 1 | CMCs and related properties of NaOl, TDM, and NaOl/TDM.

Surfactants	CMC(mmol/l)	The lowest surface tension(mN/m)	Micellization free energy (kJ/mol)
NaOl	1	25.71	−22.82
TDM	8	45.51	−17.67
NaOl/TDM	0.8	25.09	−23.37

surface tension of TDM is the largest, so its hydrophobicity is the weakest. This also explains why flotation recovery of TDM is poor when it is used as single collector. The CMC of mixed NaOl/TDM collector is slightly smaller than that of NaOl. Therefore, NaOl/TDM is more hydrophobic than that of NaOl, which also explains why the flotation effect of mixed collector NaOl/TDM is better than that of NaOl. The free energy of micellization can be calculated from the CMC using Eq where R is the gas constant and T is the absolute temperature, with T set to 298.15 K when unknown (Butt et al., 2003).

$$\Delta G_m = \mathrm{RTlnCMC}$$

The free energy of micellization can reflect the strength of the hydrophobic association of surfactants. Generally, the lower the free energy of micellization of surfactants is, the stronger the hydrophobic association is Fan et al. (2015). The order of micellization free energy is TDM > NaOl > NaOl/TDM. The micellization free energy of mixed collector NaOl/TDM is the lowest, so its hydrophobic association and collecting ability is the strongest, which is consistent with the result of flotation.

Zeta Potential Determinations

Zeta potentials of diaspore and kaolinite mixed with NaOl, TDM and NaOl/TDM collectors are shown in **Figures 8**, **9**. **Figures 8**, **9** show that the IEP (isoelectric point) of diaspore and kaolinite obtained are ∼6.6 and 3.2, respectively, which matches well with the previous reports (Guan et al., 2009; Liu et al., 2011; Huang et al., 2014; Lyu et al., 2019).

Compared with the Zeta potentials of diaspore and kaolinite in water, the Zeta potentials of diaspore and kaolinite mixed

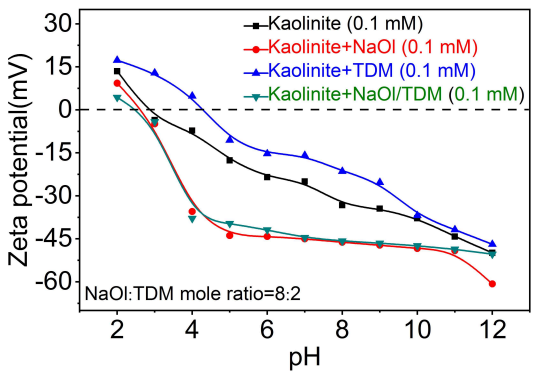

FIGURE 9 | Zeta potentials of diaspore in the presence of various flotation reagents.

with single collector NaOl are shifted negatively, which indicates that NaOl is adsorbed on the surface of diaspore and kaolinite. Because NaOl has stronger adsorption and affinity to diaspore than kaolinite, the negative shift of Zeta potentials of diaspore is larger than that of kaolinite. The Zeta potentials of diaspore and kaolinite mixed with single collector TDM are moved in the positive direction, which indicates that TDM is adsorbed on the surface of minerals. However, the Zeta potential shift of diaspore and kaolinite in the presence of TDM is smaller than that of NaOl, which indicates that the adsorption of TDM on mineral surface is less than that of NaOl. This is consistent with the conclusion of flotation. The Zeta potentials of diaspore in NaOl/TDM mixed collector are slightly negatively shifted from those in NaOl solution, indicating that the addition of TDM can enhance the change of potentials. Unlike diaspore, the Zeta potentials of kaolinite in NaOl/TDM mixed collector are shifted slightly positively than those in NaOl solution, which indicates that the addition of TDM does not enhance the negative movement of Zeta potentials of kaolinite.

From **Figure 8**, we found that Zeta potential change of mineral surface is very small in the presence of NaOl and NaOl/TDM, which indicates that the change of Zeta potentials

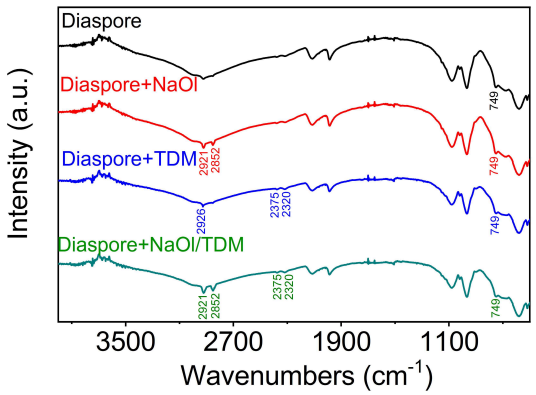

FIGURE 10 | FTIR spectra of diaspore in different collectors (NaOl: TDM mole ratio = 8:2).

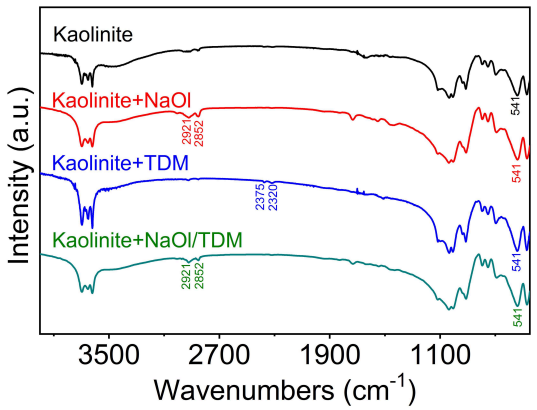

FIGURE 11 | FTIR spectra of kaolinite in different collectors (NaOl: TDM mole ratio = 8:2).

on mineral surface by mixed collector is limited, compared with NaOl. This may be due to the fact that TDM only accounts for 20% of the molar fraction of mixed collector, resulting in a limited increase in the amount of adsorption on the mineral surface. However, the addition of TDM can properly promote the adsorption of collector on diaspore surface and weaken the adsorption on kaolinite surface, so the selectivity of NaOl/TDM mixed collector is better than that of single NaOl collector.

FTIR Spectra Analysis

In the infrared spectrum of NaOl, 2,957, 2,921, and 2,852 cm^{-1} are the stretching vibration absorption peaks of $-CH_2$ in the hydrocarbon chain. The peak at 1,560 cm^{-1} belongs to the -COOC- asymmetric vibration. The peaks at 1,463 and 1,379 cm^{-1} are attributed to the symmetric stretching vibration of -COOC- (Wen et al., 2008; Wang et al., 2014). In the infrared spectrum of TDM, 2,926 and 2,852 cm^{-1} are the stretching vibration band of $-CH_3$, 2,375 and 2,320 cm^{-1} are the -SH stretching vibration absorption peaks in sulfhydryl group. And spectra has bending vibration band of $-CH_3$ and $=CH_2$ in 1,560 and 1,463 cm^{-1} (Jiao et al., 2016). The FTIR spectra of NaOl and TDM are shown in **Supplementary Material**.

Figures 10, **11** show the FTIR spectra of diaspore and kaolinite, which were in the presence of different collectors. It can be seen in **Figure 10** that after the NaOl treatment, obvious $-CH_2$ stretching vibration absorption peaks appear at 2,921 and 2,852 cm^{-1}, which indicates that NaOl is adsorbed on the surface of diaspore. However, the Al-O stretching vibration peak at 749 cm^{-1} does not show obvious band shift, which indicates that NaOl is not adsorbed on the mineral surface by the chemical action of the Al atom site, but by physical adsorption. This is similar to the results of other scholars (Xia et al., 2009; Xu et al., 2014). Under the action of TDM, -SH stretching vibration absorption peaks appear at 2,375 and 2,320 cm^{-1}. And stretching vibration band of $-CH_3$ in 2,926 cm^{-1} appears. However, no band shift is observed, so it is presumed that TDM is physically adsorbed on the surface of diaspore. After the NaOl/TDM treatment, the appearance of -SH stretching vibration peaks (2,375 and 2,320 cm^{-1}) indicates that TDM is adsorbed on the surface of diaspore. The appearance of $-CH_3$ stretching vibration peak (2,921 and 2,852 cm^{-1}) indicates that NaOl is also adsorbed on the mineral surface. Compared with the infrared spectra of diaspore treated by NaOl, the peak intensities treated by NaOl/TDM are strengthened, which indicates that diaspore treated by NaOl/TDM mixed collector has stronger adsorption. This is consistent with the conclusion of Zeta potential test.

As shown in **Figure 11**, the weak absorption vibration peaks of $-CH_3$ appear at 2,921 and 2,852 cm^{-1} after the interaction between NaOl and kaolinite. No obvious band shift is found, which indicates that NaOl is also adsorbed on the mineral surface by physical action (Elbokl and Detellier, 2006; Xia et al., 2009). However, from the intensity of absorption peaks, its adsorptive effect is not as strong as that of NaOl on diaspore surface. A weak characteristic absorption peak of TDM appears in the infrared spectra of kaolinite treated by TDM, but the band shift is not observed, indicating that TDM is physically adsorbed on the mineral surface. After the treatment of NaOl/TDM, the characteristic peaks of NaOl show that it is adsorbed on the mineral surface, but no adsorption of TDM is found. It may be that the adsorption of TDM is weak, so the adsorption effect is not obvious at low concentration. Compared with the infrared spectra of kaolinite treated by NaOl, the peak intensities treated by NaOl/TDM are weakened, which indicates that diaspore treated by NaOl/TDM mixed collector has weaker adsorption. This is consistent with the flotation test results, which further proves that the mixed NaOl/TDM can effectively separate diaspore and kaolinite.

CONCLUSION

In this work, tert dodecyl mercaptan (TDM) is first proposed as a mixed collector with NaOl for diaspore flotation. It is

proved that the selective separation of diaspore and kaolinite can be effectively achieved by using mixed collector of NaOl and TDM (NaOl: TDM mole ratio = 8:2, dosage = 0.1 mM) at pH = 9. Compared with single collector NaOl or TDM, mixed collector NaOl/TDM has stronger hydrophobic association and surface activity. Mixed collector NaOl/TDM can co-adsorb on diaspore through physical adsorption, and the adsorption strength of diaspore surface is greater than that of kaolinite with NaOl/TDM mixed collector. The addition of TDM can enhance the adsorption strength of NaOl on diaspore. And TDM also adsorbs on the surface of diaspore, thus forming a synergistic adsorption between TDM and NaOl. For kaolinite, TDM has almost no adsorption on its surface when mixed collector NaOl/TDM treats together. These experimental results show that the addition of TDM can promote the flotation separation of diaspore from kaolinite by NaOl. Mixed collector NaOl/TDM can achieve better separation of diaspore and kaolinite.

DATA AVAILABILITY STATEMENT

All datasets generated for this study are included in the article/**Supplementary Material**.

AUTHOR CONTRIBUTIONS

XMan, LO, and CW conceived the research, designed the tests, and analyzed the data, while XMan, SJ, and XMa wrote and revised the manuscript.

FUNDING

This work was financially supported by the Fundamental Research Funds for the Central Universities of Central South University (No. 2018zzts225) and the Postgraduate Survey and Research Project of Central South University (No. 2018dcyj055).

ACKNOWLEDGMENTS

We thank LL, MW, DZ, KZ, SY, and JL for their help in suggestions for the article.

SUPPLEMENTARY MATERIAL

The Supplementary Material for this article can be found online at: https://www.frontiersin.org/articles/10.3389/fchem.2019.00813/full#supplementary-material

REFERENCES

Butt, H.-J., Graf, K., and Kappl, M. (2003). *Physics and Chemistry of Interfaces.* Wiley, 1379–1380. doi: 10.1080/10426914.2013.840916

Cao, X., Gao, J., Liu, R., and Zhu, Y. (2014). Beneficiation experiment on oleic acid flotation of bauxite ore collaborated with a new synergistic agent. *Metal Mine.* 458, 65–68.

Chen, J., Chen, Y. E., Wei, Z., and Liu, F. (2010). Bulk flotation of auriferous pyrite and arsenopyrite by using tertiary dodecyl mercaptan as collector in weak alkaline pulp. *Miner. Eng.* 23, 1070–1072. doi: 10.1016/j.mineng.2010.07.006

Chernyshova, I. V., Ponnurangam, S., and Somasundaran, P. (2011). Adsorption of fatty acids on iron (hydr)oxides from aqueous solutions. *Langmuir Acs J. Surf. Colloids* 27, 10007–10018. doi: 10.1021/la2017374

Deng, L., Wang, S., Zhong, H., and Liu, G. (2015). N-(6-(hydroxyamino)-6-oxohexyl) decanamide collector: flotation performance and adsorption mechanism to diaspore. *Appl. Surf. Sci.* 347, 79–87. doi: 10.1016/j.apsusc.2015.03.138

Deng, L., Wang, S., Zhong, H., and Liu, G. (2016). A novel surfactant 2-amino-6-decanamidohexanoic acid: flotation performance and adsorption mechanism to diaspore. *Miner. Eng.* 93, 16–23. doi: 10.1016/j.mineng.2016.04.002

Elbokl, T. A., and Detellier, C. (2006). Aluminosilicate nanohybrid materials. Intercalation of polystyrene in kaolinite. *J. Phys. Chem. Solids* 67, 950–955. doi: 10.1016/j.jpcs.2006.01.008

Fan, Y., Wei, S., Hu, Y., and Long, S. (2015). Cationic flotation of scheelite from calcite using quaternary ammonium salts as collector: adsorption behavior and mechanism. *Miner. Eng.* 81, 18–28. doi: 10.1016/j.mineng.2015.07.014

Gibson, B., Wonyen, D. G., and Chehreh Chelgani, S. (2017). A review of pretreatment of diasporic bauxite ores by flotation separation. *Miner. Eng.* 114, 64–73. doi: 10.1016/j.mineng.2017.09.009

Guan, F., Zhong, H., Liu, G. Y., Zhao, S. G., and Xia, L. Y. (2009). Flotation of aluminosilicate minerals using alkylguanidine collectors. *Trans. Nonferrous Metals Soc. China* 19, 228–234. doi: 10.1016/S1003-6326(08)60257-5

Hong, Z., Liu, G., Xia, L., Lu, Y., Hu, Y., Zhao, S., et al. (2008). Flotation separation of diaspore from kaolinite, pyrophyllite and illite using three cationic collectors. *Miner. Eng.* 21, 1055–1061. doi: 10.1016/j.mineng.2008.05.007

Hu, Y., Sun, W., Jiang, H., Miller, J. D., and Fa, K. (2005). The anomalous behavior of kaolinite flotation with dodecyl amine collector as explained from crystal structure considerations. *Int. J. Miner. Process.* 76, 163–172. doi: 10.1016/j.minpro.2004.12.009

Huang, G., Zhou, C., and Liu, J. (2012). Effects of different factors during the desilication of diaspore by direct flotation. *Int. J. Mining Sci. Technol.* 22, 341–344. doi: 10.1016/j.ijmst.2012.04.010

Huang, Z., Hong, Z., Shuai, W., Xia, L., Gang, Z., and Liu, G. (2014). Gemini trisiloxane surfactant: synthesis and flotation of aluminosilicate minerals. *Miner. Eng.* 56, 145–154. doi: 10.1016/j.mineng.2013.11.006

Jarek, E., Jasinski, T., Barzyk, W., and Warszynski, P. (2010). The pH regulated surface activity of alkanoic acids. *Colloids Surf. Physicochem. Eng. Asp.* 354, 188–196. doi: 10.1016/j.colsurfa.2009.09.041

Jiang, H., Sun, Z., Xu, L., Hu, Y., Huang, K., and Zhu, S. (2014). A comparison study of the flotation and adsorption behaviors of diaspore and kaolinite with quaternary ammonium collectors. *Miner. Eng.* 65, 124–129. doi: 10.1016/j.mineng.2014.05.023

Jiang, Y.-R., Li., X.-X, Feng, R., Chen, D., and Li, J.-C. (2012). Novel alkyl bis(hydroxycarbamoyl) propionic acids for flotation separation of diaspore against aluminosilicate minerals. *Sep. Purif. Technol.* 87, 135–141. doi: 10.1016/j.seppur.2011.11.036

Jiang, Y. R., Li, W., and Feng, R. (2011). Preparation and performance of 4-alkyl-4,4-bis(hydroxycarbamoyl) carboxylic acid for flotation separation of diaspore against aluminosilicates. *Miner. Eng.* 24, 1571–1579. doi: 10.1016/j.mineng.2011.08.008

Jiang, Y. R., Yin, Z. G., Yi, Y. L., and Zhou, X. H. (2010a). Synthesis and collecting properties of novel carboxyl hydroxamic acids for diaspore and aluminosilicate minerals. *Miner. Eng.* 23, 830–832. doi: 10.1016/j.mineng.2010.05.016

Jiang, Y. R., Zhao, B. N., Zhou, X. H., and Zhou, L. Y. (2010b). Flotation of diaspore and aluminosilicate minerals applying novel carboxyl hydroxamic acids as collector. *Hydrometallurgy* 104, 112–118. doi: 10.1016/j.hydromet.2010.05.006

Jiao, F., Wu, J., Qin, W., Wang, X., and Liu, R. (2016). Interactions of tert dodecyl mercaptan with sphalerite and effects on its flotation behavior. *Colloids Surf. Physicochem. Eng. Asp.* 506, 104–113. doi: 10.1016/j.colsurfa.2016.05.095

Jing, L., Wang, X., Lin, C. L., and Miller, J. D. (2015). Significance of particle aggregation in the reverse flotation of kaolinite from bauxite ore. *Miner. Eng.* 78, 58–65. doi: 10.1016/j.mineng.2015.04.009

Kongolo, K., Kipoka, M., Minanga, K., and Mpoyo, M. (2003). Improving the efficiency of oxide copper–cobalt ores flotation by combination of sulphidisers. *Miner. Eng.* 16, 1023–1026. doi: 10.1016/S0892-6875(03)00263-2

Liang, S., Zhu, J., Liu, L., and Wang, H. (2017). Flotation of fine kaolinite using dodecylamine chloride/fatty acids mixture as collector. *Powder Technol.* 312, 159–165. doi: 10.1016/j.powtec.2017.02.032

Liu, C., Hu, Y., Feng, A., Guo, Z., and Cao, X. (2011). The behavior of N,N-dipropyl dodecyl amine as a collector in the flotation of kaolinite and diaspore. *Miner. Eng.* 24, 737–740. doi: 10.1016/j.mineng.2011.01.002

Liu, G., Zhong, H., Hu, Y., Zhao, S., and Xia, L. (2007). The role of cationic polyacrylamide in the reverse flotation of diasporic bauxite. *Miner. Eng.* 20, 1191–1199. doi: 10.1016/j.mineng.2007.05.003

Lyu, F., Gao, J., Sun, N., Liu, R., Sun, X., Cao, X., et al. (2019). Utilisation of propyl gallate as a novel selective collector for diaspore flotation. *Miner. Eng.* 131, 66–72. doi: 10.1016/j.mineng.2018.11.002

Wang, L., Sun, W., Hu, Y. H., and Xu, L. H. (2014). Adsorption mechanism of mixed anionic/cationic collectors in Muscovite – Quartz flotation system. *Miner. Eng.* 64, 44–50. doi: 10.1016/j.mineng.2014.03.021

Wang, Y., Feng, Y., Zhang, Q., Lu, D., and Hu, Y. (2017). Flotation separation of diaspore from aluminosilicates using commercial oleic acids of different iodine values. *Int. J. Miner. Process.* 168, 95–101. doi: 10.1016/j.minpro.2017.09.013

Wen, X., Yang, J., He, B., and Gu, Z. (2008). Preparation of monodisperse magnetite nanoparticles under mild conditions. *Curr. Appl. Phys.* 8, 535–541. doi: 10.1016/j.cap.2007.09.003

Xia, L., Hong, Z., Liu, G., Huang, Z., and Chang, Q. (2009). Flotation separation of the aluminosilicates from diaspore by a Gemini cationic collector. *Int. J. Miner. Process.* 92, 74–83. doi: 10.1016/j.minpro.2009.02.012

Xu, L., Hu, Y., Dong, F., Gao, Z., Wu, H., and Wang, Z. (2014). Anisotropic adsorption of oleate on diaspore and kaolinite crystals: implications for their flotation separation. *Appl. Surf. Sci.* 321, 331–338. doi: 10.1016/j.apsusc.2014.10.042

Yuehua, H., Wei, S., Haipu, L., and Xu, Z. (2004). Role of macromolecules in kaolinite flotation. *Miner. Eng.* 17, 1017–1022. doi: 10.1016/j.mineng.2004.04.012

Zhang, N., Ejtemaei, M., Nguyen, A. V., and Zhou, C. (2019). XPS analysis of the surface chemistry of sulfuric acid-treated kaolinite and diaspore minerals with flotation reagents. *Miner. Eng.* 136, 1–7. doi: 10.1016/j.mineng.2019.03.002

Zhang, N., Nguyen, A. V., and Zhou, C. (2018a). Impact of interfacial Al- and Si-active sites on the electrokinetic properties, surfactant adsorption and floatability of diaspore and kaolinite minerals. *Miner. Eng.* 122, 258–266. doi: 10.1016/j.mineng.2018.04.002

Zhang, N., Nguyen, A. V., and Zhou, C. (2018b). A review of the surface features and properties, surfactant adsorption and floatability of four key minerals of diasporic bauxite resources. *Adv. Colloid Interface Sci.* 254, 56. doi: 10.1016/j.cis.2018.03.005

Zhang, N., Zhou, C., Cong, L., Cao, W., and Zhou, Y. (2016). Semi-industrial experimental study on bauxite separation using a cell-column integration process. *Int. J. Miner. Metallurgy Mater.* 23, 7–15. doi: 10.1007/s12613-016-1205-4

Zhang, N.-N., Zhou, C.-C., Liu, C., Pan, J.-H., Tang, M.-C., Cao, S.-S., et al. (2017a). Effects of particle size on flotation parameters in the separation of diaspore and kaolinite. *Powder Technol.* 317, 253–263. doi: 10.1016/j.powtec.2017.04.049

Zhang, N. N., Zhou, C. C., Pan, J. H., Xia, W., Liu, C., Tang, M. C., et al. (2017b). The response of diasporic-bauxite flotation to particle size based on flotation kinetic study and neural network simulation. *Powder Technol.* 318, 272–281. doi: 10.1016/j.powtec.2017.06.010

Conflict of Interest: The authors declare that the research was conducted in the absence of any commercial or financial relationships that could be construed as a potential conflict of interest.

The handling editor declared a shared affiliation, though no other collaboration, with the authors LO, XMan, CW, SJ, and XMa at time of review.

frontiers in Chemistry

ORIGINAL RESEARCH
published: 24 December 2019
doi: 10.3389/fchem.2019.00886

Selectivity of Benzyl Hydroxamic Acid in the Flotation of Ilmenite

Lixia Li[1], *Chen Zhang*[1]*, *Zhitao Yuan*[1], *Zhichao Liu*[2] *and Chunfeng Li*[2]

[1] School of Resources and Civil Engineering, Northeastern University, Shenyang, China, [2] Beijing Research Institute of Chemical Engineering and Metallurgy, CNNC, Beijing, China

The decreased ground size of ilmenite-bearing ores challenges the selectivity of collectors of ilmenite. Taking advantage of flotation tests and density functional theory (DFT), the selectivity of benzyl hydroxamic acid (BHA) and the adsorption mechanism of oleate and BHA on ilmenite were systematically investigated. The flotation tests showed that BHA had good selectivity to ilmenite. In the DFT study, the favorable adsorption of BHA and oleate on the ilmenite surface were verified by the Mulliken population and the calculated interaction energies. Results indicated that the covalent bonds caused the adsorption of oleate on the ilmenite surface. The strong selectivity of BHA was due to abundant adsorption sites and solid adsorption of five-membered rings. The present investigation has important implications for further studies of BHA and will be helpful for screening and designing collectors for ilmenite flotation.

Keywords: ilmenite, benzyl hydroxamic acid, selectivity, density functional theory, flotation

OPEN ACCESS

Edited by:
Zhiyong Gao,
Central South University, China

Reviewed by:
Sugata Chowdhury,
National Institute of Standards and Technology (NIST), United States
Shuai Wang,
Central South University, China

***Correspondence:**
Chen Zhang
zc9303@126.com

Specialty section:
This article was submitted to Physical Chemistry and Chemical Physics, a section of the journal Frontiers in Chemistry

Received: *13 July 2019*
Accepted: *09 December 2019*
Published: *24 December 2019*

Citation:
Li L, Zhang C, Yuan Z, Liu Z and Li C (2019) Selectivity of Benzyl Hydroxamic Acid in the Flotation of Ilmenite. Front. Chem. 7:886. doi: 10.3389/fchem.2019.00886

INTRODUCTION

For the beneficiation of ilmenite-bearing ores, a hybrid beneficiation method of low-intensity magnetic separation (LIMS) for magnetite removal and high-intensity magnetic separation (HIMS) for ilmenite pre-concentration followed by flotation for ilmenite upgrade, is commonly commercialized. With the continuous exploitation of ilmenite-bearing ores in China, the mined resources exhibit lean, fine, and miscellaneous. In order to liberate valuable minerals to a higher degree, fine grinding is applied, which is challenging the selectivity of collectors to ilmenite in the flotation section.

As an anionic collector, benzyl hydroxamic acid (BHA) has been increasingly brought attention to the field of mineral processing in the flotation of tungsten, iron, and rare earth minerals (Bulatovic and Wyslouzil, 1999) owing to its good selectivity. Investigations also showed that BHA as a collector can effectively separate ilmenite from associated gangue minerals, especially fine particles of ilmenite disseminated in the gangue minerals (Belardi et al., 1998; Li et al., 2016).

Many researchers have used hydroxamic acid as a collector to separate different minerals by flotation. Ren et al. (1997) used naphthyl hydroxamic acid for the flotation of bastnaesite. The flotation results showed that the naphthyl hydroxamic acid had good selectivity on the bastnaesite with regards to chemisorption. Sreenivas and Padmanabhan (2002) studied the floatability and adsorption characteristics of BHA on cassiterite. The results showed that the adsorption capacity of cassiterite for octyl hydroxamic acid was greatest under acidic conditions. The optimal slurry pH also changed greatly as the carbon chain of hydroxamic acid increased and the cassiterite particle size decreased. Beyond that, the cyclohexyl hydroxamic acid (Zhao et al., 2013) and octyl hydroxamic (Meng et al., 2015) were employed in the flotation of scheelite flotation and fine wolframite flotation. Novel carboxyl hydroxamic acids (Jiang et al., 2010) were also be designed

and used for the flotation of aluminosilicate minerals. In the field of titanium minerals flotation, relevant studies have used hydroxamic acid as a collector (Buckley and Parker, 2013; Meng et al., 2015; Somasundaran, 2018; Chen et al., 2019). It can be seen that various forms of hydroxamic acid are attracting interest in mineral processing due to their unique properties.

During the flotation process, collectors can anchor on the mineral surface as a medium between mineral and air bubbles (Rao and Forssberg, 1991). In the present flotation of ilmenite ore, fatty acids and their modified products commonly serve as collectors industrially. BHA has been proving as a potential alternative to fatty acids due to its good selectivity to ilmenite (Bulatovic and Wyslouzil, 1999), and experiments demonstrate that the flotation performance of BHA is significantly better than that of oleate (shown in section Flotation Results). In view of this phenomenon, based on the mechanism of the collector, two hypotheses have been advanced: that BHA has more adsorption sites on ilmenite surfaces than that of oleate; and that the bond between BHA and the ilmenite surface is more solid than for oleate. Density functional theory (DFT) was applied to energy calculation and bond analysis to provide a quantitative comparison (Li et al., 2019).

DFT is able to reveal the reaction mechanisms that are difficult to explain by current experimental techniques at the atomic level (Pradip et al., 2002). It has been widely used (Kwon and Kubicki, 2004; Blanchard et al., 2012) to investigate properties of molecules and minerals surface as well as the interaction of adsorbent on the adsorbate. The properties of molecular, interaction energies, and Mulliken population analysis give a vivid characterization to the sorption mechanism and provide deep insight into the separation process from the aspects of physical and chemical (Rath et al., 2014). In our previous study, the mechanism of depression of hematite and the adsorption mechanism of oleate on siderite were investigated using DFT (Pradip et al., 2002; Li et al., 2018, 2019; Zhang et al., 2019, 2020).

The aim of this paper was to identify the adsorption configuration of BHA and oleate on the surface of ilmenite, using flotation tests to testify the selectivity of oleate and BHA, and applying DFT to demonstrate the adsorption mechanism. First, flotation tests were conducted at optimal conditions for BHA and sodium oleate, respectively, and the grade and recovery of ilmenite concentrate were compared. Second, the exposed surface of the ilmenite crystal was determined based on the calculation of surface energy. Finally, different models of oleate and BHA were built and screened. The models with the lowest adsorption energy were calculated to analyze the mechanism of adsorption.

MATERIALS AND METHODOLOGY

Experimental Materials

The fine ilmenite sample involved in this study was a classifier overflow materials in a titanium beneficiation plant of Panzhihua Iron & Steel Group Co. in China, with a particle size of −0.038 mm passing 86.18% and TiO_2 grade of 8.89%. After treated by a LIMS and a superconducting magnetic separator, it was upgraded to 17.01% of TiO_2. This concentrate was collected, dried, homogenized, and sampled to perform flotation experiments.

BHA and sodium oleate were used as collectors. In order to prepare the solution of sodium oleate, 50 mg of sodium oleate was put into a 500 mL beaker placed in an ultrasonic dispersion machine. Then the dispersed solution was transferred into a 1 L volumetric flask with deionized water to a final concentration of 50 mg/L. The same procedure was followed to prepare a BHA solution with a concentration of 50 mg/L. All experiments were carried out at room temperature. Lead nitrate $Pb(NO_3)_2$ had an analytical purity and was adopted as an activator, and the frother terpenic oil was commercially pure.

Flotation Experiments

An XFG flotation machine with 1 L flotation cell was used for the flotation experiments with a stirring rate of 1,800 rpm. With BHA and sodium oleate as a collector separately, experimental optimizations with parameters of slurry pH, dosages of reagents, and flotation time, have been implemented. In each experiment, 300 g of samples were added in 700 mL of water to stir for 3 min. Sulfuric acid (H_2SO_4) or hydroxide sodium (NaOH) was employed to adjust slurry pH from 4 to 12.

In the case of BHA, after pH adjustment, activator, collector, and frother were added in sequence and conditioned for 3, 5, and 1 min correspondingly. After that, the flotation test was carried out, and the froth was scrapped off every 10 s. While in the case of sodium oleate, collector, and frother were added into the slurry after pH adjustment at the same time intervals to those of BHA. When flotation completed, both floated and sunk fractions were dried in an oven at 60°C, and then weighed and chemically analyzed.

As a result, suitable flotation conditions with BHA for ilmenite were determined as pH of 7.0, $PbNO_3$ of 200 g/t, BHA of 1,300g/t, frother of 60 g/t and flotation time of 5 min. While for sodium oleate, optimized flotation conditions were pH of 4.5, sodium oleate of 1,500g/t, 40 g/t of frother and flotation time of 5 min.

Models for Ilmenite Crystal

The crystal optimization convergence tests of exchange-correlation potentials, k-point, and cutoff energy were carried out to get the optimum ilmenite crystal geometry. The exchange-correlation potentials of generalized gradient approximation (GGA) convergence test included GGA-RPBE, GGA-WC, GGA-PBE, GGA-PBESOL, and GGA-PW91. The convergence criteria of max. displacement = 0.002 Å, energy = 2.0×10^{-5} eV, max. stress = 0.1 GPa, and max. force = 0.05 eV/Å. The lattice parameters of ilmenite from the literature and experimental values were referred to ensure the suitability of optimized ilmenite crystal (Wechsler and Prewitt, 1984). In this study, the CASTEP module in Materials Studio was employed for all calculations.

Based on the results of these convergence tests, the cutoff energy of 300 eV, exchange-correlation potential of GGA-PW91 and k-point set $6 \times 6 \times 2$ were selected with the energy −22717.6637 eV and the parameter difference 1.4%, which confirmed the suitability of parameter selection for accurate calculations. **Figure 1** shows the optimum ilmenite crystal.

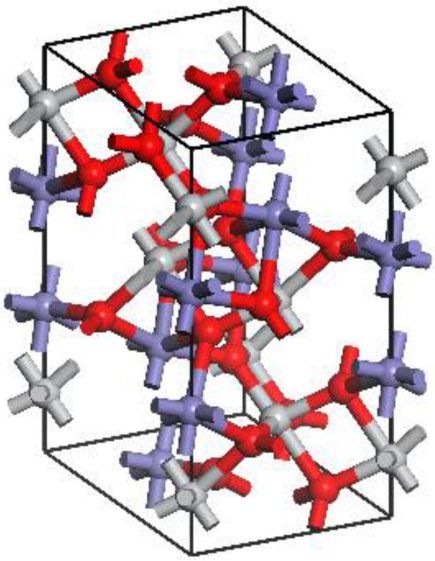

FIGURE 1 | Optimum ilmenite crystal. The red spheres represent O atoms, the gray represents Ti atoms, and the blue represents Fe atoms.

Models for the Ilmenite Surface

To get the most likely exposed crystal surface of ilmenite, the surface energy calculation was conducted. Surface energy was a thermodynamic stability measurement of an exposed crystalline surface. The smaller surface energy corresponds to a more stable surface structure (Lavina et al., 2009). In this study, the Equation (1) was used to calculate the surface energy (Hu et al., 2012).

$$E_{surf} = \frac{E_{slab} - \left(\frac{N_{slab}}{N_{bulk}}\right) \cdot E_{bulk}}{2A} \quad (1)$$

where E_{bulk} and E_{slab} are the bulk unit cell and the total energy of the slab, respectively; N_{bulk} is the number contained in each bulk unit cell and N_{slab} is the number of atoms in ilmenite slab; unit area of the surface was represented by A and the factor of 2 represents the two surfaces in the surface slab that are perpendicular to the z-axis.

In this study, the ilmenite crystal surfaces (1 0 4), (1 1 0), (1 1 −6), (0 1 2), (0 2 4), and (3 0 0) were selected for comparison with the most readily existing crystal surfaces, according to the XRD results. The selected crystal surface was then used to establish the model of ilmenite with reagents.

Models of Reagents

The representative of modeled conditions to experimental flotation conditions has been considered. Slurry pH determines the predominant functional groups of reagents. As abovementioned, with sodium oleate as a collector, the optimized flotation pH for ilmenite samples was 4.5, while for BHA it was 7.0. Well-known that the predominant group for sodium oleate at pH of 4.5 is oleate molecule, for BHA and $Pb(NO_3)_2$ at pH of 7.0, BHA molecule and $Pb(OH)^+$ are dominant species.

TABLE 1 | Flotation results of BHA and oleate.

Collector	Product	Yield/%	TiO_2 grade/%	TiO_2 recovery/%
BHA	Concentrate	16.38	39.25	37.79
	Tailings	83.62	12.65	62.21
	Feed	100.00	17.01	100.00
Oleate	Concentrate	32.95	28.42	55.06
	Tailings	67.05	11.40	44.94
	Feed	100.00	17.01	100.00

TABLE 2 | Surface energies of different ilmenite surfaces.

Crystal surface	E_{bulk}/eV	E_{slab}/eV	A/Å^2	E_{surf}/J·m^{-2}
(1 0 4)	−22717.650	−22711.667	94.25	0.509
(1 1 0)	−22717.650	−22704.376	92.57	1.149

In this study, the surface of ilmenite was the adsorbent and the BHA, oleate, and $Pb(OH)^+$ were adsorbates. The Visualizer module was employed to design the oleate, BHA and $Pb(OH)^+$ molecular structures. Before adsorption modeling, geometric optimizations of the oleate, BHA and $Pb(OH)^+$ molecular structures were conducted using the CASTEP module.

RESULTS AND DISCUSSION

Flotation Results

Using BHA and oleate as collectors, flotation tests were performed at their optimal conditions. Flotation performances in terms of grade and recovery of ilmenite are presented in **Table 1**.

As can be seen from **Table 1**, BHA enriched the TiO_2 grade from 17.01% of the feed to 39.25% of the concentrate which was higher than 28.42% obtained with oleate. In contrast, BHA displayed relatively poor floatability for ilmenite, i.e., with oleate as collector the recovery of TiO_2 in concentrate was 55.06%, which was higher than that of 37.79% with BHA. The results show that BHA has good selectivity to ilmenite and oleate has good floatability to ilmenite.

Selected Ilmenite Surfaces

The dominant crystal face of ilmenite was determined by surface energy. The crystal morphology is dominated by the crystal surfaces with a slow-growing rate, meanwhile, a slower growth rate means that a surface has lower surface energy, while fast-growing faces with higher surface energy may disappear (Prywer, 2001). Ilmenite surfaces (1 0 4), (1 1 0), (1 1 −6), (0 1 2), (0 2 4), and (3 0 0) were modeled as a six-layer slab with a vacuum thickness of 25 Å, and the most stable crystal surfaces were determined based on the calculated surface energies as shown in **Table 2**.

The calculation process for surfaces (1 1 −6), (0 1 2), (0 2 4), and (3 0 0) did not converge, which indicated that the types of atom exposed on the crystal surfaces were unlikely to exist, while the surfaces (1 0 4) with surface energy of 0.509 J·m^{-2} and (1 1 0) with 1.149 J·m^{-2} converged to a stable surface slab. The surface

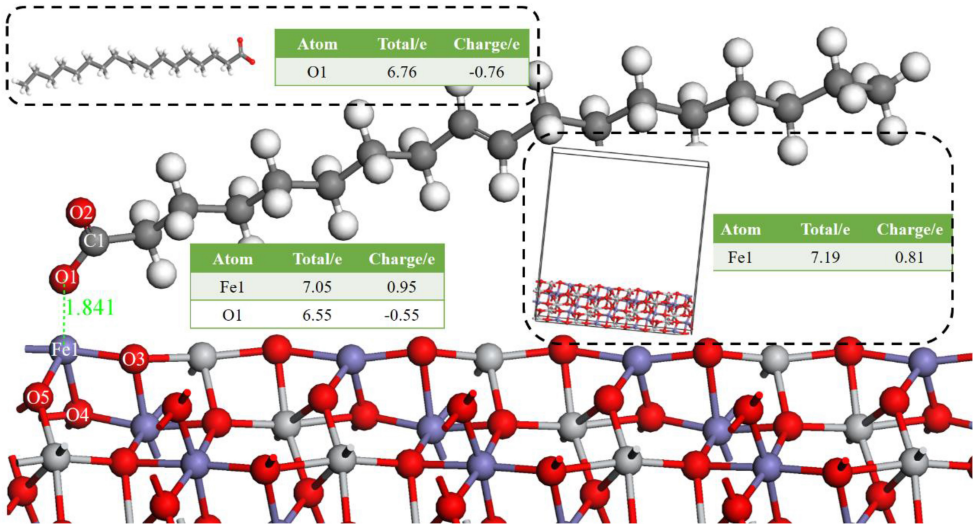

FIGURE 2 | The optimal bond of oleate on an ilmenite (1 0 4) surface, the red ball is O, the blue ball is Fe, the light gray ball is Ti, the dark gray ball is C, and the white ball is H.

energy of (1 0 4) was lower than that of (1 1 0), which implied that the surface (1 0 4) would more likely exist. Therefore, the surface (1 0 4) was adopted in the subsequent calculations to establish the mineral-reagent models.

Models for Mineral-Reagent Complex

Models of oleate and BHA on ilmenite surface were built and calculated to reveal the greater selectivity of BHA as compared with oleate. Bond strength was revealed by the adsorption energy and Mulliken bonds population. The adsorption energy (ΔE_{ads}) of reagents and optimized ilmenite (1 0 4) were quantified by Equation (2) (Hu et al., 2012):

$$\Delta E_{ads} = E_{complex} - (E_{adsorbate} + E_{mineral}) \quad (2)$$

where $E_{complex}$ is the energy of optimized ilmenite-reagent complex, $E_{adsorbate}$ refers to the total energy of the reagents and $E_{mineral}$ is the total energy of the ilmenite crystal surface. A greater (negative) magnitude of ΔE implies a stronger interaction between the mineral surface and reagent.

Mulliken population analysis was conducted to specify the bond types between adsorbent and adsorbate. The Mulliken bond population is positive for a covalent bond, and the covalent bonding becomes stronger with the increase of Mulliken population. Similarly, a negative bond population indicates antibond.

Models for Ilmenite-Oleate Complex

Figure 2 shows the apparent interaction of oleate with the atoms on ilmenite surface. The adsorption energy (Equation 2) of oleate on the surface of ilmenite was −146.501kJ/mol, which demonstrated that the oleate adsorbed on the ilmenite surface with a distance of 1.841Å between the Fe1 and O1 atoms. Mulliken population analysis was conducted to discern the bond type of oleate on ilmenite. The bond populations are listed in **Table 3**.

TABLE 3 | Mulliken population of adsorption configuration of oleate on ilmenite.

Atom	Bond	Bond population	Bond length/Å
Fe1	O1-Fe1	0.42	1.840
	O5-Fe1	0.25	1.880
	O3-Fe1	0.31	1.893
O1	O3-O1	−0.01	2.830
	C1-O1	0.74	1.340

As shown in **Table 3**, the bond population of O1-Fe1 was 0.42, indicating that a covalent bond was generated between the Fe1 on the ilmenite surface and O1 of oleate. The bond population of O1-Fe1 was lower than that of C1-O1 in oleate (0.74), yet higher than O5-Fe1 (0.25) and O3-Fe1 (0.31) in the ilmenite crystal, indicating that the interaction between the atoms of Fe and O was strong enough to trigger the adsorption of oleate on the ilmenite surface. The atom population in **Figure 2** demonstrates that the charge of O1 and Fe1 are −0.76 e and 0.81 e before the adsorption of oleate on ilmenite surface. After a series reaction, the oleate absorbed on the surface of ilmenite. The total charge of O1 changed from −0.76 e to −0.55 e with 0.21 e lose of charge. Meanwhile, the charge of Fe1 went from 0.81 e to 0.95 e, which manifests the electron transfer existed between O1 and Fe1 atom, which contributed to the formation of covalent bonds.

Models for Ilmenite—$Pb(OH)^+$—BHA Complex

In the flotation of ilmenite with BHA, the activator lead nitrate is usually added before the collector BHA. Therefore, the adsorption of $Pb(OH)^+$ on the ilmenite surface was calculated first. The different models of $Pb(OH)^+$ are shown in **Figure 3**.

During building the models of $Pb(OH)^+$ on the ilmenite surface, $Pb(OH)^+$ was placed on the top of Fe, Ti, and O atoms of the ilmenite surface to find the best adsorption site. The adsorption energy of $Pb(OH)^+$ on the ilmenite surface was

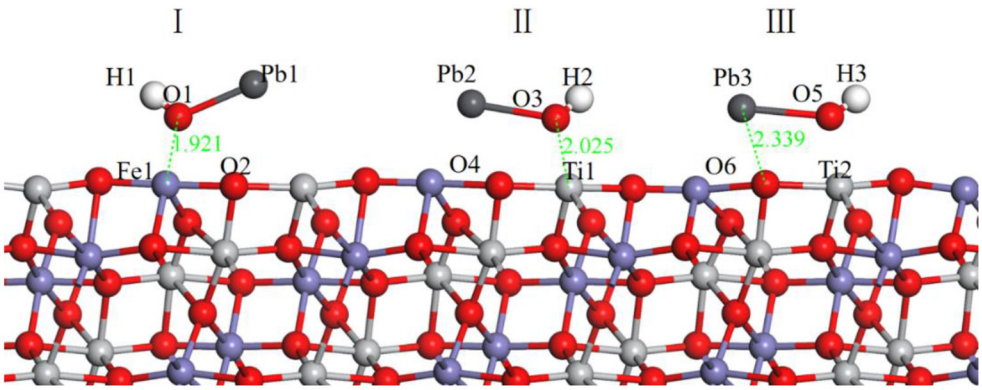

FIGURE 3 | Models of $Pb(OH)^+$ on ilmenite surface, (I) represents the $Pb(OH)^+$ on the top of Fe atom, (II) represents the $Pb(OH)^+$ on the top of Ti atom, (III) represents the $Pb(OH)^+$ on the top of O atom. The black ball is Pb.

TABLE 4 | Mulliken population of adsorption configuration of $Pb(OH)^+$ on the ilmenite surface.

$Pb(OH)^+$	Bond	Bond population	Bond length/Å
I	Fe1-O1	0.22	1.921
	O1-O2	−0.06	2.520
II	Ti1-O3	0.31	2.025
	O3-O4	−0.05	2.593
III	Ti2-O5	0.22	2.000
	O6-O5	−0.04	2.686

TABLE 5 | Atom population of $Pb(OH)^+$ on the ilmenite surface.

Atom	Status	Total/e	Charge/e
Fe1	Before adsorption	7.19	0.81
	After adsorption	7.05	0.95
O1	Before adsorption	6.66	−0.66
	After adsorption	6.58	−0.58

calculated as −16.916 kJ/mol. **Figure 3** shows that all of the $Pb(OH)^+$ was adsorbed on the ilmenite surface. **Table 4** shows the bond population of $Pb(OH)^+$.

As shown in **Table 4**, the atoms of Fe and Ti on the ilmenite surface interacted with O of $Pb(OH)^+$ with bond populations of 0.22, 0.31, and 0.22, respectively. This confirmed that the $Pb(OH)^+$ adsorbed on the ilmenite surface by covalent bonding, and that adsorption sites were abundant.

Table 5 exhibits the atom population of Fe1 and O1 before and after the adsorption of $Pb(OH)^+$.

Known from **Table 5**, both Fe1 and O1 atoms have obvious electron transfer during the reaction, and 0.14 e and 0.08 e removed from Fe1 and O1 atom, respectively, which supplement the interaction between O in $Pb(OH)^+$ and Fe in the ilmenite surface.

Having identified the adsorption of $Pb(OH)^+$, the interaction between BHA and the ilmenite surface $Pb(OH)^+$-functioned was calculated to detect the selectivity of BHA. The optimized model is shown in **Figure 4**.

As shown in **Figure 4**, BHA adsorbed on ilmenite surface via the interaction between the Pb atom of $Pb(OH)^+$ and the O atom of BHA. Pb^{2+} and the O atoms formed a five-membered ring, and this interaction was stronger than that of oleate with ilmenite. The adsorption energy was determined as −101.1528 kJ/mol and the bond population analysis indicated that the BHA adsorbed on the three sites of the ilmenite surface. The five-membered ring and the abundant adsorption sites lead to the good selectivity of BHA. From the atom population analysis, the charge of Pb1 went from 0.29 to 1.08, and the two O of BHA also had obvious charge transfer which confirmed the interaction among the two O of BHA and Pb of activated ilmenite surface.

Based on the results and discussion, both oleate and BHA could adsorb on the ilmenite surface. Covalent bonds formed between Fe of ilmenite surface and the O of oleate. Due to the activation of $Pb(OH)^+$, there were more adsorption sites of ilmenite for BHA (Meng et al., 2018; Ozsváth et al., 2019). And five-membered rings formed among lead species and BHA, which improved the selectivity of BHA.

CONCLUSION

This study highlighted the good selectivity of BHA for ilmenite. Flotation tests were performed to discover the difference in selectivity between BHA and oleate, and the DFT calculation of the reagent-ilmenite complexes was adopted to elucidate the mechanism of the good selectivity of BHA at the atomic level.

Flotation tests showed that the selectivity of BHA was better than that of oleate. DFT calculation suggested that both oleate and BHA adsorbed on the ilmenite surface. BHA had more adsorption sites on ilmenite surfaces, as it formed five-membered rings through the O atoms of BHA and Pb^{2+} of the activator. Abundant adsorption sites and solid adsorption of five-membered rings contribute to the good selectivity of BHA.

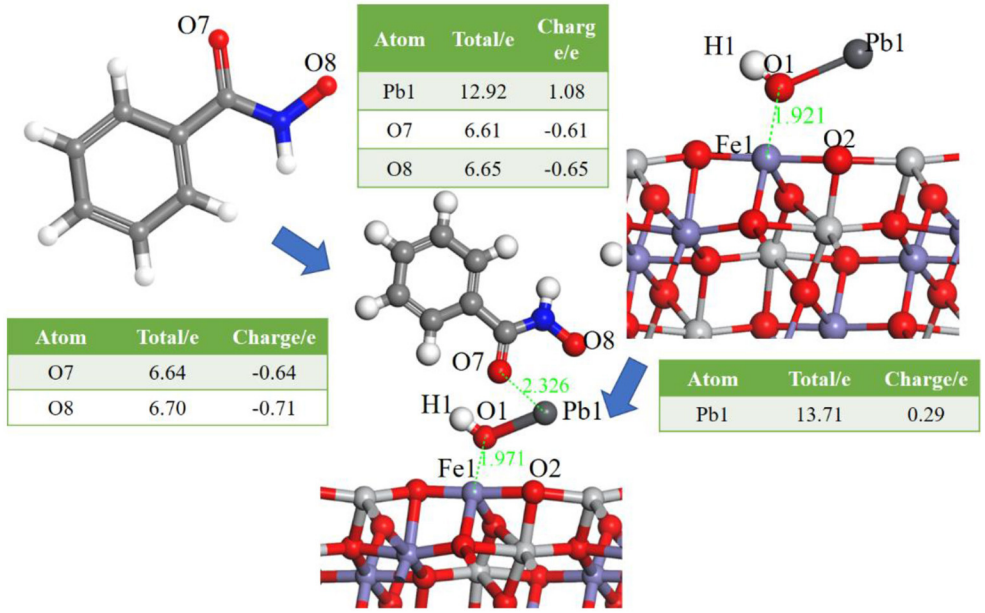

FIGURE 4 | Models of BHA on the $Pb(OH)^{+}$-functioned ilmenite surface, the Table is the atom population before and after the adsorption of BHA.

The present investigation offers insight into the good selectivity of BHA, providing a reference for designing and screening flotation reagents for ilmenite flotation.

DATA AVAILABILITY STATEMENT

The datasets generated for this study are available on request to the corresponding author.

AUTHOR CONTRIBUTIONS

During investigation and paper writing, all authors participated in their assigned tasks. LL carried out flotation experiments, drafted the flotation tests, and analyzed DFT calculation results with CZ, who performed the DFT calculation and wrote the paragraphs of DFT calculation. ZY was responsible for designing the experimental scheme and outlining the manuscript structure. ZL and CL repeated flotation tests using BHA and contributed to the interpretations of flotation results and the revision of whole manuscript.

FUNDING

This study was supported by the National Natural Science Foundation of China (No. 51574061), the Fundamental Research Funds for the Central Universities (N180106005), and the Open Foundation of State Key Laboratory of Mineral Processing (No. BGRIMM-KJSKL-2019-01).

ACKNOWLEDGMENTS

We would like to express our gratitude to editors and reviewers for their diligent work.

REFERENCES

Belardi, G., Piga, L., Quaresima, S., and Shehu, N. (1998). Application of physical separation methods for the upgrading of titanium dioxide contained in a fine waste. *Int. J. Miner. Process.* 53, 145–156. doi: 10.1016/S0301-7516(97)00076-8

Blanchard, M., Morin, G., Lazzeri, M., Balan, E., and Dabo, I. (2012). First-principles simulation of arsenate adsorption on the (1 1 2) surface of hematite. *Geochim. Cosmochim. Acta* 86, 182–195. doi: 10.1016/j.gca.2012.03.013

Buckley, A. N., and Parker, G. K. (2013). Adsorption of n-octanohydroxamate collector on iron oxides. *Int. J. Miner. Process.* 121, 70–89. doi: 10.1016/j.minpro.2013.03.004

Bulatovic, S., and Wyslouzil, D. (1999). Process development for treatment of complex perovskite, ilmenite and rutile ores. *Miner. Eng.* 12, 1407–1417. doi: 10.1016/S0892-6875(99)00130-2

Chen, W., Chen, F. F., Bu, X. Z., Zhang, G. F., Zhang, C. H., and Song, Y. H. (2019). A significant improvement of fine scheelite flotation through rheological control of flotation pulp by using garnet. *Miner. Eng.* 138, 257–266. doi: 10.1016/j.mineng.2019.05001

Hu, Y., Gao, Z., Sun, W., and Liu, X. (2012). Anisotropic surface energies and adsorption behaviors of scheelite crystal. *Colloids Surf. A Physicochem. Eng. Aspects* 415, 439–448. doi: 10.1016/j.colsurfa.2012.09.038

Jiang, Y.-R., Zhao, B.-N., Zhou, X.-H., and Zhou, L.-Y. (2010). Flotation of diaspore and aluminosilicate minerals applying novel carboxyl hydroxamic acids as collector. *Hydrometallurgy* 104, 112–118. doi: 10.1016/j.hydromet.2010.05.006

Kwon, K. D., and Kubicki, J. D. (2004). Molecular orbital theory study on surface complex structures of phosphates to iron hydroxides: calculation of vibrational frequencies and adsorption energies. *Langmuir* 20, 9249–9254. doi: 10.1021/la0487444

Lavina, B., Dera, P., Downs, R. T., Prakapenka, V., Rivers, M., Sutton, S., et al. (2009). Siderite at lower mantle conditions and the effects of the pressure-induced spin-pairing transition. *Geophys. Res. Lett.* 36. doi: 10.1029/2009GL039652

Li, F., Zhong, H., Zhao, G., Wang, S., and Liu, G. (2016). Adsorption of α-hydroxyoctyl phosphonic acid to ilmenite/water interface and its application in flotation. *Colloids Surf. A Physicochem. Eng. Aspects* 490, 67–73. doi: 10.1016/j.colsurfa.2015.11.015

Li, L., Zhang, C., Yuan, Z., Hao, H., and Zhao, C. (2018). Density functional theory and atomic force microscopy study of oleate functioned on siderite surface. *Minerals*. 8:33. doi: 10.3390/min8010033

Li, L., Zhang, C., Yuan, Z., Xu, X., and Song, Z. (2019). AFM and DFT study of depression of hematite in oleate-starch-hematite flotation system. *Appl. Surf. Sci.* 480, 749–758. doi: 10.1016/j.apsusc.2019.02.224

Meng, Q., Feng, Q., Shi, Q., and Ou, L. (2015). Studies on interaction mechanism of fine wolframite with octyl hydroxamic acid. *Miner. Eng.* 79, 133–138. doi: 10.1016/j.mineng.2015.05.015

Meng, Q., Yuan, Z., Yu, L., Xu, Y., and Du, Y. (2018). Study on the activation mechanism of lead ions in the flotation of ilmenite using benzyl hydroxamic acid as collector. *J. Indus. Eng. Chem*. 62, 209–216. doi: 10.1016/j.jiec.2017.12.059

Ozsváth, A., Farkas, E., Diószegi, R., and Buglyó, P. (2019). Versatility and trends in the interaction between Pd (ii) and peptide hydroxamic acids. *N. J. Chem*. 43, 8239–8249. doi: 10.1039/C9NJ00296K

Pradip, P., Rai, B., Rao, T., Krishnamurthy, S., Vetrivel, R., Mielczarski, J., et al. (2002). Molecular modeling of interactions of diphosphonic acid based surfactants with calcium minerals. *Langmuir* 18, 932–940. doi: 10.1021/la010625q

Prywer, J. (2001). Effect of crystal geometry on disappearance of slow-growing faces. *J. Cryst. Growth* 224, 134–144. doi: 10.1016/S0022-0248(01)00798-9

Rao, K. H., and Forssberg, K. (1991). Mechanism of fatty acid adsorption in salt-type mineral flotation. *Miner. Eng.* 4, 879–890. doi: 10.1016/0892-6875(91)90071-3

Rath, S. S., Sinha, N., Sahoo, H., Das, B., and Mishra, B. K. (2014). Molecular modeling studies of oleate adsorption on iron oxides. *Appl. Surf. Sci.* 295, 115–122. doi: 10.1016/j.apsusc.2014.01.014

Ren, J., Lu, S., Song, S., and Niu, J. (1997). A new collector for rare earth mineral flotation. *Miner. Eng.* 10, 1395–1404. doi: 10.1016/S0892-6875(97)00129-5

Somasundaran, P. (2018). *Reagents in Mineral Technology*. Routledge.

Sreenivas, T., and Padmanabhan, N. (2002). Surface chemistry and flotation of cassiterite with alkyl hydroxamates. *Colloids Surf. A Physicochem. Eng. Aspects* 205, 47–59. doi: 10.1016/S0927-7757(01)01146-3

Wechsler, B. A., and Prewitt, C. T. (1984). Crystal structure of ilmenite (FeTiO3) at high temperature and at high pressure. *Am. Mineral*. 69, 176–185.

Zhang, C., Li, L., Yuan, Z., Xu, X., Song, Z., and Zhang, Y. (2019). Probing the effect of particle imperfections on the sliming of siderite in carbonate-bearing iron ore. *Miner. Eng.* 143:106014. doi: 10.1016/j.mineng.2019.106014

Zhang, C., Li, L., Yuan, Z., Xu, X., Song, Z., and Zhang, Y. (2020). Mechanical properties of siderite and hematite from DFT calculation. *Miner. Eng.* 146:106107. doi: 10.1016/j.mineng.2019.106107

Zhao, G., Zhong, H., Qiu, X., Wang, S., Gao, Y., Dai, Z., et al. (2013). The DFT study of cyclohexyl hydroxamic acid as a collector in scheelite flotation. *Miner. Eng.* 49, 54–60. doi: 10.1016/j.mineng.2013.04.025

Conflict of Interest: ZL and CL are employed by Beijing Research Institute of Chemicals Engineering and Metallurgy, CNNC.

The remaining authors declare that the research was conducted in the absence of any commercial or financial relationships that could be construed as a potential conflict of interest.

frontiers in Materials

ORIGINAL RESEARCH
published: 18 February 2020
doi: 10.3389/fmats.2020.00035

Surface Electrical Behaviors of Apatite, Dolomite, Quartz, and Phosphate Ore

*Fang Zhou, Qi Liu, Xu Liu, Wanchun Li, Jian Feng and Ru-an Chi**

Key Laboratory for Green Chemical Process of Ministry of Education, Wuhan Institute of Technology, Wuhan, China

The phosphate ore flotation is achieved through the surface electrical behavior difference among apatite, dolomite and quartz, but it is usually affected by the dissolved ions from pulp, especially Ca^{2+} and Mg^{2+}. The zeta potentials of apatite, dolomite, quartz, and phosphate ore in different solutions were measured to discuss the surface electrical behaviors of them in this study. It was found that the apatite, dolomite and phosphate ore supernatants have limited impact on the zeta potentials of the respective surfaces themselves, but the surface electrical behaviors of apatite and dolomite in the supernatant of the other is similar to the supernatant mineral source. This will increase the separation difficulty of apatite from dolomite in the phosphate ore flotation process. The negative zeta potentials of apatite, dolomite, quartz and phosphate ore increase in the presence of Ca^{2+} and Mg^{2+}. Moreover, a more zeta potential increase in presence of Ca^{2+} than Mg^{2+} was investigated, suggesting a stronger influence of Ca^{2+} than Mg^{2+} on the surface electrical behaviors of ores.

Keywords: apatite, dolomite, quartz, phosphate ore, zeta potential

OPEN ACCESS

Edited by:
Zhiyong Gao,
Central South University, China

Reviewed by:
Hock Jin Quah,
University of Science Malaysia, Malaysia
Yuesheng Gao,
Michigan Technological University, United States

****Correspondence:***
Ru-an Chi
rac513@163.com

Specialty section:
This article was submitted to Colloidal Materials and Interfaces, a section of the journal Frontiers in Materials

Received: *07 September 2019*
Accepted: *30 January 2020*
Published: *18 February 2020*

Citation:
Zhou F, Liu Q, Liu X, Li W, Feng J and Chi R (2020) Surface Electrical Behaviors of Apatite, Dolomite, Quartz, and Phosphate Ore. Front. Mater. 7:35. doi: 10.3389/fmats.2020.00035

INTRODUCTION

Phosphorus is an important chemical raw material, and is also a primary constituent of plants. The industrial phosphorus is extracted from the phosphate ore to produce elemental phosphorus, phosphoric acid, phosphatic fertilizer and phosphate (Santana et al., 2011; Xiao et al., 2013). Phosphate ore is a significant mineral source of phosphorus, which is general floated to recover the phosphorus in the apatite minerals ($Ca_5(PO_4CO_3)_3(F, OH, Cl)$) (Zhou et al., 2017). However, most of the phosphate ore industry is currently focused on recovery of apatite from low-grade ores due to the decrease of high-grade phosphate ore. Flotation as the most important method is applied in phosphate ore processing to separate the valuable mineral of apatite from the gangue minerals, such as dolomite and quartz (Zhou et al., 2015). Mineral type and electrolyte environment will result in different surface electrical behaviors of different minerals, and even the same mineral (Alroudhan et al., 2016). Therefore, the investigation of those surface electrical behaviors, which influences interfacial process such as flotation, has obvious research significance. Apatite and dolomite belong to the group of salt-type minerals. It has thus been assumed that they have similar surface electrical behaviors due to the dissolved metal ions (Mishra, 1978; Hu and Wang, 1992). Metal ions in the bulk solution which can be adsorbed on the mineral surface by physical and/or chemical interaction exist in various forms, such as bonding to mineral lattice, generating metal

hydroxides, or carbonate hydroxides precipitated on mineral surface, producing new active center of beneficiation reagent, transferring mineral surface to improve or weaken the role of mineral processing reagents (Demir et al., 2003).

Dolomite can produce Ca^{2+} and Mg^{2+} ions into the pulp during the ore grinding and pulp-mixing processes (Amankonah et al., 1985; dos Santos et al., 2010; Li et al., 2017). The valuable mineral, apatite, in phosphate ore has the same lattice ion, Ca^{2+}, as dolomite, which results in a significant effect on the selective flotation of apatite from dolomite. In the real phosphate ore flotation process, different ions in the pulp change the surface electrical behavior of minerals and hence change the selective adsorption of beneficiation reagent on the mineral surface, which enlarges the difficulties in the selective separation of apatite from dolomite and quartz (Amankonah et al., 1985).

The surface electrical behaviors of apatite, dolomite, and quartz in mineral supernatants were discussed in this study. The surface electrical behaviors of apatite, dolomite and quartz in solutions with different Ca^{2+} and Mg^{2+} concentrations have also been studied to further confirm the effects of Ca^{2+} and Mg^{2+}. The comparison of surface electrical behaviors for phosphate ore in phosphate ore supernatants and in solutions containing Ca^{2+} and Mg^{2+} are conducted to explore the surface chemistry changes in phosphate ore flotation.

MATERIALS AND METHODS

Materials

Potassium chloride, calcium chloride, and magnesium chloride were used in reagent grade. Reagent grade hydrochloric acid and sodium hydroxide were used as pH modifiers.

The single minerals of apatite, dolomite and quartz were purchased from Canada Wards Natural Science Establishment Company, hand-crushed by a hammer, ground, and sieved to obtain particles with diameter smaller than 20 μm for zeta potential measurement. The phosphate ore from Yichang City, China, was ground by a Mortar Grinder (Fisher Scientific) to obtain the same size fractions as the single minerals for zeta potential measurement. All mineral samples prepared were analyzed by XRD shown in **Figure 1**. As seen in **Figure 1**, the XRD peaks of the tested apatite dolomite and quartz matched closely with that of the standard samples, confirming that the samples is mainly apatite, dolomite, and quartz, respectively. The phosphate ore sample is mainly fluorapatite.

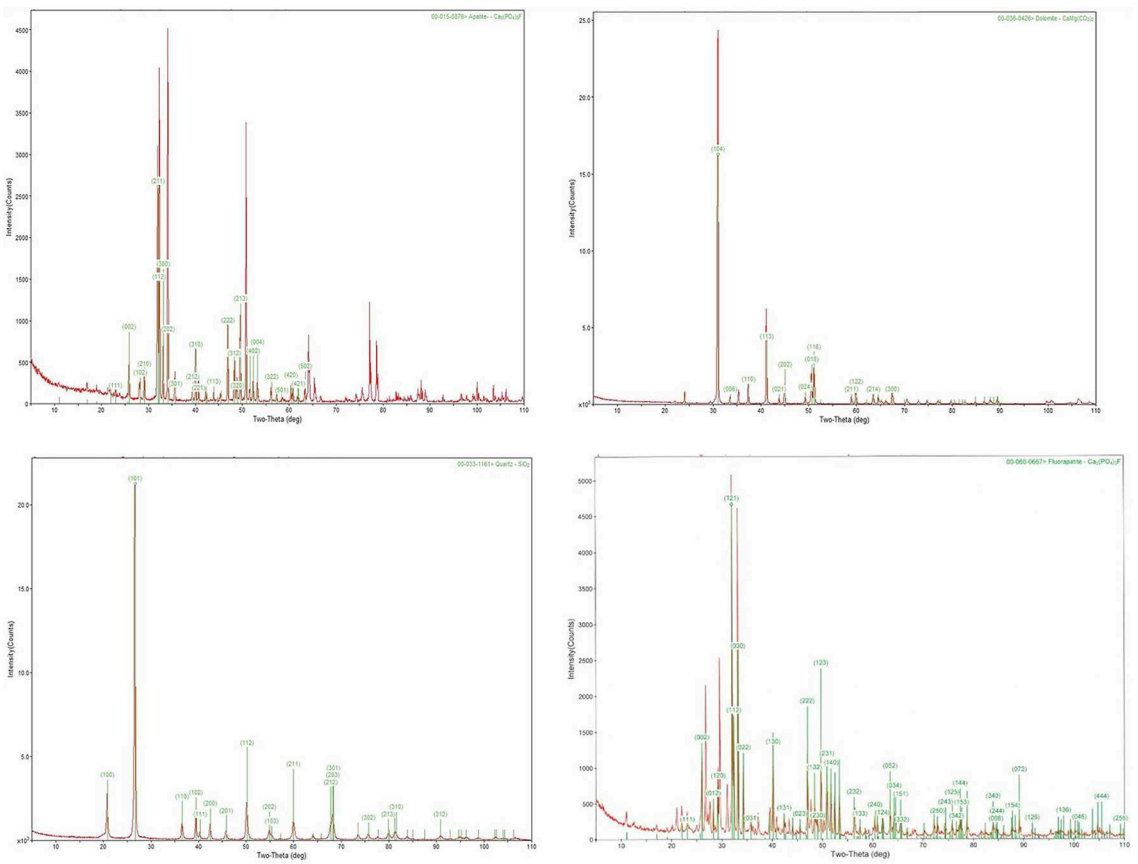

FIGURE 1 | XRD analysis of apatite, dolomite, quartz, and phosphate ore.

Methods

The mineral supernatants of apatite, dolomite, quartz, and phosphate ore were prepared by immersing the single mineral, respectively, in 10 mM KCl solutions for 48 h followed by suction filtration. The absence of mineral particles in the mineral supernatants was determined by an optical microscope. The ore samples were placed in the test solutions to prepare ore suspensions, which were hand-shaken for 2 min. After 10 min standing for mineral particles to reach equilibrium, the supernatant of the suspension was diluted by the test solutions, and then placed under an ultrasonic equipment HS2060A (Fisher Scientific) for 10 min. The detailed description can be found in the literature (Zhou et al., 2015). The obtained solutions were used for zeta potential measurement by Zetasize R-Malvern Nano-ZS. The measurements were repeated six times for the same suspension, and the average values as well as the standard deviations of a given ore sample were reported. All the experimental set-up was usually flushed by nitrogen gas to avoid the possible precipitation of calcium carbonate in the system and the formation of carbonate species on the ore surface (Amankonah et al., 1985). The measurement was conducted at ambient temperature of 22 ± 0.5°C.

RESULTS AND DISCUSSION

Zeta Potentials of Apatite, Dolomite, Quartz

Results obtained for the zeta potentials of apatite, dolomite, and quartz in 10 mM KCl solutions are given in **Figure 2**. The Zeta potentials of apatite, dolomite, and quartz decrease with the pH increasing among the tested pH range. Some literatures report that isoelectric point (IEP) value of apatite from different deposits changes from 2.0 to 8.0, and the dolomite is around 3.0–6.0, but they can shift in the presence of electrolyte (Yu et al., 1985; Merma et al., 2013; Kasha et al., 2015). Therefore, isoelectric points of apatite and dolomite in 10 mM KCl solutions are observed, but no isoelectric points of quartz are determined around the tested pH range from 3.1 to 10.2. In general, the zeta potential of apatite is larger than that of dolomite, and that of quartz is the most electrostatically charged among the three ores.

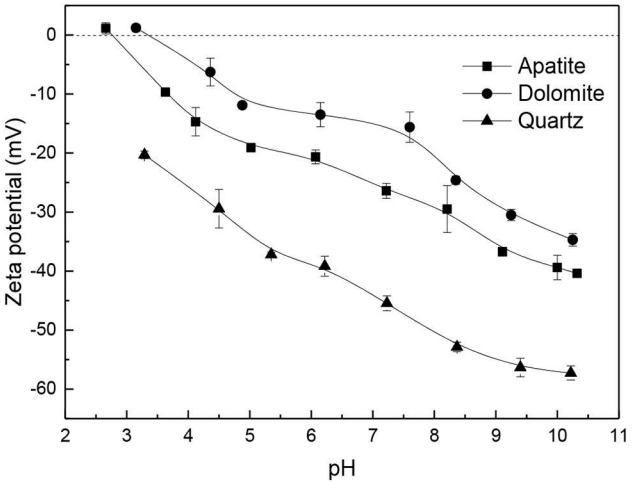

FIGURE 2 | Zeta potentials of apatite, dolomite, and quartz in 10 mM KCl solutions.

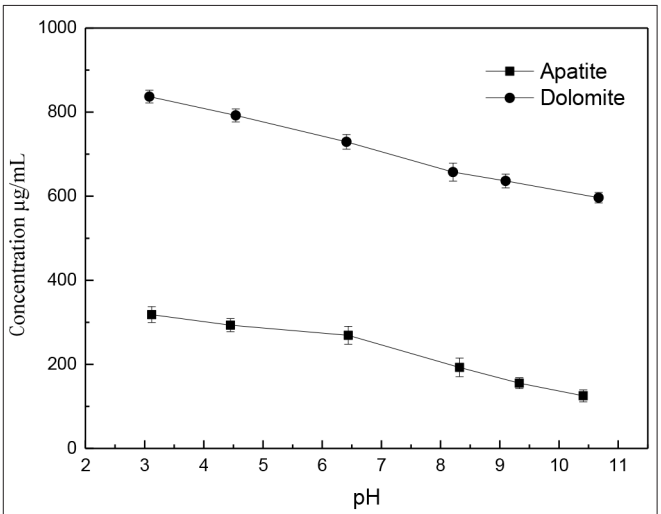

FIGURE 3 | Ca^{2+} concentration of dolomite and apatite in water as a function of pH.

Dissolution of Apatite and Dolomite

Apatite and dolomite are slightly soluble minerals, which can release the dissolved Ca^{2+} and Mg^{2+} to affect the surface electrical behaviors of minerals. Since the dissolution of apatite and dolomite can achieve equilibrium in 2 h according to the previous studies, the dissolved Ca^{2+} and Mg^{2+} contents as a function of pH were investigated with the two minerals soaked in different pH solutions for 2 h, respectively.

From **Figure 3**, the dissolved Ca^{2+} content in acid solutions is relatively high due to the carbonate and phosphate minerals reacting with hydrogen ions. But it decreases in alkaline environment, which is due to the precipitation of $Ca(OH)_2$. This phenomenon is similar to that of Mg^{2+} in **Figure 4**, where the dissolved Mg^{2+} from dolomite decreases with the solution pH increase. Furthermore, the dissolved Ca^{2+} from dolomite is more than that of apatite, which is consistent with literature (Amankonah et al., 1985). Amankonah et al. (1985) found that the dissolved Ca^{2+} from calcite is more than that of apatite when calcite and apatite are soaked in open water, closed water and 2 mM KNO_3 solution. Generally, the dissolved Ca^{2+} and Mg^{2+} will affect the surface electrical behavior of minerals in solution.

Surface Electrical Behavior of Apatite, Dolomite, and Quartz in Apatite Supernatants

Results obtained for the zeta potentials of apatite in apatite supernatants was compared to that of apatite in 10 mM KCl shown in **Figure 5A**. It can be seen that there was no marked difference in the zeta potential values because of the similar surfaces of apatite in the two solutions. The experimental dates

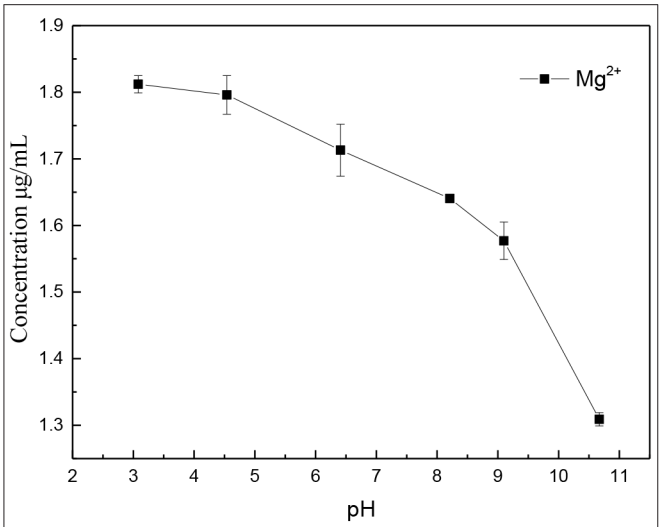

FIGURE 4 | Mg^{2+} concentration of dolomite in water as a function of pH.

suggest that the influence of dissolved ions from apatite on the degree of variation in zeta potential values of apatite can be ignored. No changes can be deduced, because the new surface formed by the dissolved ions precipitated and/or adsorbed on apatite surface is similar to the apatite surface in the absence of apatite supernatants. The dissolved ions just change the electrolyte solutions, and further the influence is tiny because of the low concentration.

For dolomite in apatite supernatants, it is interesting to find that there is no marked difference between the zeta potential-curve of dolomite in apatite supernatants and the zeta potential-curve of apatite, but both of them are distinct to the dolomite. This result is similar to the interaction of apatite and calcite reported by Somasundaran (Amankonah et al., 1985). The observations indicate that the dissolved ions from apatite change the surface of dolomite to become similar to the apatite surface due to the precipitation and adsorption of dissolved ions on the dolomite surface.

In **Figure 5C**, the zeta potential-curve of quartz in apatite supernatants shifts toward less negative zeta potential compared to the original values of quartz, suggesting that the zeta potentials of quartz increase at the same pH because of the dissolved positive ions from apatite. There may be two reasons. The one is that the dissolved ions change the electrolyte solutions due to the zeta potential depending on the electrolyte and the ionic concentration (Sze et al., 2003). The second is that the dissolved ions are adsorbed or precipitated on the quartz surface to form calcium phosphate or hydroxide so as to change its surface electrical behavior. However, the zeta potential for quartz in apatite supernatants is still distinct to that of apatite, indicating that the dissolved ions cannot transfer the quartz surface to the apatite surface, very different from its effects on the dolomite.

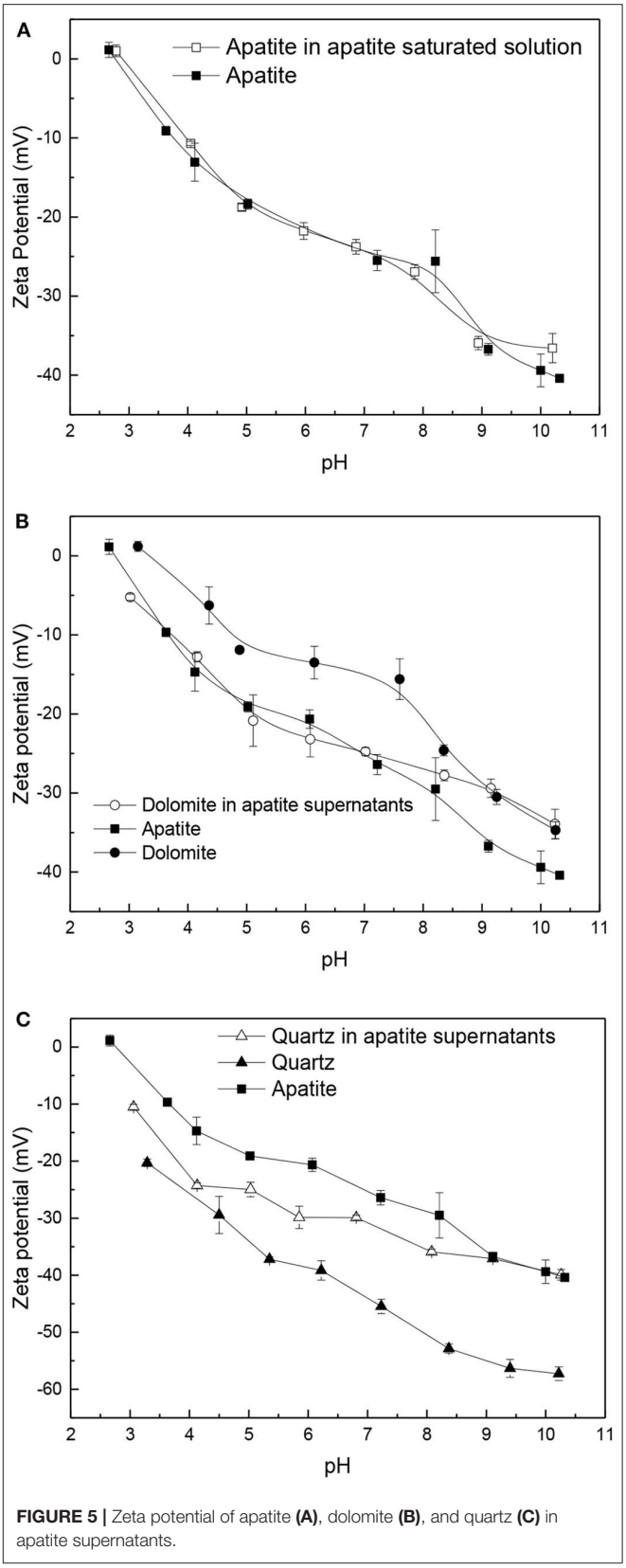

FIGURE 5 | Zeta potential of apatite **(A)**, dolomite **(B)**, and quartz **(C)** in apatite supernatants.

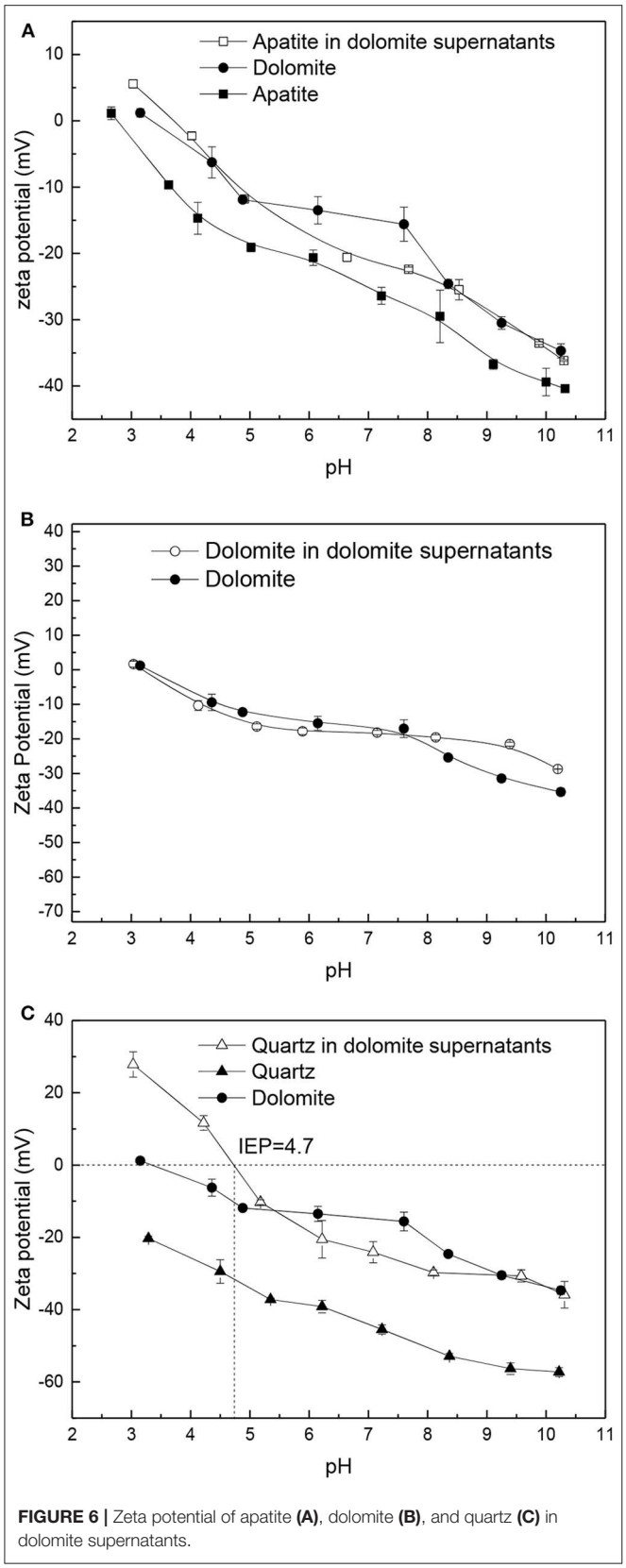

FIGURE 6 | Zeta potential of apatite **(A)**, dolomite **(B)**, and quartz **(C)** in dolomite supernatants.

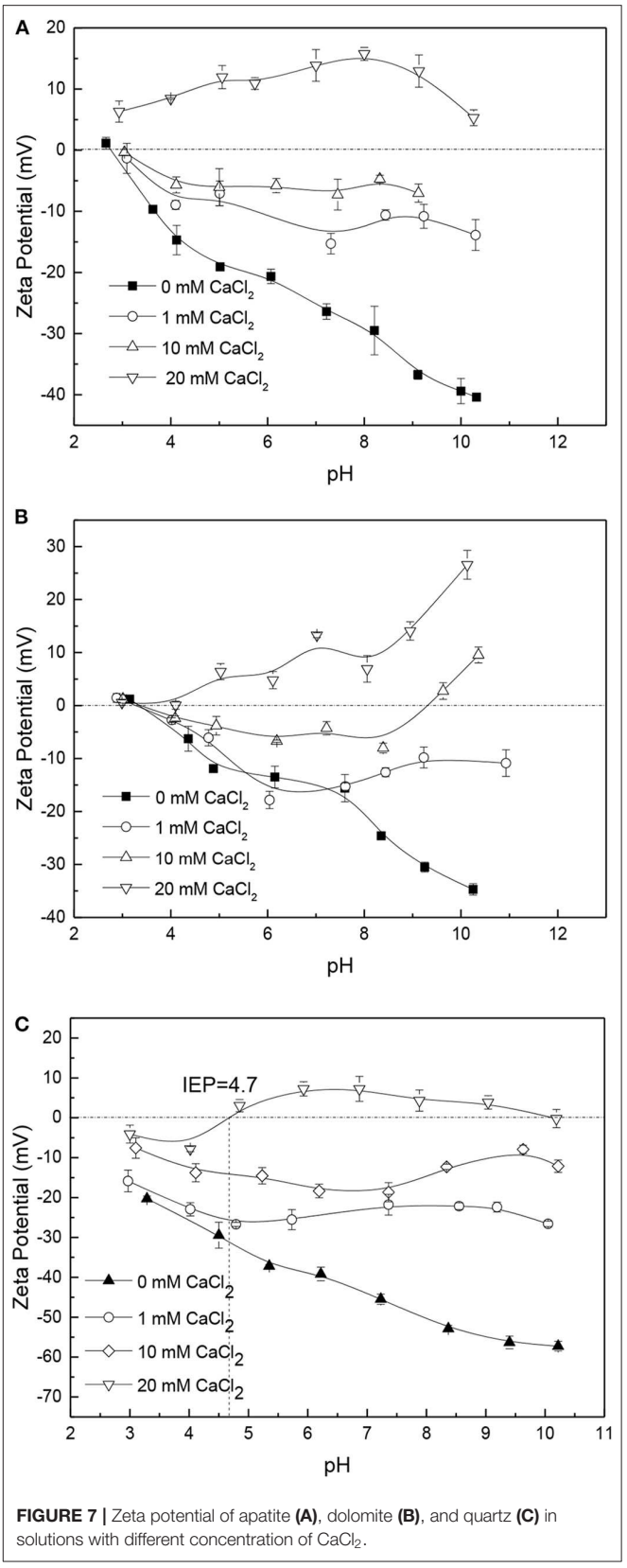

FIGURE 7 | Zeta potential of apatite **(A)**, dolomite **(B)**, and quartz **(C)** in solutions with different concentration of $CaCl_2$.

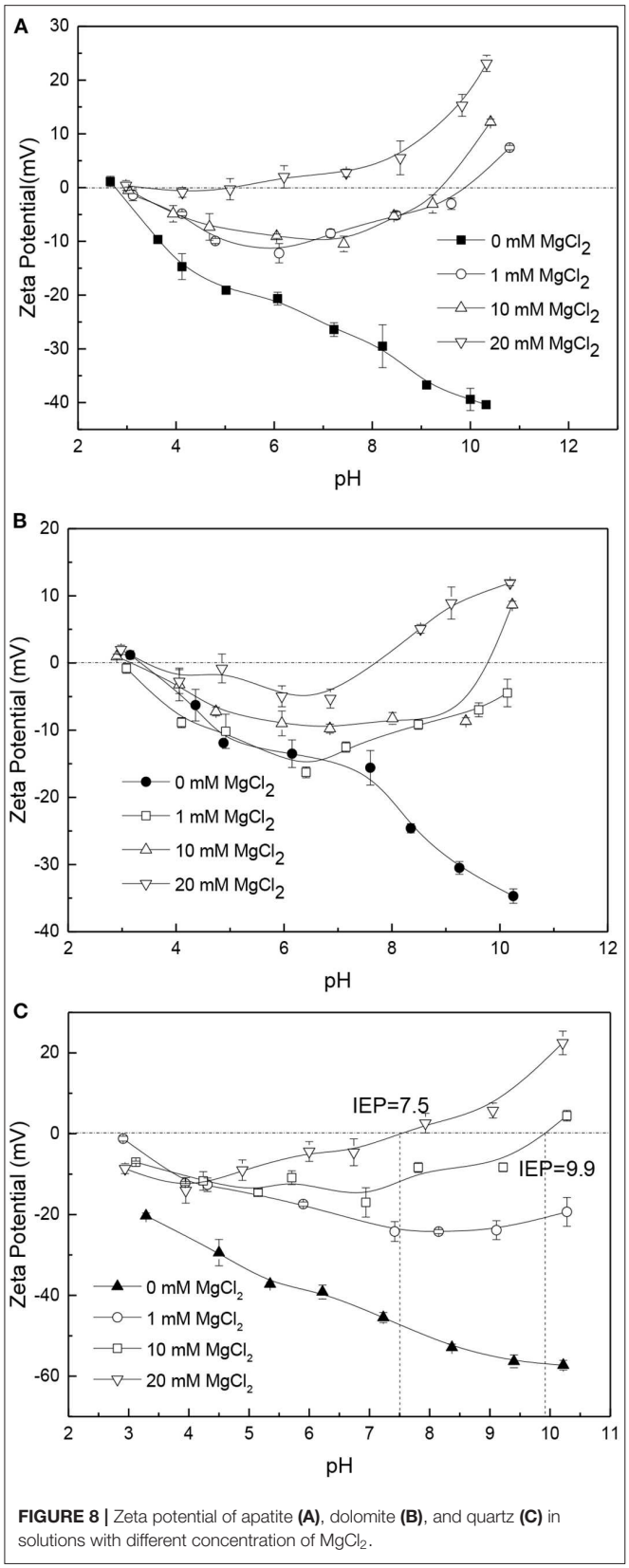

FIGURE 8 | Zeta potential of apatite **(A)**, dolomite **(B)**, and quartz **(C)** in solutions with different concentration of $MgCl_2$.

Surface Electrical Behavior of Apatite, Dolomite, and Quartz in Dolomite Supernatants

The results given in **Figure 6A** show the zeta potentials of apatite are increased by the dolomite supernatants, and move to the zeta potential-curve of dolomite, indicating the surface conversion of apatite to dolomite with the impact of dissolved ions from dolomite because the zeta potential increased with increase in ionic concentration of cations (Ozeki et al., 1989). This surface conversion from apatite to dolomite in dolomite supernatants is similar to the surface change from dolomite to apatite in apatite supernatants shown in **Figure 5B**. The zeta potentials of dolomite in dolomite supernatants are similar to that of dolomite over the entire pH range investigated shown in **Figure 6B**, indicating a less impact of the dissolved ions from dolomite on the zeta potential variation of dolomite. The results are similar to the effects of apatite supernatants on the surface electrical behavior of apatite in **Figure 5A**. The reason of the surface conversion for apatite and dolomite in the other supernatants may be the similar lattice cations of Ca^{2+} and Mg^{2+} for apatite and dolomite, which will adsorb on the surface of the minerals or form hydroxide precipitations. For quartz in dolomite supernatants shown in **Figure 6C**, the original negative zeta potential of quartz is increased and IEP at pH 4.7 is observed because of the increasing of dissolved ions from dolomite, which can be deduced they are divalent Ca^{2+} and Mg^{2+} ions due to the chemical component of dolomite, $CaMg(CO_3)_2$ (Pokrovsky et al., 1999).

Effects of Ca^{2+} on the Surface Electrical Behavior of Apatite, Dolomite, and Quartz

The effect of Ca^{2+} on the surface electrical behavior of apatite, dolomite and quartz is shown in **Figure 7**, respectively. Examination of the results shows that the zeta potentials of the three ores are more positively charged in solutions containing Ca^{2+} than in 10 mM KCl among the tested pH range, and the Ca^{2+} can alter the zeta potentials of these ores from negative to positive. The affinity between the Ca^{2+} and the zeta potentials of apatite, dolomite, and quartz is affected by the concentration of Ca^{2+}. The greater the concentration of Ca^{2+} is, the higher the zeta potentials of these ores in calcium chloride solution is. The increase in the zeta potential values resulting from the concentration of calcium ions could be attributed to the compression of the double layer under high ionic strength conditions (Amankonah et al., 1985). Furthermore, a high concentration of $CaCl_2$ can be expected to cause the precipitation such as calcium hydroxide on the surface of ores to produce more positive zeta-potential values.

Effects of Mg^{2+} on the Surface Electrical Behavior of Apatite, Dolomite, and Quartz

The effect of Mg^{2+} at different concentration on the surface electrical behaviors of apatite, dolomite, and quartz is shown in **Figure 8**. The Mg^{2+} causes the zeta potentials of these ores to be increased similar to the effect of Ca^{2+} among the tested pH

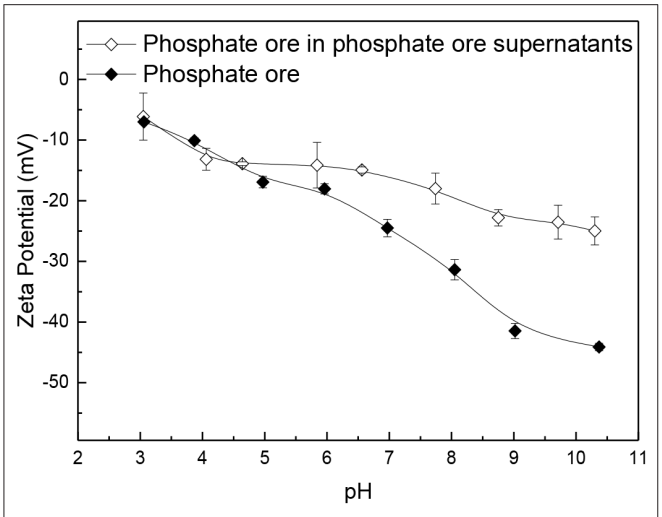

FIGURE 9 | Zeta potential of phosphate ore and phosphate ore in phosphate ore supernatants.

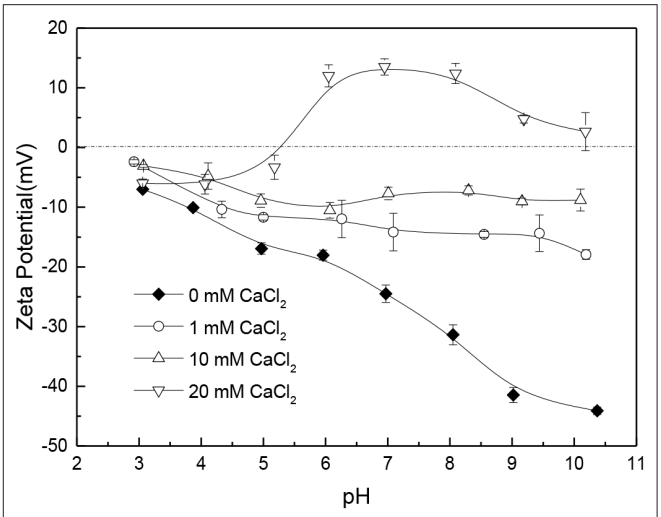

FIGURE 10 | Zeta potential of phosphate ore in solutions with different concentration of $CaCl_2$.

range. A higher concentration of Mg^{2+} has a greater impact on the surface electrical behaviors of apatite, dolomite and quartz. At a relative high concentration, 20 mM $MgCl_2$, the original negative zeta potentials of apatite, dolomite, and quartz change to be positive. The isoelectric points of these ores shift to a relatively small values. In the acidic solution, Mg^{2+} is in the form of positioning ion adsorbed on the surface of apatite and dolomite in the form of characteristic adion. Under the condition of high pH value, the adsorption of Mg^{2+} and OH^- may create precipitation on the surface of ores to produce more positive zeta potential values (Tang et al., 2010).

Electrokinetic Behavior of Phosphate Ore

Surface Electrical Behavior of Phosphate Ore in Phosphate Ore Supernatants

To understand the surface electrical behavior of phosphate ore, a phosphate rock from China was chosen to investigate the effects of its supernatants, Ca^{2+} and Mg^{2+}, on its zeta potentials which can affects interfacial process such as flotation. **Figure 9** shows the comparison of zeta potential-curves of phosphate ore and phosphate ore in phosphate ore supernatants. The two curves are basically coincident when pH < 6, but as pH increases, they separate gradually. In general, the zeta potential of phosphate ore in phosphate ore supernatants is greater than that of phosphate ore. The phosphate ore supernatants contain metal cations dissolved from phosphate ore. When pH > 8, these cations can attach and cause precipitation to the surface of phosphate ore to produce more positive zeta potential values.

Effects of Ca^{2+} on the Surface Electrical Behavior of Phosphate Ore

The effects of Ca^{2+} with different concentrations on the zeta potential of phosphate ore are shown in **Figure 10**. The results show that the zeta potentials of phosphate ore in 0 mM $CaCl_2$, 1 mM $CaCl_2$, and 10 mM $CaCl_2$ are negative over the entire pH range investigated. The isoelectric point of phosphate ore in 20 mM $CaCl_2$ is about 5.2. Data given in **Figure 10** for the zeta potential of phosphate ore in calcium chloride of several concentrations show that the Ca^{2+} has the same impact on the zeta potential of phosphate ore to the other three ores, apatite, dolomite, and quartz. The greater the concentration of Ca^{2+} is, the higher the zeta potential of phosphate ore in $CaCl_2$ solution is.

Effects of Mg^{2+} on the Surface Electrical Behavior of Phosphate Ore

Figure 11 shows the effects of Mg^{2+} on the zeta potential of phosphate ore. The original negative zeta potential of phosphate ore is increased in the presence of Mg^{2+}. The results suggest that the Mg^{2+} reveals the similar influence on the zeta potential of phosphate ore as Ca^{2+}. However, the Ca^{2+} shows a greater impact than the Mg^{2+} on the zeta potential of phosphate ore among the tested pH range according to the comparison of **Figures 10**, **11**. The isoelectric points of phosphate ore in 20 mM $MgCl_2$ solutions, is about 6.6, but the isoelectric points in 20 mM $CaCl_2$ solutions is about 5.2. A relatively higher influence of $CaCl_2$ solutions than $MgCl_2$ solutions are also investigated for the zeta potentials of apatite, dolomite, and quartz according to the **Figures 7**, **8**, which is consistent with the results on silica reported in literature (Datta et al., 2009). Mammen et al. (1997) used a simple model of a silica surface to present that a higher degree of association of Ca^{2+} to the silica surface are consistent with the experimental zeta potentials tested by Datta et al. (2009). The higher zeta potentials of Ca^{2+} observed for comparison to Mg^{2+} may result from the increase in association of Ca^{2+} to the mineral surface and the larger ion radius of Ca^{2+} leading to lower polarizability than Mg^{2+} as well as its smaller influence to the electrons on the outer surface of minerals.

CONCLUSION

No impact or limited impact of the apatite, dolomite and phosphate ore supernatants are found on the surface electrical

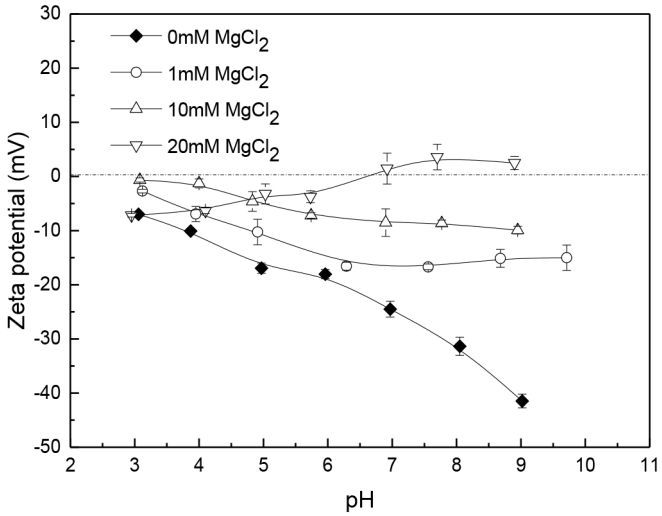

FIGURE 11 | Zeta potential of phosphate ore in solutions with different concentration of $MgCl_2$.

behaviors of the respective surfaces. The zeta potentials of quartz in apatite or dolomite supernatants increase compared to the original negative zeta potential of quartz. When apatite and dolomite are conditioned in the supernatants of each other, they interchange their zeta potential-curves over the entire pH range investigated. The zeta potential-curve of apatite in dolomite supernatants moves from that of apatite to dolomite, while the zeta potential-curve of dolomite in apatite supernatants moves from that of dolomite to apatite similarly. At high Ca^{2+} and Mg^{2+} concentration, especially 20 mM, the zeta potentials of apatite, dolomite, quartz and phosphate ore increase with IEP investigated, which is distinctly different from the original negative charge. Furthermore, it is interesting to find that the effects of Ca^{2+} is greater than that of Mg^{2+} on the surface electrical behaviors of apatite, dolomite, quartz, and phosphate ore.

These results are significant for the phosphate ore flotation. In the flotation circuit, the calcium and magnesium species from dissolved ores, not only increase the consumption of flotation reagents, but also change the surface properties of apatite, dolomite and quartz. Especially for apatite and dolomite, the similar variation on surface charge will enlarge the difficulty of selective flotation of phosphate ore.

DATA AVAILABILITY STATEMENT

All datasets generated for this study are included in the article/supplementary material.

AUTHOR CONTRIBUTIONS

FZ designed experiments and wrote the manuscript. QL, XL, WL, and JF carried out experiments. RC analyzed experimental results.

FUNDING

Project (51404171) was supported by the National Nature Science Foundation of China. Project (T201506) was supported by the Hubei Provincial Department of Education, China.

REFERENCES

Alroudhan, A., Vinogradov, J., and Jackson, M. D. (2016). Zeta potential of intact natural limestone:impact of potential-determining ions Ca, Mg and SO_4. *Colloids Surf. A Physicochem. Eng. Aspects* 493, 83–98. doi: 10.1016/j.colsurfa.2015.11.068

Amankonah, J. O., Somasundaran, P., and Ananthapadmabhan, K. P. (1985). Effects of dissolved mineral species on the dissolution/precipitation characteristics of calcite and apatite, *Colloids Surf.* 15:295. doi: 10.1016/0166-6622(85)80080-9

Datta, S., Conlisk, A. T., Li, H. F., and Yoda, M. (2009). Effect of divalent ions on electroosmotic flow in microchannels. *Mech. Res. Commun.* 36, 65–74. doi: 10.1016/j.mechrescom.2008.07.006

Demir, C., Bentli, I., Gulgonul, I., and Celik, M. S. (2003). Effects of bivalent salts on the flotation separation of Na-feldspar from K-feldspar. *Miner. Eng.* 16, 551–554. doi: 10.1016/S0892-6875(03)00078-5

dos Santos, M. A., Santana, R. C., Capponi, F., Ataíde, C. H., and Barrozo, M. A. (2010). Effect of ionic species on the performance of apatite flotation. *Sep. Purifi. Technol.* 76, 15–20. doi: 10.1016/j.seppur.2010.09.014

Hu, Y. H., and Wang, D. Z. (1992). Dissolution/surface property of salt-type minerals and design of schemes of flotation separation. *J. Central-South Inst. Mining Metallurgy* 23, 273–279.

Kasha, A., Al-Hashim, H., Abdallah, W., Taherian, R., and Sauerer, B. (2015). Effect of Ca^{2+}, Mg^{2+}, and SO_4^{2-}, ions on the zeta potential of calcite and dolomite particles aged with stearic acid. *Colloids Surf A Physicochem. Eng. Aspects* 482, 290–299. doi: 10.1016/j.colsurfa.2015.05.043

Li, D., Yin, W. Z., Xue, J. W., Yao, J., Fu, Y. F., and Liu, Q. (2017). Solution chemistry of carbonate minerals and its effects on the flotation of hematite with sodium oleate. *Int. J. Miner. Metallurgy Mater.* 24, 736–744. doi: 10.1007/s12613-017-1457-7

Mammen, M., Carbeck, J. D., Simanek, E. E., and Whitesides, G. M. (1997). Treating electrostatic shielding at the surface of silica as discrete siloxide·cation

interactions. *J. Am. Chem. Soc.* 119, 3469–3476. doi: 10.1021/ja9638115

Merma, A. G., Torem, M. L., Morán, J. J., and Monte, M. B. (2013). On the fundamental aspects of apatite and quartz flotation using a Gram positive strain as a bioreagent. *Miner. Eng.* 48, 61–67. doi: 10.1016/j.mineng.2012.10.018

Mishra, S. K. (1978). The electrokinetics of apatite and calcite in inorganic electrolyte environment. *Int. J. Miner. Process.* 5, 69–83. doi: 10.1016/0301-7516(78)90006-6

Ozeki, S., Takano, I., Shimizu, M., and Kaneko, K. (1989). ζ-potential of synthetic chrysotile asbestos in aqueous simple salt solutions. *J. Colloid Interface Sci.* 132, 523–531. doi: 10.1016/0021-9797(89)90266-X

Pokrovsky, O. S., Schott, J., and Thomas, F. (1999). Dolomite surface speciation and reactivity in aquatic systems. *Geochimica et Cosmochimica Acta.* 63, 3133–3143. doi: 10.1016/S0016-7037(99)00240-9

Santana, R. C., Duarte, C. R., Ataíde, C. H., and Barrozo, M. A. S. (2011). Flotation selectivity of phosphate ore:effects of particle size and reagent concentration. *Sep. Sci. Technol.* 46, 1511–1518. doi: 10.1080/01496395.2011.561268

Sze, A., Erickson, D., Ren, L., and Li, D. (2003). Zeta-potential measurement using the Smoluchowski equation and the slope of the current–time relationship in electroosmotic flow. *J. Colloid Interface Sci.* 261, 402–410. doi: 10.1016/S0021-9797(03)00142-5

Tang, C. Q., Zhang, Q., and Mao, S. (2010). Study on differences of flotation behavior of pure minerals in collophanite and dolomite. *Indust. Miner. Process.* 13, 1–4 (in Chinese).

Xiao, C., Chi, R., and Fang, Y. (2013). Effects of Acidiphilium cryptum on biosolubilization of rock phosphate in the presence of *Acidithiobacillus ferrooxidans*. *Trans. Nonferrous Met. Soc. China* 23, 2153–2159. doi: 10.1016/S1003-6326(13)62711-9

Yu, J., Ge, Y., and Hou, J. (1985). Behavior and mechanism of collophane and dolomite separation using alkyl hydroxamic acid as a flotation collector. *Colloids Surf.* 15, 295–307.

Zhou, F., Wang, L., Xu, Z., Liu, Q., and Chi, R. (2015). Reactive oily bubble technology for flotation of apatite, dolomite and quartz. *Int. J. Miner. Process.* 134, 74–81. doi: 10.1016/j.minpro.2014.11.009

Zhou, F., Wang, L., Xu, Z., Ruan, Y., Zhang, Z., and Chi, R. (2017). Role of reactive oily bubble in apatite flotation. *Colloids Surf. A Physicochem. Eng. Aspects* 513, 11–19. doi: 10.1016/j.colsurfa.2016.11.024

Conflict of Interest: The authors declare that the research was conducted in the absence of any commercial or financial relationships that could be construed as a potential conflict of interest.

frontiers in Materials

ORIGINAL RESEARCH
published: 21 February 2020
doi: 10.3389/fmats.2020.00040

On the Role of Hydrolyzable Metal Cations in the Adsorption of Anionic Surfactants on Negatively Charged Surfaces

Christian Weber and Urs A. Peuker*

Mechanical Engineering and Mineral Processing, TU Bergakademie Freiberg, Freiberg, Germany

The role of hydrolyzable metal ions in the adsorption of anionic surfactants on a negatively charge surface is studied by electrophoresis and phase transfer experiments. The notion that the presence of such hydrolyzable species (activators) can promote flotation is not new, but a detailed mechanistic explanation is lacking. We relate the role of activators to the phenomenon of overcharging, which has been studied rather extensively within colloid and interface science. The experiments conducted in this article show that overcharging is a necessary condition for the adsorption of an anionic surfactant on a negatively charged surface and that the hydrophobization of the studied particles is most effective when overcharging is most pronounced.

Keywords: SDS, phase transfer, two liquid flotation, overcharging, zeta potential, aluminum chloride, hydrolysis, activators

OPEN ACCESS

Edited by:
Zhiyong Gao,
Central South University, China

Reviewed by:
Wengang Liu,
Northeastern University, China
Snežana Papović,
University of Novi Sad, Serbia

****Correspondence:***
Christian Weber
chris.weber@mvtat.tu-freiberg.de

Specialty section:
This article was submitted to Colloidal Materials and Interfaces, a section of the journal Frontiers in Materials

Received: *13 September 2019*
Accepted: *05 February 2020*
Published: *21 February 2020*

Citation:
Weber C and Peuker UA (2020) On the Role of Hydrolyzable Metal Cations in the Adsorption of Anionic Surfactants on Negatively Charged Surfaces. Front. Mater. 7:40. doi: 10.3389/fmats.2020.00040

1. INTRODUCTION

In the flotation of mineral particles, one often relies on the adsorption of collectors for an effective hydrophobization of the target particles. If the ore to be floated has a very diverse mineralogical composition, there is quite a number of collectors that may selectively adsorb on the target particles. If, however, one is concerned with mineral assemblies that are majorly composed of oxides and silicates, the issue of finding a sufficiently selective collector becomes considerably more difficult. In principle one could try ionic surfactants and rely on electrostatics to achieve selectivity. For an anionic surfactant this would require that the valuable particles are positively charged and all other particles be negatively charged for the anionic surfactant to be electrostatically repelled. Here one relies on a sufficiently large difference between the points of zero charge of the minerals. However, as many oxides and silicates are negatively charged in practical pH ranges this is not a universal option for silicate-oxide systems. Similar reasoning applies to the selective separation of fine particles across liquid-liquid interfaces, a process the present authors are concerned with Machunsky et al. (2009), and Leistner et al. (2014, 2019).

An appealing alternative to the hydrophobization routes just described is the use of certain inorganic electrolytes to promote the adsorption of an ionic surfactant. Within the flotation literature these inorganic electrolytes are known as activators (Schubert, 1996; Furstenau and Pradip, 2005). Common to all activators is the fact that they show a more or less pronounced, pH-dependent speciation in aqueous solution. By speciation it is understood that hydrolyzed metal cations exist in certain pH ranges and these are precisely the pH ranges where best flotation results are obtained with negatively charged particles and anionic collectors (Fuerstenau et al., 1965). The mechanistic idea behind these activators is that they act as a linker between the anionic surfactant

and the similarly charged surface. Schubert (1996) summarizes that the probable mechanism is the adsorption of the activator in the Stern layer and Furstenau and Pradip (2005) state that the hydrolyzed species show such a high surface activity that they adsorb on any sort of adsorbent and thus provide said link.

The behavior of such hydrolyzed metal electrolytes has attracted interest in colloid and interface science as well (for reviews see Lyklema, 2006, 2013), where it was noticed that the colloid stability is affected quite drastically by such electrolytes. Furthermore, the phenomenon of overcharging—a more or less sudden sign reversal of the ζ-potential as a function of electrolyte concentration—was studied quite intensively.

In this article we will bring the information collected on the overcharging phenomenon in context with the activating electrolytes in flotation. This necessarily requires the description of electric double layers with inorganic electrolytes. The following sections are intended to briefly review the structure of electric double layers and to define the role of charge determining-, indifferent- and specifically adsorbed electrolytes. Furthermore, some information on overcharging and the necessary conditions for it to occur will be presented before proceeding with the experimental section where phase transfer under overcharging conditions will be experimentally investigated. The presentation will focus on the adsorption of the hydrolyzed species rather than on the adsorption of surfactants. This latter step in the adsorption process has been extensively studied by others (see Fuerstenau and Colic, 1999 for a review and many references) and we have little to add on this topic.

2. SHORT OVERVIEW ON ELECTRIC DOUBLE LAYERS AND OVERCHARGING

2.1. Double Layer Structure With Simple Inorganic Electrolytes

Virtually all minerals acquire a surface charge when immersed in an aqueous electrolyte solution. The processes by which the surface charge is established may vary from system to system. Quite often the surface charge results from the ad-/desorption of *charge determining ions*, which are ions that have a particularly high affinity for the surface and become part of the adsorbent after adsorption (Lyklema, 1991). Which ions are charge determining depends on the system under consideration. For AgI, for instance, Ag^+ and I^- have been identified as charge determining and for $BaSO_4$, Ba^{2+}, and SO_4^{2-} are charge determining. In the case of (hydr-) oxides and and many silicates H^+ and OH^- are charge determining and therefore the surface charge density can be changed by pH control. Typical reactions at the surface can be formulated as ad-/desorption equilibria:

$$> \mathrm{ROH} \longleftrightarrow > \mathrm{RO^-} + \mathrm{H^+} \quad \text{and}$$
$$> \mathrm{ROH} + \mathrm{H_2O} \longleftrightarrow > \mathrm{ROH_2^+} + \mathrm{OH^-}$$

In this notation >R denotes an atom of the solid. The surface charge density σ^0 is defined as the difference between the surface excess of H^+ and OH^-, which can be determined experimentally by potentiometric titrations. Only by such methods can a point of zero charge be established.

Once a surface has acquired a charge, the surface charge density has to be compensated in equal and opposite amount on the solution side of the surface: an electric double layer will form, whose detailed structure varies from system to system. In the easiest case the surface charge density will be entirely compensated by *indifferent electrolytes*, which, by definition, experience purely Coulombic attraction/repulsion from the surface (Lyklema, 1991). When this is the case, the electrical double layer is said to be entirely diffuse and the variation of the electrical potential perpendicular to the surface follows Gouy-Chapman theory. The electroneutrality condition for such a double layer reads $\sigma^0 + \sigma^d = 0$, in which σ^d is the charge density of the diffuse double layer. This parameter can be calculated via Gouy-Chapman theory if the diffuse layer potential is known. For a flat double layer in a symmetrical electrolyte diffuse layer charge density and potential are related by (Lyklema, 1995):

$$\sigma^d = -\sqrt{8\varepsilon\varepsilon_0 cRT}\sinh(zy^d/2) \tag{1}$$

Here $\varepsilon\varepsilon_0$ is the dielectric constant of the solvent, R the ideal gas constant, T the temperature, c the concentration of the electrolyte, z the charge, and $y^d = F\psi^d/RT$. Note that the relationship between charge and potential of diffuse layer looks quite different when non-symmetrical electrolytes or electrolyte mixtures are considered.

In order to decide whether an electrolyte is truly indifferent or not, one has basically two options: (1) Measure either surface charge or diffuse layer charge density with electrolytes of the same charge but different nature and (2) measure the surface charge density and the diffuse layer charge density simultaneously. In the framework of option (1), an indifferent electrolyte would give the very same parameters for every electrolyte of the same charge. The more direct and quantitative option (2) allows testing of the electroneutrality condition. For an indifferent electrolyte this condition would always be fulfilled, implying that the point of zero charge (pH at which $\sigma^0 = 0$) and the isoelectric point (pH at which $\sigma^d = 0$) coincide. Experimental evidence collected over the past decades shows that in many systems presumably indifferent electrolytes are not quite indifferent. Not only is this based on the shift of isoelectric points vs. points of zero charge, but violations of the simple electroneutrality condition have been observed as well (see for instance Lyklema, 1989, 1994). The basic tendency is $|\sigma^0| > |\sigma^d|$, which implies that there has to be another location where charges can accumulate in order for the double layer to be electroneutral.

Such observations, together with experimental evidence from electrokinetic studies (see Dukhin and Derjaguin, 1974; Hunter, 1981; Delgado et al., 2007), make the introduction of a Stern layer necessary, a modification of the diffuse double layer structure suggested by Stern (1924). The resulting double layer configuration is schematically shown in **Figure 1**.

In this figure there is a negatively charged surface with charge density σ^0 and associated surface potential ψ^0. The region between the surface and the inner Helmholtz plane (iHp), where the electric potential is ψ^i, is charge free. The iHp is the plane where specifically adsorbed ions reside (creating a charge density σ^i) and its distance to the surface is often said to be

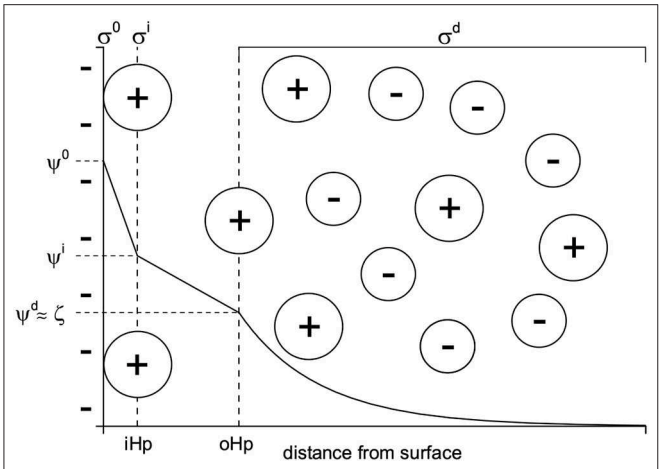

FIGURE 1 | Schematic model of the electric double layer including a Stern- and a diffuse layer.

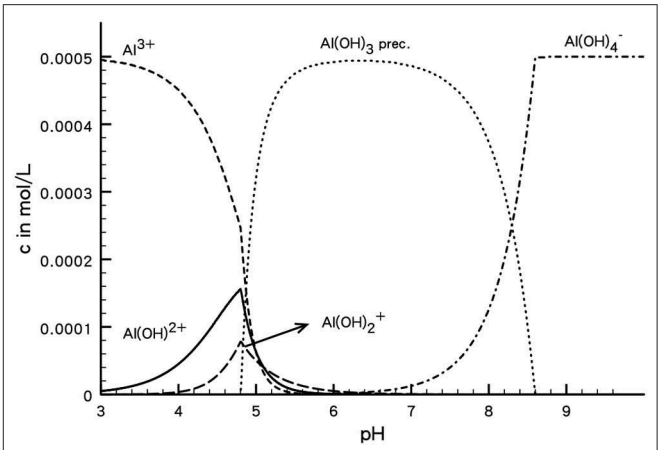

FIGURE 2 | Speciation of Al in 0.5 mM $AlCl_3$ solution, assuming that all Al available can be precipitated into amorphous $Al(OH)_3$. Only dominant species are shown.

determined by the size of the specifically adsorbed species. Note that *specifically adsorbing ions* experience, in addition to the purely electrostatic attraction, additional attraction to the surface. Due to the additional force(s) operating at the iHp equations like Eq. 1 that only consider an electrical attraction/repulsion no longer hold in this region of the double layer. For the charge density σ^i one has to formulate an adsorption isotherm. Among the many options to do so, we quote Hunter and Wright (1971):

$$\sigma^i = z_i e N_s e^{-(z_i e \psi^i + \Delta G_{ne})/kT} \tag{2}$$

Here e is the elementary charge, ψ^i the electric potential at the iHp, k Boltzmann's constant, ΔG_{ne} a specific adsorption free energy and N_s the site density available for specific adsorption, which is not necessarily the same as the total number of surface sites. The specific adsorption free energy simply reflects the additional work terms that are needed to bring an ion from the free solution to the iHp and is of a non-electric nature. Examples include solvent structure mediated interactions, complex formation or hydrophobic bonding.

Going further to the solution side of the double layer, there is again a charge free region up to the outer Helmholtz plane (oHp). In **Figure 1** we have not made a distinction between the oHp and the *slip plane*. Consequently the electrical potentials ψ^d and ζ are approximated to be equal. For a discussion on the positioning of the slip plane relative to the oHp and the distinctions between ψ^d and ζ we refer to Lyklema (2011) and Hunter (1981). The oHp, no matter if equated to the slip plane or not, marks the start of the diffuse part of the double layer, where the Gouy-Chapman theory applies. The electroneutrality condition for such a double layer reads $\sigma^0 + \sigma^i + \sigma^d = 0$.

This picture of the double layer, although physically not the most precise, is sufficiently simple and able to account for many experimental results.

2.2. Overcharging

The phenomenon of overcharging describes a situation in which the addition of an electrolyte containing multivalent counterions can lead to a sign reversal of the ζ-potential, which is not induced by pH changes. Note that overcharging is also called charge reversal, electrokinetic charge inversion and superequivalent adsorption. There are two popular explanations that may account for this: ion-ion correlations and a drastic specific adsorption of certain species within the Stern layer. Both of these options are discussed in Jiménez et al. (2012) and Lyklema (2009) where many references can be found. Briefly one may state that ion correlation theories require simultaneously high surface charge densities and high concentrations of multivalent counterions. Experimentally such situations have been observed in surface force studies (e.g., Kekicheff et al., 1993).

With respect to specific adsorption, the observation is that multivalent electrolytes that tend to form hydrolysis species can reverse the sign of the ζ-potential at rather low concentrations and often at quite low surface charge densities[1] (e.g., Matijević et al., 1962, 1964, 1971; James and Healy, 1972; James et al., 1977; Lyklema and Golub, 2007; Jiménez et al., 2012). The usual reasoning is that such hydrolysis products appear to have a rather high affinity for specific adsorption at the iHp. This statement derives from the fact that the effect is usually only observed in a limited pH window for a given electrolyte.

As an example one may consider the speciation in an $AlCl_3$ solution as a function of pH (**Figure 2**). The calculations have been performed with ChemEQL (Mueller, 1996) assuming that all the available Al can be precipitated as amorphous $Al(OH)_3$. Immaterial of this assumption one can see that at acidic pH values hydrolyzed species are present and that not all the Al in the system is trivalent. At about pH = 5 the precipitation of $Al(OH)_3$ sets in and in the alkalic range the dominant species in $Al(OH)_4^-$.

For aluminum chloride and nitrate solutions it was indeed observed that overcharging will only occur in the acidic range, being most effective around pH = 4–5. Such reasoning is of course applicable to many other electrolytes that form hydrolyzed

[1]Depending on the system just some 10–100 μmol/L and charge densities $\mathcal{O}(10^0)$ μC/cm^2 are sufficient.

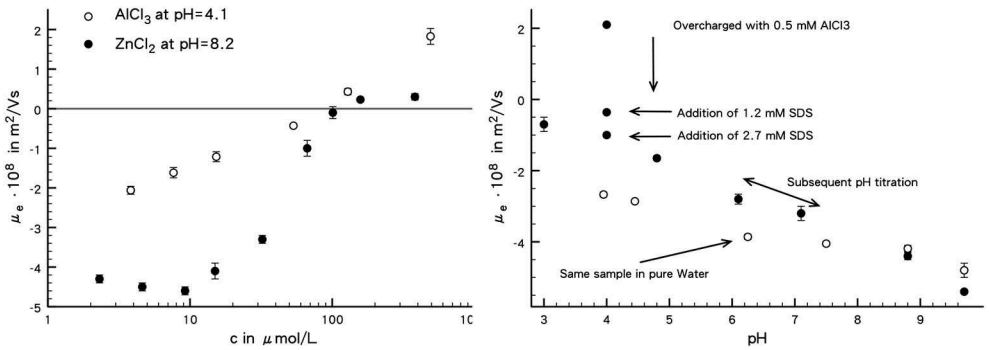

FIGURE 3 | (Left) electrophoretic mobility of SFP-30M as a function of $AlCl_3$ at pH = 4.1 and $ZnCl_2$ at pH = 8.2. **(Right)** electrophoretic mobility of SFP-30M in pure water (open circles) and of the same sample at pH = 4 (full circles), overcharged with 0.5 mM $AlCl_3$. To this sample SDS was added with a subsequent pH titration. See text for detailed explanation. The error bars represent the standard deviation from three measurements.

species in other pH ranges and was observed for many different solids. This suggests that the phenomenon as such is quite generic. A further discussion of overcharging will be given at the end of the article.

An important point to make is, that the effect does not mean that the sign of the surface charge density changes, it is the diffuse layer charge density that changes sign (see Lyklema and Golub, 2007 for comprehensive experimental evidence). At a given concentration of electrolyte the surface charge density is determined by the pH in the case of oxides. If there is more specific adsorption at the iHp than is needed to compensate the surface charge, electroneutrality dictates that the diffuse layer charge density has to change sign, which is experimentally observed as a change in sign of the ζ-potential.

To promote overcharging, one has to look for multivalent electrolytes that form hydrolyzed species in aqueous solution. Popular candidates include Al(III), La(III), Fe(III), and Zn(II) chlorides and nitrates. Typically, there will be certain pH windows where hydrolyzed species are stable and these are precisely the pH ranges one wishes to investigate for overcharging.

3. MATERIALS AND METHODS

The experiments reported in here have been conducted with a commercial spherical silica (SFP-30M from Denka, Japan). According to the manufacturer, the particle size is in the range between 0.1 and 2 μm with a median diameter of 0.6 μm and the specific surface area of the sample is 5.6 m^2/g.

The chemicals used in the experiments have been used without further purification. The purity of the metal chlorides was at least 99% [CAS Numbers: 7784-13-6 ($AlCl_3$), 7646-85-7 ($ZnCl_2$)], n-Hexane (CAS Number: 110-54-3) was obtained from Merck as chromatographic grade and SDS was also obtained from Merck with a quoted homologue C_{12} purity of $\geq$ 98% (CAS Number: 151-21-3).

Electrophoretic mobilities were measured with a Malvern Zetasizer Nano in folded capillary cells. The suspension has been stirred in a double-walled glass vessel that was connected to a water thermostad. Measurements have been carried out at 25°C with a drive voltage of max. 40 V. For each point 3 measurements have been made, each consisting of 50–100 sub runs.

Phase transfer experiments have been conducted in the following manner: An aqueous stock suspension was prepared with the desired concentration of a given metal salt, after which 2g/L silica were immersed in the solution. This suspension was then sonicated for $\approx$ 2 min in order to properly disperse the particles. The desired amount SDS was added to this suspension in dry form. Different pH values were then adjusted by the addition of HCl or NaOH. For each tube 20 mL of aqueous suspension were withdrawn and 5 mL n-Hexane were added. These tubes were then shaken in order to observe whether a successful phase transfer is accomplished.

The transmittance (relative to pure water) of the aqueous phase was measured with an Agilent Technologie Cary 60 UV-Vis spectrometer at 800 nm in order to obtain a qualitative indication of the efficiency of the phase transfer.

4. RESULTS AND INTERPRETATION

The electrophoretic mobilities (μ_e) measured in different electrolyte solutions and in pure water are shown in **Figure 3**. Absolute electrophoretic mobilities will be used in discussing trends of this quantity.

First of all it is noted that the electrophoretic mobility in pure water is negative in the entire pH range studied. This is usual for silica and crystalline SiO_2 phases. Although the surface charge density is not at our disposal for this specific sample, it seems reasonably safe to say that the point of zero charge is not reached for the sample since there is rather good agreement in the literature that silicas have points of zero charge below pH = 3 if one is found at all (see Lyklema, 1995).

Based on the speciation of $AlCl_3$ and $ZnCl_2$ pH ranges were selected where overcharging can be suspected to occur. For aluminum chloride this is in the acidic range (roughly pH = 4–5) and for zinc chloride this is in the alkalic range (roughly pH = 8–9). Suspension were prepared with the desired pH and a titration with the corresponding electrolyte was conducted (see **Figure 3**, left). For aluminum chloride a steady increase of the electrophoretic mobility is observed and a change in its sign

FIGURE 4 | Pictures of the phase transfer experiments. **(A)** 0.5 mM $AlCl_3$ with 2 mM SDS, **(B)** $ZnCl_2$ with 2 mM SDS, **(C)** 0.5 mM $CaCl_2$ with 2 mM SDS and **(D)** 11 μmol $AlCl_3$ at pH = 4.6 with different SDS concentrations. pH values in **(A–C)** are indicated and the SDS concentration in **(D)** is given in mM.

occurs at $\approx$ 0.1 mM. Upon further addition of electrolyte the mobility increases further, which indicates that the adsorption in the Stern layer is not completed after the change of sign.

The mobilities of zinc chloride suspensions are somewhat more complicated. At rather low concentration a decrease in mobility is noted. This is a definitive hint for Stern layer adsorption in conjunction with mobile ionic species in this part of the double layer. Such mobility maxima are observed on a standard basis in electrokinetic studies and can be traced back to surface conductance in the Stern layer (Delgado et al., 2007). Upon further addition of electrolyte, the mobility starts to increase rapidly and eventually changes sign at about 0.1 mM. Further addition of electrolyte does not change the mobility markedly anymore which can be taken as a sign that Stern layer adsorption of this species is completed.

Now that the solution compositions for overcharging are established, SDS was added to a suspension overcharged with 0.5 mM $AlCl_3$ at pH = 4 was measured (see **Figure 3**, right). The first addition of 1.2 mM SDS decreases the mobility from initially $2{\cdot}10^{-8}$ m^2/Vs to about $-0.5 \cdot 10^{-8}$ m^2/Vs. Further addition of SDS (equivalent to 2.7 mM) decreases the mobility further to $\approx -1 \cdot 10^{-8}$ m^2/Vs. This can be taken as an indication that the adsorbed aluminum species act as adsorption sites for the negative part of the SDS. In order to investigate the stability of these Stern layer species, a pH titration was carried out after the addition of 2.7 mM SDS. The general shape of the mobility vs. pH curve is quite similar to the one recorded in pure water. Up to pH $\approx$ 9 the absolute mobilities in the SDS system are lower that those of pure water and in the alkalic range they do not differ too much from each other. Furthermore, it is interesting to note that the pH titration is reversible.

Figure 4 shows the results of the qualitative phase transfer experiments. The lower phase is the aqueous phase and the upper one is n-Hexane. It can immediately be concluded that the success of the phase transfer depends on the type and concentration of the electrolyte and the pH.

The transmittance measurements of the aqueous parts of these systems are presented in **Figure 5**. Note that these measurements should be interpreted qualitatively, because in $AlCl_3$ - SDS systems precipitation of a Al-SDS phase occurs which will be discussed later.

Even without a detailed mechanistic explanation one can conclude from **Figures 4**, **5** that the phase transfer in the system containing 0.5 mM $AlCl_3$ with 2mM SDS is most effective. Within this system there is a pronounced pH dependency of the transfer efficiency as indicated by the transmission measurements. At low pH, where overcharging is most pronounced, the phase transfer is almost complete, decreasing toward the alkalic range where a quite low amount of particles is transferred. Considering the system with 11 μmol/L $AlCl_3$ at pH = 4.6, where the Al concentration is too low to overcharge the silica, one cannot observe a phase transfer at all, immaterial of the SDS concentration. In the $ZnCl_2$ system one observes a partial, but pH independent phase transfer. As a comparison to this system, we have conducted the same experiment with $CaCl_2$, which does not hydrolyze significantly in the studied pH range and does not cause overcharging. No phase transfer at all is observed in this system. All these observations, although largely qualitative, show that overcharging is a necessary condition

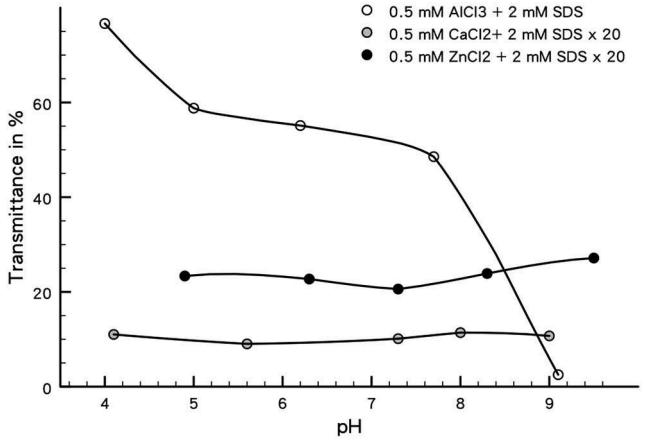

FIGURE 5 | Transmittance (at 800 nm) of the aqueous phase of the phase transfer experiments shown in **Figure 4**. Note that the data for 0.5 mM $CaCl_2$ and $ZnCl_2$ have both been multiplied by a factor of 20 in order to make them visible with respect to the $AlCl_3$ system.

for a successful phase transfer in our system. The following section is intended to provide a more detailed explanation for these observations.

5. DISCUSSION

Before discussing the details of overcharging and the subsequent adsorption of DS^-, it is necessary to point out that we have observed the formation of a precipitate in solutions of $AlCl_3$ and SDS. Visually this can be observed at a ratio of SDS/$AlCl_3$ $\approx$1. Upon further addition of SDS the precipitation proceeds until a ratio of SDS/$AlCl_3$ $\approx$12 is attained, where the solution is entirely transparent again. This effect is known for $AlCl_3$ sulfonate systems (Somasundaran et al., 1988) and goes by the name precipitation-redissolution phenomena. In the $Al(NO_3)_3$-dodecylsulfate system similar observations have been made (Pereira et al., 2009). Regardless of the specific details of these processes, it must be noted that our $AlCl_3$ experiments have been conducted in a concentration range (SDS/$AlCl_3 = 4$) where precipitation occurs. It is therefore logical to question whether the successful phase transfer is due to the presence of the precipitate or due to the effect of overcharging with concomitant adsorption of DS^-. It is for this reason that we have conducted the same experiments with a lower concentration of $AlCl_3$, where overcharging does not occur. In these experiments the SDS concentration was varied to cover a range of SDS/$AlCl_3 = 4$–178, where both precipitation and redissolution occur.

As mentioned in the previous section, no phase transfer was observed in these experiments. This suggests that overcharging is the dominating mechanism leading to the adsorption of DS^-. To see this point, consider the experiments with $ZnCl_2$ and $CaCl_2$. Here we observe no phase transfer for $CaCl_2$, but observe a partial one for $ZnCl_2$. This is due to the ability of Zn to overcharge the silica at alkalic pH, whereas Ca is not able to do so at such low concentration. Furthermore, we have not observed (visually) a precipitation of $ZnCl_2$ + SDS solutions.

The experimental data presented in here and the numerous experimental observations cited in conjunction with the overcharging phenomenon demonstrate that the sign reversal of the electrophoretic mobility is at least in part due to the specific adsorption of hydrolyzed species. One may now wonder why such hydrolyzed species, which have a lower charge than the unhydrolyzed metal cation, adsorb so effectively.

In addition to the electrostatic adsorption energy at the iHp, which is $\Delta G_{el}=ze\psi^i$, one may quite generally add a solvation term (see for instance James and Healy, 1972). The free energy change associated with ion solvation describes the process of transferring an ion from a region of high dielectric constant to a region of lower dielectric constant. These authors derived a relationship for the solvation work required to bring an ion from the free solution to the iHp:

$$\Delta G_{solv} = \left(\frac{z_i^2 e^2}{16\pi\varepsilon_0}\right)\left(\frac{1}{r_i + 2r_w} - \frac{r_i}{2(r_i + 2r_w)^2}\right)\left(\frac{1}{\varepsilon_{iHp}} - \frac{1}{\varepsilon_w}\right) + \left(\frac{z_i^2 e^2}{32\pi\varepsilon_0}\right)\left(\frac{1}{r_i + 2r_w}\right)\left(\frac{1}{\varepsilon_s} - \frac{1}{\varepsilon_{iHp}}\right) \quad (3)$$

In this relation z_i is the charge of the ions, e the elementary charge, ε_0 the permitivitty of free space, ε_w the relative dielectric constant of water, ε_s the one of the solid, ε_{iHp} the effective relative dielectric constant at the iHp, r_i the radius of the ion and $2r_w$ the diameter of a water molecule. Note that James and Healy (1972) place the iHp at a distance $2r_w + r_i$ away from the surface. The difficult point is to define and calculate reasonable values for the dielectric constant at the iHp, since at such small length scales a definition of a macroscopic quantity becomes somewhat ambiguous. James and Healy (1972) chose to relate this dielectric constant to the field strength in the double layer. This step, however, is somewhat inconsistent, because diffuse double layer theory is applied up to the iHp in order to obtain the required relationship. Moreover, the change of dielectric constant close to a solid surface is a general property of structurable solvents. This is why we choose a relationship suggested by Podgornik et al. (1987) to construct the dielectric profile:

$$\varepsilon_w(x) = \frac{\varepsilon_w}{1 + (\varepsilon_w/\varepsilon_s - 1)e^{-x/l}} \quad (4)$$

where x is the distance to the solid surface and l the correlation length of water. Last but not least, James and Healy (1972) added a chemical contribution to the adsorption free energy. This chemical contribution embraces all specific interactions that may occur in the system and, just like the electrical contribution, it is a favorable energy change. It is furthermore assumed that this term is constant and applies to all species present. Within this simple model the total adsorption free energy at the iHp is written as the sum of the discussed contributions: $\Delta_{ads}G=\Delta G_{el} + \Delta G_{solv} + \Delta G_{chem}$. An example calculation along these lines is shown in **Figure 6**. The parameters chosen for the calculation are

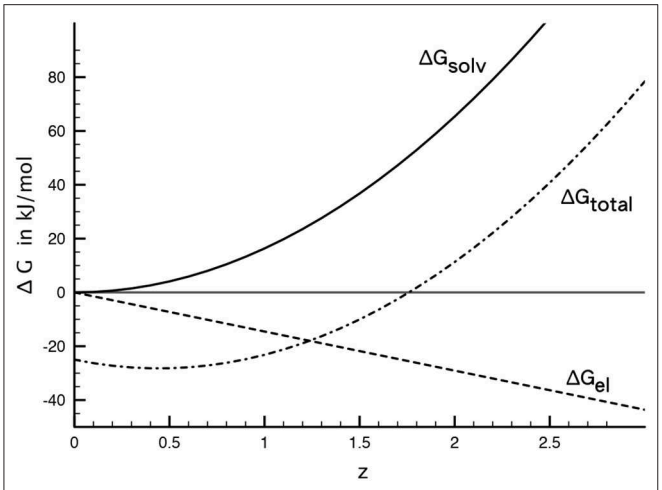

FIGURE 6 | Solvation and electrostatic contribution to total free energy of adsorption in the Stern layer. For parameters see text. The chemical contribution of $\Delta G_{chem} = -25$ kJ/mol (not shown) is added to the total adsorption free energy.

as follows: As already mentioned above, the position of the iHp is fixed as $2r_w + r_i$, where $2r_w = 0.284$ nm and r_i=0.05 nm (Al^{3+}) (Marcus, 1988). The dielectric constant of SiO_2 has be taken as $\varepsilon_s = 4$ (Hunter, 2000) and the correlation length of water has been set to $2r_w = 0.284$ nm. With these values the dielectric constant at $2r_w + r_i$=0.33 nm is ε_{iHp}=10. Finally the electric potential at the iHp has ben set $\psi^i = -0.15$ V and the chemical part of the adsorption free energy has been chosen as $\Delta G_{chem} = -25$ kJ/mol (an intermediate value from James and Healy, 1972).

It can be seen that the electrical and chemical contributions represent a favorable energy change, i.e., they promote adsorption. While the chemical part has, as usual, been assumed constant, the electrical part increases lineraly with z. The energy penalty represented by the solvation term, however, scales with z^2. It thus represents an energy barrier for the adsorption of higher-valence ions. In the example presented here, the adsorption would be favorable for species with $z \lessapprox 2$.

Due to the quite large number of unknown parameters such calculations should not be taken as quantitative unless more experimental data is available. They do, however, highlight the decisive role of solvation in the adsorption of hydrolyzed species. James and Healy (1972) used a similar approach to fit adsorption isotherms in such systems and were able to describe their experimental results with reasonable parameter choices. The difference being that they related the dielectric constant to the field strength in the double layer (see above). The simple treatment of the dielectric constant profile presented above is somewhat more attractive in that it does not involve the application of Gouy-Chapman theory in the inner part of the double layer and that it is applicable to structurable solvents in general.

The pH titration of overcharged SiO_2 in the presence of 2.7 mM SDS shown in **Figure 3** is reversible with respect to pH changes. This is an important observation, because it shows that the Al-DS^- complexes are adsorbed quite strongly in the Stern layer. When SDS is added to the overcharged silica, part of the SDS adsorbs to the positive Al sites in the Stern layer. The amount of SDS added in our system is high enough to reverse the overcharging, meaning that $|\sigma^0| > |\sigma^i|$, which is indicated by the electrophoretic mobility going to negative values again. The fact that at pH = 4 the mobility remains well above the mobility of the sample in water suggests that there is still a finite charge density located in the Stern layer when $AlCl_3$ and SDS are added. If this charge density is more or less pH-independent, a titration to high pH will increase the surface charge density σ^0 while σ^i remains more or less constant. At alkalic pH σ^0 becomes eventually so large that that the contribution of σ^i becomes less notable and similar diffuse layer charge densities are obtained again (with respect to the pure water case). This is precisely what can be observed from the electrophoretic mobilities.

Moreover it was observed that the phase transfer as such is reversible. In the presence of 0.5 mM $AlCl_3$ + 2mM SDS at pH = 4, a rather effective phase transfer is observed (see **Figures 4**, **5**). When NaOH is added to the aqueous phase and the tube is shaken again, most of the particles are transferred to the aqueous phase again. This is a remarkable observation, for which we do not have a definitive explanation up to now.

Apart from the energetic changes occurring at the aqueous-solid interface it is also permissible that the interface tension of the aqueous-Hexane interface is influenced by the precipitates in the $AlCl_3$-SDS system. Preliminary measurements indicate that at acidic pH the interface tension is lower at acidic pH than at alkalic pH, which can also contribute to the efficiency of the phase transfer. Altogether these results show that the systems studied here are quite complicated ones and that multiple adsorption processes at different interfaces as well as the liquid chemistry as such deserve further attention.

6. CONCLUSION

Using electrophoresis measurements and phase transfer experiments it was shown that overcharging by hydrolyzed metal species is responsible for the adsorption of an anionic collector (SDS) to a negatively charged surface. The phase transfer, and thus the hydrophobization of particles, was found to be most effective when overcharging is most pronounced. The complicated interactions between SDS and multivalent cations, however, hamper an in-depth understanding of the multiple adsorption phenomena at the different interfaces.

What appears to be established is that overcharging by hydrolyzed species is a necessary condition for a phase transfer in our systems. The processes leading to overcharging by inorganic ions were discussed an it was emphasized that ion solvation can play a decisive role by creating an energetic barrier for the adsorption of multivalent ions.

DATA AVAILABILITY STATEMENT

All datasets generated for this study are included in the article/supplementary material.

AUTHOR CONTRIBUTIONS

CW designed, conducted, and interpreted the experiments. UP designed experiments and critically examined the results.

FUNDING

CW appreciates funding by the DFG (SPP2045, 313858373).

ACKNOWLEDGMENTS

CW acknowledges insightful discussions with Dr. Martin Rudolph and Edgar Schach (Helmholtz-Zentrum Dresden-Rossendorf). Paul Knüpfer and Klaus Graebe are thanked for experimental assistance and B. von Klitzing from Denka for supply of the silica.

REFERENCES

Delgado, A. V., Gonzalez-Caballero, F., Hunter, R., Koopal, L. K., and Lyklema, J. (2007). Measurement and interpretation of electrokinetic phenomena. *J. Colloid Interface Sci.* 209, 194–224. doi: 10.1016/j.jcis.2006.12.075

Dukhin, S. S., and Derjaguin, B. V. (1974). "Chapter 2: Electrokinetic phenomena," in *Surface and Colloid Science*, ed V. Matijević (New York, NY: John Wiley and Sons), 356.

Fuerstenau, D. W., and Colic, M. (1999). Self-association and reverse hemimicelle formation at solid-water interfaces in dilute surfactant solutions. *Colloids Surfaces A Physicochem. Eng. Aspects* 146, 33–47. doi: 10.1016/S0927-7757(98)00795-X

Furstenau, D. W., and Pradip (2005). Zeta potentials in the flotation of oxide and silicate minerals. *Adv. Colloid Interface Sci.* 9-26, 114–115. doi: 10.1016/j.cis.2004.08.006

Furstenau, M. C., Rice, D. A., Somasundaran, P. and Furstenau, D. W. (1965). Metal ion hydrolysis and surface charge in beryl flotation. *Trans. Am. Inst. Mining Metallur. Eng.* 74, 381–391.

Hunter, R. (1981). "Zeta potential in colloid science - Principles and applications," in *Colloid Science: A Series of Monographs*, eds R. H. Ottewill and R. L. Rowell (London: Academic Press), 386.

Hunter, R. (2000). *Foundations of Colloid Science, 2nd Edn.* New York, NY: Oxford University Press Press,

Hunter, R., and Wright, H. J. L. (1971). The dependence of electrokinetic potential on concentration of electrolyte. *J. Colloid Interface Sci.* 37, 564–580. doi: 10.1016/0021-9797(71)90334-1

James, R. O., and Healy, T., W. (1972). Adsorption of hydrolyzable metal ions at the oxide-water interface iii. a thermodynamic model of adsorption. *J. Colloid Interface Sci.* 40, 65–81. doi: 10.1016/0021-9797(72)90174-9

James, R. O., Wiese, G. R., and Healy, T., W. (1977). Charge reversal coagulation of colloidal dispersions by hydrolysable metal ions. *J. Colloid Interface Sci.* 59, 381–385. doi: 10.1016/0021-9797(77)90023-6

Jiménez, M. L., Delgado, A. V., and Lyklema, J. (2012). Hydrolysis versus ion correlation models in electrokinetic charge inversion: establishing application ranges. *Langmuir* 28, 6786–6793. doi: 10.1021/la3010773

Kekicheff, P., Marcelja, S., Senden, T. J., and Shubin, V. E. (1993). Charge reversal seen in electrical double layer interaction of surfaces immersed in 2:1 calcium chloride solutions. *J. Chem. Phys.* 99, 6098–6113.

Leistner, T., Müller, M., Erler, J. V., Rudolph, M., and Peuker, U. A. (2014). Selektive trennung sehr feiner partikelsysteme mittels flüssig/flüssig-flotation. *Chem. Ingenieur Technik* 86, 831–839. doi: 10.1002/cite.201400011

Leistner, T., Türk, M., Weber, A., Weber, C., and Peuker, U. A. (2019). Selective separation using fluid-liquid interfaces. *Mater. Sci. Forum* 959, 113–124. doi: 10.4028/www.scientific.net/MSF.959.113

Lyklema, J. (1989). Discrimination between physical and chemical adsorption of ions on oxides. *Colloids Surfaces* 37, 197–204. doi: 10.1016/0166-6622(89)80118-0

Lyklema, J. (1991). Electrified interfaces in aqueous dispersions of solids. *Pure Appl. Chem.* 61, 895–906.

Lyklema, J. (1994). On the slip process in electrokinetics. *Colloids Surfaces A Phys. Eng. Aspects* 92, 41–49. doi: 10.1016/0927-7757(94)02727-7

Lyklema, J. (1995). *Fundamentals of Interface and Colloid Science - Volume II: Solid-Liquid Interfaces*. London: Academic Press.

Lyklema, J. (2006). Overcharging, charge reversal: chemistry or physics. *Colloids Surfaces A Phys. Eng. Aspects* 291, 3–12. doi: 10.1016/j.colsurfa.2006.06.043

Lyklema, J. (2009). Quest for ion-ion correlations in electric double layers and overcharging phenomena. *Adv. Colloid Interface Sci.* 147-148, 205–213. doi: 10.1016/j.cis.2008.12.002

Lyklema, J. (2011). Surface charges and electrokinetic charges: Distinctions and juxtapositionings. *Colloids Surfaces A Phys. Eng. Aspects* 376, 2–8. doi: 10.1021/jp057096

Lyklema, J. (2013). Coagulation by multivalent counterions and the schulze-hardy rule. *J. Colloid Interface Sci.* 392, 102–104. doi: 10.1016/j.jcis.2012.09.066

Lyklema, J., and Golub, T. (2007). Electrical double layer on silver iodide and overcharging in the presence of hydrolyzable cations. *Croatica Chem. Acta* 80, 303–311.

Machunsky, S., Grimm, P., Schmid, H. J., and Peuker, U. A. (2009). Liquid-liquid phase transfer of magnetite nanoparticles. *Colloids Surfaces A Phys. Eng. Aspects* 348, 186–190. doi: 10.1016/j.colsurfa.2009.07.014

Marcus, Y. (1988). Ionic radii in aqueous solution. *Chem. Rev.* 88, 1475–1498. doi: 10.1021/cr00090a003

Matijević, E., Janauer, G. E., and Kerker, M. (1964). Reversal of charge of lyophobic colloids by hydrolyzed metal ions i. aluminum nitrate. *J. Colloid Interface Sci.* 19, 333–346. doi: 10.1016/0095-8522(64)90035-2

Matijević, E., Mangravite, F. J., and Cassell, E. A. (1971). Stability of colloidal silica iv. the silica-alumina system. *J. Colloid Interface Sci.* 35, 560–568. doi: 10.1016/0021-9797(71)90214-1

Matijević, E., Mathai, K. G., and Kerker, M. (1962). Detection of metal ion hydrolysis by coagulation v. zirconium. *J. Phys. Chem.* 66, 1799–1803. doi: 10.1021/j100816a006

Mueller, B. (1996). *ChemEQL. A Program to Calculate Chemical Speciation and Chemical Equilibria*. Eidgenössische Anstalt für Wasserversorgung.

Pereira, R. F. P., Valente, A. J. M., Burrows, H. D., Ramos, M. L., Ribeiro, C. F., and Lobo, V. M. M. (2009). Flocculation and micellization of sodium dodecyl sulfate solutions in the presemce of aluminum nitrate: effect of concentration and temperature. *Acta Chim. Slovenica* 56, 45–52.

Podgornik, R., Cevc, G., and Zeks, B. (1987). Solvent structure effects in the macroscopic theory of van der waals forces. *J. Chem. Phys.* 87, 5957–5967. doi: 10.1063/1.453519

Schubert, H. (1996). *Aufbereitung Fetster Stoffe Band II: Sortierprozesse*. Stuttgart: Deutscher Verlag für Grundstoffindustrie Stuttgart.

Somasundaran, P., Ananthapadmanabhan, K. P., and Celik, M. S. (1988). Precipitation-redissolution phenomena in sulfonate-alcl$_3$ solutions. *Langmuir* 4, 1061–1063.

Stern, O. (1924). Zur theorie der elektrolytischen doppelschicht. *Zeitschrift für Elektrochemie und Angewandte Physikalische Chemie* 30, 508–516.

Conflict of Interest: The authors declare that the research was conducted in the absence of any commercial or financial relationships that could be construed as a potential conflict of interest.

frontiers in Materials

ORIGINAL RESEARCH
published: 12 March 2020
doi: 10.3389/fmats.2020.00047

Adsorption Behaviors of Different Water Structures on the Fluorapatite (001) Surface: A DFT Study

Weiyong Cui[1], Xueli Song[2], Jianhua Chen[1,3], Ye Chen[1,3]*, Yuqiong Li[3] and Cuihua Zhao[3]*

[1] School of Chemistry and Chemical Engineering, Guangxi University, Nanning, China, [2] First Affiliated Hospital of Guizhou University of Traditional Chinese Medicine, Guiyang, China, [3] School of Resources, Environment and Materials, Guangxi Key Laboratory of Processing for Non-ferrous Metals and Featured Materials, Guangxi University, Nanning, China

To investigate the effect of hydration behavior on the fluorapatite structure, single H_2O molecule and three-layer water cluster adsorptions on the fluorapatite (001) surface were performed by means of density functional theory. The results show that a single H_2O molecule can form stable chemisorption structures with the fluorapatite (001) surface in the form of single-site, two-site, and three-site adsorption and that the corresponding adsorption energies are 64.817, 98.712, and 139.620 kJ/mol, respectively. The interacting length of the Ca atom and the O atom of the H_2O molecule is close to the length of the Ca–O bond in the bulk, and their overlap is mainly contributed by the O 2p and Ca 4s states. The fluorapatite (001) surface shows serious hydration reconstruction after adsorbing three layers of water molecules; these atoms in the surface layer are highly distorted, and the Ca and the PO_4 are shifted in opposite directions along the *z*-axis direction. Further analysis shows that these surface Ca atoms are critical to the hydration behaviors of the transition area, as they can bind strongly to the H_2O molecules, with the newly formed Ca–O bonds being between 2.164 and 2.486 Å.

Keywords: fluorapatite, hydration behavior, density-functional theory, water cluster, transitional interfacial layer

OPEN ACCESS

Edited by:
Zhiyong Gao,
Central South University, China

Reviewed by:
Xuming Wang,
The University of Utah, United States
Fanfei Min,
Anhui University of Science and Technology, China
Chenyang Zhang,
Central South University, China

***Correspondence:**
Jianhua Chen
jhchen@gxu.edu.cn
Ye Chen
fby18@126.com;
yechen@gxu.edu.cn

Specialty section:
This article was submitted to Colloidal Materials and Interfaces, a section of the journal Frontiers in Materials

Received: *18 December 2019*
Accepted: *12 February 2020*
Published: *12 March 2020*

Citation:
Cui W, Song X, Chen J, Chen Y, Li Y and Zhao C (2020) Adsorption Behaviors of Different Water Structures on the Fluorapatite (001) Surface: A DFT Study. Front. Mater. 7:47. doi: 10.3389/fmats.2020.00047

INTRODUCTION

Apatites have attracted more and more attention due to their complex structures and unique properties. On the one hand, because they are the most important bone material, the study of apatites occupies a huge market in the field of life science (Palazzo et al., 2007; Rey et al., 2014; Okada and Matsumoto, 2015); on the other hand, there are many valuable elements in them, such as rare earths, uranium, and thorium, which play significant roles in the development of future energy, high-end equipment, and other advancements of various key technologies (Li et al., 2014; Zhang, 2014; Emsbo et al., 2015). However, we should not ignore the fact that apatites, and mostly fluorapatite, are the main phosphorus-bearing minerals and play an irreplaceable role in industrial and agricultural production (Scholz et al., 2014). Data reveals that more than 90% of the fluorapatite resource is used to produce fertilizer, with other applications being in animal feed, detergents, food and beverages, and water treatment (Rawashdeh and Maxwell, 2011). Not all phosphate ores can be used directly, and this is becoming more and more of an issue as rich fluorapatite resources become even scarcer. With the further depletion of the apatite resources, billions of tons of apatite ores need to be pretreated by flotation. It is reported that more than half of the world's marketable

phosphate is concentrated via the flotation process, which takes place at the complex solid, water, and gas phase interface (Santos et al., 2010).

The existence of a water environment is a necessity for flotation, and the hydration behavior of the surface is very important. However, corresponding research is still needed, and progress has been slow. Due to the development of modern microscopic detection equipment, this trend has improved dramatically. Park et al. (2005) studied the structure of the Durango fluorapatite (100)–water interface with high-resolution X-ray reflectivity and found that the presence of a layered interfacial water structure exhibits two distinct water layers and that the heights of the first and second layers are 2.64 and 4.17 Å, respectively. Dan et al. (2006) conducted research on calcium surface sites at aqueous fluorapatite by means of ^{1}H and ^{31}P MAS NMR. Meanwhile, Pareek et al. (2008, 2009) made a systematic study of the role of water in the surface relaxation of the fluorapatite (100) surface with grazing incidence *x*-ray diffraction. In recent years, with the continuous progress of computer technology, the density functional theory method (DFT), which can be used to describe collector-mineral adsorption at the molecular level in 3D space, has triggered intense research and is providing valuable primary information on various interface systems (Mkhonto and de Leeuw, 2002; Rulis et al., 2004, 2007; Haverty et al., 2005; Chappell et al., 2008; Menéndez-Proupin et al., 2011). Mkhonto and de Leeuw (2002) studied the effect of water on the surface structure and morphology of fluorapatite and found that the hydration of the surfaces occurs by physisorption and shows Langmuir behavior. Mkhonto and de Leeuw (2002) studied the interaction of (001) carbonated hydroxylapatite surfaces with water. They found that a single molecule of water can be strongly adsorbed by the apatite surface and that the carbonate ion may lower both the adsorbate/surface interaction energy and the energy needed to deform the COHAp surface and the water molecule. However, many questions relating to the details of water adsorption on the fluorapatite surface at the molecular level remain without clear answers.

In this paper, the fluorapatite (001) surface was chosen to investigate the interactions between the fluorapatite (001) surface and single H_2O molecule as well as water cluster, respectively. Different configurations were optimized, and the mechanism of water adsorptions on the fluorapatite (001) surface and their influence are discussed. The results provide an important insight into the structure of and enable investigation of flotation reagent interactions on the fluorapatite surface, which may aid current experimental efforts to understand the flotation process further.

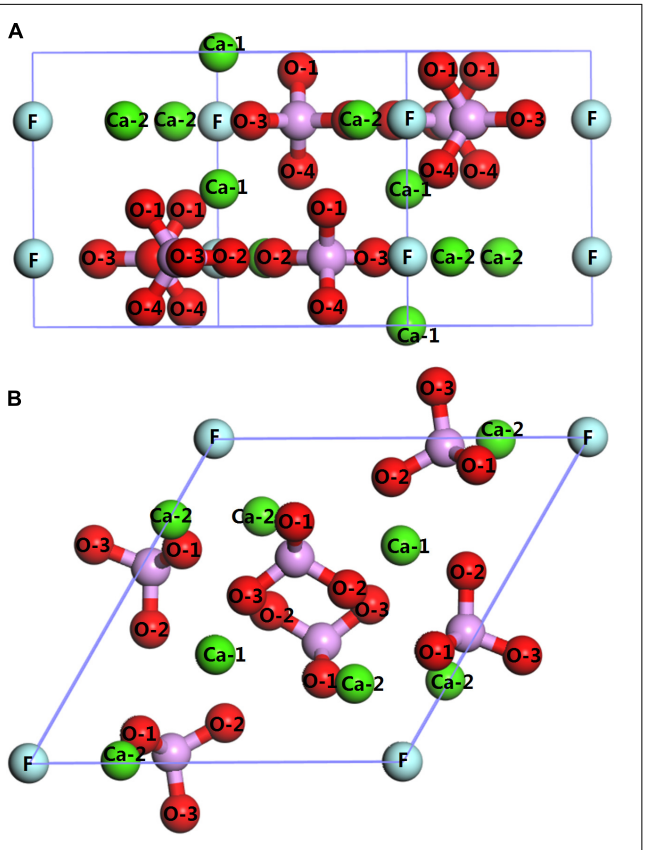

FIGURE 1 | Crystal structure of fluorapatite: **(A)** side view (perpendicular to the fluorapatite (001) surface); **(B)** top view (parallel to the fluorapatite (001) surface).

MATERIALS AND METHODS

Computational Methods

Calculations for the fluorapatite (001) surface and single H_2O molecule adsorptions were performed within Cambridge Serial Total Energy Package (CASTEP) (Clark et al., 2005).

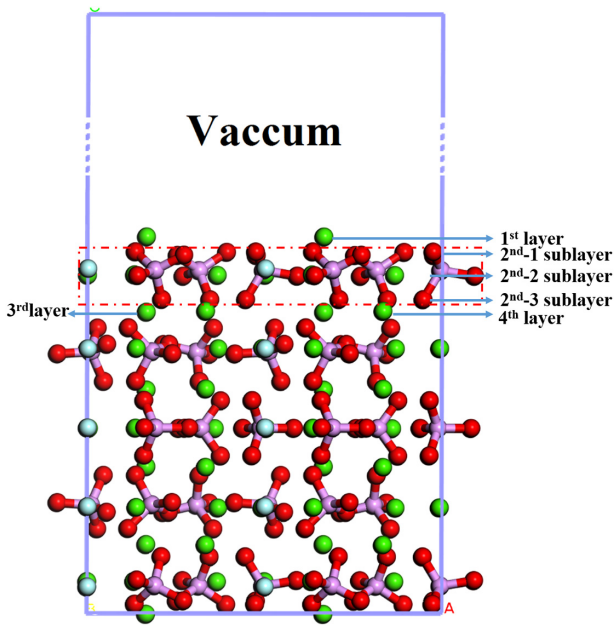

FIGURE 2 | Structure of the fluorapatite (001) surface.

For the former calculations, the ultrasoft pseudo-potential was employed to describe the electron–ion interactions. The exchange correlation function used in the present study was the generalized gradient approximation (GGA), which was extended by the Perdew-Wang generalized-gradient approximation (PW91). The plane-wave cutoff of 400 eV was chosen, and the Brillouin zone was sampled with k-points of a 2 × 2 × 2 grid, which were found to be enough for the system. The convergence tolerances were set as follows: the maximum displacement was 0.002 Å, the maximum force was 0.08 eV·Å^{-1}, the maximum energy change was 2.0 × 10^{-5} eV·atom^{-1}, the maximum stress was 0.1 GPa, and the SCF convergence tolerance was 2.0 × 10^{-6} eV·atom^{-1}. The valence electron configurations considered in all the studies were H 1s^1, O 2s^2 2p^4, F 2s^2 2p^5, P 3s^2 3p^3, Ca 3s^2 3p^6 4s^2.

Computational Models

The bulk crystal structure of the fluorapatite was obtained from the American Mineralogist Crystal Structure Database (AMCSD). The lattice parameters were calculated as $a = b = 9.457$ Å and $c = 6.883$ Å, which were in good agreement with the experimental results ($a = b = 9.375$ Å and $c = 6.887$ Å) (Comodi et al., 2001). As shown in **Figure 1**, each fluorapatite bulk possesses two $Ca_5(PO_4)_3F$ structures along the (001) plane, with the stacking sequence of Ca-$Ca_3(PO_4)_3F$-Ca-Ca-$Ca_3(PO_4)_3F$-Ca. These adjacent Ca-1 and Ca-2 sites are rather different in that the columnar Ca-1 site is coordinated to nine oxygen atoms in the arrangement of a tricapped trigonal prism, while the mirror Ca-2 site is in the $Ca_3(PO_4)_3F$ layer and bonds to six oxygen atoms and the column anion F (Hughes and Rakovan, 2002). However, the oxygen atoms are not very different, and they are marked for the sake of data discussion. The most stable surface was chosen, though there are different kinds of terminations along the (001) plane (Qiu et al., 2017). After testing, the (22) fluorapatite (001) surface structure with fifteen atomic layers was constructed, and the five bottom-most atomic layers were fixed to the bulk (see **Figure 2**). The vacuum gap of 30 Å in the z-direction was sufficient for our investigation.

The optimization of a single H_2O molecule was performed in a 10 × 10 × 10Å cubic cell, and the calculated results (see **Figure 3A**) are close to the experimental observations (Zhao et al., 2014; Chen et al., 2017). Adsorption clusters of three layers of water molecules (see **Figure 3B**) were optimized with the same condition, which was used to simulate the natural state of water.

The adsorption energy of H_2O on the fluorapatite surface is calculated by the following equation (Zhao et al., 2015):

$$E_{ads} = E_{H_2O/surface} - E_{H_2O} - E_{surface} \quad (1)$$

where E_{ads} is the adsorption energy, E_{H_2O} is the energy of the H_2O calculated in a cubic cell, $E_{surface}$ is the energy of the fluorapatite slab, and $E_{H_2O/surface}$ is the energy of the fluorapatite slab with adsorbed H_2O.

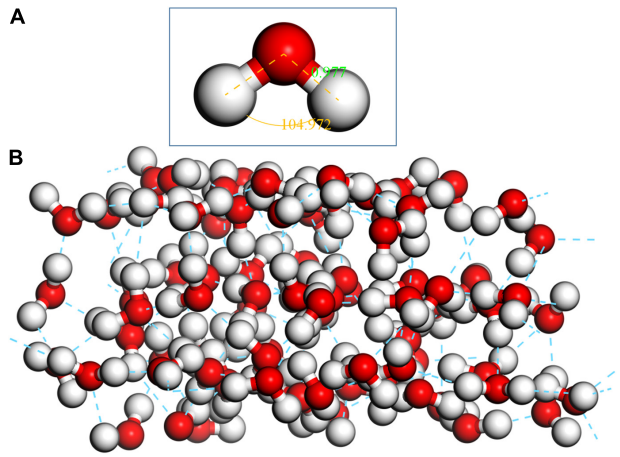

FIGURE 3 | Optimized single H_2O molecule and three-layer water cluster, **(A)** single H_2O molecule; **(B)** three-layer water cluster.

RESULTS AND DISCUSSION

Adsorption of a Single H_2O Molecule on the Fluorapatite (001) Surface

As shown in **Figure 2**, the exposed atoms of the fluorapatite (001) surface can be divided into three parts. The Ca-1 atoms occupy the first layer, and the other atoms in the second layer can be divided into two parts, the O-1 atom in the first sublayer and Ca-2, P, O-2, and O-3 atoms in the second sublayer. So from top to bottom are Ca-1 atoms, O-1 atoms, and then Ca-2, P, O-2,

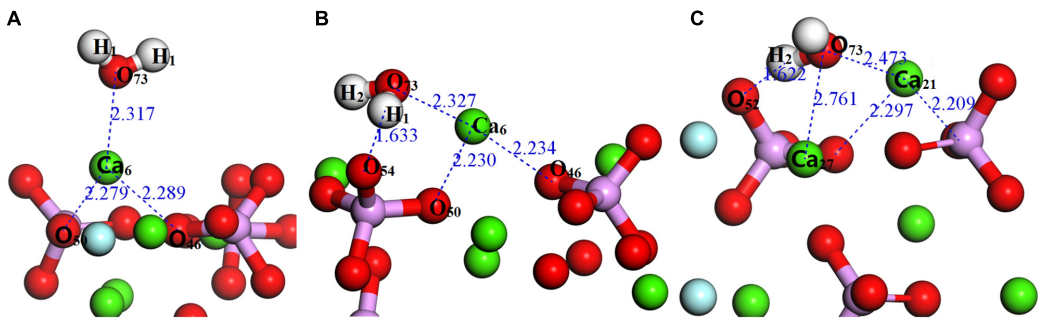

FIGURE 4 | Configurations of a single H_2O molecule on the fluorapatite (001) surface: **(A)** single-adsorption; **(B)** double-site adsorption; **(C)**: three-site adsorption.

and O-3 atoms. Usually, the tetrahedral PO_4-group is considered indivisible in reactions, so the potential centers are divided into four parts, Ca-1, Ca-2, PO_4-group, and F sites. It is worth noting that the F and Ca-2 atoms are not as active as other atoms, such as Ca-1 and O atoms, during the single H_2O molecule adsorption; the optimized stable configurations are shown in **Figure 4**.

As seen in **Figure 4A**, the length between O_{73} and Ca_6 is 2.317 Å, which is close to that of the Ca–O bond in the bulk. Meanwhile, the calculated E_{ads} is −64.817 kJ/mol, confirming that the interaction between the Ca and O atoms is rather strong. As shown in **Table 1**, the O_{73} atom exhibits the ability to gain electrons, and its 2p state increases from 5.13 to 5.16e, while the Ca_6 atom shows some electron-donating behavior and the main electron loss orbital is its 4s state (from 2.20 to 2.12e). The configuration of the H_2O molecule changes very little, which suggests that this kind of adsorption is insufficient to initiate the decomposition of the H_2O molecule.

For further study, DOS analysis of the single-site H_2O adsorption on the fluorapatite (001) surface is presented. As revealed in **Figure 5**, the DOS of the H_2O molecule has a distinct shift to the lower energy area after absorbing on the (001) surface of fluorapatite. For the Ca_6, the peak in the conduction band contributed by the 3s state has been greatly weakened. Significant overlap is seen in the range from 2 to 3.5 eV, which is contributed by the O 2p and Ca 3s states. In addition, some bonding interactions also can be observed in the range from −8 to −4eV and 2 to 3eV.

Figure 4B shows the double-site adsorption configuration of the H_2O molecule on the fluorapatite (001) surface. It is found that strong bonding interaction exists between O_{73} and Ca_6, with a distance of 2.327 Å (see **Table 2**). Meanwhile, a hydrogen bond is also observed with a $H_1 \ldots O_{54}$ distance of 1.633 Å, and the corresponding angle of O_{73}–H_2–O_{54} is 160.89°. In addition, the bonding length of O_{73} and H_1, O_{73}, and H_2 in the H_2O molecule is increased from 0.974 to 1.038 Å and 0.9780 Å, respectively, and

TABLE 1 | Charge transfer and bond properties of single-site adsorption.

	Atom	s (before)	p (before)
H_2O molecule	H_1	0.45 (0.48)	0 (0)
	H_2	0.45 (0.48)	0 (0)
	O_{73}	1.89 (1.90)	5.16 (5.13)
Fluorapatite	Ca_6 (Ca-1 site)	2.12 (2.20)	5.99 (6.02)
Bond		**Population (before)**	**Length/Å (before)**
O_{73}–H_1		0.52 (0.51)	0.977 (0.974)
O_{73}–H_2		0.52 (0.51)	0.978 (0.974)
O_{73}–Ca_6		0.09	2.317
Angle			**θ/°**
H_1–O_{73}–H_2			106.54

TABLE 2 | Charge transfer and bond properties of the double-site adsorption.

	Atom	s (before)	p (before)
H_2O molecule	H_1	0.55 (0.48)	0 (0)
	H_2	0.48 (0.48)	0 (0)
	O_{73}	1.89 (1.90)	5. (5.13)
Fluorapatite	O_{54} (O-1 site)	1.88 (1.89)	5.18 (5.22)
	Ca_6 (Ca-1 site)	2.11 (2.2)	5.99 (6.02)
Bond		**Population (before)**	**Length/Å (before)**
O_{73}–H_1		0.47	1.038 (0.974)
O_{73}–H_2		0.53	0.978 (0.974)
$O_{54}\ldots H_1$		0.17	1.633
O_{73}–Ca_6		0.12	2.320
Angle			**θ/°**
H_1–O_{73}–H_2			104.14
O_{73}–$H_2\ldots O_{54}$			160.89

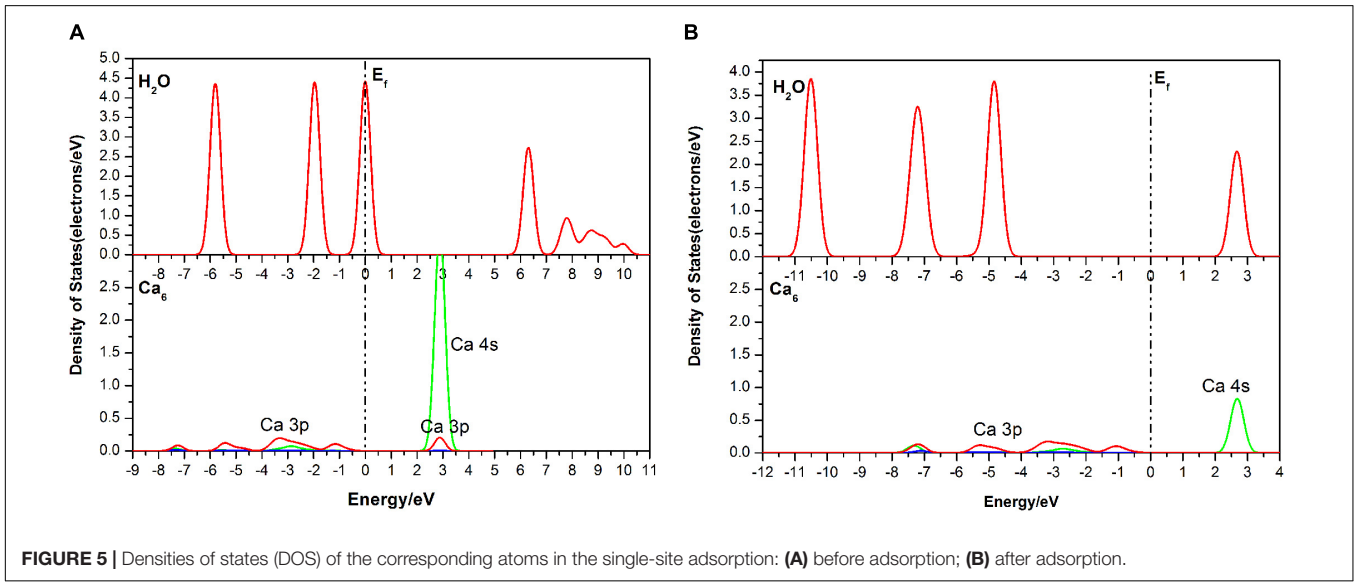

FIGURE 5 | Densities of states (DOS) of the corresponding atoms in the single-site adsorption: **(A)** before adsorption; **(B)** after adsorption.

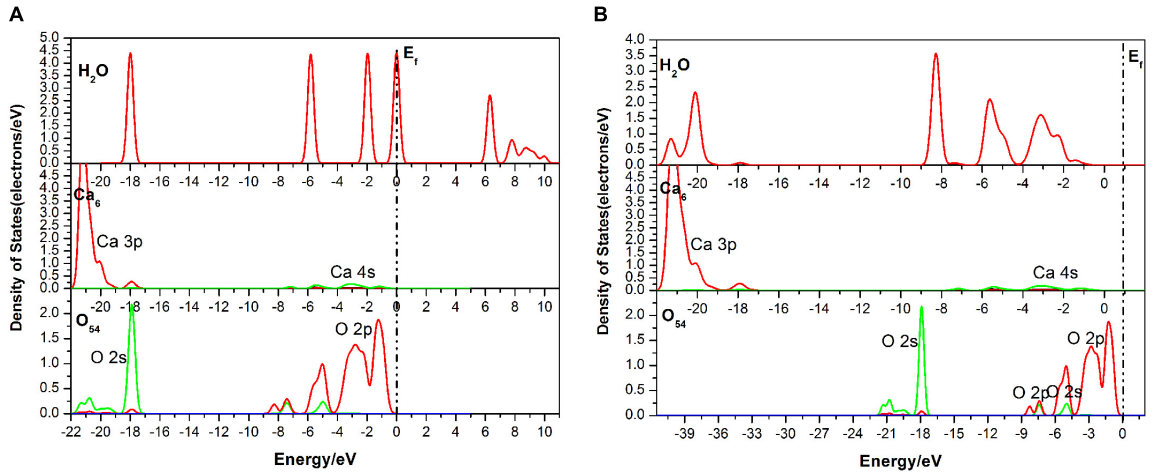

FIGURE 6 | Densities of states (DOS) of the corresponding atoms of the double-site adsorption: **(A)** before adsorption; **(B)** after adsorption.

TABLE 3 | Charge transfer and bond properties of the three-site adsorption.

	Atom	s (before)	p (before)
H_2O molecule	H_1	0.56 (0.48)	0 (0)
	H_2	0.62 (0.48)	0 (0)
	O_{73}	1.88 (1.90)	5.19 (5.13)
Fluorapatite	O_{50} (O-2 site)	1.88 (1.89)	5.2 (5.23)
	O_{54} (O-1 site)	1.89 (1.89)	5.22 (5.22)
	Ca_{21} (Ca-1 site)	2.16 (2.20)	6.11 (6.02)
	Ca_{27} (Ca-2 site)	2.20 (2.20)	6.04 (6.18)
Bond		**Population (before)**	**Length/Å (before)**
O_{73}–H_1		0.61	1.003 (0.974)
O_{73}–H_2		0.53	1.065 (0.974)
O_{52}...H_2		0.16	1.622
O_{73}–Ca_{12}		0.08	2.473
O_{73}–Ca_{27}		−0.06	2.761
Angle			**θ/°**
O_{73}–H_2...O_{52}			135.16
H_1–O_{73}–H_2			108.28

the calculated E_{ads} is −98.712 kJ/mol, which indicates that the H_2O molecule can be tightly adsorbed on the fluorapatite (001) surface. Further analysis shows that there are electron transfers between O_{73} and Ca_6 atoms and H_1 and O_{54} and that the O_{73} and H_1 gain electrons from 5.13 to 5.19e and 0.48 to 0.55e by their 2p state and 1s state, respectively.

As seen in **Figure 6**, the DOS of the H_2O molecule has the same distinct shift to the left and the structure changes greatly, with the valence bands mixing together from −6.51 to 0.05 eV, indicating strong charge transfer during the adsorption process. The apparent change for the Ca_6 is these peaks in the conduction band, which are contributed by 3p and 3d states. For the O_{54}, all of the bands move to the lower energy area. Meanwhile, the parts near the Fermi level contributed by the 2p state broaden, but the peak next to the Fermi level shows a decrease from 2.5 to 2 eV. The potential bonding interactions both for the H_2O–Ca_6 and H_2O–O_{54} systems are distributed near the top of the valence band.

As shown in **Figure 4C**, the length of O_{73} and Ca_{12}, Ca_{27} is 2.473 Å and 2.761 Å, and the obvious hydrogen bond of H_2 and O_{52} is 1.622 Å. Our calculated result shows that the E_{ads} is as large as −139.620 kJ/mol, which indicates that this configuration is very stable. **Table 3** shows that the 1s state of the H_1 and H_2 atoms in the H_2O increases from 0.52 to 0.44e and 0.38e, respectively, and that the O_{73} atom gains electrons mainly by the 2p state from 5.13 to 5.19e. At the fluorapatite (001) surface, the Ca_{21} in the Ca-1 site gains more charge and its value increase from 1.66 to 1.73e, while the 3s and 3p states lose 0.04 and 0.07e electrons, respectively. The change in the O–H bond length in the H_2O seems more apparent than in the other two configurations, but the results are still very minor; too small to cause the H_2O molecule to decompose. The angles of O_{73}–H_2...O_{52} are 135.16°.

It is seen in **Figure 7** that the DOS of the H_2O molecule has a distinct shift to the left, and the structure change greatly too, which indicates a strong charge transfer during the adsorption process. The obvious change of the Ca_{21} is that its peak at 2.7 eV contributed by the 4s state is weakened. For the Ca_{27}, its valence band, which is contributed by the 3p state, is broadened, and the peak at 20.5 eV is weakened from 7.32 to 5386 eV. The top valence band of the O_{52}, which is contributed by its 2p state, becomes wider and moves away from the Fermi level, which may affect its chemical properties. Meanwhile, the peak next to the Fermi level drops to 0.75 eV.

Adsorption Configurations of a Water Cluster on the Fluorapatite (001) Surface

The adsorption configuration of three layers of water molecules on the fluorapatite (001) surface was optimized and is shown in **Figure 8**. It is an interesting phenomenon that a transitional interfacial layer is formed containing water molecules and Ca atoms, which suggests that strong hydration occurs in this

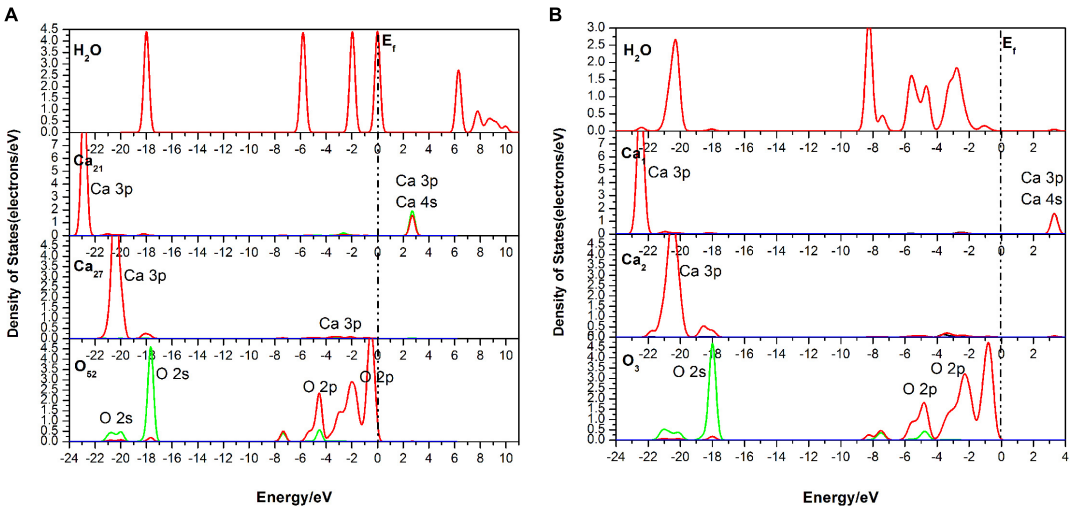

FIGURE 7 | Densities of states (DOS) of the corresponding atoms of the three-site adsorption: **(A)** before adsorption; **(B)** after adsorption.

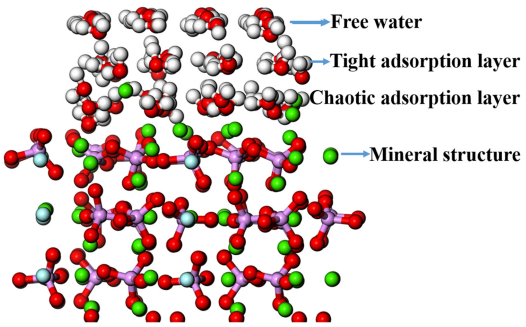

FIGURE 8 | Adsorption configuration of three layers of water molecules on the fluorapatite (001) surface.

region and that the fluorapatite (001) surface undergoes a drastic reconstitution. The whole area can be divided into four parts: the upmost layer is near-free water, the second is a tight adsorption layer, the third is a chaotic adsorption layer, and finally, the fourth layer is the mineral structure.

Table 4 shows the atomic displacement of the fluorapatite (001) surface. The calculation formula (Cui and Liu, 2010) is as follows:

$$\Delta d_i = \frac{d_{after} - d_{before}}{a} \times 100\% \quad (2)$$

Here, Δd_i represents the relative atomic coordinate shift of O, P, Ca, and F atoms; d_{before} is the corresponding pre-adsorption atomic coordinate; d_{after} represents the coordinate after adsorption; a refers to the bulk lattice parameter along the x-axis before geometry optimization.

The relative atomic displacements of the fluorapatite (001) surface are presented in **Table 4**. It is found that the Ca-1 sites in the first layer have the largest distorted displacements and

TABLE 4 | Atomic displacements of the fluorapatite (001) surface before and after adsorption.

Layer	Atom	Displacement/%		
		Δ*x*	Δ*y*	Δ*z*
1st	Ca-1	−16.961 ~ 7.427	−9.188 ~ 5.285	5.273 ~ 20.042
2nd	O1	0.165 ~ 3.963	−1.029 ~ −0.389	−5.448 ~ −3.194
	Ca-2	−6.576 ~ 6.318	−5.959 ~ 1.712	−3.046 ~ 14.153
	F	−1.262 ~ 3.834	−2.563 ~ 2.160	−10.521 ~ 1.933
	P	0.182 ~ 2.954	−2.152 ~ −0.389	−4.654 ~ −4.551
	O2	−0.318 ~ 5.443	−1.298 ~ 0.776	−6.842 ~ −5.102
	O3	0.894 ~ 32.275	2.133 ~ 16.534	−11.763 ~ −3.286
	O4	−2.319 ~ 0.375	−2.417 ~ −1.167	−3.018 ~ 6.352
3rd	Ca-1	−1.244 ~ −0.082	−1.167 ~ −1.442	−2.413 ~ 7.731
4th	Ca-2	−3.664 ~ −0.908	−4.433 ~ −1.263	−0.244 ~ 1.667

TABLE 5 | Summary of the current calculation and previous experimental results of the layer spacing of adsorbing water.

Structure	Surface	Distance/Å	
		First layer	Second layer
Current result	(001)	2.1	1.8
Park et al.*	(100)	2.64	1.53
Pareek et al. (partially hydrated)*	(001)	1.8	/
Pareek et al. (fully hydrated)*	(001)	1.6	1.58
Mkhonto, D. et al.	(001)	About 2.39	

**represents the test value.*

that the corresponding movements along the x-, y-, and z-axis directions are −16.961% ~ 7.427%, −9.188% ~ 5.285%, and 5.273% ~ 20.042%. The Ca-2 sites in the second layer possess the second-largest distorted displacements, and the main movement is −3.046% ~ 14.153% in the z-axis direction. The PO_4 group moves toward the vacuum region strongly in the negative z-axis

direction, which is in the opposite direction from the previous two Ca sites. The Ca-1 sites in both the third and fourth layers are quite stable, and their displacements along the *z*-axis direction are about 3 and 1%, respectively.

As shown in **Figure 8**, the displacement of the PO_4 group seems not to be large; however, the Ca-1 atoms have entered the water environment, and the Ca-2 atoms also show significant upward displacement, which means that the fluorapatite (001) surface is severely dissociated. This result can well explain the source of Ca^{2+} in slurry. However, we have noted that some experimental reports on the adsorption behavior on the fluorapatite (100) surface (Park et al., 2005; Pareek et al., 2007, 2008) seem a little different from our calculations, though the adsorption behaviors of the two surfaces are not much different. This discrepancy may be attributable to the dissolution of sensitive Ca-1 atoms during sample preparation. As shown in **Table 5**, if we take away the chaotic adsorption layer, then the result will be very close to the experimental value.

The bindings of the mineral structure and the chaotic adsorption layer are mainly contributed by the Ca-2 atoms with the Ca–O ionic bond. Each Ca atom is bonded to six O atoms, half of which come from the H_2O molecule, and the length of these newly formed bonds is 2.215∼ 2.439 Å. In addition, a few weak hydrogen bond interactions can be seen, which are contributed by the O atoms from PO_4 groups and the H atoms from H_2O molecules; their length is between 2.164 and 2.472 Å. The interactions in the chaotic adsorption layer are mainly due to the Ca–O ionic bond and the hydrogen bond; the latter comes from the H_2O molecule. Each Ca is surrounded by six H_2O molecules, which usually contain three molecules from the tight sorption layer. The lengths of the Ca–O bond and hydrogen bond are between 2.237 and 2.486 Å and from 1.903 to 1.956 Å, respectively. The lengths of the hydrogen bonds of the tight adsorption layer and free water layer are not much different and are basically between 1.913 and 1.967 Å; however, the lengths of the interlaminar hydrogen bonds of the latter are slightly greater than those of the former.

CONCLUSION

To investigate the effect of hydration behavior on the structure of fluorapatite, single H_2O molecule and three-layer cluster adsorptions on the fluorapatite (001) surface were performed by means of density functional theory. The conclusions can be summarized as follows:

(1) The H_2O molecule can form stable chemisorption structures with the fluorapatite (001) surface in the form of single-site, two-site, and three-site adsorption, each of which is associated with surface Ca atoms, especially those at the Ca-1 sites; the corresponding adsorption energies are 64.817, 98.712, and 139.620 kJ/mol. Ca atom can bind with the O of the H_2O molecule, with ionic interaction mainly contributed by the O 2p and Ca 4s states, and the length is about 2.3 Å, which is close to that of the Ca–O bond in the fluorapatite bulk.

(2) The adsorption configuration of a three-layer water cluster on the fluorapatite (001) surface shows serious hydration reconstruction at the interface and a transitional interfacial area containing water molecules where Ca atoms are formed. The lower layer of the transition area is dominated by Ca–O ionic bonding and the upper parts by hydrogen bonding. Further analysis shows that these six-coordinated Ca atoms are critical to the hydration behaviors of the transition area, as they can bind strongly to the H_2O molecules, with the newly formed Ca–O bonds being between 2.164 and 2.486 Å.

DATA AVAILABILITY STATEMENT

The datasets generated for this study are available on request to the corresponding authors.

AUTHOR CONTRIBUTIONS

JC: conceptualization and scheme. YC, WC, and XS: data curation. WC, XS, YL, YC, and CZ: formal analysis. JC, YC, and WC: investigation. JC: project administration. WC: writing–original draft.

ACKNOWLEDGMENTS

This research was funded by the National Natural Science Foundation of People's Republic of China (NSFC 51864003 and NSFC 51874106), Guangxi Natural Science Foundation (2018GXNSFAA050127 and 2018GXNSFAA281355), and Guangxi Key Laboratory of Processing for Non-ferrous Metals and Featured Materials (GXYSYF1811). The authors are thankful for this support.

REFERENCES

Chappell, H., Duer, M., Groom, N., Pickard, C., and Bristowe, P. (2008). Probing the surface structure of hydroxyapatite using NMR spectroscopy and first principles calculations. *Phys. Chem. Chem. Phys.* 10, 600–606. doi: 10.1039/B714512H

Chen, J., Chen, Y., Long, X., and Li, Y. (2017). DFT study of coadsorption of water and oxygen on galena (PbS) surface: an insight into the oxidation mechanism of galena. *Appl. Surf. Sci.* 420, 714–719. doi: 10.1016/j.apsusc.2017.05.199

Clark, S. J., Segall, M. D., Pickard, C. J., Hasnip, P. J., Probert, M. I. J., Refson, K., et al. (2005). First principles methods using CASTEP. *Z. Krist.* 220, 567–570. doi: 10.1524/zkri.220.5.567.65075

Comodi, P., Liu, Y., Zanazzi, P. F., and Montagnoli, M. (2001). Structural and vibrational behaviour of^{-} uorapatite with pressure . Part I: in situ single-crystal X-ray diffraction investigation. *Phys. Chem. Miner.* 28, 219–224.

Cui, J., and Liu, W. (2010). First-principles study of the (001) surface of cubic BiAlO3. *Phys. B Condens. Matter.* 405, 4687–4690. doi: 10.1016/j.physb.2010.08.063

Dan, E. S., Jarlbring, M., Antzutkin, O. N., and Forsling, W. (2006). A spectroscopic study of calcium surface sites and adsorbed iron species at aqueous fluorapatite by means of 1H and 31P MAS NMR. *Langmuir* 22:11060. doi: 10.1021/la0602158

Emsbo, P., McLaughlin, P. I., Breit, G. N., du Bray, E. A., and Koenig, A. E. (2015). Rare earth elements in sedimentary phosphate deposits: solution to the global REE crisis? *Gondwana Res.* 27, 776–785. doi: 10.1016/j.gr.2014.10.008

Haverty, D., Tofail, S. A. M., Stanton, K. T., and McMonagle, J. B. (2005). Structure and stability of hydroxyapatite: density functional calculation and rietveld analysis. *Phys. Rev. B* 71:094103. doi: 10.1103/PhysRevB.71.094103

Hughes, J. M., and Rakovan, J. (2002). The crystal structure of apatite, Ca5(PO4)3(F,OH,Cl). *Rev. Miner. Geochem.* 48, 1–12. doi: 10.2138/rmg.2002.48.1

Li, X., Zeng, H., Teng, L., and Chen, H. (2014). Comparative investigation on the crystal structure and cell behavior of rare-earth doped fluorescent apatite nanocrystals. *Mater. Lett.* 125, 78–81. doi: 10.1016/j.matlet.2014.03.151

Menéndez-Proupin, E., Cervantes-Rodríguez, S., Osorio-Pulgar, R., Franco-Cisterna, M., Camacho-Montes, H., and Fuentes, M. E. (2011). Computer simulation of elastic constants of hydroxyapatite and fluorapatite. *J. Mech. Behav. Biomed. Mater.* 4, 1011–1020. doi: 10.1016/j.jmbbm.2011.03.001

Mkhonto, D., and de Leeuw, N. H. (2002). A computer modelling study of the effect of water on the surface structure and morphology of fluorapatite: introducing a Ca10(PO4)6F2 potential model. *J. Mater. Chem.* 12, 2633–2642. doi: 10.1039/b204111

Okada, M., and Matsumoto, T. (2015). Synthesis and modification of apatite nanoparticles for use in dental and medical applications. *Jpn. Dent. Sci. Rev.* 51, 85–95. doi: 10.1016/j.jdsr.2015.03.004

Palazzo, B., Iafisco, M., Laforgia, M., Margiotta, N., Natile, G., Bianchi, C. L., et al. (2007). Biomimetic hydroxyapatite-drug nanocrystals as potential bone substitutes with antitumor drug delivery properties. *Adv. Funct. Mater.* 17, 2180–2188. doi: 10.1002/adfm.200600361

Pareek, A., Torrelles, X., Angermund, K., Rius, J., Magdans, U., and Gies, H. (2008). Structure of interfacial water on fluorapatite (100) surface. *Langmuir* 24, 2459–2464. doi: 10.1021/la701929p

Pareek, A., Torrelles, X., Angermund, K., Rius, J., Magdans, U., and Gies, H. (2009). Competitive adsorption of glycine and water on the fluorapatite (100) surface. *Langmuir* 25, 1453–1458. doi: 10.1021/la802706y

Pareek, A., Torrelles, X., Rius, J., Magdans, U., and Gies, H. (2007). Role of water in the surface relaxation of the fluorapatite (100) surface by grazing incidence x-ray diffraction. *Phys. Rev. B Condens. Matter Mater. Phys.* 75, 1–6. doi: 10.1103/PhysRevB.75.035418

Park, C., Fenter, P., Zhang, Z., Cheng, L., and Sturchio, N. C. (2005). Structure of the fluorapatite (100)-water interface by high-resolution X-ray reflectivity. *Am. Miner.* 89, 1647–1654. doi: 10.2138/am-2004-11-1209

Qiu, Y.-Q., Cui, W.-Y., Li, L.-J., Ye, J.-J., Wang, J., and Zhang, Q. (2017). Structural, electronic properties with different terminations for fluorapatite (001) surface: a first-principles investigation. *Comput. Mater. Sci.* 126, 132–138. doi: 10.1016/j.commatsci.2016.09.027

Rawashdeh, R., and Maxwell, P. (2011). The evolution and prospects of the phosphate industry. *Miner. Econ.* 24, 15–27. doi: 10.1007/s13563-011-0003-8

Rey, C., Combes, C., Drouet, C., Cazalbou, S., and Sarda, S. (2014). Surface properties of biomimetic nanocrystalline apatites; applications in biomaterials. *Prog. Cryst. Growth Charact. Mater.* 60, 63–73. doi: 10.1016/j.pcrysgrow.2014.09.005

Rulis, P., Ouyang, L., and Ching, W. Y. (2004). Electronic structure and bonding in calcium apatite crystals: hydroxyapatite, fluorapatite, chlorapatite, and bromapatite. *Phys. Rev. B Condens. Matter Mater. Phys.* 70, 1–8. doi: 10.1103/PhysRevB.70.155104

Rulis, P., Ouyang, L., and Ching, W. Y. (2007). Electronic structure, bonding, charge distribution, and x-ray absorption spectra of the (001) surfaces of fluorapatite and hydroxyapatite from first principles. *Phys. Rev. B. Condens. Matter* 24, 1–8. doi: 10.1103/PhysRevB.76.245410

Santos, M. A., Santana, R. C., Capponi, F., Ataíde, C. H., and Barrozo, M. A. S. (2010). Effect of ionic species on the performance of apatite flotation. *Sep. Purif. Technol.* 76, 15–20. doi: 10.1016/j.seppur.2010.09.014

Scholz, R. W., Roy, A. H., Brand, F. S., and Hellums, D. T. (eds) (2014). *Sustainable Phosphorus Management*. Berlin: Springer, doi: 10.1007/978-94-007-7250-2

Zhang, P. (2014). Comprehensive recovery and sustainable development of phosphate resources. *Proc. Eng.* 83, 37–51. doi: 10.1016/j.proeng.2014.09.010

Zhao, C., Chen, J., Li, Y., Huang, D. W., and Li, W. (2015). DFT study of interactions between calcium hydroxyl ions and pyrite, marcasite, pyrrhotite surfaces. *Appl. Surf. Sci.* 355, 577–581. doi: 10.1016/j.apsusc.2015.07.081

Zhao, C., Chen, J., Long, X., and Guo, J. (2014). Study of H2O adsorption on sulfides surfaces and thermokinetic analysis. *J. Ind. Eng. Chem.* 20, 605–609. doi: 10.1016/j.jiec.2013.05.021

Conflict of Interest: The authors declare that the research was conducted in the absence of any commercial or financial relationships that could be construed as a potential conflict of interest.

frontiers in Chemistry

ORIGINAL RESEARCH
published: 18 March 2020
doi: 10.3389/fchem.2020.00079

The Behavior of Gangue During the Flotation of a Sulfidic PGM-Bearing Ore in Response to Various Monovalent and Divalent Ions in Process Water

Malibongwe Shadrach Manono, Kirsten Claire Corin and Jennifer Gael Wiese*

Centre for Minerals Research, Department of Chemical Engineering, University of Cape Town, Cape Town, South Africa

OPEN ACCESS

Edited by:
Zhiyong Gao,
Central South University, China

Reviewed by:
Thuat Thanh Trinh,
Norwegian University of Science and Technology, Norway
Sugata Chowdhury,
National Institute of Standards and Technology (NIST), United States

****Correspondence:***
Malibongwe Shadrach Manono
malibongwe.manono@uct.ac.za

Specialty section:
This article was submitted to Physical Chemistry and Chemical Physics, a section of the journal Frontiers in Chemistry

Received: *29 October 2019*
Accepted: *23 January 2020*
Published: *18 March 2020*

Citation:
Manono MS, Corin KC and Wiese JG (2020) The Behavior of Gangue During the Flotation of a Sulfidic PGM-Bearing Ore in Response to Various Monovalent and Divalent Ions in Process Water. Front. Chem. 8:79. doi: 10.3389/fchem.2020.00079

Mineral concentrators are becoming increasingly aware of the importance of the quality of the water that they feed into their milling and flotation circuits. It is speculated that different inorganic constituents of process water may yield different flotation results owing to the electrolyte–reagent–mineral interactions occurring in the pulp phase. These interactions are said to be specific to ion type, reagent type, and mineral or ore type. It therefore stands to reason that there is a need to develop an understanding of the specific ion effects on both the pulp phase and the froth phase phenomena, such that the chemistry and the quality of process water can be monitored and controlled in a manner that does not negatively affect the flotation performance. Previous research has shown that inorganic electrolytes may impact the hydrophobicity and the floatability of mineral particles and could in turn affect froth stability, entrainment, and thus mineral grades and recoveries. In this study, the floatability of a Cu-Ni-PGM-bearing Merensky ore is tested on a bench-scale flotation system in various single salt solutions, *viz*., $CaCl_2$, $CaSO_4$, $Ca(NO_3)_2$, $MgCl_2$, $Mg(NO_3)_2$, $MgSO_4$, NaCl, $NaNO_3$, and Na_2SO_4, in order to examine specific ion effects on gangue recovery. Coagulation and zeta potential tests are conducted in order to establish the nature of the impact that specific ions have on the behavior of gangue in flotation. The findings of this work have shown that single salt solutions containing NO_3^- ions resulted in a strong depression of gangue compared to those solutions containing Cl^- and SO_4^{2-} ions. It was also shown that the divalent Ca^{2+} and Mg^{2+} showed a stronger depression of gangue compared to the monovalent Na^+. Ca^{2+}, in comparison to Na^+, resulted in an increase in the coagulation of the ore as well as an increase in the zeta potential of talc. Overall, the findings of this paper suggest that the presence of Ca^{2+} and Mg^{2+} in process water would most likely create conditions that promote gangue depression.

Keywords: flotation, gangue, inorganic electrolytes, ions, sulfides, talc, water

RESEARCH KEY HIGHLIGHTS

- Solutions containing NO_3^- and Ca^{2+} increased the depression of gangue as shown by lower gangue recoveries.
- The concentrate grades were higher in solutions containing Ca^{2+} and NO_3^- compared to those which contained Na^+, Cl^-, and SO_4^{2-}.
- Ca^{2+} and NO_3^- resulted in a less negative zeta potential compared to Na^+ and SO_4^{2-}.
- Coagulation was enhanced in Ca^{2+}- and NO_3^--containing solutions.
- Ca^{2+}-containing process waters could be beneficial for floatable gangue depression.

INTRODUCTION

It is acknowledged that water should be considered as a reagent in flotation and, as such, the quality of process water becomes an important factor to consider as it may alter the pulp chemistry and thereby affect the flotation (Corin et al., 2011; Corin and Wiese, 2014). Previous work considered specific ions present in process water and their effects on the flotation of a Cu-Ni-PGM ore (Manono et al., 2016). Much of the conclusions made from Manono et al. (2016) gave rise to speculations of ions, being there in process water, which promoted gangue depression better than others. However, there was no fundamental evidence to support the speculation of an enhancement of gangue depression. Thus, the purpose of this study is to ascertain whether there are specific ion effects on gangue depression. As the separation of value-bearing minerals from the non-value-bearing gangue minerals is the core and fundamental purpose of flotation, the depression of gangue as a critical aspect of flotation is important to consider. Rao and Finch (1989) demonstrated that recycled water may negatively affect mineral recoveries and grades owing to an accumulation of inorganic and organic substances which alter the pulp chemistry and thereby affect the flotation. A study conducted by Muzenda (2010) showed that recycled process water containing Cu^{2+}, Pb^{2+}, and Fe^{2+} had adverse effects on the flotation of a PGM ore from the UG2 reef of the Bushveld Igneous Complex of South Africa in that there occurred an inadvertent activation of non-sulfide gangue which decreased the concentrate grades. This could be explained by a more recent study by Liu et al. (2014) which suggested that some electrolytes in process water could inhibit the adsorption of xanthates on sulfide minerals due to competition for adsorption onto the mineral surface. Also, Castro et al. (2013) showed that the flotation of molybdenite in the presence of Mg^{2+} ions resulted in molybdenite depression due to the presence of magnesium hydroxyl complexes and colloidal magnesium hydroxide coatings on molybdenite particles, rendering them hydrophilic. Laskowski et al. (2007) also showed that the presence of high Ca^{2+} concentration in process water improved the adsorption of CMC onto talc through an acid–base interaction and thus promoted the depression of talc. Biçak et al. (2012) concluded that dissolved metal ions and sulfide ions mainly in the form of SO_4^{2-} and $S_2O_3^{2-}$ alter the surface chemistry of minerals in the pulp phase. Ikumapayi et al. (2012) also showed that galena was

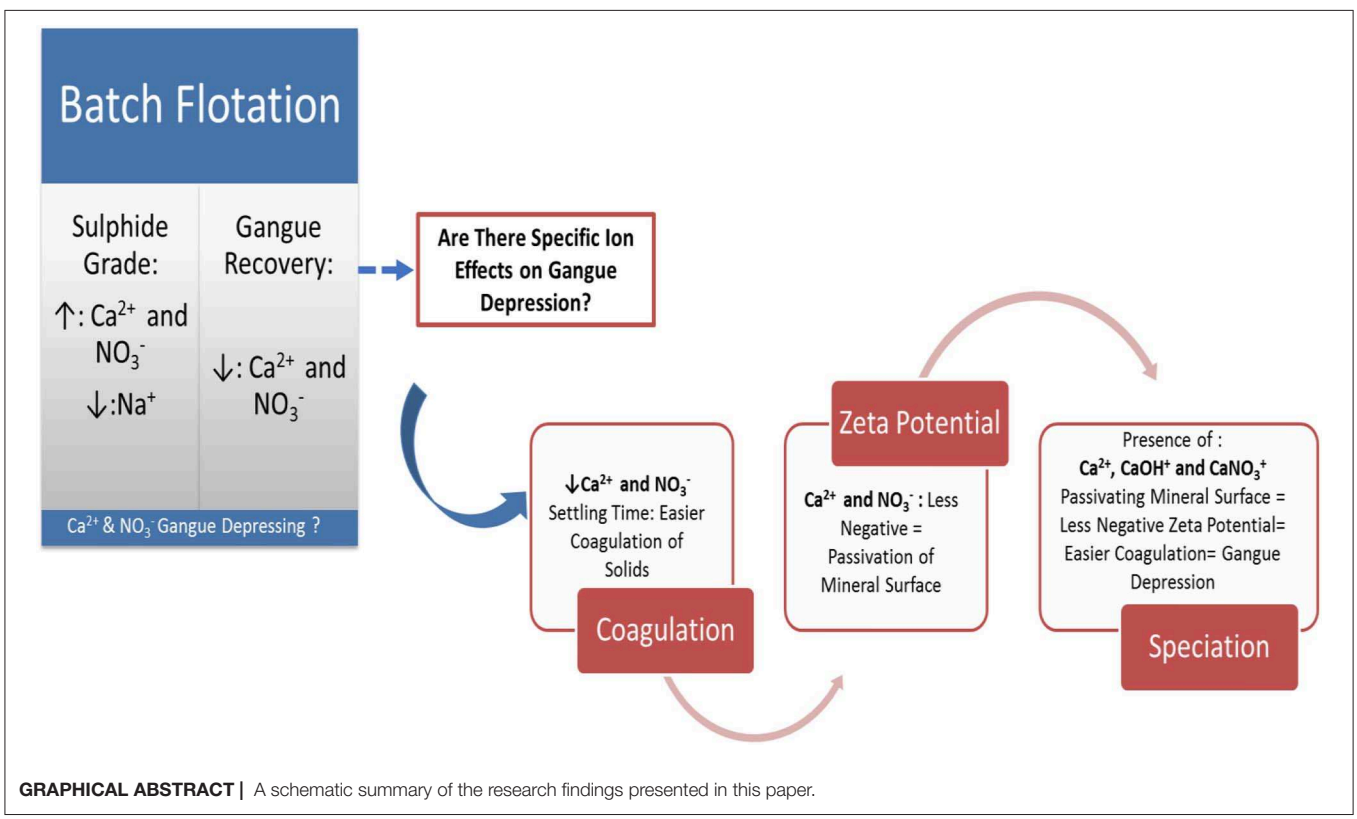

GRAPHICAL ABSTRACT | A schematic summary of the research findings presented in this paper.

TABLE 1 | Chemical compositions of synthetic plant water and the various single salt solutions tested in this study.

Water type	Ca^{2+} (mg/l)	Mg^{2+} (mg/l)	Na^{+} (mg/l)	Cl^{-} (mg/l)	SO_4^{2-} (mg/l)	NO_3^{-} (mg/l)	CO_3^{2-} (mg/l)	Total dissolved solids (mg/l)	Ionic strength [M]
1SPW	80	70	153	287	240	176	17	1,023	0.0213
NaCl	-	-	490	755	-	-	-	1,245	0.0213
Na_2SO_4	-	-	326	-	682	-	-	1,009	0.0213
$NaNO_3$	-	-	490	-	-	1,321	-	1,810	0.0213
$CaCl_2$	285	-	-	503	-	-	-	788	0.0213
$CaSO_4$	213	-	-	-	512	-	-	725	0.0213
$Ca(NO_3)_2$	285	-	-	-	-	880	-	1,165	0.0213
$MgCl_2$	-	173	-	503	-	-	-	676	0.0213
$MgSO_4$	-	129	-	-	512	-	-	641	0.0213
$Mg(NO_3)_2$	-	173		-	-	880	-	1,053	0.0213

more passivated in Ca^{2+} and SO_4^{2-} and, as a result, mineral recoveries were reduced. Shackleton et al. (2012) investigated the water quality effects on moncheite–pyroxene and pentlandite–pyroxene composites and proposed that ions found in process waters passivated the mineral surfaces and inhibited the collector adsorption, thereby reducing the floatability of moncheite, pentlandite, and pyroxene. Their findings also suggested that the specific ions in the process water played a far more significant role compared to the overall ionic strength of the process water. This therefore forms the basis of the work carried out in the study presented in this paper. It is evident, from the literature presented, that fundamental, robust, and more comprehensive studies on the effects of specific inorganic electrolytes on the floatability of sulfidic PGM ores are needed. Knowledge of the influence of each specific process water constituent on flotation is vital as it would potentially have both technical and financial benefits in that costs could be saved on wastewater treatment if research proves that some flotation circuits could still perform at their best in recycled process water containing constituents such as inorganic electrolytes which would have been removed due to limited knowledge of their specific impact on flotation performance. Such in-depth research knowledge is crucial in the development and implementation of closed water circuits in mineral concentrators. It is anticipated that understanding the impact of different process water constituents, leading to a successful implementation of closed water circuits, will contribute toward the sustainability of mineral concentrators as a result of minimal or zero process water discharge to the environment, minimal make-up water requirement, a reduction in process water treatment before reuse, savings on treatment costs, and a reduction in fresh reagent dosing. Thus, the aim of this study is to ascertain whether there are ions in flotation with dominant effects on the gangue depression of a Merensky ore. Talc is used as proxy for the naturally floatable gangue common in Merensky ores.

MATERIALS AND METHODS

Synthetic Plant Water and Single Salt Quality

Synthetic plant water (hereafter referred to as 1SPW or 1Plant) and various single salt solutions of the ionic strength and the chemical compositions shown in **Table 1** were prepared. These aqueous synthetic plant water and single salt solutions were made from distilled water and inorganic salts to ensure that the concentration of the water contained the required total dissolved solids and ionic strength as shown in **Table 1**.

Ore Preparation and Milling

A Cu-Ni-PGM-containing ore from the Merensky reef, within the Bushveld Igneous Complex of South Africa, was used throughout the bench-scale flotation tests. The bulk sample was crushed, riffled, and split into samples weighing 1 kg using a rotary splitter. The 1-kg ore samples were milled in a tumbling mill in the presence of the particular water type under study in order to make a slurry of 66% solids in the mill at the end of milling. Sodium isobutyl xanthate, which was supplied by Senmin, was used as the collector and dosed into the mill at a dosage of 150 g/t. The mill was operated so as to achieve a grind size of 60% passing 75 μm. It is important to note that this grind is typical of industrial concentrator rougher circuits concentrating on Merensky ores. The grinding media was comprised of 20 stainless steel rods with varying diameters: 6 × 25 mm, 8 × 20 mm, 6 × 16 mm. The milled slurry was transferred into a 3-L UCT Barker batch flotation cell immediately. The mineral composition of this ore is shown in **Table 2**. Pyrrhotite, pentlandite, and chalcopyrite are the main base metal sulfides; these form about 1% of the overall ore feed grade, with the rest being gangue minerals.

Batch Flotation

The standard UCT bench-scale batch flotation procedure was employed on a 3-L Barker cell. The milled slurry was transferred to the cell, and the single salt solution under investigation was added to the cell in order to ensure a pulp density of 35%; thereafter, the impeller was switched on and set to an agitation speed of 1,200 rpm. A syringe was used to draw out a feed sample (which would later be filtered, dried, and weighed for Cu, Ni, and S assays). A polyglycol frother in the form of DOW 200 supplied by Betachem was added to the cell at a dosage of 40 g/t and allowed to condition for 1 min, after which the air supply valve to the cell was opened in order to ensure a constant volumetric air flow rate of 7 L/min. A froth build-up occurred until a constant froth height of 2 cm. Four concentrates were scraped in 15-s

intervals and collected at 2, 4, 6, and 10 min into concentrate dishes named C1, C2, C3, and C4, respectively. Once all of the four concentrates were collected, the air supply was switched off; a tails sample was also taken thereafter. The concentrates were weighed in order to account for the amount of water reporting to the concentrate, and thereafter the samples were filtered, dried, weighed, and analyzed for Cu, Ni, and S in the UCT Chemical Engineering Analytical Services Laboratory using XRF and Leco. All tests were performed in duplicates, and the error bars are shown in the batch flotation results. Batch flotation tests were performed at room temperature (25°C).

Solid Settling Tests

Settling tests were performed for single salt solutions of $CaCl_2$, $CaSO_4$, $Ca(NO_3)_2$, NaCl, $NaNO_3$, and Na_2SO_4 at a total ionic strength of 0.0213 mol dm^{-3}, with each test performed in duplicate. These salts were carefully selected as they showed the most interesting effects on gangue recovery during the flotation of the selected Cu-Ni-PGM ore. Nine grams of Merensky ore were added to 90 ml of the water under investigation in a 100-ml glass beaker to make a slurry containing 10% solids. The contents of the glass beaker were mixed adequately for 1 min using a magnetic stirrer. The pH of the suspension was adjusted to pH 9 using stock/dilute solutions of NaOH or HCl. The suspension was allowed to mix at 500 rpm for 4 min in order to disperse the mixture immediately after pH adjustment. The slurry was then carefully transferred to a 100-ml graduated cylinder. The graduated cylinder was carefully monitored until a clear supernatant liquid was observed against a clear background. A picture was taken, printed, and stuck next to the working bench to serve as a basis for the clear supernatant liquid for the remaining tests. The time taken to reach equivalent settling was recorded. Settling tests were conducted at room temperature (25°C).

Zeta Potential Measurements on Talc

A Malvern Zetasizer 4 was used to measure the zeta potential of talc at varying pH values. Talc was crushed using a hammer and pulverized thereafter. This was sieved and screened to 100% passing 25 μm. Single salt solutions of $Ca(NO_3)_2$, $CaSO_4$, $NaNO_3$, and Na_2SO_4 were used as dispersants on the Malvern Zetasizer 4. Mg^{2+} salts were excluded since Ca^{2+} and Mg^{2+} showed similar flotation results. Na^{+} salts were included since these showed different flotation results compared to the two (Ca^{2+} and Mg^{2+}) divalent cations. Furthermore, zeta potential measurements on talc, performed in the presence of $CaCl_2$, $MgCl_2$, and NaCl, are reported in Manono et al. (2019); hence, they are not shown in this paper. For each tested single salt solution [i.e., $Ca(NO_3)_2$, $CaSO_4$, $NaNO_3$, or Na_2SO_4], six aliquots of 25 ml were measured and were adjusted to pH values of 2, 4, 6, 8, 10, and 12 using NaOH and HCl. These were allowed to condition for 20 min. Thereafter, 0.0625 g of talc was added to the 25 ml conditioned dispersant, stirred, and left to stand for 1 min. Two milliliters of the supernatant solution was then pipetted into the capillary tube and placed into the Malvern Zetasizer 4. A calibration time of 2 min was allowed, and each reading was taken three times. This procedure was repeated for all the different dispersants. Zeta potential measurements were conducted at room temperature (25°C).

TABLE 2 | Modal composition: sulfide and gangue minerals present in the ore as determined by QEMSCAN.

Mineral	%
Pentlandite	0.31
Chalcopyrite	0.25
Pyrrhotite	0.44
Pyrite	0.08
Other sulfides	0.02
Total sulfides	1.09
Plagioclase	43.38
Orthopyroxene	32.60
Olivine	0.59
Clinopyroxene	7.48
Talc	3.51
Serpentine	0.80
Chlorite	0.83
Phlogopite	0.46
Quartz	0.67
Calcite	0.18
Oxides	8.10
Other	0.32
Total	100.00

Inorganic Electrolyte Speciation

In order to investigate specific ion effects on interactions occurring in the pulp phase of flotation at the solid–water interface, inorganic electrolyte speciation calculations were carried out using the Visual MINTEQ (version 3.1). The Visual MINTEQ is an open-source chemical equilibrium modeling software for the prediction or calculation of ion speciation in water based on thermodynamic equilibrium data (Wang et al., 2016). Only single salt solutions of $Ca(NO_3)_2$, $CaSO_4$, $NaNO_3$, and Na_2SO_4 were subjected to the Visual MINTEQ for ion speciation over a pH range of 2–12. Temperature was set at 25°C.

Statistical Analyses

Statistical analyses were carried out using the Minitab 18.1 Analysis of Means (ANOM). This method uses the output means (e.g., %S grades) for all conditions and calculates an overall or grand mean. It then compares the single test condition output against the total grand mean calculated from all conditions. This would be such that if an output mean for a specific condition falls below the lower bound of the confidence interval, it would be said that the specific test condition resulted in an output mean significantly lower than the total grand mean, whereas if the output fell outside the upper bound of the 95% confidence interval, that condition is said to have resulted in an output that is significantly higher than the total grand mean. However, if a specific test condition resulted in an output that fell within the confidence interval, that output is said to be comparable with the total grand mean (i.e., there is no discernable statistical

difference between that specific test condition's finding and the total grand mean, and therefore it cannot be said that the specific test condition resulted in a lower or higher impact compared to the other tested conditions).

RESULTS

The Effect of Single Salts on Total Sulfides, Gangue and Water Recoveries, and Total Sulfide Grades

Figure 1 shows the total mass pull (i.e., the total amount of solids reporting to the concentrate) for all the inorganic electrolytic solutions. The mass pull is presented as two fractions, namely, the sulfides and the gangue. It is shown that the amount of sulfides reporting to the concentrate did not change with single salt type and the recovered mass of sulfides was the same as that recovered in the presence of synthetic plant water; these results are further supported by the ANOM performed on these data in **Figures 2, 3**, where it is shown that there is no significant difference between the means of the mass of sulfides obtained with different single salts and of that obtained with synthetic plant water. However, the amount of gangue reporting to the concentrate showed a dependence on the ions present in the single salt solution. $Ca(NO_3)_2$ and $CaCl_2$ resulted in a significant decrease in total gangue recovery compared to other single salts, while $NaNO_3$ resulted in a significant increase in gangue reporting to the concentrate as shown in **Figure 3**.

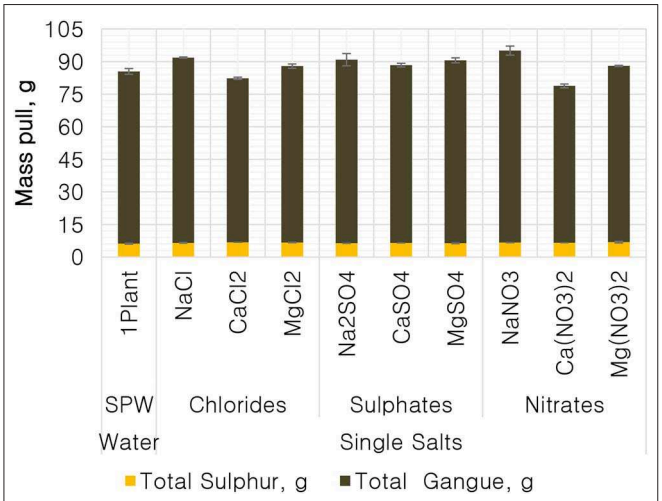

FIGURE 1 | The amount of solids, split into total sulfides and total gangue, reporting to the concentrate for all conditions tested.

Figure 4 shows the total sulfide recoveries and grades for all tested single salts and synthetic plant water. It is clear that the %S recovery remained unaffected by changes in the inorganic electrolyte solution type, whereas the %S grade proved to be susceptible to changes in the quality of the ionic solution as illustrated in **Figures 5**, **6**. $Ca(NO_3)_2$ and $CaCl_2$ resulted in significantly higher concentrate grades compared to all the other single salts as can be seen in **Figure 6**. It is also interesting to note that the Na^+-containing single salt solutions resulted in grades slightly lower than the grand mean shown by the ANOM presented in **Figure 6**.

Figure 7 shows the %S recovery as a function of the amount of water recovered for all tested single salts. According to **Figure 7**, all tested single salt solutions and synthetic plant water generally followed the same trend of a first-order model. It is shown that there was no difference in the recovery of total sulfides per gram of water regardless of the inorganic electrolyte solution used.

Figure 8 depicts the recovery of gangue per gram of water for the various single salts and the synthetic plant water. It is evident

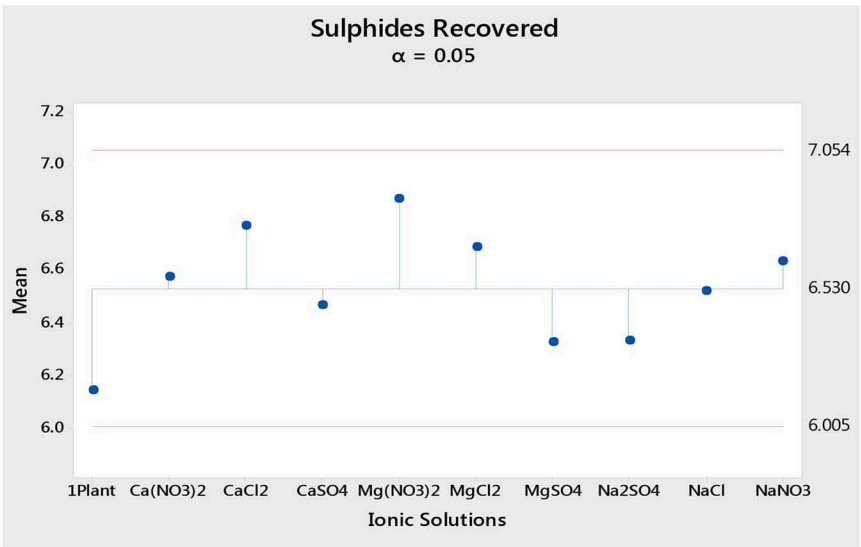

FIGURE 2 | Analysis of means of the amount of sulfides (in grams) reporting to the concentrate for all single salts and synthetic plant water.

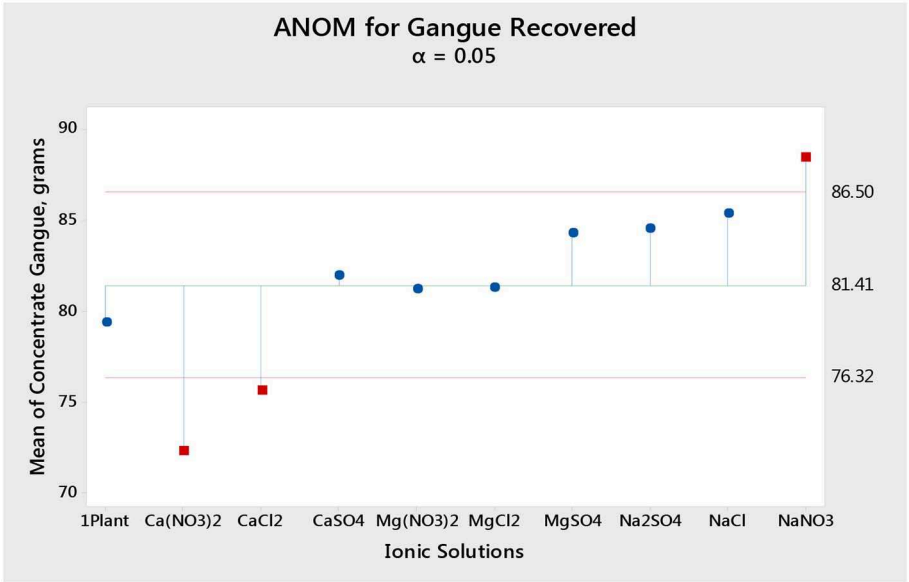

FIGURE 3 | Analysis of means (ANOM) of the amount of gangue reporting to the concentrate for all single salts and synthetic plant water.

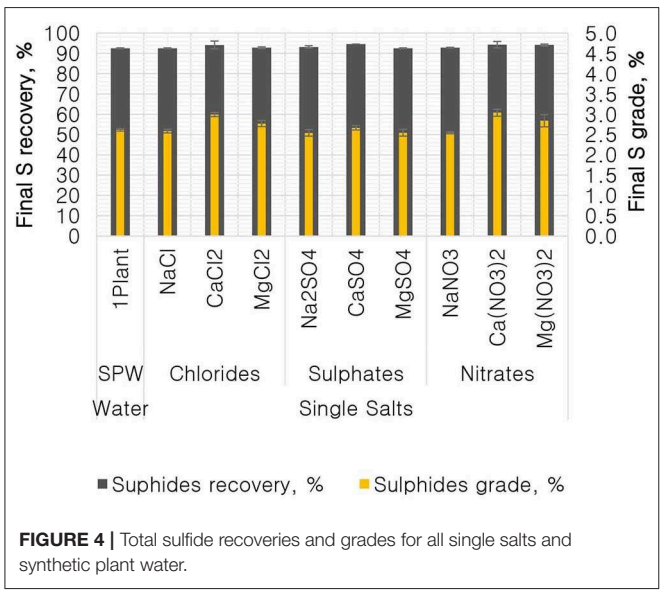

FIGURE 4 | Total sulfide recoveries and grades for all single salts and synthetic plant water.

that all single salt solutions containing the monovalent Na^+ resulted in higher gangue recovery per gram of water compared to that of the synthetic plant water and the single salt solutions containing divalent cations (Ca^{2+} and Mg^{2+}). Ca^{2+}- and Mg^{2+}-containing single salt solutions resulted in lower gangue per gram of water compared to that of synthetic plant water. Furthermore, for the Na^+ single salts, gangue recovery per gram of water was higher in the SO_4^{2-} solution compared to the Cl^-- and NO_3^--containing solutions. Moreover, of the divalent cation-containing single salts, Ca^{2+} resulted in lower gangue recovery per gram of water compared to Mg^{2+}.

The Effect of Single Salts on the Coagulation of the Selected Merensky Ore

Figure 9 shows the settling time of solids for a Merensky ore for various single salts as a proxy to cationic and anionic effect on coagulation. The Na^+-containing solutions resulted in longer settling times compared to the Ca^{2+}-containing solutions for every corresponding anion, suggesting a cation effect on coagulation with the divalent cation having a stronger coagulation effect compared to the monovalent cation. Moreover, for a fixed cation, SO_4^{2-} resulted in the longest settling time followed by Cl^-, while the NO_3^- anions resulted in the shortest settling time.

The Effect of Single Salts on the Zeta Potential of Talc

Figure 10 depicts the zeta potential of talc as a function of pH in various single salt solutions in order to investigate whether there are any ion (anion and cation)-specific effects on the zeta potential of talc. Firstly, it is evident that the monovalent Na^+ resulted in a highly negative zeta potential of talc across the studied pH range compared to solutions containing the divalent Ca^{2+}. Secondly, for both cations, NO_3^- resulted in a less negative zeta potential compared to SO_4^{2-} across the studied pH range. Generally at pH >4, Ca^{2+}-containing single salt solutions resulted in an increase in the potential of talc with increasing pH, to an extent that the zeta potential of talc became positive after pH 8 for $Ca(NO_3)_2$. However, an increase in pH resulted in a further decrease in the potential of talc in Na^+-containing solutions. A point of zero potential for talc is seen at pH 2 in $NaNO_3$, while two points of zero potential for talc are seen with $Ca(NO_3)_2$ at pH 3 and pH 9. It is worth noting that at pH 4 the two SO_4^{2-}-containing solutions resulted in similar talc potentials.

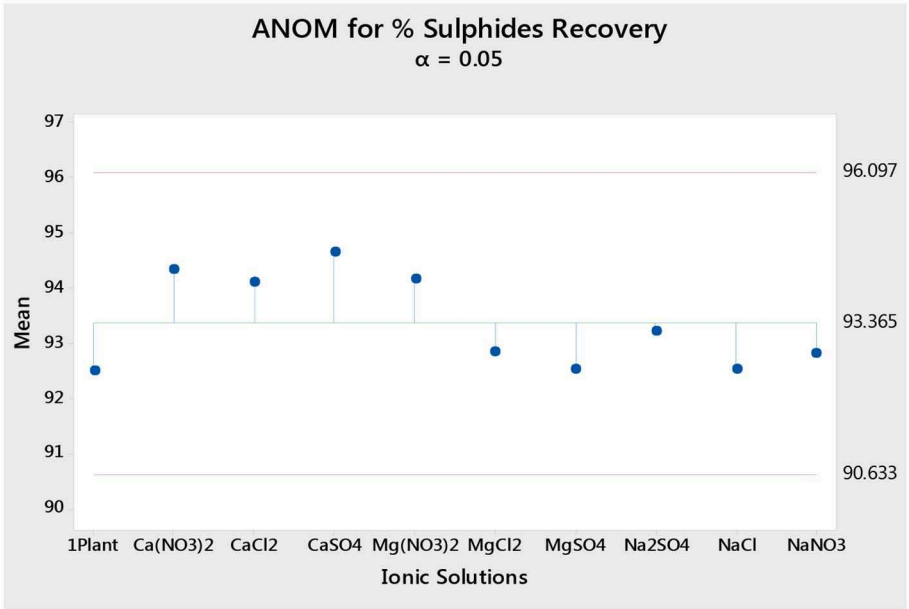

FIGURE 5 | Analysis of means (ANOM) of the total sulfide recovery for all single salts and synthetic plant water.

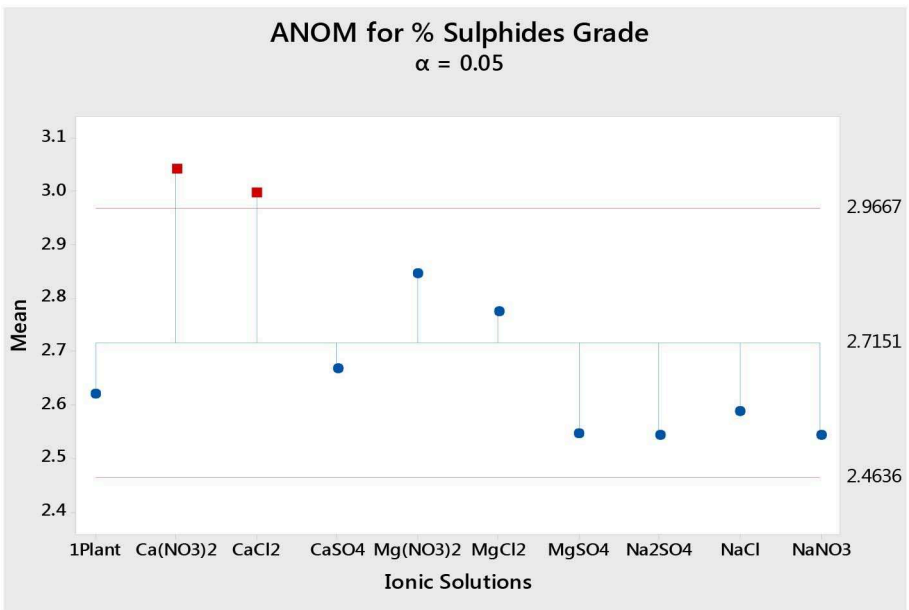

FIGURE 6 | Analysis of means (ANOM) of the total sulfides grade for all single salts and synthetic plant water.

The Speciation of Selected Single Salt Solutions

Figure 11 depicts the speciation of a $NaNO_3$ solution, with an ionic strength of 0.0213 mol dm^{-3}, generated through the Visual MINTEQ 3.1 software. The speciation of $NaNO_3$ shows that at pH 4 and below, the dominant species are Na^+, NO_3^-, and H^+, with all of the other species existing at comparably insignificant concentrations. At the pH range of 4–10, only Na^+ and NO_3^- are dominant and present in solution. Beyond pH 10, the concentration of OH^- rises together with the apparent formation of NaOH(aq) and $NaNO_3$(aq).

Figure 12 depicts the speciation of a Na_2SO_4 solution, with an ionic strength of 0.0213 mol dm^{-3}, generated through Visual MINTEQ 3.1 software. The speciation of Na_2SO_4 shows that

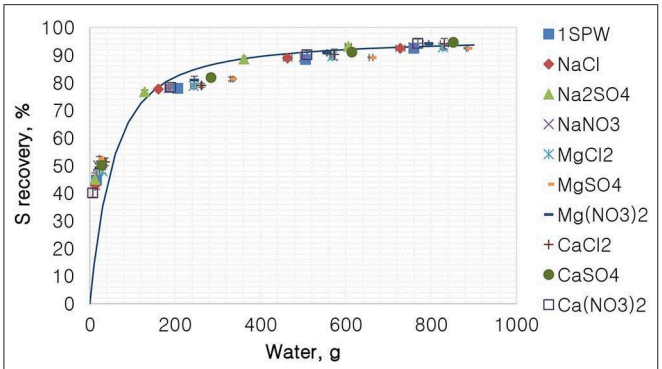

FIGURE 7 | The %S recovery vs. water for all single salts and synthetic plant water.

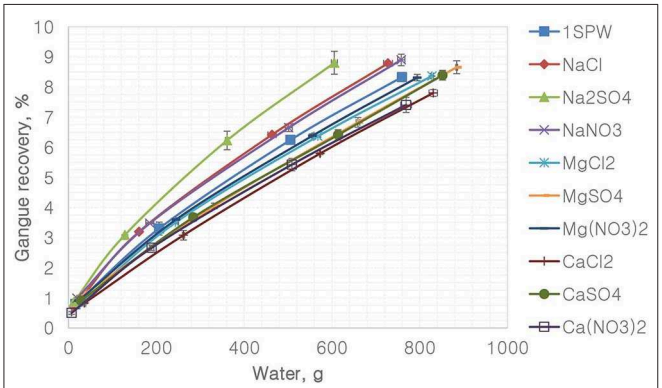

FIGURE 8 | Gangue recovery vs. water for all single salts and synthetic plant water.

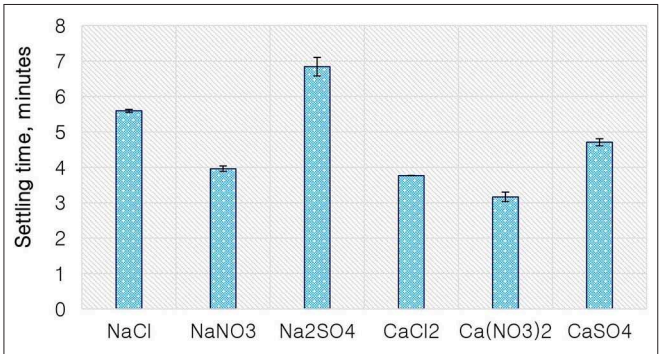

FIGURE 9 | Merensky ore solids settling time as a function of the single salts.

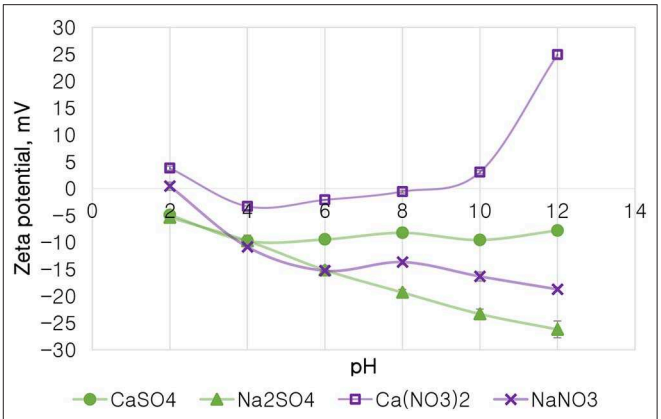

FIGURE 10 | The zeta potential of talc in single salt solutions of 0.0213 mol dm^{-3} ionic strength as a function of pH.

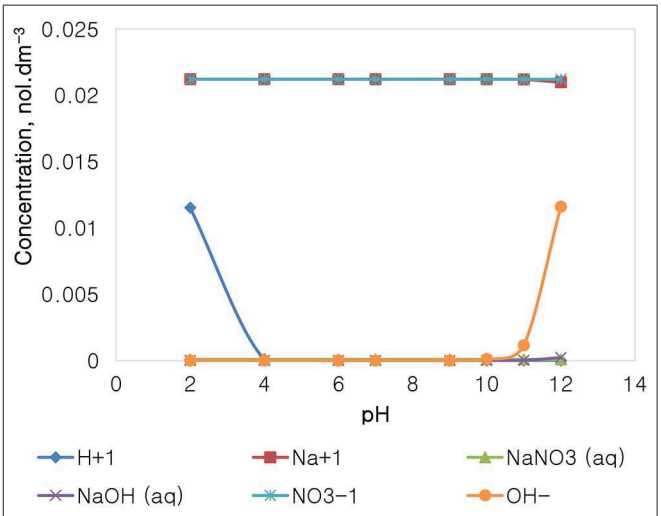

FIGURE 11 | $NaNO_3$ speciation for a solution of 0.0213 mol dm^{-3} ionic strength.

below pH 4, contrary to the $NaNO_3$ speciation, the dominant species are Na^+, H^+, and $SO_4{}^{2-}$, HSO_4^- as well as $NaSO_4$. The concentration of these species remains fairly constant in the pH 4–10 range, except for HSO_4^- and H^+ which become virtually insignificant, while the concentration of OH^- rises together with an appearance of NaOH(aq) and $NaSO_4^-$ when the pH is increased beyond pH 10. It is important to note that the specific Na^+ concentration in Na_2SO_4 is roughly 0.014 mol dm^{-3}, relatively lower than that of 0.021 mol dm^{-3} in $NaNO_3$ as reported in **Figure 11**, although both single salts have a fixed similar ionic strength of 0.021 mol dm^{-3}. The NO_3^- ion in $NaNO_3$ also has a higher concentration compared to the concentration of $SO_4{}^{2-}$ seen in Na_2SO_4.

Figure 13 depicts the speciation of a $Ca(NO_3)_2$ solution, with an ionic strength of 0.0213 mol dm^{-3}, generated through the Visual MINTEQ 3.1. The speciation of $Ca(NO_3)_2$ shows that at pH 4 and below, the dominant species are Ca^{2+}, NO_3^-, and H^+, with all of the other species existing at comparably insignificant concentrations. At the pH range of 4–10, only Ca^{2+} and NO_3^- are dominant and present in the solution, with a concentration of 0.014 mol dm^{-3} for the NO_3^- anions compared to that of the other species. It is also shown that above pH 10, the concentration of OH^- rises; however, that concentration is still relatively lower than that of the nitrate anions.

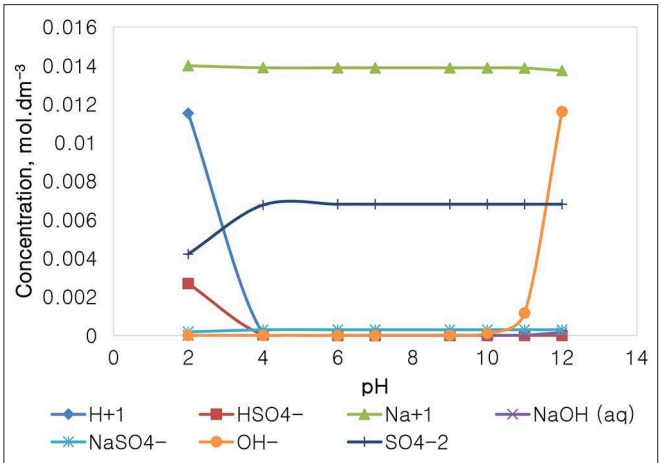

FIGURE 12 | Na_2SO_4 speciation for a solution of 0.0213 mol dm^{-3} ionic strength.

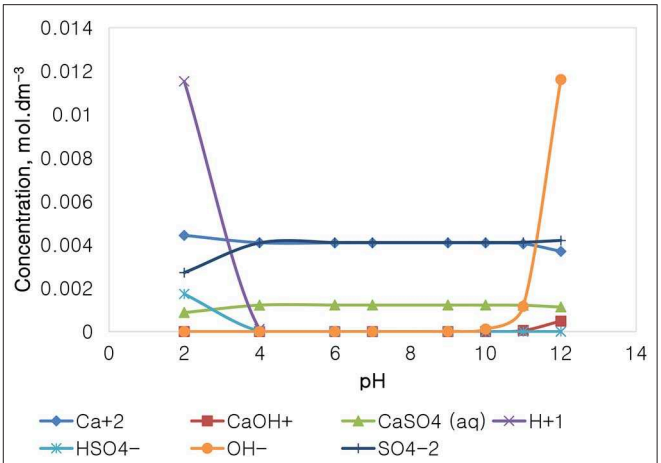

FIGURE 14 | $CaSO_4$ speciation for a solution of 0.0213 mol dm^{-3} ionic strength.

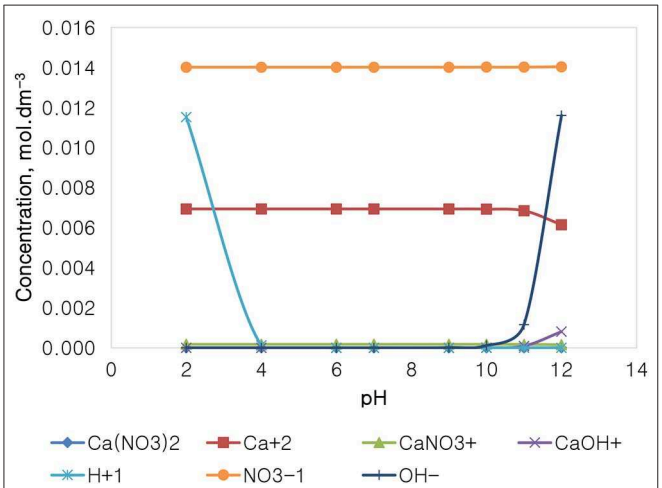

FIGURE 13 | $Ca(NO_3)_2$ speciation for a solution of 0.0213 mol dm^{-3} ionic strength.

Figure 14 depicts the speciation of a $CaSO_4$ solution, with an ionic strength of 0.0213 mol dm^{-3}, generated through the Visual MINTEQ 3.1. The speciation of Na_2SO_4 shows that below pH 4, contrary to the $NaNO_3$ speciation and similarly with that of Na_2SO_4, the dominant species are Ca^{2+}, H^+, and $SO_4 2-$, HSO_4^-, and $CaSO_4$. The concentration of these species remains fairly constant in the pH 4–10, while H^+ becomes obsolete. The concentration of OH^- and of $CaOH^+$ increases with an increase in the solution alkalinity, while the concentration of Ca^{2+} decreases with an increase in pH beyond pH 10. It is worth noting that the specific Ca^{2+} concentration in $CaSO_4$ is roughly 0.004 mol dm^{-3}, which is relatively lower than that of 0.014 mol dm^{-3} in $Ca(NO_3)_2$ as reported in **Figure 12**, although both single salts have a fixed similar ionic strength of 0.0213 mol dm^{-3}. NO_3^- is also present in higher concentrations (0.062 mol dm^{-3}) compared to $SO_4 2-$ (0.003 mol dm^{-3}).

DISCUSSION

Figures 1, **2** showed no evidence of specific ion effects on sulfide recoveries for the tested ore. Also, **Figure 5** shows that the recovery of sulfides per gram of water did not change with ion type, indicating that specific ion effects on froth stability (as measured by the recovery of water) had little or no impact on the behavior of sulfides. However, specific ion effects were observed on the behavior of gangue in that $Ca(NO_3)_2$ and $CaCl_2$ resulted in the lowest total amount of gangue reporting to the concentrate compared to those of all the other single salts. **Figure 3** shows that $NaNO_3$, Na_2SO_4, and NaCl resulted in the highest total recovery of gangue, while solutions containing Mg^{2+} were comparable to 1SPW. **Figure 8** shows that the monovalent Na^+ solutions resulted in the highest gangue recovery per gram of water compared to the divalent Ca^{2+} and Mg^{2+}; this behavior is attributed to the effects on froth stability and the resulting impact on entrainment (Manono et al., 2018a). This behavior could imply that Na^+ resulted in an activation of gangue, hence the higher gangue recovery per gram of water.

The specific ion effects seen on the behavior of gangue led to $Ca(NO_3)_2$ and $CaCl_2$ resulting in the highest sulfide grades, whereas all the Na^+ salts resulted in the lowest sulfide grades compared to the Ca^{2+} and Mg^{2+} single salt solutions. Thus, it can be said that the divalent Ca^{2+} and Mg^{2+} depressed the gangue more effectively. It was also apparent that in all cations (Ca^{2+}, Mg^{2+}, and Na^+), solutions containing NO_3^- depressed the gangue more readily compared to solutions containing Cl^- and $SO_4 2-$. This effect was stronger in the presence of Ca^{2+} compared to when a combination of Na^+ and NO_3^- was present in the solution.

Findings from the flotation results gave rise to the need to conduct further investigative work into the mechanism of the gangue depression effects seen, hence the determination of specific ion effects on the coagulation and the surface charge of talc. Talc was selected as a proxy for the naturally floatable gangue minerals needing to be depressed during the flotation

of base metal sulfides-PGM-bearing ores. Single salts which showed the greatest impact on gangue depression and sulfide grades were selected for further investigative test work. **Figure 9** shows that the divalent Ca^{2+} resulted in the shortest settling time compared to the monovalent Na^{+}. This indicates that talc particles coagulated far easier in solutions containing Ca^{2+} compared to those in Na^{+}-containing solutions. This trend is similar to the observations made in an earlier study by Manono et al. (2019) which showed enhanced coagulation and depression of talc in $CaCl_2$ and $MgCl_2$ compared to those in NaCl. Also, the solutions containing NO_3^- resulted in a shorter settling time compared to those containing Cl^- and SO_42-. This implies that the NO_3^--containing solutions resulted in increased coagulation of talc particles compared to the solutions containing Cl^- and SO_42-. These results are in line with the lower gangue recovery in the solutions containing Ca^{2+} and NO_3^- compared to those in the solutions containing Na^{+}, Cl^-, and SO_42- as seen in **Figure 3**.

On the basis of the gangue recovery and the coagulation trends seen in **Figures 8**, **9**, it can be said that there exists specific ion effects on the behavior of gangue in that specific ions such as Ca^{2+} resulted in slightly more pronounced effects. These effects emanate from the passivation of gangue mineral particle surfaces due to the presence of species such as Ca^{2+}, $CaOH^{+}$, and $CaNO_3+$ as shown in **Figures 11–14**. It is evident that beyond pH 9, oxyhydroxo species and metal complexes become dominant; these alter the surface chemistry of the mineral particles. These oxyhydroxo species are known to impart a more hydrophilic nature on the naturally hydrophobic gangue and thus cause a greater depression of gangue. Zeta potential measurements for talc were taken in various single salts of monovalent and divalent cations to probe the effect of inorganic electrolytes on the particle surface charge. **Figure 10** shows that the zeta potential of talc was less negative in Ca^{2+} compared to that in Na^{+}. These results correlate well with the greater depression and coagulation of gangue in Ca^{2+} compared to those in Na^{+} as shown in **Figures 3, 9**. This implies that the non-sulfide gangue mineral particles were more passivated by the presence of the divalent Ca^{2+} and its resulting oxyhydroxo species in solution such that the surface of the gangue mineral particles would become more hydrophilic. The resulting hydrophilicity would in turn enhance the coagulation of particles and thereby enhance their depression. A similar finding was observed for the anions which resulted in greater depression and coagulation of gangue in that the NO_3^--containing solutions in all cation types resulted in a less negative zeta potential, particularly at the natural flotation pH 9, compared to that of the SO_42--containing solutions. Furthermore, the zeta potential results as a function of pH correlate well with the speciation diagrams shown in **Figures 11–14** in that the dominant oxyhydroxo species seen at $pH > 9$ are said to passivate mineral surfaces and thereby induce their hydrophilic nature, creating an environment conducive for gangue mineral depression (Laskowski et al., 2007; Ikumapayi et al., 2012; Feng et al., 2013). The coagulation findings of this work are in agreement with those of Dishon et al. (2009) who found that in highly concentrated electrolyte solutions, the adsorption of cations onto the mineral surface changed the surface charge of the particles and resulted in strong attractive forces between particles which consequently formed hydrophilic agglomerates. Similar to what has been shown in this present work on the depression of gangue, an investigation into the role of Ca^{2+} ions on the surface properties of molybdenite in copper porphyries by Li et al. (2015) showed that the floatability of fine molybdenite particles decreased significantly when Ca^{2+} ions and silica coexisted in the flotation pulp. Raghavan and Hsu (1984) relate this phenomenon to the adsorption of Ca^{2+} ions on mineral particles, reducing the magnitude of the negative surface charge and therefore causing the coagulation of mineral particles. As recorded in literature, it is worth mentioning that zeta potential changes also occur as a result of the influence of adsorption of ions onto the mineral surface (Manono et al., 2018b; Michaux et al., 2018). The adsorption of ions on the mineral surface and the resulting change in zeta potential are said to occur either by electrostatic attraction, chemisorption, or chemical reaction. The findings of this work confirm Gaudin (1932) and Gaudin and Charles (1953) who proposed that changes in the potential determining the ion concentration in the solution can cause a reduction in the zeta potential. Furthermore, the resulting correlation between the coagulation and zeta potential trends seen in this work confirms the proposal of a qualitative parallel between coagulation and zeta potential made by Fuerstenau and Mishra (1980) and Fuerstenau et al. (1988).

It is thus evident that the presence of divalent Ca^{2+} and the resulting oxyhydroxo species in process water causes an adsorption of these inorganic electrolytes onto the mineral surface. These consequently reduce the negative surface charge of the mineral particle as shown by the more positive zeta potential and passivated mineral surface in **Figure 10**. This in turn leads to enhanced coagulation and depression of gangue.

Graphical Summary of Findings

From **Graphical Abstract**, it is therefore proposed that zeta potential measurements and coagulation tests can be used as a tool to test for effects that specific process water constituents will have on the surface chemistry response and floatability of naturally hydrophobic gangue minerals during the flotation of Cu-Ni-PGM ores. Knowledge of such gangue mineral surface chemistry responses to water quality changes may prove beneficial in determining the desired water quality and reagent regimes for uninterrupted flotation performance.

CONCLUSIONS

The findings of this work have shown that the monovalent Na^{+} did not promote coagulation. However, in Ca^{2+}, coagulation was favored as less gangue was recovered into the concentrate, indicating an increased gangue depression in the presence of Ca^{2+} compared to Na^{+}. This trend was more pronounced when Ca^{2+} was in combination with NO_3^-. The zeta potential results showed a less negative zeta potential of talc with Ca^{2+} compared to that with Na^{+}, showing a greater passivation of the mineral surface in Ca^{2+}-containing single salt solutions. The greater

depression in NO_3^- was confirmed by the less negative zeta potential, the lower gangue recoveries, and the shorter settling time. Thus, the key findings of this work are:

- Both NO_3^- and Ca^{2+} increased the depression of gangue as shown by the lower gangue recoveries.
- The concentrate grades were greater in Ca^{2+} compared to those in Na^+.
- Coagulation and zeta potential tests indicated that Ca^{2+} and NO_3^- would mostly likely create a pulp chemistry environment that promotes gangue depression.
- The presence of Ca^{2+} in flotation process waters could be beneficial for the depression of floatable gangue.

This work has also shown that the depressive action of inorganic electrolytes was more pronounced on gangue, whereas little or no depression action was seen on the valuable sulfides as total sulfide recoveries were generally the same for this specific PGM ore.

DATA AVAILABILITY STATEMENT

All datasets generated for this study are included in the article/supplementary material.

AUTHOR CONTRIBUTIONS

All authors listed have made a substantial, direct and intellectual contribution to the work, and approved it for publication. MM conceptualized the work, carried out the research experiments, analyzed the experimental data, wrote the manuscript while KC and JW assisted with conceptualisation, advised on the experimental test work and data analyses, proofread and edited the manuscript.

FUNDING

This work was supported in part by the National Research Foundation (NRF) of South Africa (Grant number 118062—Water Quality in Flotation: Causes, Impacts, and Process Management Strategies). Any opinions, findings, conclusions, or recommendations expressed in any publication generated by NRF supported research is that of the authors and the NRF accepts no liability whatsoever in this regard. Financial and technical contributions from the South African Minerals to Metals Research Institute (SAMMRI) and its members are also acknowledged.

REFERENCES

Biçak, Ö., Ekmekçi, Z., Can, M., and Öztürk, Y. (2012). The effect of water chemistry on froth stability and surface chemistry of the flotation of a Cu-Zn sulfide ore. *Int. J. Miner. Process.* 102–103, 32–37. doi: 10.1016/j.minpro.2011.09.005

Castro, S., Miranda, C., Toledo, P., and Laskowski, J. S. (2013). Effect of frothers on bubble coalescence and foaming in electrolyte solutions and seawater. *Int. J. Miner. Process*. 124, 8–14. doi: 10.1016/j.minpro.2013.07.002

Corin, K. C., Reddy, A., Miyen, L., Wiese, J. G., and Harris, P. J. (2011). The effect of ionic strength of plant water on valuable mineral and gangue recovery in a platinum bearing ore from the Merensky reef. *Miner. Eng.* 24, 131–137. doi: 10.1016/j.mineng.2010.10.015

Corin, K. C., and Wiese, J. G. (2014). Investigating froth stability: a comparative study of ionic strength and frother dosage. *Miner. Eng.* 66, 130–134. doi: 10.1016/j.mineng.2014.03.001

Dishon, M., Zohar, O., and Sivan, U. (2009). From repulsion to attraction and back to repulsion: the effect of NaCl, KCl and CsCl on the force between silica surfaces in aqueous solution. *Langmuir* 25, 2831–2836. doi: 10.1021/la803022b

Feng, Q., Feng, B., and Lu, Y. (2013). Influence of copper ions and calcium ions on adsorption of CMC on chlorite. *Trans. Nonferrous Met. Soc. China* 23, 237–242. doi: 10.1016/S1003-6326(13)62451-6

Fuerstenau, D. W., and Mishra, R. K. (1980). "On the mechanism of pyrite flotation with xanthate collectors," in *Complex Sulphide Ores,* eds M. J. Jones (London: I.M.M), 271–277.

Fuerstenau, M. C., Lopez-Valdivieso, A., and Fuerstenau, D. W. (1988). Role of hydrolyzed cations in the natural hydrophobicity of talc. *Int. J. Miner. Process.* 23, 161–170. doi: 10.1016/0301-7516(88)90012-9

Gaudin, A. M. (1932). *Flotation, 1st Edn*. New York, NY: McGraw-Hill Book Company.

Gaudin, A. M., and Charles, W. D. (1953). Adsorption of calcium and codium on pyrite. *Trans. AIME – Min. Eng.* 196, 195–200.

Ikumapayi, F., Makitalo, M., Johansson, B., and Rao, K. H. (2012). Recycling of process water in sulphide flotation: effect of calcium and sulphate ions on flotation of galena. *Miner. Eng.* 39, 77–88. doi: 10.1016/j.mineng.2012.07.016

Laskowski, J. S., Liu, Q., and O'Connor, C. T. (2007). Current understanding of the mechanism of polysaccharide adsorption at the mineral/aqueous solution interface. *Int. J. Miner. Process.* 84, 59–68. doi: 10.1016/j.minpro.2007.03.006

Li, M. Y., Wei, D. Z., Shen, Y. B., Liu, W. G., Gao, S. L., and Liang, G. Q. (2015). Selective depression effect in flotation separation of copper-molybdenum sulfides using 2,3-disulfanylbutanedioic acid. *Trans. Nonferrous Met. Soc. China* 25, 3126–3132. doi: 10.1016/S1003-6326(15)63942-5

Liu, W., Moran, C. J., and Vink, S. (2014). A review of the effect of water quality on flotation. *Miner. Eng.* 53, 91–100. doi: 10.1016/j.mineng.2013.07.011

Manono, M., Corin, K., and Wiese, J. (2018a). Water quality effects on a sulfidic PGM ore: Implications for froth stability and gangue management. *Physicochem. Probl. Miner. Process.* 54, 1253–1265. doi: 10.5277/ppmp18181

Manono, M., Corin, K., and Wiese, J. (2018b). Perspectives from literature on the influence of inorganic electrolytes present in plant water on flotation performance. *Physicochem. Probl. Miner. Process.* 54, 1191–1214. doi: 10.5277/ppmp18157

Manono, M. S., Corin, K. C., and Wiese, J. G. (2016). The influence of electrolytes present in process water on the flotation behaviour of a Cu-Ni containing ore. *Miner. Eng.* 96–97. doi: 10.1016/j.mineng.2016.06.015

Manono, M. S., Corin, K. C., and Wiese, J. G. (2019). "Inorganic electrolytes on the efficacy of a carboxymethyl cellulose as a coagulant for talc: implications for talc depression in flotation," in: *Mine Water – Technological and Ecological Challenges*, eds E. Khayrulina, C. H. Wolkersdorfer, S. Polyakova, and A. Bogush (Perm: Perm State University), 217–225.

Michaux, B., Rudolph, M., and Reuter, M. A. (2018). Challenges in predicting the role of water chemistry in flotation through simulation with emphasis an emphasis on the influence of electrolytes. *Miner. Eng.* 125, 252–264. doi: 10.1016/j.mineng.2018.06.010

Muzenda, E. (2010). An investigation into the effect of water quality on flotation performance. *World Acad. Sci. Eng. Technol.* 4, 237–241.

Raghavan, S., and Hsu, L. L. (1984). Factors affecting the flotation recovery of molybdenite from porphyry copper ores. *Int. J. Miner. Process.* 12, 145–162. doi: 10.1016/0301-7516(84)90026-7

Rao, S. R., and Finch, J. A. (1989). A review of water re-use in flotation. *Miner. Eng.* 2, 65–85. doi: 10.1016/0892-6875(89)90066-6

Shackleton, N. J., Malysiak, V., De Vaux, D., and Plint, N. (2012). Water quality - a comparative study between moncheite and pentlandite in mixture with pyroxene. *Miner. Eng.* 36–38, 53–64. doi: 10.1016/j.mineng.2012.02.004

Wang, X., Liu, R., Ma, L., Qin, W., and Jiao, F. (2016). Depression mechanism of the zinc sulfate and sodium carbonate combined inhibitor on talc. *Colloids Surf. A Physicochem. Eng. Aspects* 501, 92–97. doi: 10.1016/j.colsurfa.2016.04.057

Conflict of Interest: The authors declare that the research was conducted in the absence of any commercial or financial relationships that could be construed as a potential conflict of interest.

frontiers in Materials

ORIGINAL RESEARCH
published: 20 March 2020
doi: 10.3389/fmats.2020.00053

A Study on the Electric Surface Potential and Hydrophobicity of Quartz Particles in the Presence of Hexyl Amine Cellulose Nanocrystals and Their Correlation to Flotation

Robert Hartmann and Rodrigo Serna-Guerrero**

Department of Chemical and Metallurgical Engineering, School of Chemical Engineering, Aalto University, Aalto, Finland

OPEN ACCESS

Edited by:
Jan Zawala,
Institute of Catalysis and Surface Chemistry (PAN), Poland

Reviewed by:
Onur Guven,
Adana Science and Technology University, Turkey
Way Foong Lim,
University of Science Malaysia, Malaysia

****Correspondence:***
Robert Hartmann
robert.hartmann@aalto.fi
Rodrigo Serna-Guerrero
rodrigo.serna@aalto.fi

Specialty section:
This article was submitted to Colloidal Materials and Interfaces, a section of the journal Frontiers in Materials

Received: *29 November 2019*
Accepted: *18 February 2020*
Published: *20 March 2020*

Citation:
Hartmann R and Serna-Guerrero R (2020) A Study on the Electric Surface Potential and Hydrophobicity of Quartz Particles in the Presence of Hexyl Amine Cellulose Nanocrystals and Their Correlation to Flotation. Front. Mater. 7:53. doi: 10.3389/fmats.2020.00053

In this work, the study of hexyl amine cellulose nanocrystal (HAC) as a renewable and environmentally-friendly reagent for the flotation of quartz (QRZ) is expanded with a focus on the changes of electrical states at the solid-liquid interface, the range of solid-gas interactions, and their impact on flotation operations under a turbulent regime. Furthermore, particle-bubble attachment probabilities were measured with the recently engineered automated contact timer apparatus (ACTA), a versatile technique used to deduce the wettability of microparticles and potentially predict their floatability. Therefore, the findings of the ACTA proved that, with sufficiently hydrophobic QRZ (i.e., HAC concentration $\geq$ 0.667 mg_{HAC}/m^2_{QRZ}), stable particle-bubble attachments occur at particle-bubble distances in the range of tens of micrometers. The distances for the successful attachment of HAC-coated QRZ particles exceed the range of interactions reported in literature so far and imply the existence of structural or hydrodynamic phenomena acting between particle and bubble surfaces. The occurrence of so-called non-compressive particle-bubble attachments is shown to correlate with a significant increase in the floatability of QRZ, where recoveries up to 90% were obtained. Based on the experimental results, some insights on the nature of the long-range interactions responsible for the particle-bubble attachment of hydrophobic particles are provided.

Keywords: cellulose-derived reagent, surface (zeta-) potential, hydrophobicity, particle-bubble-attachment, induction timer, floatability

INTRODUCTION

Froth flotation is a widely used industrial process for the concentration of mineral particles. Despite its widespread application in the field of mineral processing, the process performance has not changed significantly during the last decades and the understanding of phenomena responsible of flotation is still strongly based on empirical knowledge. Nowadays, this traditional approach is

challenged by the demand to process ores with decreasing grades (Calvo et al., 2016) and thus, many efforts have been recently undertaken to better understand the various aspects of flotation processes with the aim of enhancing their efficiency. Simultaneously, the growing concerns in terms of environmental impact and consumption of natural resources urge for the design of mineral flotation processes with minimal impact, including for example, efficient water recycling strategies and the employment of more environmentally-friendly chemicals (Bridge, 2004; Pearse, 2005; Liu et al., 2013; Nuorivaara et al., 2019).

To that end, chemicals derived from renewable sources, for instance cellulose, hemicellulose or lignin, are promising substitutes to the State-of-the-Art reagents in various fields, although their use in the mineral processing industry remains largely unexplored (Klemm et al., 2005; Ago et al., 2016). In terms of flotation, the relatively high chemical complexity of functionalized nanocellulose leads, on one hand, to challenges concerning their surface interaction mechanisms, but on the other hand, to opportunities to modify macromolecules with tailored properties that selectively interact with specific mineral species rendering them more hydrophobic. So far, cellulose-based chemicals (e.g., starch dextrin, guar gum, carboxymethyl cellulose or chitosan) have proven useful as depressants (Mu et al., 2016; Hernandez et al., 2017). In addition, research was recently initiated to investigate the efficiency of artificial nanoparticles as collectors, however, the behavior of nanoparticles differs significantly from conventionally used soluble organic molecules (Yang et al., 2011; Yang et al., 2013; Dong et al., 2017; Abarca et al., 2018). In a study of Abarca et al. (2018), polystyrene nanoparticles were modified by click chemistry to incorporate several functional groups on the nanoparticles surface. In such work, tests were performed to study colloidal stability and hydrophobicity, leading to flotation recoveries up to 90% for the most suitable candidates. The employment of nanoparticles as collector in froth flotation introduces novel aspects of study, such as the colloidal stability of the hydrophobic nanoparticles in the pulp or the occurrence of "wet-patch" adhesions, in which only the adsorbed hydrophobic nanoparticles attach to an air bubble, while the mineral particles remains completely wetted by water (Yang et al., 2011). So far, most of the work with nanoparticles was performed with artificial polymers, which are not biodegradable and their synthesis is rather complicated (Al-Shatty et al., 2017). In this study, hexyl amine cellulose nanocrystal (HAC) was used as an alternative of commercial amine-based collectors or artificial nanoparticles for quartz (QRZ) flotation. To our best knowledge, aminated celllose nanocrystals are the first bio-based nanoparticle used as collector in froth flotation (Laitinen et al., 2016; Hartmann et al., 2017, 2018).

The behavior of different aminated cellulose nanocrystals dispersed in an aqueous solution, as well as the change of the wetting properties of quartz surfaces after its adsorption, was part of previous studies by the authors (Hartmann et al., 2016, 2017, 2018; Lopéz et al., 2019). In such studies, the influence of nanocellulose on the surface charge of QRZ was identified using zeta potential and it was correlated with the floatability of QRZ using a single-bubble Hallimond tube. While such studies showed promising results, it was also found that the performance of HAC as collector differs fundamentally from conventional reagents, due to its greater spatial dimensions, the water-insoluble nature of HAC nanoparticles, and its complex chemical constitution. Indeed, the origin of the pulp and the modification route of HAC may have an effect on its chemical constitution. In case of HAC, amine groups can be incorporated into the cellulose structure in a way that the nitrogen atom forms a covalent bond with an oxygen atom of the cellulose backbone, while its hydrocarbon chain is oriented toward the exterior. Therefore, the amine functional groups in HAC can be considered different from amine functionalities in conventional amphiphilic water-soluble molecules, where the nitrogen atom is only bound to a carbon atom of its linked hydrocarbon chain. It has been shown that the aqueous environment affects the protonation of the amine groups in HAC and their reactivity (Hartmann et al., 2016). Another fundamental difference to conventional reagents is the random distribution of functional groups throughout the entire structure of HAC. Consequently, the amine groups relevant for interactions with surrounding phases are rather isomorphically distributed than positioned toward a single direction. Interestingly, the degree of protonation of the amine groups has positive effects on its adsorption on QRZ, but may have antagonistic effects on the rupture of the liquid intervening film between a particle and a bubble (Hartmann et al., 2018). For these reasons, it is worth to continue exploring the behavior of HAC in the mineral processing field.

To characterize the efficiency of flotation processes, efforts have been placed to define physico-chemical parameters, which could be capable to reliably predict the floatability of a mineral species without expensive experimental schemes. The use of three-phase contact angle, for example, has proven unreliable due to the difficulties of measuring contact angles of microparticles or on rough surfaces (Crawford and Ralston, 1988). Recently, the use of thermodynamic properties of minerals were investigated, such as the free energy of interaction between a particle and a bubble immersed in water (ΔG_{pwb}) (Hartmann et al., 2017; Rudolph and Hartmann, 2017) or the enthalpy of immersion (ΔH_{imm}) (Taguta et al., 2018, 2019). These parameters allow a more precise determination of the energetic state of a mineral surface, but their measuring techniques are limited. For example, there is no aqueous phase during measurements in case of the inverse gas chromatography (Hartmann et al., 2017; Rudolph and Hartmann, 2017), and particles with sizes significantly finer as the ones processed in real flotation practice are required in case of calorimetric measurements (Taguta et al., 2018, 2019). In addition, these techniques measure properties at equilibrium states instead of dynamic systems.

Another approach to predict floatability of a particular mineral system is the study of induction time, defined as the time required to drain the intervening liquid film between a particle and a bubble leading to the formation of a stable, orthokinetic three-phase contact. In a review published by Verrelli and Albijanic (2015), the strengths and weaknesses of several methods to measure the induction time were summarized. To overcome the current limitations of the previously available experimental methods, a novel automated contact timer apparatus (ACTA) was engineered by our research group (Aspiala et al., 2018).

This apparatus offers various technical advantages, such as a controlled preparation of a particle bed, the ability of setting and recording contact times, approach and receding speeds, and the measurement of hundreds of individual attachment events in a few hours. In addition, the ACTA allows the possibility to mimic environments present in flotation cells and the use of particles with relevant sizes. Most importantly, the ACTA is capable of analyzing both, the time and distance at which a particle-bubble attachment occurs with a certain probability. The establishment of particle-bubble attachment probability distributions as a function of contact time and distance may be the key to characterize the degree of hydrophobization of a particulate sample and predict its floatability. In a recent work by the authors, it was found that, with sufficiently hydrophobic particles, a stable particle-bubble attachment occurs even at distances of tens of micrometers (Hartmann and Serna-Guerrero, 2020). This has a tremendous effect on the understanding of particle-bubble attachments, further demonstrating that hydrophobic forces may lead to capillary forces that have a further reach than the interactions derived for instance from surface force apparatus or atomic force microscopy using the extended DLVO theory, which are generally accepted to act within distances in the nanometer-range (Derjaguin and Churaev, 1989; William et al., 1994; Yoon and Moa, 1996; van Oss, 2003).

The present work thus combines a series of experimental studies to determine the changes at the surface level of QRZ in the presence of HAC and its influence on the particle-bubble attachment. Firstly, the evolution of the electrical state of QRZ particles in the presence of different HAC concentrations and environments is analyzed. Subsequently, the probability of particle-bubble attachments dependent on the contact time and particle-bubble distance is analyzed using the above-described ACTA. As will be discussed, non-compressive particle-bubble attachments were observed at distances beyond the limits of measurable effects of interaction energies known in literature and may hold the key for an objective assessment of floatability using attachment probabilities. To demonstrate the practical applicability and hydrophobic nature of HAC, bench-scale flotation tests were performed, showing that HAC is an efficient collector for QRZ. Furthermore, this study shows for the first time a correlation between high QRZ recoveries and the presence of non-compressive attachments between particles and bubbles in ACTA measurements.

MATERIALS, METHODS, AND MODELS

Quartz and Aminated Cellulose Nanocrystals

Quartz (QRZ) was supplied by Nilsiä (Sibelco, Nilsiä, Finland, 99.2% purity, 100–600 μm) and ground in a mill (Fritsch *PULVERISETTE*, planetary micro mill) for 15 s. The ground QRZ powder was dry sieved (Fritsch *ANALYSETTE*, vibratory sieve shaker) between sieves with 75 and 180 μm mesh-opening sizes. Afterward, the QRZ fraction was immersed in de-mineralized water, treated for 3 min with ultrasound (Branson 5510 Ultrasonic Cleaner) at 40 kHz, placed on a 75 μm mesh size sieve and washed with de-mineralized water to remove fines. The wet-sieved material was collected and dried in an oven overnight at 50°C. The sample thus obtained was used for the ACTA and flotation experiments. For the electrophoretic mobility analysis, a sample of a fine quartz powder was prepared as previously described (Hartmann et al., 2018). The granulometric properties of the fine and coarse quartz fractions are summarized in **Table 1**, based on laser diffraction (Beckman Coulter LS 320) and nitrogen adsorption (ASAP 2020 N_2, micromeritics) following the Brunauer-Emmet-Teller method.

As collector reagent, hexyl-amine cellulose nanocrystals (HAC) were synthesized according to the procedure of Visanko (Visanko et al., 2014; Hartmann et al., 2016). Using this method, a suspension of 0.1-wt% HAC was obtained with nanocrystals possessing a length of 137 nm ± 6 nm and diameter of 5 nm ± 0.2 nm (Hartmann et al., 2018).

The Electric Surface Potentials From Electrophoresis

The electrophoretic mobility of QRZ in the presence of HAC with different concentrations, background salts and pH values was measured with a Delsa Nano C zeta-potential analyzer (Beckman Coulter, United States). Prior to the experiments, different background salt solutions were prepared using de-mineralized water with controlled pH values of 5, 7, or 9 (Mettler Toledo Seven Excellence) obtained by the addition of diluted HCl or NaOH solutions. After the pH value remained constant for 24 h, background salts were added to obtain either a 10 mM NaCl solution or a 1 mM $MgSO_4$ solution. It was assumed that the addition of salts did not alter the initial pH value. For each experiment, 10 mg of quartz were dispersed in 30 ml of background salt solution and stirred for 5 min. Meanwhile, HAC was treated in an ultrasonic bath for 3 min. Subsequently, different amounts of HAC were added to the QRZ suspension to reach concentrations of 0.5, 1, 1.5, 2, 2.5, or 3 mg/l. The suspension thus obtained was stirred for one additional minute to promote HAC adsorption on QRZ. After stirring, the suspension stood still for 2 min for coarse particles or flocculates to settle and then approximately 3 ml of the

TABLE 1 | Size quantiles and specific surface areas and Sauter diameters ($D_{3,2}$) of quartz fractions based on particle size distributions obtained through laser diffraction and the Brunauer-Emmet-Teller method.

Granulometric properties	Quartz	
	Fine (electrophorese)[a]	Coarse (ACTA/flotation)
D_{10}/μm	1.3	94
D_{50}/μm	6.1	154
D_{90}/μm	21.2	249
$D_{3,2}$/μm	1.3	151
$S_{spec,calc}/m^2g^{-1}$[b]	0.772	0.015
$S_{spec,BET}/m^2g^{-1}$	1.7009	0.045

[a]*From Hartmann et al. (2018).* [b]*Specific surface area calculated from laser diffraction results.*

suspension were transferred into the Delsa Nano C analyzer. During the measurement, the temperature was kept constant at 25°C and three measurements were performed on each sample for reproducibility. For each HAC concentration, measurements were performed on duplicates. For the determination of the electric surface (ζ−) potential, the Einstein-Smoluchowski equation was applied (Zembala, 2004).

$$\zeta = \frac{\eta \cdot u_{el.-phor.}}{\varepsilon_0 \cdot \varepsilon_{rel}} \quad (1)$$

where η is the dynamic viscosity of water at 25°C, $u_{el.-phor.}$ the detected electrophoretic mobility, ε_0 the permittivity of a vacuum and ε_{rel} the relative permittivity of water.

The Automated Contact Time Apparatus (ACTA)

For measurements with the ACTA, identical background salt solutions as previously described were used. For conditioning, 10 g of QRZ were transferred into a glass beaker containing 100 ml of background salt solution and stirred for 5 min. Meanwhile, a suspension of HAC was treated for 3 min with ultrasound. Afterward, the HAC suspension was mixed with the QRZ-containing suspension and the conditioning continued under stirring for 5 min. The concentrations of HAC in the suspension were set to either 3 or 5 mg/l. After conditioning, QRZ particles and background salt solution were transferred into a transparent plastic pool. The plastic pool was placed into the ACTA and a particle bed with a 2 mm thickness prepared by the automatically controlled shovel in the ACTA setup. Once a flat particle bed was obtained, the measurements were started. The contact times between bubbles and the particle bed were set at 20, 40, 60, 80, or 100 ms. The presence of an attached particle and the diameter of each bubble was recorded and measured using a microscopic camera positioned at the bottom of the pool (see **Figure 1**). The distance between needle tip and particle bed were measured with a high-speed camera positioned perpendicular to the movement of the needles to obtain the particle-bubble distance (see **Figure 1**). Each experiment consisted of 396 particle-bubble attachment events, which were individually analyzed on whether this resulted in a successful attachment, depending on the contact time and position. The operating principle of the ACTA measurement is visualized in **Figure 1** and a detailed description of the operation and data processing methodology can be found in Hartmann and Serna-Guerrero (2020). Since the previous work, the illumination of the bubbles during the recording with the high speed camera video has been improved, leading to a more accurate determination of the bubble-particle bed distance.

Flotation Tests

Bench-scale flotation tests were carried out in a 1.5 l Outokumpu flotation cell. A fresh background solution was prepared for each experiment with 10 mM NaCl or 1 mM $MgSO_4$. In addition, DowFroth 250 (DF250) at a concentration of 10 ppm was used as frother. The pH of the solution was controlled at either 5, 7, or 9. Approximately 300 g of QRZ were transferred into the flotation cell and the background salt solution added. The suspension was stirred for 5 min at 1300 rpm. At the same time, the HAC suspension was treated with ultrasound for 3 min. The rotational speed of the rotor was then reduced to 900 rpm and HAC suspension was added to the flotation cell for a concentration of either 3 or 5 mg/l and further conditioned for 5 min. Then, air was introduced at a flow of 4 l/min, at which point the flotation experiment was considered to have started. The total flotation time was 10 min and subsequently the over- and underflow were collected. In case of strong froth formation, additional background salt solution was added throughout the experiment to keep the water level constant. After each experiment, the over- and underflow was vacuum filtered and dried in an oven at 50°C, before their masses were measured. All experiments were performed as duplicates.

Overview of Examined Conditions for the Comparability of the Results

In the sections above, the concentration of HAC was presented as a relation of the dry mass of HAC to the volume of aqueous solution. However, to account for the different sizes and masses of the QRZ samples used in the various analysis methods described above, the results are presented as the relation of the mass of HAC in suspension to the free surface area of QRZ obtained with the BET method as an approximation for the fair comparison of the results. The HAC concentrations used in the different experiments of this work are summarized in **Table 2**. Please note that the values presented as $mg_{HAC}/m^2{}_{QRZ}$ may not necessarily represent the actual mass of HAC adsorbed on QRZ.

RESULTS AND DISCUSSION

Electrophoretic Mobility of Quartz Coated With Hexyl-Amine Cellulose

The importance of electric surface (ζ−) potentials on the physisorption of ionic molecular surfactants on QRZ and of the obtained particle-surfactant aggregate ζ-potential on their floatability is well accepted (Fuerstenau and Jia, 2004; Fuerstenau and Pradip, 2005). However, the replacement of conventional amphiphilic molecules by macromolecular HAC is not trivial. The presence of free surface charges on the HAC surface significantly affects both its adsorption on a mineral surface and the formation of a stable three-phase contact during flotation processes. This was presented and discussed in a previous work examining the selective flotation of QRZ from a mixture with hematite (Hartmann et al., 2018). The change of the derived ζ-potential of QRZ in the presence of different HAC concentrations is shown in **Figure 2**. For a better understanding, the results of the ζ-potentials of pure particles are shown from previous work (Hartmann et al., 2018) together with the results for a bubble dispersed in a 10 mM NaCl and 1 mM CaCl solution from Yang et al. (2001), assuming that Ca^{2+}- ions have a comparable behavior to Mg^{2+}- ions due to their physico-chemical similarity.

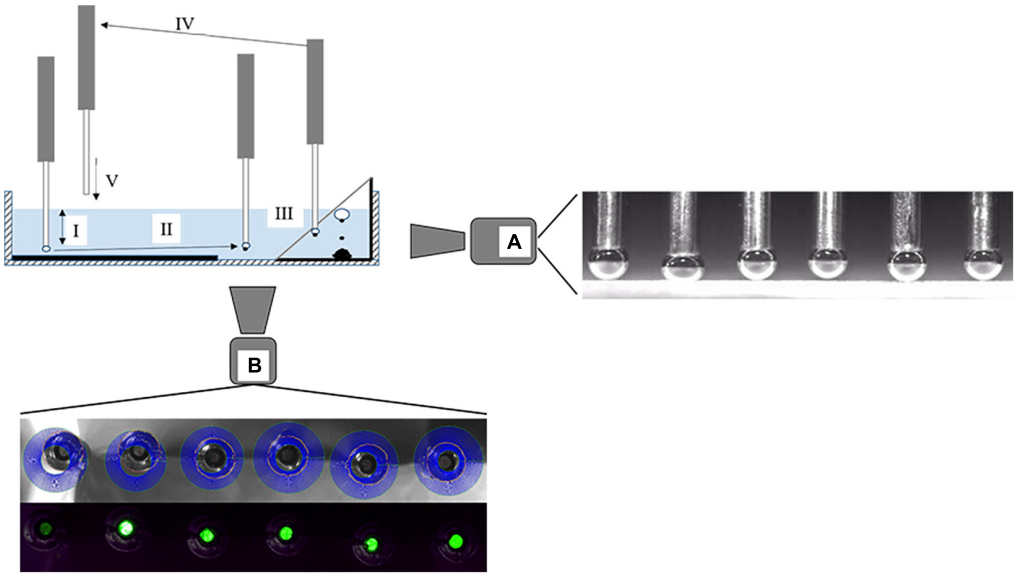

FIGURE 1 | Operating diagram of the ACTA with typical steps of a measurement cycle: (I) Bubbles are formed and approach the particle bed, rest for a set contact time and recede afterward again to the initial position. The initial distances of the needles varied to obtain different H between bubbles and the particle bed for a set contact time and the approach, rest and retraction of the bubbles are recorded with a high-speed camera (A). A representative image of the position of the bubbles relative to the particle bed at closest approach is given next to camera (A). (II) Bubbles are moved to the viewing window and images are taken by a digital microscope (B), representative images for the bubble size analysis and particle detection are shown below microscope (B). (III) Bubbles are moved to a collection bin and detached from the needles. (IV) The needles are lifted up until the needle tips are above the liquid, flushed with air for cleaning and simultaneously moved horizontally. (V) The needles are lowered slowly over an untouched spot of the particle bed into the liquid and the next cycle starts (as adapted from Hartmann and Serna-Guerrero, 2020).

The ζ-potential of pure substances shows that HAC possesses a positive ζ-potential for the examined pH range, approaching a neutral potential at pH 9, while QRZ is negatively charged, indicating a potential for attractive electrostatic interaction between them. By comparing the effect of the background solutions, the interactions between QRZ and polyvalent SO_4^{2-}- and Mg^{2+}- ions are stronger compared to monovalent Na^{+}- and Cl^{-}- ions, leading to a more pronounced compensation of its ζ-potential. For HAC, the reduction of the ζ-potential was only slightly stronger for the polyvalent background salts, taking in mind that the concentration of NaCl was ten times higher than of $MgSO_4$. Consequently, HAC is expected to physisorb on the mineral surface, which is proven by the two plots showing the distribution of the ζ-potential of QRZ for different HAC concentrations in the two salt solutions hereby studied. In general, all distributions show an evolution of the ζ-potential toward a maximum value with increasing HAC concentration. Eventually, the ζ-potential values reach a plateau, indicating the complete occupation of active sites at the QRZ surface. For QRZ and HAC dispersed in NaCl, HAC overcompensates the ζ-potential of QRZ in pH 5 and 7 with an isoelectric point at 0.4 $mg_{HAC}/m^2{}_{QRZ}$ and 1.4 $mg_{HAC}/m^2{}_{QRZ}$, respectively. At pH 9 (**Figures 2B,C**), the ζ-potential of modified QRZ remains negative throughout the examined concentration range of HAC, likely due to the absence of free positive surface charges in the HAC structure (as seen in **Figure 2A**). Similar distributions were obtained when QRZ and HAC are dispersed in $MgSO_4$ with a slightly greater compensation of the ζ-potential of QRZ by HAC. The isoelectric point is reached in this case at approximately 0.4 $mg_{HAC}/m^2{}_{QRZ}$ in pH 5 and 0.8 $mg_{HAC}/m^2{}_{QRZ}$ in pH 7 solution. Whether the comparatively stronger change of the ζ-potential of QRZ is attributed to an enhanced adsorption of HAC or a stronger interaction with SO_4^{2-} ions compared to Cl^{-} ions cannot be unequivocally concluded at this point. However, the evolution of the ζ-potential of the mineral surface for all pH values proves that adsorption of HAC occurred and indicates the occupation of its active sites. The next stage of this work is to determine whether such differences in the ζ-potential

TABLE 2 | The used HAC concentrations in mass of HAC related to the volume of the aqueous suspension for the electrophoretic mobility tests, ACTA experiments and their equivalents displayed as mass of HAC related to the surface area of QRZ.

	Hexyl-amine cellulose nanocrystal concentration		
mg_{HAC}/l	Electrophoretic mobility $mg_{HAC}/m^2{}_{QRZ}$	ACTA $mg_{HAC}/m^2{}_{QRZ}$	Flotation $mg_{HAC}/m^2{}_{QRZ}$
0.5	0.8	–	–
1	1.6	–	–
1.5	2.4	–	–
2	3.2	–	–
2.5	4	–	–
3	4.8	0.667	0.38
5	–	1.111	0.7

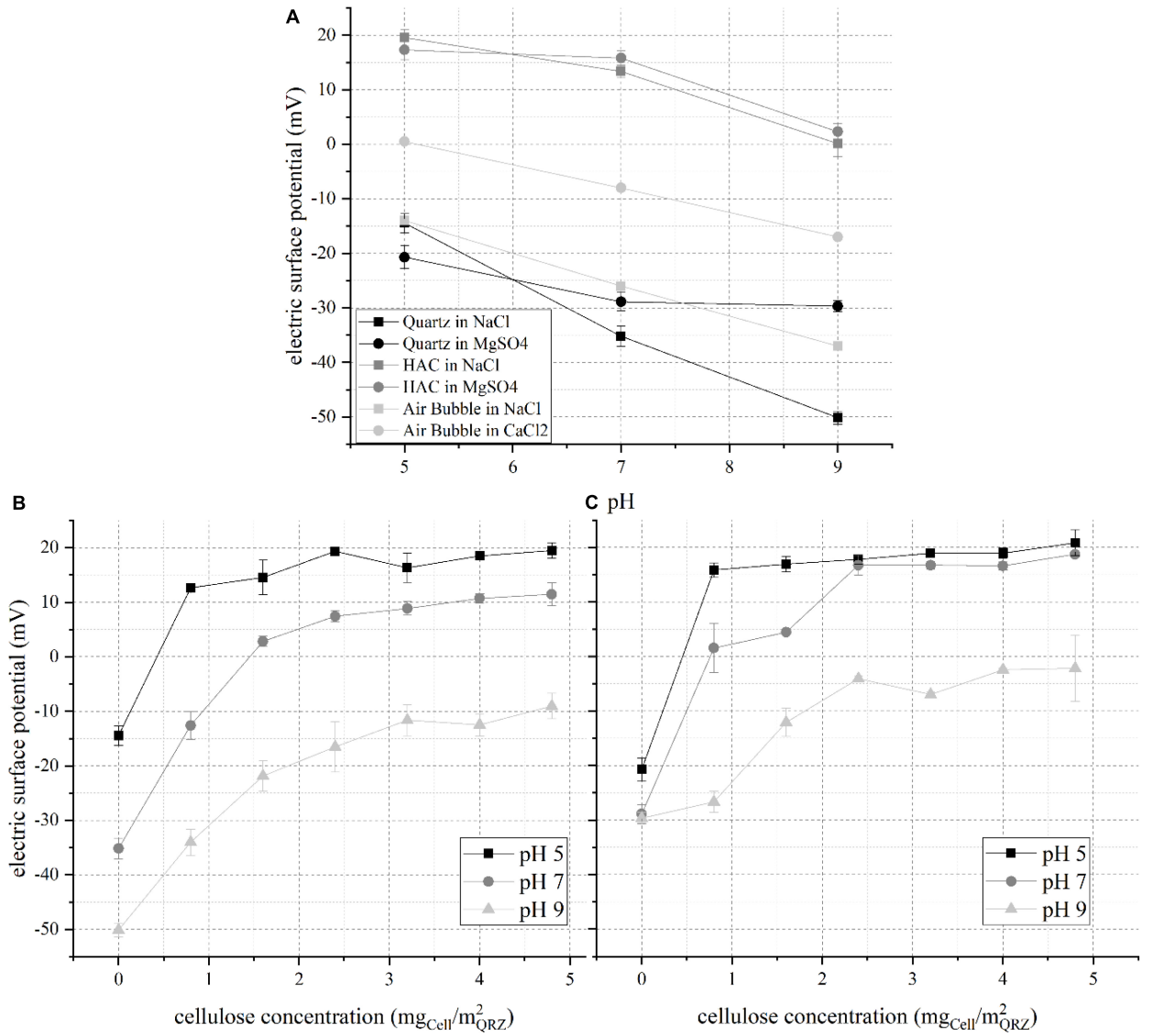

FIGURE 2 | Electric surface (ζ–) potential of **(A)** pure quartz, HAC and a bubble at different pH values according to previously published results (Yang et al., 2001; Hartmann et al., 2018), **(B)** QRZ at different HAC concentrations in NaCl, and **(C)** QRZ at different HAC concentrations in $MgSO_4$; error bars are 95% confidence intervals and lines are only visual guidelines.

are correlated to higher particle-bubble attachment probabilities and floatability.

Probability of Quartz-Bubble Attachments in the Presence of Hexyl-Amine Cellulose

As mentioned in section Materials, Methods, and Models, the probability for a QRZ particle to attach to an air bubble as a function of the particle-bubble distance (H), contact time and HAC concentration was measured by means of the ACTA. As a representative example, the results for the attachment probability are shown for pH 7 in **Figure 3**, while the results for pH 5 and pH 9 are presented in **Supplementary Figures S1, S2**.

As seen in **Figure 3**, in the absence of HAC, the bubbles had to be compressed against the particle bed (i.e., compression > 0) for attachment to occur. To obtain an attachment probability higher than 50%, bubbles were compressed for approximately 150 μm against the particle bed, which is in the range of the D_{50}-value for the QRZ particles (see **Table 1**), indicating that an attachment only occurred in the presence of an additional mechanical force acting upon the intervening liquid film rather than as a result of any attractive interfacial force. When HAC is present in solution, stable particle-bubble attachments were obtained at distances between 25 and 50 μm (P > 50%) without compressing a bubble against the particle bed (in **Figure 3**, positive distance = negative compression). In several instances, these distances exceed significantly the generally

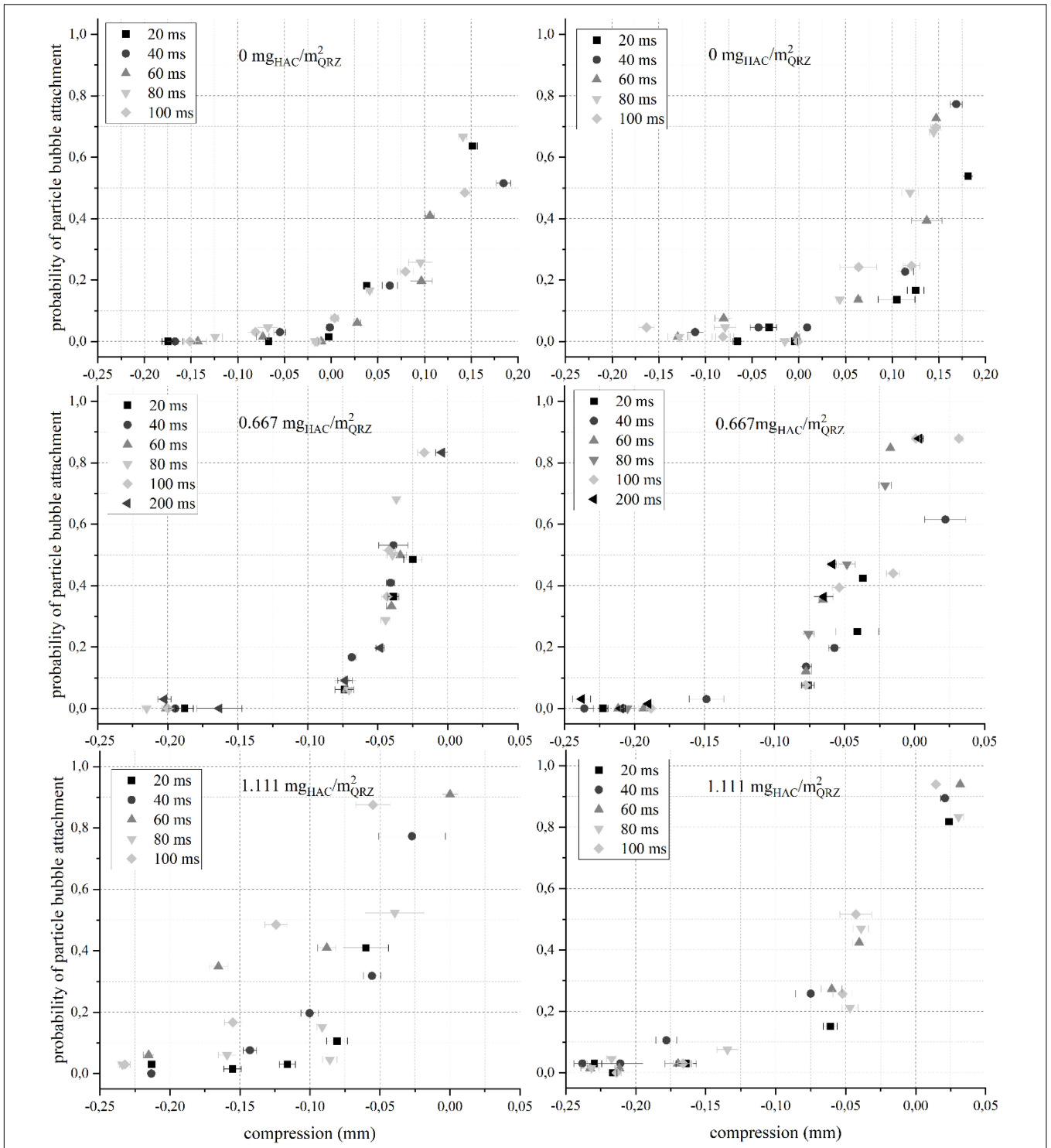

FIGURE 3 | The probability for an attachment between a QRZ particle and an air bubble immersed in a NaCl **(left)** or $MgSO_4$ **(right)** solution at pH 7 over the particle-bubble distance (compression = −H) for different contact times and HAC concentrations. The error bars are 95% confidence intervals. Note that the abscissa value range is not the same in all graphs.

accepted ranges for particle-bubble interactions (Israelachvili and Pashley, 1982; Eriksson et al., 1989; Ducker et al., 1994; Yao et al., 2016). Already when the HAC concentration was 0.667 mg$_{HAC}$/m$^2_{QRZ}$, non-compressive attachments between QRZ particles and air bubbles occurred, proving that HAC renders the mineral surface more hydrophobic, in line with earlier studies

(Laitinen et al., 2016; Hartmann et al., 2017, 2018). Interestingly, at 0.667 mg_{HAC}/m^2_{QRZ} in NaCl, the attachment probability seems rather independent from the influence of contact times, but remains sensitive to distance with a sudden increase of the attachment probability in the range between 20 and 50 μm. An additional experiment with 200 ms contact time was performed at the lower HAC concentration, however not showing a significant increase of the attachment probability in any of the background salt solutions. The independence of the attachment probability distribution in terms of the set contact time has not been reported before, but may be interpreted as a spontaneous rupture of the intervening film occurring at a significantly shorter time than the minimum contact time used in these experiments. As will be discussed next, a stronger hydrophobicity makes the influence of contact time more evident, but the emergence of a non-compressive attachment between a particle and a bubble may be already indicative of a turning point on its floatability.

As seen, when the HAC concentration was increased to 1.111 mg_{HAC}/m^2_{QRZ}, two trends were observed: (i) an extension of the particle-bubble distance at which high attachment probabilities were measured, and (ii) an evident correlation of higher attachment probabilities with increasing contact time for each given particle-bubble distance. These trends are most significant for particle-bubble attachments in NaCl solution, but were consistently seen for the attachment probabilities of QRZ for both background solutions in pH 5 or 9 (see **Supplementary Figures S1, S2**). The dependence of attachment probability to particle size was shown in a previous work to follow the efficiency of particle-bubble aggregate stability, which diminishes with increasing particle size (Hartmann and Serna-Guerrero, 2020). Admittedly, the sensitivity of attachment probabilities for different contact times in this work may be limited by the relatively broad particle size distribution, i.e., 75–180 μm. Nevertheless, non-compressive attachment has been recorded for all samples in which HAC was present and a higher sensitivity in regards of the contact time was always observed at higher HAC concentrations, demonstrating the ability of ACTA to distinguish different degrees of hydrophobicity for a particular mineral sample.

When the results are put in context with the ζ-potential of QRZ coated with HAC under identical environments, a higher adsorption capacity is expected with increasing HAC concentrations, as reflected by the compensation of the ζ-potential in **Figure 2**. Thus, at higher HAC concentrations, it can be expected that a more complete coverage of QRZ particles occurs, resulting in a higher degree of hydrophobicity. In turn, this leads to longer distances for which high attachment probabilities occur, generating an evident dependence of attachment probabilities with contact times. As shown in **Figure 2**, when the HAC concentration is 0.666 mg_{HAC}/m^2_{QRZ}, the ζ-potential of HAC-coated QRZ is more negatively charged in NaCl compared to $MgSO_4$ solution. Interestingly, the results of the particle-bubble attachment probability in $MgSO_4$ solution show a comparatively higher sensitivity in terms of contact time. By increasing the HAC concentration to 1.111 mg_{HAC}/m^2_{QRZ} at pH 7, the ζ-potential of HAC-coated QRZ approaches its iso-electric point in NaCl solution, while the potential is overcompensated in $MgSO_4$ solution. In the case of ACTA analysis, the increase of HAC concentration from 0.666 mg_{HAC}/m^2_{QRZ} to 1.111 mg_{HAC}/m^2_{QRZ} in NaCl solution led to an increase of the attachment distance and a higher sensitivity in terms of the contact time for non-compressive attachments. Surprisingly, no significant change occurred by increasing the HAC concentration in $MgSO_4$ solution, which may be explained by an antagonistic effect in terms of floatability obtained when the ζ-potential of QRZ is overcompensated by HAC, as described in an earlier work (Hartmann et al., 2018). This is an indication of the different behavior of nanocellulose compared to traditional collectors, as one may not obtain a better flotation performance simply by increasing the concentration of the former due to the random distribution of amine groups on its surface.

The obtained non-compressive particle-bubble attachments are in line with previous results obtained for the attachment of silanized glass beads to air bubbles (Hartmann and Serna-Guerrero, 2020). These results exhibit the existence of a force acting over far longer distances or perhaps changes in the properties of water molecules within the intervening liquid film have to be assumed. Although the nature of the long-range attraction cannot be analyzed in detail based on the results obtained in this work, the results of the ACTA may be a good foundation to draw some conclusions. An estimation of the length scale of micro-eddies is given after Kolmogorov (Nguyen and Schulze, 2004) by:

$$\lambda_K = \left(\frac{\nu^3}{\varepsilon}\right)^{\frac{1}{4}} \tag{2}$$

When a value for the kinematic viscosity ν of 10^{-6} m^2/s and the mean dissipation rate ε between 1 and 100 W/kg is assumed, the length of a microscale eddy is estimated between 10 and 30 μm, which is in the range of the particle-bubble distance shown in **Figure 3**. However, the results of hydrophilic QRZ particles (in the absence of HAC) show that microscale eddies do not have a significant effect on the particle-bubble attachment and particles only attach when a bubble is compressed against a particle. In other words, it is possible that microscale eddies contribute to the transportation of microparticles, but particle-bubble agglomerates result only when attractive forces are present. Admittedly, the presented values for the kinematic viscosity of vicinal water and the dissipation rate in polarized water molecules are rough estimations.

Another phenomenon that is worth considering is the ability of fluid molecules to propagate forces along their structure, which was firstly described by Hardy (1931) using the term "*diachysis*" (after the Greek *diáchysis* meaning "diffusion"). A review of experimental data suggesting the existence of an abnormal behavior of water molecules was presented 70 years ago by Henniker (1949) and some 20 years later, Padday (1970) studied the rupture of thin liquid films between surfaces with different wettability and air. In the latter work, the rupture of thin water films was detected to be initiated at thicknesses between 100 and 500 μm over surfaces with low surface energy. Although long-range forces are expected to be of structural nature (Ducker et al., 1994; Yoon and Moa, 1996),

based on an entropic effect of the re-arrangement of water molecules near hydrophobic surfaces, no conclusive physical explanation for their strength and extension has been found. One important aspect of *diachysis* is that the origin of forces is not locally restricted to the surface of particles or bubbles, but forces are acting along clusters of structured water molecules (Eriksson et al., 1989). In other words, the liquid phase is not solely a passive medium through which forces act, but it energetically merits from the presence of a solid or gaseous phase, which induce a structure into the liquid film, leading to the propagation of forces over relatively long distances. The examination of the structure of water molecules near solid or gaseous surfaces is an ongoing field of research, challenged by the complexity of the system under investigation, which at present exceeds the ability of molecular modeling (Akaishi et al., 2017). The ACTA may be a valuable technique to quantify the strength and range of interactions between microparticles and bubbles in quiescent environments. To investigate if the particle-bubble attachments occur and are stable under turbulent conditions, the flotation recovery of QRZ in the presence of HAC is presented next.

Flotation of Quartz Using Hexyl-Amine Nanocrystals

The results for the flotation of QRZ with HAC are presented in **Figure 4**, showing a significant increase of the flotation recovery between 0.38 and 0.7 mg_{HAC}/m^2_{QRZ}. The lower HAC concentration was not sufficient to render QRZ sufficiently hydrophobic and the high turbulences in the flotation cell did not contribute to produce stable three-phase contacts. For the results obtained with 0.7 mg_{HAC}/m^2_{QRZ} in NaCl solution, an increasing flotation recovery with increasing pH value was obtained, while similar recoveries were obtained at pH 7 and 9 in $MgSO_4$. The relatively high flotation recoveries obtained with 0.7 mg_{HAC}/m^2_{QRZ} also prove that, even though physisorption of HAC is assumed, it withstood its detachment from the particle surface under the action of turbulent currents in the flotation cell.

Figure 4 also compares the results of two experiments performed using HAC solution in the presence of fresh and recirculated QRZ at pH 7 and 9 in NaCl solution. While the flotation of fresh QRZ resulted in low flotation recoveries, flotation performance improved significantly after drying and re-suspension in the presence of HAC. This is understandable since, due to characteristics of the flotation setup, the amount of HAC suspension used was not excessive, which likely resulted in the reduction of the HAC bulk concentration in the suspension during physisorption of HAC on the QRZ surface. As a result, the adsorbed amount of HAC on fresh QRZ does not represent saturation at target HAC concentration. By re-dispersing QRZ in HAC suspension, the HAC adsorption approached equilibrium at the target of 5 mg/l (0.7 mg_{HAC}/m^2_{QRZ}). The same procedure was performed for the lower HAC concentration, but no increase of the floatability obtained (0.38 mg_{HAC}/m^2_{QRZ}), proving that QRZ is not rendered sufficiently hydrophobic at the low HAC concentration. An additional finding by following the aforementioned procedure is that HAC remains adsorbed throughout the process of vacuum filtration, drying and re-dispersion of the sample in the HAC solution. These observations suggest that the desorption of HAC does not occur spontaneously, at least under the conditions hereby used.

The dramatic increase of recovery from 0.38 to 0.7 mg_{HAC}/m^2_{QRZ} indicates that the change from a non-floatable to a floatable behavior takes place within a narrow window of HAC adsorption. Consequently, the flotation results obtained show that ACTA is sensible enough to detect the point at which floatability of particles become significant. Indeed, according

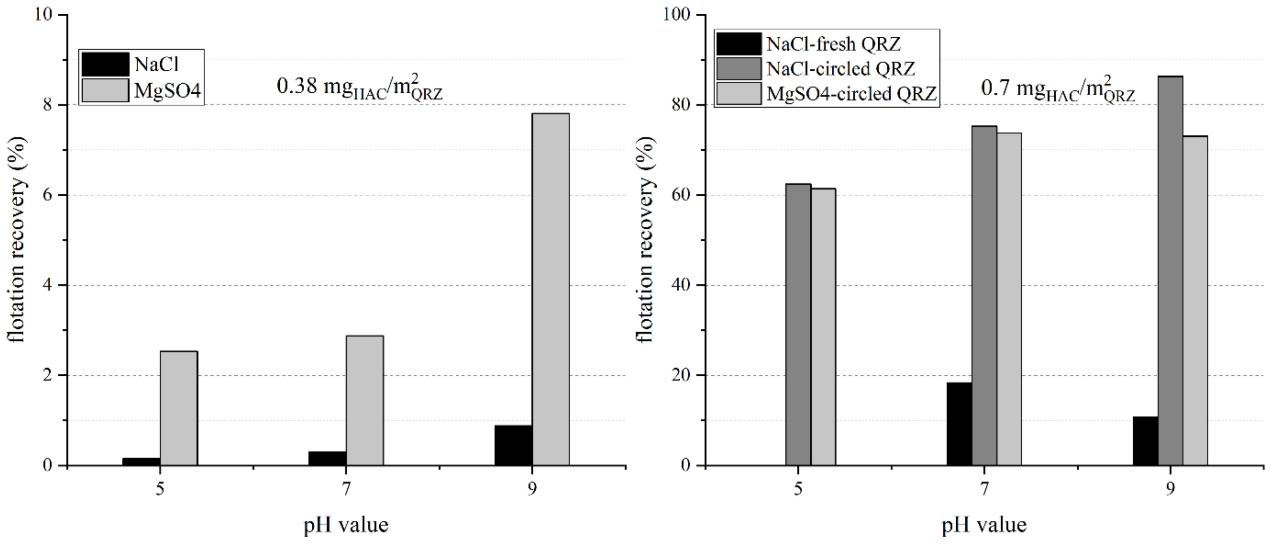

FIGURE 4 | The flotation recovery of quartz using hexyl-amine nanocrystals as collector with a concentration of 0.38 mg_{HAC}/m^2_{QRZ} **(left)** and 0.7 mg_{HAC}/m^2_{QRZ} **(right)** in different background salt solutions (shown is the mean value of two experiments).

to the ACTA results, successful non-compressive attachment is detected at 0.667 mg_{HAC}/m^2_{QRZ}. In other words, non-compressive attachments with high probability may be a suitable indicator for efficient flotation.

The correlation of the flotation results to the state of the ζ-potential of QRZ under identical conditions shows that an increasing potential does not correspond to a higher floatability. In contrast, the more negative the ζ-potential of QRZ at a HAC concentration of 0.7 mg_{HAC}/m^2_{QRZ}, the higher flotation recoveries were obtained for experiments performed in NaCl solutions. Further, the electrophoretic mobility tests indicate that at a concentration of 0.7 mg_{HAC}/m^2_{QRZ} HAC does not cover the entire QRZ surface, assuming that HAC has a tendency to form a monolayer on the QRZ surface. In accordance to the general knowledge in flotation, this shows that high flotation recoveries are also obtained for cellulose-based reagents even without the formation of an ideal monolayer on the mineral surface.

CONCLUSION

In this study, HAC was tested as an environmentally-friendly collector for the flotation of QRZ. Bench-scale flotation experiments revealed that adsorbed HAC rendered the QRZ surface more hydrophobic, leading to recoveries up to 90% at 0.7 mg_{HAC}/m^2_{QRZ}, proving that the application of cellulose-based macromolecules is feasible in turbulent froth flotation processes. The adsorption of HAC on QRZ was indicated with the help of ζ-potential measurements showing a consistent reduction of the ζ-potential of QRZ in the presence of HAC. Induction time experiments with the ACTA exhibited that high probabilities for non-compressive attachments can be obtained at distances between 25 and 50 μm in the presence of HAC, while pure QRZ only attached to air bubbles under the action of significant compression. In consequence, the ACTA and flotation results demonstrate the relevance of hydrophobic forces in the attraction between HAC-coated QRZ and air bubbles. In addition, an increase of the floatability of QRZ in a bench-scale flotation cell coincided with conditions where non-compressive particle-bubble attachments appeared in ACTA measurements. Although additional studies have to be performed to elaborate on its degree of accuracy, this work also shows the potential of the ACTA to be used for the prediction of the hydrophobicity and thus floatability of a mineral phase.

DATA AVAILABILITY STATEMENT

The datasets generated for this study are available on request to the corresponding author.

AUTHOR CONTRIBUTIONS

RH performed and overviewed the experimental work and prepared the first draft of the manuscript. RS-G reviewed the manuscript. Both had regular meetings during the experimental work and writing phase.

FUNDING

This work is part of the ACTA project supported by the Finnish Metals Producers Fund. RH would like to thank the Academy of Finland for their financial support with the "BioMInt" Postdoctoral Research project. This research benefited from the RAMI- RawMatTERS Finland Infrastructure.

ACKNOWLEDGMENTS

We would like to thank Prof. Dr. Mirja Illikainen and her group of the Fibre and Particle Engineering Research Unit at the University of Oulu for the preparation of the hexyl amine cellulose nanocrystal suspension and the opportunity to share the equipment for electrophoretic mobility measurements. Further, we would like to express their special thanks to Ms. Pia Höner for her contribution to the laboratory work.

SUPPLEMENTARY MATERIAL

The Supplementary Material for this article can be found online at: https://www.frontiersin.org/articles/10.3389/fmats.2020.00053/full#supplementary-material

FIGURE S1 | The probability for an attachment between a QRZ particle and an air bubble immersed in a NaCl or $MgSO_4$ solution at pH 5 over the particle-bubble compression for different contact times and HAC concentrations.

FIGURE S2 | The probability for an attachment between a QRZ particle and an air bubble immersed in a NaCl or $MgSO_4$ solution at pH 9 over the particle-bubble compression for different contact times and HAC concentrations.

REFERENCES

Abarca, C., Ali, M. M., and Pelton, R. H. (2018). Choosing mineral flotation collectors from large nanoparticle libraries. *J. Coll. Interf. Sci.* 2018, 423–430. doi: 10.1016/j.jcis.2018.01.080

Ago, M., Huan, S., Borghei, M., Raula, J., Kauppinen, E. I., and Rojas, O. J. (2016). High-throughput synthesis of lignin particles (∼30 nm to ∼2 μm) via aerosol flow reactor: size fractionation and utilization in pickering emulsions. *ACS Appl. Mater. Interf.* 8, 23302–23310. doi: 10.1021/acsami.6b07900

Akaishi, A., Yonemaru, T., and Nakamura, J. (2017). Formation of water layers on graphene surfaces. *ACS Omega* 2017, 2184–2190. doi: 10.1021/acsomega.7b00365

Al-Shatty, W., Lord, A. M., Alexander, S., and Barron, A. R. (2017). Tunable surface properties of aluminum oxide nanoparticles from highly hydrophobic to highly hydrophilic. *ACS Omega* 2017, 2507–2514. doi: 10.1021/acsomega.7b00279

Aspiala, M., Schreithofer, N., and Serna-Guerrero, R. (2018). Automated contact time apparatus and measurement procedure for bubble-particle interaction analysis. *Minerals Eng.* 2018, 77–82. doi: 10.1016/j.mineng.2018.02.018

Bridge, G. (2004). Contested terrain: mining and the environment. *Annu. Rev. Environ. Resour.* 29, 205–259. doi: 10.1146/annurev.energy.28.011503.163434

Calvo, G., Mudd, G., Valero, A., and Valero, A. (2016). Decreasing ore grades in global metallic mining: a theoretical issue or a global reality? *Resources* 5:36. doi: 10.3390/resources5040036

Crawford, R., and Ralston, J. (1988). The influence of particle size and contact angle in mineral flotation. *Int. J. Mineral Process.* 1988, 1–24. doi: 10.1016/0301-7516(88)90002-6

Derjaguin, B. V., and Churaev, N. V. (1989). The current state of the theory of long-range surfaec forces. *Coll. Surf.* 1989, 223–237. doi: 10.3109/10799893.2014.980950

Dong, X., Price, M., Dai, Z., Xu, M., and Pelton, R. (2017). Mineral-mineral particle collisions during flotation remove adsorbed nanoparticle flotation collectors. *J. Coll. Interf. Sci.* 2017, 178–185. doi: 10.1016/j.jcis.2017.05.050

Ducker, W. A., Xu, Z., and Israelachvili, J. N. (1994). Measurements of hydrophobic and DLVO forces in bubble-surface interactions in aqueous solutions. *Langmuir* 1994, 3279–3289.

Eriksson, J. C., Ljunggren, S., and Claesson, P. M. (1989). A phenomenological theory of long-range hydrophobic attraction forces based on a square-gradient variational approach. *J. Chem. Soc. Faraday Trans. 2* 85, 163. doi: 10.1039/f29898500163

Fuerstenau, D. W., and Jia, R. (2004). The adsorption of alkylpyridinium chlorides and their effect on the interfacial behavior of quartz. *Coll. Surf. A* 2004, 223–231. doi: 10.1016/j.colsurfa.2004.04.090

Fuerstenau, D. W., and Pradip, (2005). Zeta potentials in the flotation of oxide and silicate minerals. *Adv. Coll. Interf. Sci.* 2005, 9–26. doi: 10.1016/j.cis.2004.08.006

Hardy, W. (1931). Problems of the boundary state. *Philos. Trans. R. Soc. Lond.* 1931, 1–37.

Hartmann, R., Kinnunen, P., and Illikainen, M. (2018). Cellulose-mineral interactions based on the DLVO theory and their correlation with flotability. *Minerals Eng.* 2018, 44–52. doi: 10.1016/j.mineng.2018.03.023

Hartmann, R., Rudolph, M., Ämmälä, A., and Illikainen, M. (2017). The action of cellulose-based and conventional flotation reagents under dry and wet conditions correlating inverse gas chromatography to microflotation studies. *Minerals Eng.* 2017, 17–25. doi: 10.1016/j.mineng.2017.09.004

Hartmann, R., and Serna-Guerrero, R. (2020). Towards a quantitative analysis of the wettability of microparticles using an automated contact timer apparatus. *Minerals Eng.* 149:106240. doi: 10.1016/j.mineng.2020.106240

Hartmann, R., Sirviö, J. A., Sliz, R., Laitinen, O., Liimatainen, H., Ämmälä, A., et al. (2016). Interactions between aminated cellulose nanocrystals and quartz: adsorption and wettability studies. *Coll. Surf. A* 2016, 207–215. doi: 10.1016/j.colsurfa.2015.10.022

Henniker, J. C. (1949). The depth of the surface zone of a liquid. *Rev. Mod. Phys.* 1949, 322–341. doi: 10.1103/revmodphys.21.322

Hernandez, V. A., Ulloa, A., and Gutierrez, L. (2017). Use of wood hemicelluloses to improve copper recovery from high clay Cu-Mo ores. *Minerals Eng.* 2017, 198–200. doi: 10.1016/j.mineng.2017.06.023

Israelachvili, J. N., and Pashley, R. (1982). The hydrophobic interaction is long range, decaying exponentially with distance. *Nature* 1982, 341–342. doi: 10.1038/300341a0

Klemm, D., Heublein, B., Fink, H. P., and Bohn, A. (2005). Cellulose: fascinating biopolymer and sustainable raw material. *Angewandte Chemie* 44, 3358–3393. doi: 10.1002/anie.200460587

Laitinen, O., Hartmann, R., Sirviö, J. A., Liimatainen, H., Rudolph, M., Ämmälä, A., et al. (2016). Alkyl aminated nanocelluloses in selective flotation of aluminium oxide and quartz. *Chem. Eng. Sci.* 2016, 260–266. doi: 10.1016/j.ces.2016.01.052

Liu, W., Moran, C. J., and Vink, S. (2013). A review of the effect of water quality on flotation. *Minerals Eng.* 53, 91–100. doi: 10.1016/j.mineng.2013.07.011

Lopéz, R., Jordão, H., Hartmann, R., Ämmälä, A., and Carvalho, M. T. (2019). Study of butyl-amine nanocrystal cellulose in the flotation of complex sulphide ores. *Coll. Surf. A* 2019:123655. doi: 10.1016/j.colsurfa.2019.123655

Mu, Y., Peng, Y., and Lauten, R. A. (2016). The depression of pyrite in selective flotation by different reagent systems – A Literature review. *Minerals Eng.* 9, 143–156. doi: 10.1016/j.mineng.2016.06.018

Nguyen, A. V., and Schulze, H. J. (2004). *Colloidal Science of Flotation*. Boca Raton, FL: CRC Press.

Nuorivaara, T., Björkqvist, A., Bacher, J., and Serna-Guerrero, R. (2019). Environmental remediation of sulfidic tailings with froth flotation: reducing the consumption of additional resources by optimization of conditioning parameters and water recycling. *J. Environ. Manag.* 236, 125–133. doi: 10.1016/j.jenvman.2019.01.107

Padday, J. F. (1970). Cohesive properties of thin films of liquids adhering to a solid surface. *Specif. Discuss. Faraday Soc.* 1970, 64–74.

Pearse, M. J. (2005). An overview of the use of chemical reagents in mineral processing. *Minerals Eng.* 18, 139–149. doi: 10.1016/j.mineng.2004.09.015

Rudolph, M., and Hartmann, R. (2017). Specific surface free energy component distributions and flotabilities of mineral microparticles in flotation–An inverse gas chromatography study. *Coll. Surf. A* 2017, 380–388. doi: 10.1016/j.colsurfa.2016.10.069

Taguta, J., McFadzean, B., and O'Connor, C. (2019). The relationship between the flotation behaviour of a mineral and its surface energy properties using calorimetry. *Minerals Eng.* 2019:105954. doi: 10.1016/j.mineng.2019.105954

Taguta, J., O'Connor, C. T., and McFadzean, B. (2018). The relationship between enthalpy of immersion and flotation response. *Coll. Surf. A* 2018:263–270. doi: 10.1016/j.colsurfa.2018.08.059

van Oss, C. J. (2003). Long-range and short-range mechanisms of hydrophobic attraction and hydrophilic repulsion in specific and aspecific interactions. *J. Mol. Recogn.* 2003, 177–190. doi: 10.1002/jmr.618

Verrelli, D. I., and Albijanic, B. (2015). A comparison of methods for measuring the induction time for bubble–particle attachment. *Minerals Eng.* 2015, 8–13. doi: 10.1111/jre.12546

Visanko, M., Liimatainen, H., Sirviö, J. A., Heiskanen, J. P., Niinimäki, J., and Hormi, O. (2014). Amphiphilic cellulose nanocrystals from acid-free oxidative treatment: physicochemical characteristics and use as an oil-water stabilizer. *Biomacromolecules* 2014, 2769–2775. doi: 10.1021/bm500628g

William, A. D., Zhenghe, X., and Jacob, N. I. (1994). Measurements of hydrophobic and DLVO forces in bubble-surface interactions in aqueous solutions. *Langmuir* 1994, 3279–3289. doi: 10.1021/la00021a061

Yang, C., Dabros, T., Li, D., Czarnecki, J., and Masliyah, J. H. (2001). Measurement of the zeta potential of gas bubbles in aqueous solutions by microelectrophoresis method. *J. Coll. Interf. Sci.* 2001, 128–135. doi: 10.1006/jcis.2001.7842

Yang, S., Pelton, R., Abarca, C., Dai, Z., Montgomery, M., Xu, M., et al. (2013). Towards nanoparticle flotation collectors for pentlandite separation. *Int. J. Mineral Process.* 2013, 137–144. doi: 10.1016/j.minpro.2013.05.007

Yang, S., Pelton, R., Raegen, A., Montgomery, M., and Dalnoki-Veress, K. (2011). Nanoparticle flotation collectors: mechanisms behind a new technology. *Langmuir* 2011, 10438–10446. doi: 10.1021/la2016534

Yao, J., Han, H., Hou, Y., Gong, E., and Yin, W. (2016). A method of calculating the interaction energy between particles in minerals flotation. *Math. Probl. Eng.* 2016, 1–13. doi: 10.1155/2016/8430745

Yoon, R. H., and Moa, L. (1996). Application of Extended DLVO Theory, IV. Derivation of flotation rate equation from first principles. *J. Coll. Interf. Sci.* 181, 613–626. doi: 10.1006/jcis.1996.0419

Zembala, M. (2004). Electrokinetics of heterogeneous interfaces. *Adv. Coll. Interf. Sci.* 2004, 59–92. doi: 10.1016/j.cis.2004.08.001

Conflict of Interest: The authors declare that the research was conducted in the absence of any commercial or financial relationships that could be construed as a potential conflict of interest.

frontiers in Chemistry

REVIEW
published: 16 April 2020
doi: 10.3389/fchem.2020.00230

The Challenge of Tungsten Skarn Processing by Froth Flotation: A Review

Yann Foucaud[1]*, *Lev Filippov*[1,2], *Inna Filippova*[1] and *Michael Badawi*[3]*

[1] Université de Lorraine, CNRS, GeoRessources, Nancy, France, [2] National University of Science and Technology MISIS, Moscow, Russia, [3] Université de Lorraine, CNRS, Laboratoire de Physique et Chimie Théoriques, Nancy, France

Recently, tungsten has drawn worldwide attention considering its high supply risk and economic importance in the modern society. Skarns represent one of the most important types of tungsten deposits in terms of reserves. They contain fine-grained scheelite ($CaWO_4$) associated with complex gangue minerals, i.e., minerals that display similar properties, particularly surface properties, compared to scheelite. Consistently, the froth flotation of scheelite still remains, in the twenty first century, a strong scientific, industrial, and technical challenge. Various reagents suitable for scheelite flotation (collectors and depressants, mostly) are reviewed in the present work, with a strong focus on the separation of scheelite from calcium salts, namely, fluorite, apatite, and calcite, which generally represent significant amounts in tungsten skarns. Albeit some reagents allow increasing significantly the selectivity regarding a mineral, most reagents fail in providing a good global selectivity in favor of scheelite. Overall, the greenest, most efficient, and cheapest method for scheelite flotation is to use fatty acids as collectors with sodium silicate as depressant, although this solution suffers from a crucial lack of selectivity regarding the above-mentioned calcium salts. Therefore, the use of reagent combinations, commonly displaying synergistic effects, is highly recommended to achieve a selective flotation of scheelite from the calcium salts as well as from calcium silicates.

Keywords: scheelite, collectors, depressants, fatty acids, calcium minerals

OPEN ACCESS

Edited by:
Zhiyong Gao,
Central South University, China

Reviewed by:
Bo Feng,
Jiangxi University of Science and Technology, China
Yuesheng Gao,
Michigan Technological University, United States

***Correspondence:**
Yann Foucaud
yann.foucaud@univ-lorraine.fr
Michael Badawi
michael.badawi@univ-lorraine.fr

Specialty section:
This article was submitted to Physical Chemistry and Chemical Physics, a section of the journal Frontiers in Chemistry

Received: *20 December 2019*
Accepted: *10 March 2020*
Published: *16 April 2020*

Citation:
Foucaud Y, Filippov L, Filippova I and Badawi M (2020) The Challenge of Tungsten Skarn Processing by Froth Flotation: A Review. Front. Chem. 8:230. doi: 10.3389/fchem.2020.00230

INTRODUCTION: GENERAL CONTEXT

Tungsten: an Overview

Tungsten is a transition metal with the symbol W and atomic number 74, part of the same family as molybdenum and chromium. Its name comes from the former Swedish in which scheelite, the calcium tungstate, was named *tungsten*, i.e., "heave stone." Tungsten displays very interesting properties for industrial applications. First, it is one of the densest metals on Earth with a specific gravity of 19.3, very similar to that of gold and significantly higher than that of other transition metals. Besides, it exhibits a melting point of 3,422°C, which constitutes the highest melting point among all the metals (only exceeded by graphite). Along with its thermal dilatation coefficient, the lowest among all metals, this makes tungsten an excellent refractory material. Furthermore, this latter displays a substantial hardness (7.5 on the Mohs's scale), especially when it is combined with carbide anions in tungsten carbide (WC), which exhibits a hardness of 9. Tungsten presents a low abundance in the Earth crust, around 1.3 ppm, which is significantly lower than the other lithophile

elements but about the same as that of tin (2 ppm) and molybdenum (1.2 ppm). Rarely found under its metal form, tungsten is mostly encountered bound to oxygen atoms (tungstate anions), although it can form sulfides.

Tungsten Properties, Applications, and Prices

The aforementioned interesting properties of tungsten induce a wide range of industrial applications for this metal, including the production of tungsten carbide (55%), tungsten alloys and supra-alloys (25%), metal tungsten (13%), and chemical compounds (7%) (Audion and Labbé, 2012; U. S. Geological Survey, 2019). In particular, cemented tungsten carbide is traditionally used for machining of metallic parts and products where it constitutes the friction parts of drills and mills. Besides, tungsten alloys and supra-alloys are commonly used for refractory metallic pieces in aircraft engines, munitions, or metallurgical furnaces. Since cemented tungsten carbide cannot be recovered, the recycling rate of tungsten is around 20–25%, which represents a considerably low value (Audion and Labbé, 2012) compared to other metals. Moreover, the noticeable properties of tungsten induce a difficult substitution for this element (Audion and Labbé, 2012; U. S. Geological Survey, 2019): it can be substituted with molybdenum, titanium, or niobium in carbides and alloys, while metal tungsten can be replaced with depleted uranium. However, most of these substitutions decrease, rather than replace, the amount of tungsten used, and generally induce health problems (for uranium), increased cost, or significant loss of product performances (Audion and Labbé, 2012; U. S. Geological Survey, 2019).

Before the twentieth century, tungsten was marginally used for industrial applications. Its consumption significantly rose with the development of heavily armored warships, penetrative ammunitions, and automotive industry at the beginning of the twentieth century. Tungsten inflation-adjusted price has remained constant in average over the twentieth century (**Figure 1**). Nonetheless, it exhibited considerable peaks (**Figure 1**), in particular in 1915–1918 (World War I), 1951–1956 (Korean War), 1973–1978, and 2005, with a moderate rise during World War II. In the 1980s, an extra tungsten production ensured by China led to a tremendous decrease in the tungsten price (Audion and Labbé, 2012). Subsequently, most of the European tungsten mines, including the Salau French mine, closed, and very few tungsten mines in the world remained in operation. Since these closures, China has held a monopoly on the global tungsten production and has maintained the tungsten price significantly low. Nevertheless, in 2005, some exportations quotas were applied by China on its tungsten production, inducing a global increase in the tungsten price and, therefore, a gain of interest for tungsten exploration in the rest of the world, including in the EU.

Tungsten Deposits, Resources, and Supply

Several tungsten minerals have been reported in the literature, but only scheelite ($CaWO_4$) and wolframite [$(Fe,Mn)WO_4$] are of economic importance and nowadays exploited for primary tungsten extraction (Pitfield et al., 2011; Audion and Labbé, 2012; Schmidt, 2012a,b; Yang, 2018). Wolframite is a continuous solid series between ferberite ($FeWO_4$) and hubnerite ($MnWO_4$); the Fe/Mn ratio in the mineralized rock defines the dominance of one on another. Four major types of tungsten ore deposits have been reported in the literature: skarns, veins/stockworks, porphyries, and stratabound deposits (Werner et al., 1998; Schubert et al., 2006; Pitfield et al., 2011; Jébrak et al., 2016). As an overview, the typical WO_3 grades, deposit sizes, tungsten-bearing mineral(s),

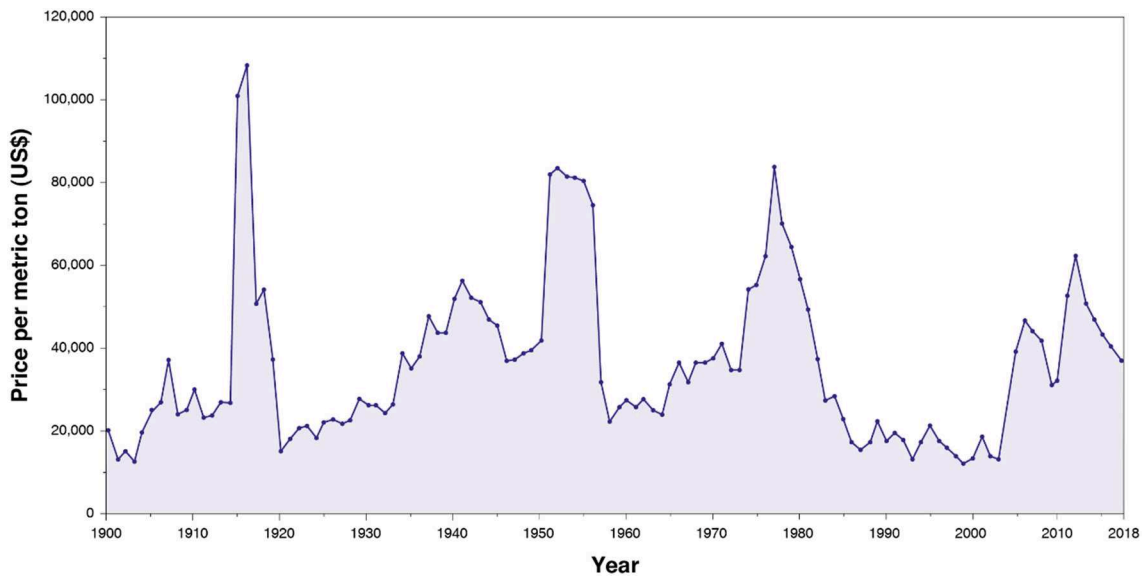

FIGURE 1 | Evolution of the tungsten inflation-adjusted price per metric ton from 1900 to actual, from Metalary website.

TABLE 1 | The four major types of tungsten ore deposits with typical deposit sizes, WO_3 grades, tungsten minerals and mines, adapted from Werner et al. (1998), Schubert et al. (2006), Pitfield et al. (2011), and Yang (2018).

Deposit type	Deposit sizes	Typical grade, %WO_3	Tungsten mineral(s)	% of total	Mines
Skarn	10^4-5 × 10^7 t	0.3–1.4	Scheelite	41	Cantung (Canada); Los Santos (Spain); Vostok-2 (Russia)
Vein/stockwork	10^5-10^8 t	Variable	Wolframite	35	Pasto Bueno (Peru); Panasqueira (Portugal); San Fix (Spain); Chollja (Bolivia);
Porphyry	10^7-10^8 t	0.1–0.4	Wolframite Scheelite	16	Xingluokeng (China); Yangchuling (China); Northern Dancer (Canada); Climax (USA)
Stratabound	10^6-10^7 t	0.2–1.0	Scheelite	3	Mittersill (Austria); Damingshan (China); Mount Mulgine (Australia)

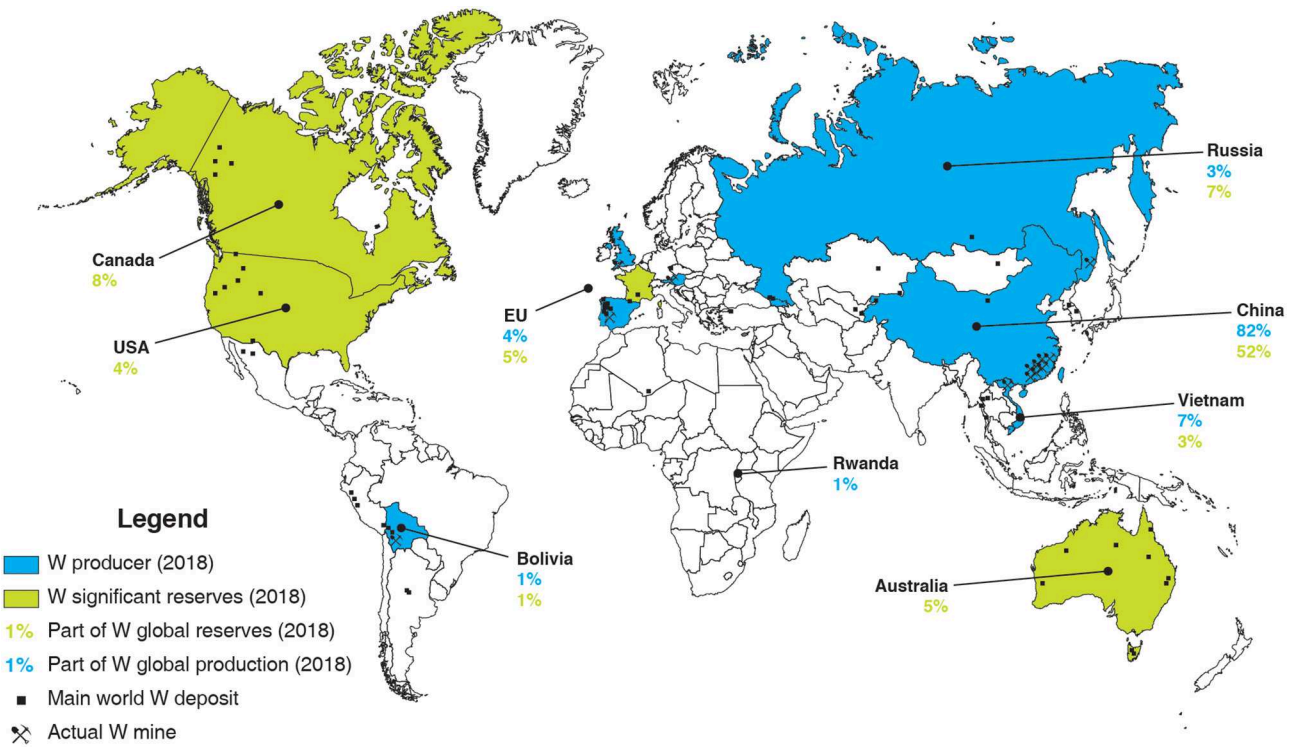

FIGURE 2 | World map of main W world deposit, W mines, W producers and countries with significant W reserves, and their respective part in the global W reserves/production in 2018, built with data from the U. S. Geological Survey (2019).

and mines corresponding to the four major types of tungsten ore are summarized in **Table 1**. Overall, skarn ores exhibit low tonnages and moderately high grades compared to the three other tungsten deposits, mainly the porphyry deposits.

At the moment, the world tungsten production is mainly ensured by China, which produced, in 2018, more than 80% of the 82,000 t of tungsten produced worldwide (U. S. Geological Survey, 2019). More than 10 major tungsten mines, with an annual output of over 1,300 t of WO_3, are reported in China, most of them being located in southern China (Werner et al., 1998; Pitfield et al., 2011; Audion and Labbé, 2012; Yang, 2018). In particular, the Xianglushan and Shizhuyuan deposits represent the two largest tungsten mines in China, with over 5,700 and 5,500 t of WO_3 produced each year, respectively (Yang, 2018). Some other countries such as Vietnam, Russia, and a few European countries produce low amounts of tungsten (**Figure 2**). Vietnam operates one of the largest tungsten mine worldwide, the Nui Phao mine, whose reserves have been estimated to 66 million tons of ore with an average grade of 0.2% WO_3 (Masan Resources, 2012). Besides, Russia has been mining the Vostok-2 sulfide–scheelite skarn ore since 1969, with around 1 million tons of remaining ore with a high average grade of around 1.7% WO_3 (Soloviev and Krivoshchekov, 2011). Despite the decrease in tungsten price in the 1980s, Austria and Portugal succeeded in maintaining the Mittersill and Panasqueira mines in operation. They produced, in 2018, 980 and 770 t of tungsten, respectively, which, however, represent a very minor part of the world production (**Figure 2**). Recently, considering

the significant increase in tungsten price in the middle of the 2000s, new tungsten mining projects have been launched in the world, including in the EU (Suárez Sánchez et al., 2015). In particular, the Los Santos mine (Spain) started operations in 2008 and produced, in 2018, 750 t of tungsten, with estimated reserves of 3.58 million tons with an average grade of 0.23% WO_3 (Wheeler, 2015). Furthermore, operations started in the Hemerdon mine (UK) in 2015, which reserves have been estimated at 35.7 million tons of ore at 0.18% WO_3 (Yang, 2018). Nonetheless, despite a production of 900 t of tungsten in 2018, the Hemerdon mine ceased trading operations in October 2018, mainly due to a decrease in tungsten price along with poor processing performances.

Overall, the EU tungsten production amounts to <3,000 t, while its consumption is estimated at about 10,000 t per year, with a slight continuous increase predicted for the next decade (Yang, 2018). Increasing the tungsten primary production as well as the tungsten recycling rate is, therefore, crucial to afford the EU independency in terms of tungsten consumption. Nowadays, the global tungsten reserves and resources are estimated at 3.3 million tons (U. S. Geological Survey, 2019) and 4.0 million tons of tungsten (Pitfield et al., 2011; Yang, 2018), respectively, with around 52% in China (**Figure 2**). Nevertheless, many tungsten occurrences have been reported in the EU, including the UK, Spain, Austria, Portugal, and France (**Figure 3**), some of which exhibiting significant resources and being suitable for exploitation.

Based on the previous considerations, tungsten has been classified as a critical raw material (CRM) in the EU since 2011. Hence, some research programs have been launched over the past few years to stimulate the tungsten extraction, such as the FAME (Flexible and Mobile Economic Processing Technologies) H2020 project. In particular, the stress has been put on tungsten skarns, which represent, within the four major tungsten deposit types, more than 40% of the global tungsten reserves (Werner et al., 1998; Schubert et al., 2006; Pitfield et al., 2011). However, despite significantly high WO_3 grades, most skarn ores are still considered complex for mineral processing: the development of efficient, environment-friendly, and mobile processing routes for tungsten skarns beneficiation is therefore of paramount interest.

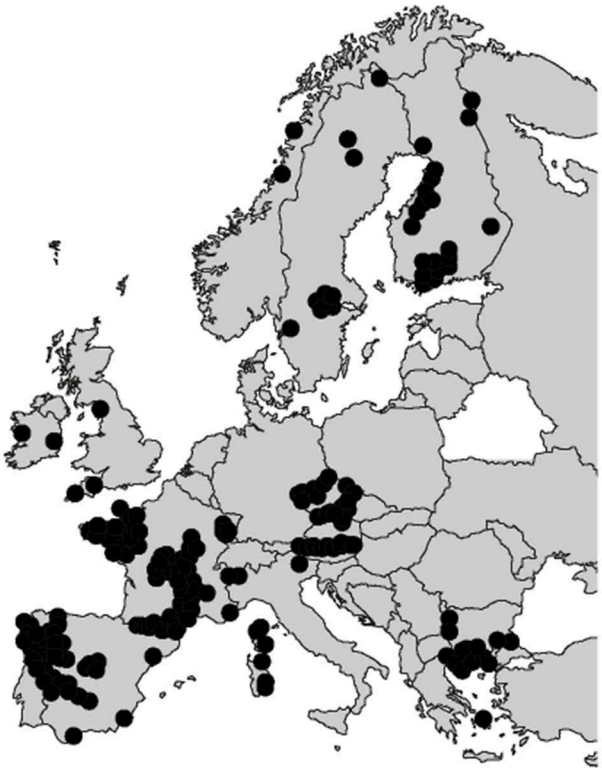

FIGURE 3 | Reported tungsten occurrences in the EU according to the main databases. Adapted from Lauri et al. (2018).

Tungsten Skarns

What Is a Skarn?

Skarn deposits are one of the most abundant ore types in the Earth's crust and have been intensively studied over the past decades (Meinert et al., 2005). Around 150 publications per year contain the term "skarn," which indicates a high constant interest of researchers and industrials for such deposits. Initially, skarns were defined by their mineralogical composition, usually dominated by calc-silicates such as pyroxene or garnets, the formation of which is enabled by the significant amounts of calcium in protolithic rocks (Einaudi and Burt, 1982; Kwak, 1987; Dawson, 1996; Misra, 2000; Meinert et al., 2005). However, skarns can also be considered in a more broad way, as rocks produced by the replacement of calcite or dolomite marble regardless of the presence of calcic or magnesian silicates (Kwak, 1987). Skarn deposits occur throughout a wide range of geological backgrounds, from Precambrian to Cenozoic, although most economic deposits are young and associated with magmatic–hydrothermal activity related to plutonism in orogenic belts (Einaudi and Burt, 1982). Traditionally, skarns are formed during contact metamorphism that goes along with a variety of metasomatic processes involving fluids of magmatic, metamorphic, meteoric, and/or marine origin (Meinert et al., 2005). Hence, most skarns are encountered adjacent to plutons albeit they can occur along faults, major shear zones, and various other structural backgrounds (**Figure 4**). Skarns can be classified by considering several major criteria, e.g., their calcite/dolomite initial content (calcic vs. magnesian skarns), their Fe^{3+}/Fe^{2+} ratio (oxidized vs. reduced skarns), or their distance to the pluton (proximal vs. distal skarns), to name but a few (Einaudi and Burt, 1982; Kwak, 1987; Meinert et al., 2005). Overall, though some skarns occur in not-calcic rocks, most of economic tungsten skarns are hosted in rocks with significant calcium contents (and/or magnesium) since this element is essential for scheelite deposition in the ore. This induces a common dominance of calcium minerals associated with scheelite in such ores.

The Economic Importance of Skarns

Mining of skarn deposits dates back to at least 4,000 years, and clear evidences of the mining of skarns can be encountered in the ancient Chinese, Greek, and Roman empires (Meinert et al., 2005). Historically, skarns have been mined for a large

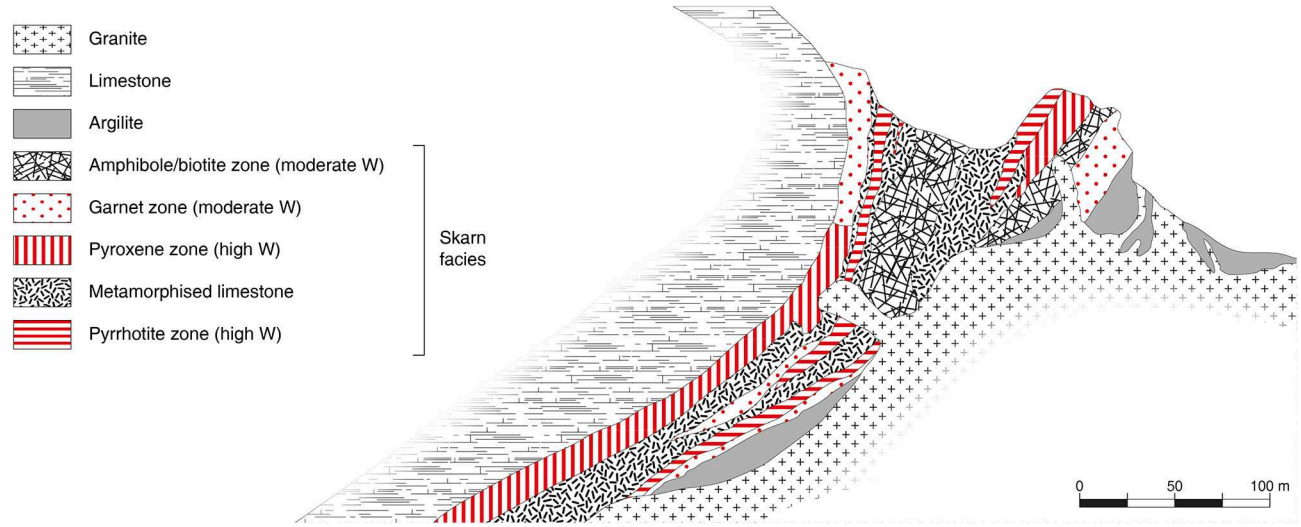

FIGURE 4 | Cross-section of a typical tungsten skarn (Cantung skarn, Canada) showing the granite, the limestone, and the different skarn facies at their interface, including the tungsten-bearing lithologies. Modified from Dawson (1996) with permission from the Geological Survey of Canada.

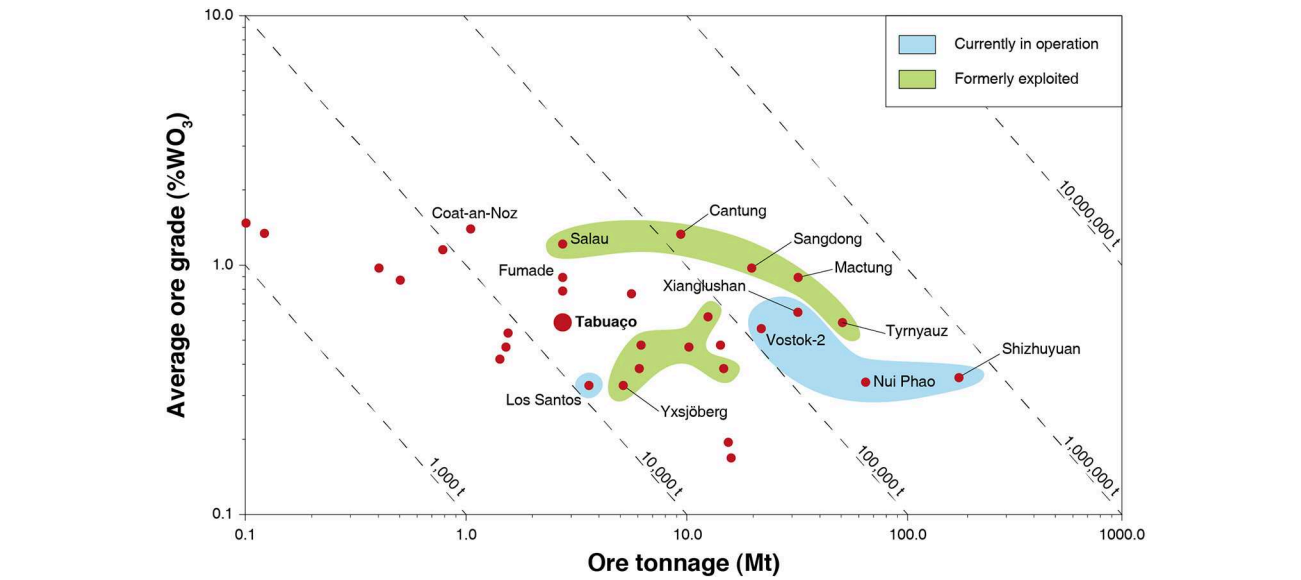

FIGURE 5 | Grade vs. tonnage of significant tungsten skarn deposits in the world, currently or formerly in operations. Modified and updated from Dawson (1996) with permission from the Geological Survey of Canada.

variety of metals, including iron, tin, tungsten, copper, zinc (along with lead), molybdenum, and gold (Einaudi and Burt, 1982; Kwak, 1987; Meinert, 1992; Dawson, 1996; Meinert et al., 2005). Considering actual economic deposits, skarns display either too low grades (for iron) or tonnages, e.g., for lead, zinc, or copper (Kwak, 1987) and, therefore, are no more exploited. Nonetheless, tungsten skarns commonly display average WO_3 grades ranging from 0.3 to 1.5%, which are significantly higher than for the other major types of tungsten deposits (see Tungsten Deposits, Resources and Supply section) (**Table 1** and **Figure 5**). Hence, despite lower tonnages compared to other major types of tungsten deposits (**Table 1**), many tungsten skarns are of economic importance. They have been continuously exploited for decades (**Figure 5**), supplying most of the world's tungsten demand (>70%) during some periods such as in the 1980s (Kwak, 1987). Nowadays, China ensures 82% of the world tungsten production (U. S. Geological Survey, 2019) with a considerable part of the Chinese tungsten coming from skarn deposits (Audion and Labbé, 2012). Indeed, the Xianglushan and Shizhuyuan world class tungsten deposits, which account for more than 11,000 tons (14%) in the annual global tungsten production, are considered as tungsten skarns (Lu et al., 2003;

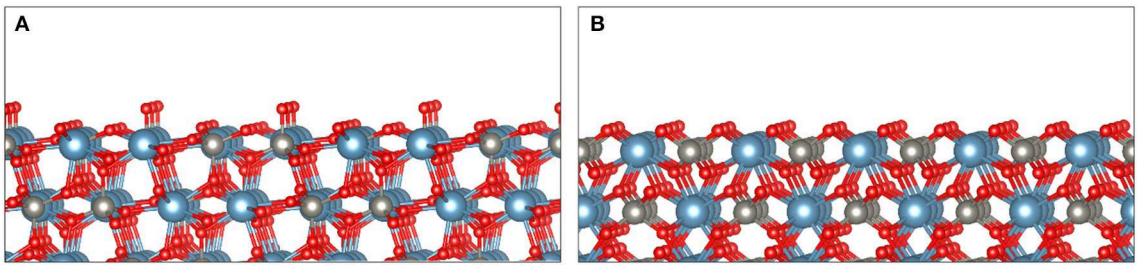

FIGURE 6 | The two main exposed surfaces during scheelite cleavage, namely, the (112) surface **(A)** and the (001) surface **(B)**, based on the literature cited in the text. These surfaces exhibit two dangling bonds per calcium atom, while each calcium atom is eight coordinated in the scheelite lattice.

Cheng, 2016; Dai et al., 2018). Additionally, the Nui Phao and Vostok-2 mines, which together produce 10% of the world tungsten, are also exploiting tungsten skarns (Soloviev and Krivoshchekov, 2011; Masan Resources, 2012) Hence, tungsten skarns represent a significant part in the current tungsten production, and some authors estimate that they account for more than 40% of the global tungsten reserves (Werner et al., 1998; Schubert et al., 2006; Pitfield et al., 2011). Besides, many tungsten skarns have been reported in the world, including in the EU; some are currently exploited, while the other largest ones were exploited in the second half of the twentieth century (**Figure 5**).

Processing Problematics and Options

Considering the high economic potential of tungsten skarn ores, the classification of tungsten as a CRM resulted in a global resurgence of interest for these ores (Suárez Sánchez et al., 2015; Kupka and Rudolph, 2018a; Yang, 2018). However, most authors working on tungsten skarns, either in the geology or in the mineral processing fields, have noticed complex gangues for the tungsten extraction, in particular for the ore dressing stage. Indeed, skarns generally occur in limestone protoliths, which induce high amounts of calcium and, therefore, the formation of calcium-bearing minerals. Owing to these metallogenetic processes, scheelite is found in fine-grained mineralization disseminated thorough the ore body and commonly associated with calcium silicates such as garnet, pyroxene, epidote, vesuvianite, wollastonite, etc., as well as with calcium salts such as fluorite (CaF_2), apatite [$Ca_5(PO_4)_3(OH,Cl,F)$], and calcite ($CaCO_3$) (Einaudi and Burt, 1982; Kwak, 1987; Meinert, 1992; Dawson, 1996; Lu et al., 2003; Meinert et al., 2005; Cheng, 2016; Jébrak et al., 2016; Dai et al., 2018).

The aforementioned gangue calcium-bearing minerals comprise elements such as P, Si, C, and F that are considered (along with sulfur) as penalizing elements either for the scheelite concentrates processed by hydrometallurgy or for the final metal–tungsten product (Pastor, 2000; Pitfield et al., 2011; Yang et al., 2016). Moreover, tungsten is traditionally extracted from scheelite concentrates by the hydrometallurgy process that requires >60% WO_3 in the concentrates (Pastor, 2000; Pitfield et al., 2011), while skarn ores usually assay between 0.5 and 1.5% WO_3 (**Figure 5**). Hence, removal of fluorite, apatite, calcite, and calcium-bearing silicates prior to any hydrometallurgical treatment is mandatory. The development of an efficient mineral processing flowsheet for the rejection of the abovementioned minerals from a given skarn ore allows to make this skarn of economic potential, i.e., exploitable.

The beneficiation of scheelite ores generally consists of crushing and grinding, followed by successive purification stages to produce a concentrate assaying 65-75% WO_3 to meet the product specifications imposed by the international trading (Lassner and Schubert, 1999; Pastor, 2000). As wolframite, scheelite is brittle and, therefore, tends to form fine particles during the milling stage. Traditionally, the comminution is carefully designed to avoid overgrinding with regular and appropriate classifying stages all over the process. In terms of processing, scheelite is diamagnetic as most of the gangue minerals, including fluorite, apatite, calcite, and some silicates such as quartz, feldspars. Therefore, magnetic separations are most of the time unsuitable for scheelite ores. Second, scheelite exhibits a significant specific gravity (6.1), which enables the use of gravity separations for scheelite processing. However, skarn ores generally display fine liberation sizes at which the classical gravity separation apparatuses are poorly efficient, inducing high WO_3 losses. In addition, the losses during the physical separation stages are significantly increased by the trend of scheelite to form fine particles (<10 μm), which are known to be lost in such separations. Consequently, scheelite has traditionally been beneficiated by froth flotation since the 1930s, when this process became a powerful route for fine particle processing. When the liberation size allows it, skarn ores can be processed by a combination of gravity separation and froth flotation. Scheelite flotation was thoroughly investigated during World War II in the USA and USSR as the tungsten demand was significantly high for military applications. However, scheelite flotation has been widely spread in the 1970s, which resulted in a sudden increase in the scientific interest for scheelite flotation and, hence, in the publication of many studies dealing with this topic (Kupka and Rudolph, 2018a). Owing to the depletion of wolframite reserves in China along with the European Metal policy, scheelite flotation has gathered considerable interest in the world over the past few years (Pitfield et al., 2011; Suárez Sánchez et al., 2015; Kupka and Rudolph, 2018a; Yang, 2018). Nonetheless, skarn deposits commonly exhibits complex gangues (Kwak, 1987; Dawson, 1996; Misra, 2000; Meinert et al., 2005; Jébrak et al., 2016), i.e., gangue minerals that display similar surface properties to that

of scheelite. Hence, although the two main processing options, namely, gravity separation and froth flotation, can be suitable for tungsten skarns, they have to be thoroughly investigated and finely adapted to the rock characteristics, particularly the froth flotation process.

THE FROTH FLOTATION, A MANDATORY STAGE IN THE SCHEELITE PROCESSING?

Surface Properties of Scheelite

Scheelite is an ionic mineral composed of Ca^{2+} cations and WO_4^{2-} anions, occurring in the $I4_1/a$ space group (tetragonal system). The most exposed surfaces have been extensively studied by means of atomistic calculations as well as of various experimental methods. Scheelite cleaves mostly forming the (112) and (001) surfaces since they present the lowest surface dangling bond densities (Mogilevsky et al., 2004; Hu et al., 2012; Gao et al., 2013, 2016b; Li and Gao, 2017). The average W–O bond length is 1.777 Å compared to 2.458 Å for the Ca–O bond length. Consistently, this induces significant differences in bond energies between W–O (610 kJ mol^{-1}) and Ca–O (130 kJ mol^{-1}) (Neiman, 1996). Hence, during the cleavage process, most WO_4^{2-} anions remain intact, while the Ca–O bonds break, resulting in a surface constituted of large polyatomic WO_4^{2-} anions bonded with Ca^{2+} cations (**Figure 6**). The (001) and (112) cleavage surfaces exhibit two dangling bonds per calcium atom (**Figure 6**). As each calcium atom is eight coordinated in the scheelite lattice, the (001) and (112) surfaces comprise six-coordinated calcium atoms, which results in a significant reactivity of the surface calcium atoms.

Considering the significant electronegativity difference existing between WO_4^{2-} and Ca^{2+}, scheelite is a sparingly soluble polar salt-type mineral. Hence, it displays a significant free energy value at its surface, which induces a favored adsorption of water molecules or hydroxyl anions on its surface, making it significantly hydrophilic (Hu et al., 2012; Wills et al., 2016; Gao et al., 2016b). Some authors have investigated the solubility of scheelite in water at room temperature (25°C): the solubility product remains roughly constant at pH > 6 with a value of 8.9×10^{-9} (Marinakis and Kelsall, 1987a) or 4.9×10^{-10} (Atademir et al., 1979), which substantiates the semi-soluble behavior. The solubility increases significantly below pH 6 (Arnold and Warren, 1974; Atademir et al., 1979; Marinakis and Kelsall, 1987a), which can be mainly attributed to the displacement of the dissolution equilibrium by the formation of isopolytungstate species (polymerized tungstate) in solution (Marinakis and Kelsall, 1987a). Interestingly, the molar concentration of WO_4^{2-} above pH 6 is significantly higher than that of Ca^{2+}, resulting in an excess of WO_4^{2-} anions near the surface, i.e., in the inner plane. This explains the negative zeta potential of scheelite over the whole pH range (Arnold and Warren, 1974; Atademir et al., 1979; Marinakis and Kelsall, 1987a; Hicyilmaz and Özbayoglu, 1992; Ozcan and Bulutcu, 1993; Gao et al., 2016b), although high Ca^{2+} concentrations can conduct to a zero zeta potential. This is attributed to increased amounts of Ca^{2+} ions in the inner plane that balance the WO_4^{2-} provided by the scheelite dissolution (Atademir et al., 1979; Hicyilmaz and Özbayoglu, 1992).

Collection of Scheelite

Since scheelite is a polar mineral, water molecules are adsorbed as soon as surfaces are generated during the milling stage, making them hydrophilic. Hence, it is required to add flotation collectors to make scheelite hydrophobic and recover it in the froth (Bulatovic, 2007). Two main surface properties can be exploited for the adsorption of flotation collectors onto scheelite: the existence of undercoordinated surface calcium atoms (Mogilevsky et al., 2004; Hu et al., 2012; Gao et al., 2013, 2016b; Li and Gao, 2017), i.e., with two dangling bonds (**Figure 6**) and the negative zeta potential of scheelite surfaces over the whole pH range (Arnold and Warren, 1974; Atademir et al., 1979; Marinakis and Kelsall, 1987a; Hicyilmaz and Özbayoglu, 1992; Ozcan and Bulutcu, 1993; Gao et al., 2016b). These two properties suggest the use of anionic and cationic collectors, respectively, which can both be employed for scheelite flotation.

Anionic Collectors

Anionic collectors are composed of a polar group exhibiting a negative charge available to establish a chemical bond with undercoordinated surface cations of many minerals, including scheelite. Hence, anionic collectors are widely used for a large range of minerals (Leja, 1981; Bulatovic, 2007). Notably, the negatively charged atoms of the polar group are traditionally adapted to the target mineral: oxygen atoms (oxhydril) for oxide minerals and sulfur atoms (sulfhydryl) for sulfide minerals (Fuerstenau and Healy, 1972; Fuerstenau and Palmer, 1976; Leja, 1981; Bulatovic, 2007). Therefore, oxhydril collectors are generally used for scheelite (**Figure 7**), which is an oxide mineral. Most oxhydril collectors correspond to the basic form of an acid–base couple, since the existence of an extra valence electron, i.e., a negative charge, located on the polar group of the collector is induced by the deprotonation of the acidic form.

Sulfates, phosphates, and their derivatives

Some authors have investigated the use of sulfate collectors such as sodium dodecyl sulfate (SDS) for scheelite flotation (Grosman and Sukhoval'skaya, 1955; Grosman, 1962; Atademir et al., 1981; Marinakis and Kelsall, 1987b). Nevertheless, they reported a significant lack of selectivity between scheelite and other calcium minerals such as calcite (Atademir et al., 1981; Marinakis and Kelsall, 1987b). The adsorption is related to an exchange between the tungstate anion, WO_4^{2-}, and the sulfate collector, on the surface (Atademir et al., 1981), supported by the solubility results previously discussed (Atademir et al., 1979; Marinakis and Kelsall, 1987a). Albeit these collectors have been poorly investigated for scheelite flotation over the past decades, they have been extensively studied for other calcium salts such as fluorite. Interestingly, SDS provided high performances for fluorite flotation (Sørensen, 1973), which are mainly attributed to a chemisorption onto surface calcium atoms (Shergold, 1972; Sørensen, 1973; Mielczarski et al., 1983; González-Martín et al., 1996). Furthermore, the

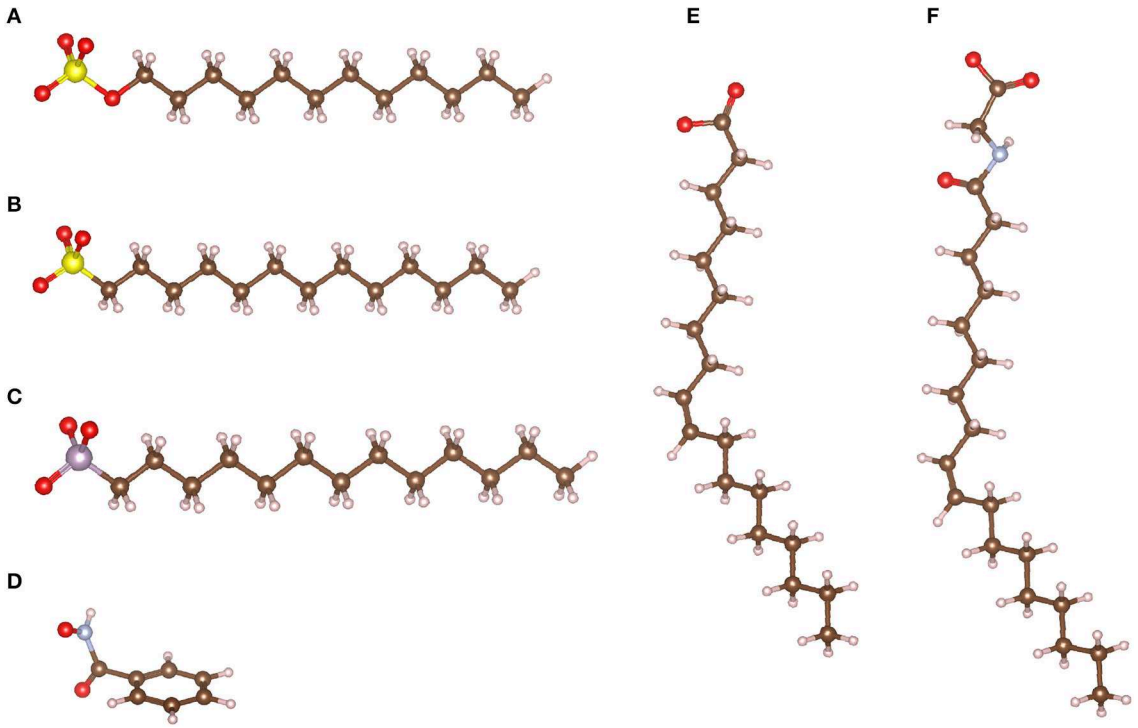

FIGURE 7 | The different anionic collector families used for scheelite flotation: sulfates **(A)**, sulfonates **(B)**, phosphonates **(C)**, hydroxamates **(D)**, carboxylates **(E)**, and sarcosinates **(F)**. The maroon, white, red, yellow, purple, and blue-gray balls represent the carbon, hydrogen, oxygen, sulfur, phosphorous, and nitrogen atoms, respectively.

calcium sulfate salts exhibit a significant solubility compared to other anionic collectors salts, indicating that no precipitation occurred at the studied concentrations (Fuerstenau and Palmer, 1976). Hence, such collectors are promising despite the crucial lack of selectivity displayed throughout the flotation tests. Besides, sulfonate collectors, which display a chemical structure very similar to that of sulfate collectors (**Figure 7**), demonstrated acceptable performances for calcium mineral flotation, including scheelite (Fukazawa, 1977; Gao et al., 2015a) and fluorite (Zheng et al., 2018; Chen et al., 2019). However, as for sulfates, sole sulfonates provided poor selectivity between scheelite and other calcium minerals despite good recoveries (Gao et al., 2015a).

In phosphonate molecules, the sulfur atom from a sulfonate is replaced with a phosphorous atom in the polar group (**Figure 7**). Nonetheless, while sulfur establishes two double bonds with the surrounding oxygen atoms, phosphorous forms only one double bond (**Figure 7C**). As for sulfates, phosphonates are used in basic conditions to favor the anionic form, i.e., the phosphonate, rather than the acidic form (Marinakis and Kelsall, 1987b). The adsorption studies conducted with phosphonate suggested that a chemisorption occurs between the polar group and the surface calcium atoms of scheelite and calcite (Marinakis and Kelsall, 1987b). However, considering the very close calculated adsorption energies of phosphonate on scheelite (-42.9 kJ.mol^{-1}) and on calcite (-38.8 kJ.mol^{-1}), the adsorption selectivity and, therefore, the flotation selectivity are traditionally very low using those collectors (Marinakis and Kelsall, 1987b).

Hydroxamates

Hydroxamates, the anionic forms of hydroxamic acids, have been significantly used for two decades, mainly because of their noticeable chelating abilities. Basically, their polar group contain a carbon atom linked to an oxygen and a nitrogen, these latter being linked to an oxygen atom, which can be both deprotonated to form the anionic forms (**Figure 7D**). The use of hydroxamic acids has been deeply investigated in the literature by many research articles published between 2000 and 2019 (Pradip and Fuerstenau, 1983, 1985; Zhao et al., 2013, 2015; Feng et al., 2017; Han et al., 2017; Tian et al., 2018; Wei et al., 2018, 2019; Yue et al., 2018). First, Zhao et al. (2013) demonstrated that cyclohexylhydroxamate (CHA) exhibits performances significantly better than benzohydroxamate (BHA) for scheelite collection (Zhao et al., 2013). Nonetheless, the flotation recovery was not as high as other collectors such as fatty acids and hydroxamates commonly suffer from a lack of selectivity (Zhao et al., 2013). Hence, most studies have shown that BHA should be combined with lead ions to increase notably the flotation selectivity, providing an acceptable separation of scheelite from gangue minerals, including the calcium salts (Zhao et al., 2015; Feng et al., 2017; Tian et al., 2018; Wei et al., 2018, 2019). The activation mechanism is mainly related to the specific adsorption of Pb^{2+} ions onto scheelite surfaces, since the lead tungstate

species are known to be thermodynamically stable. In addition, the chelation ability of BHA is significantly higher for lead ions compared to calcium ions, especially because these latter are included in the crystallographic structure.

Sarcosinates

The acyl sarcosinates represent another family of collectors that were developed in the early 1990s by the chemical reaction between a fatty acid and an amino-acid (Schubert et al., 1990). They exhibited very good performances for fluorite flotation from calcite-rich gangues, albeit some specific depressants were used to depress calcite (Schubert et al., 1990). The oleoyl sarcosine (**Figure 7F**), which is synthesized from oleic acid, also displayed satisfactory performances for scheelite flotation from a siliceous gangue (Ozcan and Bulutcu, 1993; Ozcan et al., 1994). Nevertheless, this molecule provided a poor selectivity between scheelite and calcite, and modifiers were added in a first stage of conditioning to reach an acceptable separation. This method was applied to an ore assaying 0.3% WO_3, which was first conditioned with 400 g/t of alkyloxine (a hydroxyquinoline) at pH 8, then with 50 g/t of quebracho to depress calcite, and finally with 200 g/t of oleoyl sarcosine as scheelite collector (Ozcan et al., 1994). This flowsheet afforded good separation performances: these authors obtained a concentrate assaying 56.1% WO_3 with 79.4% WO_3 recovery. Nonetheless, the ore considered by Ozcan et al. (1994) comprised only calcite as calcium salt, strongly depressed by the use of quebracho. In addition, sarcosinates have been successfully used for fluorite collection (Schubert et al., 1990), indicating a significant affinity of these collectors for fluorite, as well as for scheelite (Ozcan et al., 1994). This is mainly due to the adsorption mechanisms, which are reported to be very similar to that of fatty acids since the polar group of sarcosinates contain a carboxylate group (Xian-Ping et al., 2017).

Carboxylates

Carboxylates, which correspond to the anionic form of carboxylic acids (**Figure 7E**), are the most used collectors worldwide for the collection of a large range of oxide (and fluoride) minerals, including silicates and sparingly soluble minerals. These latter are composed of an alkaline-earth, a lanthanide, or a transition metal associated with a mono- or a polyatomic anion. On the one hand, the valuable metal can correspond to the cation, as is the case for rare earth elements [in monazite $(La,Ce,Nd)PO_4$ or in bastnäsite $(La,Ce,Nd)CO_3$], barium (in barite, $BaSO_4$), orstrontium (in celestite, $SrSO_4$). On the other hand, the valuable metal can correspond to the cation that forms the polyatomic anion, as niobium, tantalum, tungsten, or boron, which constitute niobate-/tantalite-based minerals [e.g., columbite $(Fe,Mn)Nb_2O_6$], tungstate-based minerals (e.g., scheelite and wolframite), and borate-based minerals (e.g., colemanite, $Ca_2B_6O_{11}, 5\ H_2O$), respectively. Besides, the metallic commodity can be the whole anion of the semi-soluble salt such as F^- and PO_4^{3-}, extracted from fluorite and apatite, respectively. All the above mentioned minerals have been successfully collected by carboxylates (Fuerstenau and Palmer, 1976; Leja, 1981; Bulatovic, 2010; Wills et al., 2016) as well as many silicates (Fuerstenau and Palmer, 1976), including andalusite/kyanite (Jin et al., 2019), spodumene (Xu et al., 2016, 2017a; Zhu et al., 2018), feldspars (Xu et al., 2016, 2017a,b), activated quartz (Gaudin and Fuerstenau, 1956; Fuerstenau and Palmer, 1976), muscovite (Alekseev and Morozov, 1975), and beryllium silicates (Walsh and Vidal, 2009). In addition, pure oxides such as cassiterite (Angadi et al., 2015) or hematite (Nakhaei and Irannajad, 2018) have been collected using fatty acids with satisfactory performances. These collectors have been commonly used for scheelite collection considering their low cost, high efficiency, and environment friendliness. The high collection ability of carboxylates for a large range of minerals is mainly related to their significant affinity for metallic cations (alkali-earth, lanthanide, or transition metals). Traditionally, carboxylate collectors are called fatty acids since they are composed of a carboxylic group and a linear aliphatic chain with between 12 and 18 carbon atoms that frequently comprises unsaturations (Leja, 1981). They occur naturally under their acidic form in many vegetal organisms such as trees (mostly pine) or oleaginous plants (olive, colza, peanuts, etc.), which store their energy in the form of lipid molecules. For their use in the froth flotation process, fatty acids are usually treated with a strong base (sodium hydroxide or potassium hydroxide) to form carboxylates anions (metal soaps). The fatty acid deprotonation results in a significant increase in their solubility: authors reported higher solubility products of metal soaps in solution compared to fatty acids, these latter being nearly zero at room temperature (Leja, 1981; Khuwijitjaru et al., 2002), although a significant decrease in the solubility of carboxylate salts occurs when the chain length increases (Fuerstenau and Miller, 1967). Besides, the deprotonation allows adding an extra valence electron, i.e., a negative charge, on the polar group ($-COO^-$), which enables the chemisorption of the carboxylate onto the surface metallic cations (Hanumantha Rao and Forssberg, 1991; Foucaud et al., 2018b). In solution, four major species have been reported for the oleic acid/oleate species, depending on the pH and the total concentration (**Figure 8**). They can be under $RCOO^-$, $(RCOO)_2^{2-}$, $(RCOO)_2H^-$, and RCOOH forms, the two first being the most dominant at alkaline pH and for usual concentrations in flotation (Miller and Misra, 1984).

For one century, the *cis*-octadec-9-enoic acid, also named oleic acid, has been the most used carboxylic acid in the flotation worldwide (Leja, 1981; Bulatovic, 2007; Kupka and Rudolph, 2018a), for its high natural abundance and its low melting point (induced by its unsaturation). Hence, it displays low operating costs and considerable ease to work with. Nevertheless, many other fatty acids, with different chain lengths and unsaturation degrees, are used, most of the time in mixtures with oleic acid. Indeed, this latter is difficult to purify from vegetal extracts (trees or oleaginous compounds) and is, therefore, commonly associated with other abundant fatty acids such as the saturated lauric acid (12 carbon atoms), myristic acid (14 carbon atoms), palmitic acid (16 carbon atoms), and stearic acid (18 carbon atoms), or the unsaturated linoleic acid (18 carbon atoms, two unsaturations) and linolenic acid (18 carbon atoms, three unsaturations). Thus, most fatty acid-based collectors are mixtures of the aforementioned fatty acids in different proportions. In particular, tall oil Fatty Acids (TOFA) are fatty

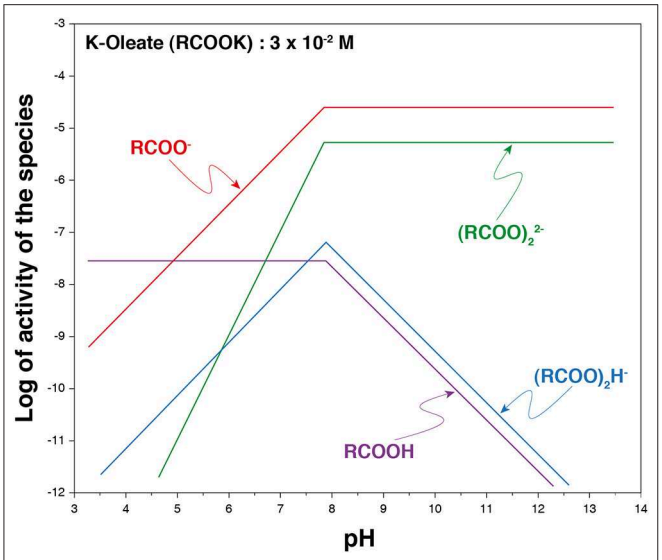

FIGURE 8 | Species distribution diagram for an aqueous (potassium) oleate solution. Adapted from Miller and Misra (1984).

acid mixtures derived from the saponification and distillation of pine resin (Logan, 1979). These by-products of the Kraft process in paper industry represent a significant amount of the fatty acids used for froth flotation at industrial scale. In such collector's mixtures, the classical above-described fatty acids are also associated with rosin acids, large-sized hydrophobic terpene-derived compounds among which abietic, pimaric, and palustric acids are dominant (Logan, 1979). Albeit authors suggested that rosin acids do not adsorb onto mineral surfaces (Pearse, 2005), recent studies highlighted their negative impact on the flotation of sparingly soluble minerals: they increase the recoveries of all the minerals therefore inducing a considerable decrease in selectivity (Filippov et al., 2018).

Cationic Collectors

Considering the high negative zeta potential of scheelite on the whole pH range, cationic collectors have a high potential for scheelite collection since they are known to adsorb through electrostatic interactions. Among the cationic collectors, amines are the most commonly used for the collection of silicates, oxides, and various other minerals including scheelite. In the literature, some authors investigated the use of amines for scheelite flotation. In particular, Arnold et al. (1978) studied the floatabilities of scheelite and calcite with amines by microflotation as well as their separation by microflotation tests performed on mixtures. They concluded that, despite the good floatabilities of each mineral, the flotation separation of scheelite from calcite remained very difficult using amines (Arnold et al., 1978). In addition, Atademir et al. (1981) demonstrated very good scheelite recovery using dodecylamine hydrochloride which, however, was not suitable for industrial application due to the high silicate contents in traditional ores (Atademir et al., 1981). Later on, Hiçyìlmaz et al. (1993) tested several different amines and showed that amine D acetate (a dodecylamine neutralized with acetate radicals) provided acceptable scheelite recoveries (91%) but poor selectivity between scheelite and calcite (Hiçyìlmaz et al., 1993). Recently, Gao et al. (2015b) investigated the use of dodecylamine (DDA) for the flotation separation of scheelite from calcite with a strong focus on adsorption mechanisms. Interestingly, they showed that, at low pH, electrostatic bonds are established between positively charged amine (NH_3^+ head group) and WO_4^{2-} surface sites (Gao et al., 2015b). Also, DDA adsorbs better on scheelite than on calcite by creating a more compact monolayer, therefore enhancing the contact angle of scheelite (Gao et al., 2015b).

Besides, the use of quaternary ammonium salts (QAS) as collectors for scheelite has also been investigated (Hu et al., 2011; Yang et al., 2015). Such molecules afforded good scheelite flotation performances along with very good selectivity between scheelite and other calcium minerals such as calcite. For instance, dioctyl dimethyl ammonium bromide was used on a mixture of calcite and scheelite at pH 8 and exhibited high selectivity as well as high scheelite recovery, which were significantly better than those obtained with oleic acid (Hu et al., 2011). Similar performances were attained with didecyl dimethyl ammonium and trioctylmethylammonium chlorides (Yang et al., 2015), but none of them was tested on an ore.

Collector Mixtures

To increase selectivity between scheelite and the other calcium minerals, one can use collector mixtures, including anionic/anionic, cationic/non-ionic, and anionic/non-ionic reagent mixtures. In particular, the use of a mixture of sodium oleate and fatty alcohols, i.e., non-ionic reagents, provided interesting performances for gypsum separation from a gangue comprising calcium minerals (Filippova et al., 2014). A similar mixture, involving sodium oleate and a fatty alcohol, conducted to an efficient flotation separation of scheelite from calcite (Filippov et al., 1993; Filippov and Filippova, 2006). It is assumed that mixing ionic and non-ionic reagents allows to reduce the electrostatic repulsions existing between the ionic groups of anionic collectors by introducing, in the adsorption layer, non-ionic compounds. These latter are supposed to adsorb on the cationic sites by means of electrostatic interactions and/or hydrogen bonding. In addition, while reducing the polar repulsions, they also maintain significant hydrophobic chain–chain interactions inside the adsorption layer (Filippov et al., 1993, 2012, 2019; Filippov and Filippova, 2006; Filippova et al., 2014) since they are composed of aliphatic chains of 10 to 16 carbon atoms. They induce higher quantities of collector adsorbed onto a mineral from another (**Figure 9**), due to a better organization of the adsorption layer. All the above mentioned studies clearly noticed significant variations in flotation selectivity and/or recoveries of various minerals. Similar results were observed using a combination of sodium oleate and polyoxyethyiene reagents (Chen C. et al., 2017; Chen et al., 2018).

Besides, a similar methodology was applied for anionic/anionic reagent mixtures by Yin and Wang (2014), who blended BHA and sodium oleate and observed an increase

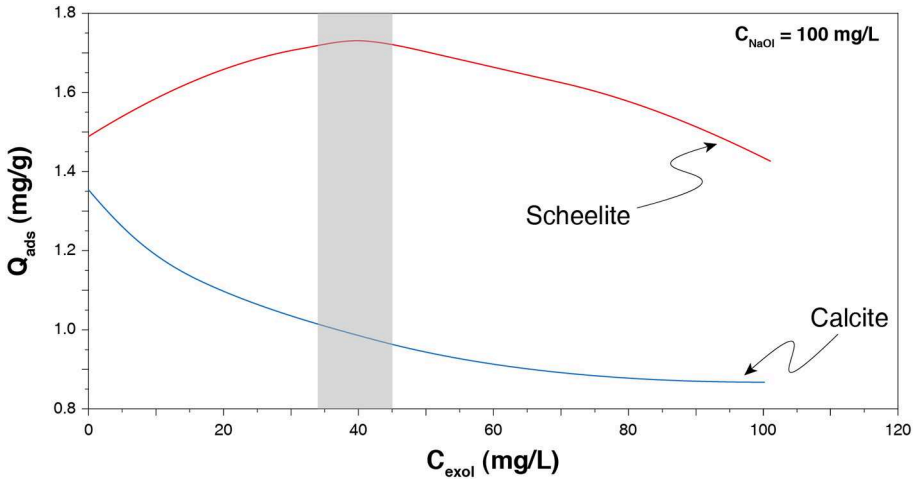

FIGURE 9 | Effect of the quantity of an alcohol reagent (Exol-B) on the sodium oleate adsorption onto scheelite and calcite. Adapted from Filippov and Filippova (2006). The optimum zone is displayed in gray, which roughly corresponds to a 2.5:1 mass ratio.

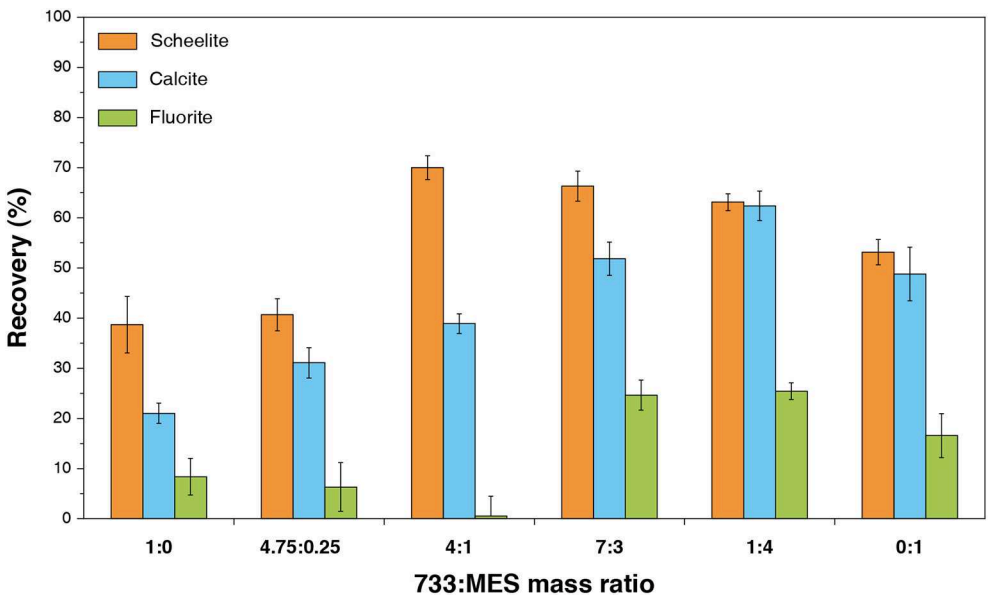

FIGURE 10 | Effect of mass ratio of a fatty acid collector combined with methyl ester sulfonate on flotation behavior of scheelite, fluorite, and calcite. Adapted from Gao et al. (2015a) with permission of Elsevier.

in the scheelite recovery, without yet performing any test on an ore (Yin and Wang, 2014). Another mixture of two different anionic collectors was studied recently: Gao et al. (2015a) blended a sulfonate with a fatty acid-based mixture with interesting results in terms of scheelite/fluorite selectivity (**Figure 10**). They obtained a concentrate assaying 65.8% WO_3 with 66.0% WO_3 recovery. This mixture not only improved the selectivity compared to sole sodium soap but also reduced the quantity of sodium soap and water glass required, with, finally, a high tolerance to water hardness (Gao et al., 2015a). Furthermore, recently, some authors demonstrated that mixing two molecules with the same polar group but different aliphatic chains can modulate the selectivity in flotation, particularly between scheelite and fluorite (Filippov et al., 2018). This achievement was attained by introducing saturated fatty acids (palmitate) in the unsaturated fatty acid-based formulations, which allowed increasing significantly the WO_3 grade in the flotation concentrates. It demonstrates the importance of the chain geometry in the adsorption selectivity since this latter can be led by the auto-organization of the adsorption layer.

Depressants for Common Gangue Minerals

According to the previous part, the most commonly used collectors for scheelite flotation are anionic reagents, mainly

the carboxylates. Owing to their anionic groups, they all suffer from a significant lack of selectivity between the calcium salts, namely, scheelite, fluorite, apatite, and calcite. Therefore, the use of depressants is necessary to attain an acceptable selectivity in favor of scheelite. In particular, most collectors can afford a good selectivity between scheelite and a given mineral, while tungsten skarns generally comprise a dozen of minerals. The combination of a collector with a depressant is, therefore, mandatory to reach an acceptable separation between scheelite and several gangue minerals.

Sodium Silicate

Sodium silicate (Na_2SiO_3) is one of the most common reagents used in the froth flotation process (Leja, 1981). This environment-friendly reagent is a very efficient dispersant since it decreases the particle–particle interactions. Moreover, it is known to adsorb with a high affinity on the gangue mineral surfaces, mostly silicates, and therefore, it constitutes a strong depressant in the froth flotation process. Over the past decades, Na_2SiO_3 has been successfully used in the flotation separation of rare earth minerals (Filippov et al., 2016), zinc minerals (Ejtemaei et al., 2012), iron minerals (Rao et al., 2011), scheelite ($CaWO_4$) (Kupka and Rudolph, 2018a; Yang, 2018; Foucaud et al., 2019c), fluorite (Song et al., 2006; Zhou et al., 2013), apatite (Qi et al., 1993; Sis and Chander, 2003), and many other minerals. The behavior of Na_2SiO_3 in aqueous solutions have been intensively investigated: depending on the pH of the solution and the total silica concentration, the silica tetrahedral (SiO_4) can be under SiO_4^{4-}, $SiO_3(OH)^{3-}$, $SiO_2(OH)_2^{2-}$, $SiO(OH)_3^-$, and $Si(OH)_4$ forms (Engelhardt et al., 1975; Marinakis, 1980; Marinakis and Shergold, 1985; Bass and Turner, 1997; Halasz et al., 2007; Jansson et al., 2015). Furthermore, the pH, total silica concentration, and SiO_2:Na_2O ratio affect the polymerization degree of silica tetrahedra, a high ratio inducing a high polymerization degree (Lentz, 1964; Marinakis, 1980; Bass and Turner, 1997; Dimas et al., 2009; Nordström et al., 2011; Jansson et al., 2015). In the froth flotation process, according to the SiO_2:Na_2O ratio and the total silica concentrations commonly used, the main species of Na_2SiO_3 are $Si(OH)_4$ for pH < 9.4 and $SiO(OH)_3^-$ for 9.4 < pH < 12.6 (Marinakis, 1980; Han et al., 2016) (**Figure 11**). Also, the polymerization degree depends strongly on the $SiO(OH)_3^-$ and $SiO_2(OH)_2^{2-}$ concentrations in solution (Roller and Ervin, 1940; Marinakis, 1980). Most of the flotation processes worldwide are performed at pH 7–11, at which the silica monomers are dominant, under both $Si(OH)_4$ and $SiO(OH)_3^-$ forms.

The above-mentioned silica species in aqueous solution are assumed to interact strongly with the surface cations, i.e., Ca^{2+} in the case of calcium salts. Depending on the surface calcium speciation (Ca or Ca–OH) and the most dominant silica species in solution, silica adsorption can result in the formation of Ca–$Si(OH)_4$ or Ca–O–$Si(OH)_3$ on the surface (Marinakis, 1980; Marinakis and Shergold, 1985). However, various adsorption mechanisms have been suggested, including the physical adsorption of silica gel and water glass (Cheng et al., 1963), silicate ions (Glembotskii and Uvarov, 1964; Fuerstenau et al., 1972), colloidal silica, and polymeric silicic acid (Nikiforov and Skobeev, 1968) apart from chemisorptions (Fuerstenau et al., 1972; Marinakis, 1980; Marinakis and Shergold, 1985). Besides, the soda amount as well as the age of the Na_2SiO_3 solution is likely to play a role in the depressing effect of Na_2SiO_3 (Berlinskii, 1962; Marinakis, 1980; Marinakis and Shergold, 1985). Recently, the adsorption of silica species onto fluorite, an archetypal calcium salt, has been investigated by DFT calculations (Foucaud et al., 2019d) the acidic form of the monomers and the dimers, $Si(OH)_4$ and $Si_2O(OH)_6$, respectively, physisorbs onto surface calcium atoms, while the anionic form, namely, $SiO(OH)_3^-$, chemisorbs onto surface calcium atoms, eventually substituting a fluorine surface atom. Also, the monomers adsorb with a considerable higher adsorption energy compared to the dimers (Foucaud et al., 2019d), which could explain the high depressing effect of acidified water glass (AWG). This reagent corresponds to sodium silicate treated with acid (sulfuric, hydrochloric, etc.) prior to its use in flotation. Over the past years, some authors demonstrated a high efficiency of AWG for depressing gangue minerals, in particular, calcite, significantly better than classical sodium silicate (Zhou et al., 2013; Bo et al., 2015; Dong et al., 2018; Kupka et al., 2019). According to these authors, this higher efficiency could be linked to higher amounts of depolymerized silica species (i.e., monomers) when sodium silicate is acidified (Zhou et al., 2013; Bo et al., 2015; Dong et al., 2018; Kupka et al., 2019).

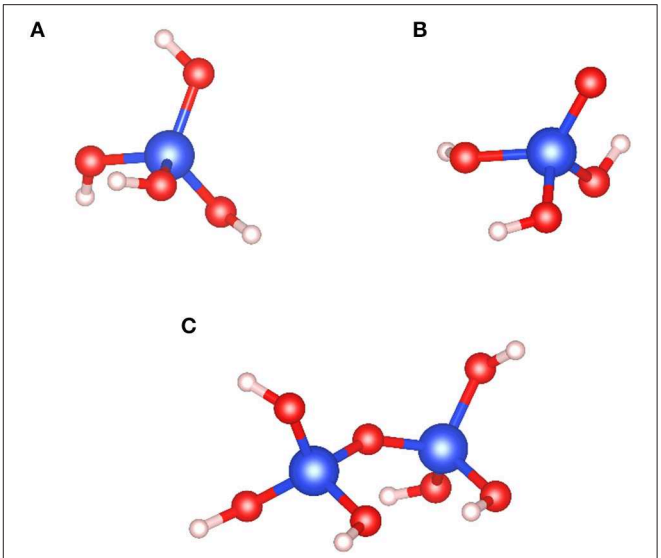

FIGURE 11 | Most dominant forms of Na_2SiO_3 in aqueous solutions for realistic froth flotation conditions: **(A)** acidic monomer, $Si(OH)_4$, **(B)** basic monomer, $SiO(OH)_3^-$, and **(C)** acidic dimer, $Si_2O(OH)_6$. The blue, red, and white balls represent the silicon, oxygen, and hydrogen atoms, respectively.

Sodium Carbonate

Sodium carbonate (Na_2CO_3) is mostly described as a buffering pH modifier (Bulatovic, 2010) as well as a pulp dispersant (Kupka and Rudolph, 2018b), and eventually as a depressant (Zheng and Smith, 1997). Some authors highlighted positive synergistic effects when Na_2SiO_3 is used in flotation systems where the pH is controlled beforehand by Na_2CO_3 (Agar, 1984;

Kupka and Rudolph, 2018a; Foucaud et al., 2019c). In other terms, the prior treatment of the minerals by Na_2CO_3 results in a higher efficiency of Na_2SiO_3 in terms of gangue mineral depression, which provides a better flotation selectivity and, therefore, considerably higher metal grades in the flotation concentrates (Martins and Amarante, 2013; Kupka and Rudolph, 2018b). Recently, Kupka and Rudolph (2018b) suggested that fluorite would be first depressed followed by calcite, silicates, and scheelite when Na_2CO_3 dosage is increased, with negligible dependence on the pH and the other pH modifiers used (Kupka and Rudolph, 2018b). The effect of Na_2CO_3 can be related to the precipitation of calcium ions in suspension (Bahr et al., 1968; Kupka and Rudolph, 2018b) as well as a surface carbonation of the calcium minerals (Bahr et al., 1968; Miller and Hiskey, 1972; Rahimi et al., 2017; Foucaud et al., 2019d). Indeed, the precipitation of calcium ions probably decreases the gangue mineral activation induced by their adsorption (Kupka and Rudolph, 2018b). Besides, the formation of calcium carbonate onto gangue mineral surfaces (silicates, apatite, fluorite, etc.), demonstrated by spectroscopic studies on fluorite (Foucaud et al., 2019d) results in a better depression of these minerals by Na_2SiO_3, which is known to strongly depress calcite (Filippov et al., 2018; Kupka and Rudolph, 2018b).

The addition of 1,150 g/t of sodium carbonate prior to the addition of sodium silicate (1,220 g/t) allowed to reach 11.2% WO_3 with 95% recovery from a flotation feed containing 1.09% WO_3 (Filippov et al., 2018). The synergistic effect highlighted is linked to the carbonation of the fluorite surfaces, calcite being well-depressed by sodium silicate. The combination of depressants was optimized to create the best conditions to estimate as well as possible the influence of the collector on the selectivity of flotation. Notably, *ab initio* calculations substantiated recent experimental investigations, which demonstrated that those synergistic effects are related to an acid–base reaction on the surface between the pre-adsorbed sodium carbonate layer and the silica species, added after (Foucaud et al., 2019d).

Metallic Salts

Studies have demonstrated that the addition of metallic cations, such as Fe^{3+}, Al^{3+}, Pb^{2+}, Zn^{2+}, etc. in the flotation process allows to modulate the selectivity of the separation (Abeidu, 1973; Mercade, 1975; Hanna and Somasundaran, 1976; Detienne, 1978; Patil and Nayak, 1985; Oliveira and Sampaio, 1988; Schubert et al., 1990; Raatz, 1992; Feng et al., 2017) (see **Figure 12**). However, using sole metallic salts results in a limited improvement of the flotation performances (Hiçyìlmaz et al., 1993). Combined with Na_2SiO_3, these cations are assumed to form strongly hydrophilic hydrosols, which depress gangue minerals efficiently (Changgen and Yongxin, 1983). In particular, Patil and Nayak (1985) efficiently depressed calcite using a hydrosol composed of Na_2SiO_3 and ferrous sulfate with no negative impact on scheelite (Patil and Nayak, 1985). Interestingly, they noted an increase in the flotation recovery when the two reagents were added simultaneously. The use of iron salts combined with Na_2SiO_3 systematically conducted to an increase in the flotation selectivity in favor of scheelite (Dean and Schack, 1964; Foucaud et al., 2019c), which could be attributed to the specific adsorption of iron compounds (mostly hydroxides) on scheelite along with a strong depression of calcite by Na_2SiO_3. Nevertheless, the mechanisms involved in the depression/activation phenomena observed when Na_2SiO_3 is combined with metallic cations is still poorly understood.

Organic Molecules

Moreover, organic polymers such as tannins, carboxymethyl cellulose, and starch (Ozcan and Bulutcu, 1993; Rutledge and Anderson, 2015; Liu et al., 2016; Wang et al., 2018a) as well as chelating agents, e.g., citric acid (Bulatovic, 2015; Gao et al., 2016a), are known to depress calcium-bearing minerals in some cases. In particular, starch is widely known to strongly depress silicate minerals and calcite (Bulatovic, 2010), as well as quebracho and carboxymethyl cellulose (Wang et al., 2018a). Classical organic molecules were tested on a typical tungsten skarn without affording an acceptable selectivity between scheelite and the gangue minerals, mainly the calcium salts (Foucaud et al., 2019c). Nonetheless, many studies have been recently conducted to investigate the use of new organic depressants for the selective flotation of scheelite. Interestingly, Chen et al. (2017a) attained a satisfactory selectivity between scheelite and fluorite/calcite using sodium alginate as depressant and fatty acids as collector. They demonstrated that sodium alginate chemisorbs selectively onto fluorite and calcite, therefore preventing the adsorption of sodium oleate onto those minerals without affecting scheelite (Chen et al., 2017a). Similar performances were obtained using dextran sulfate sodium, which adsorbs selectively onto calcite and fluorite surfaces and, hence, increases significantly the flotation selectivity (Chen et al., 2017b). Some depressants were successfully used to depress specifically a given gangue mineral such as calcium lignosulfonate for calcite (Feng et al., 2018) or sodium polyacrylate for fluorite (Zhang et al., 2017). Overall, it has been demonstrated that all these abovementioned organic molecules adsorb by interactions between their polar groups (–OH or –COOH) and the surface cations, mainly Ca^{2+} (Somasundaran, 1969; Filho et al., 2000; Wang and Somasundaran, 2005; Filippov et al., 2013). These interactions can be of various types, including chemisorption of the $–COO^-$ group onto calcium atoms, physisorption of the –OH or –COOH groups onto the same cations, or hydrogen bonding between the –OH or –COOH groups and hydroxylated surface cations [$Ca(OH)^+$]. The selectivity obtained in the depression is most probably related to the steric hindrance of those organic molecules and the correlations between their functional groups (–OH or –COOH) and the surface cationic sites.

Phosphate Derivatives

Phosphate derivatives such as sodium hexametaphosphate [$(NaPO_3)_6$], sodium phosphate (Na_3PO_4), sodium pyrophosphate ($Na_4P_2O_7$), and 1-hydroxyethylidene-1,1-diphosphonic acid (HEDP) (Wang et al., 2018b) are also widely used inorganic depressants for scheelite flotation from calcite and fluorite (Yongxin and Changgen, 1983; Bel'kova et al., 1993; Bulatovic, 2015; Liu et al., 2016). The depressing effect of phosphate derivatives has been extensively discussed, with,

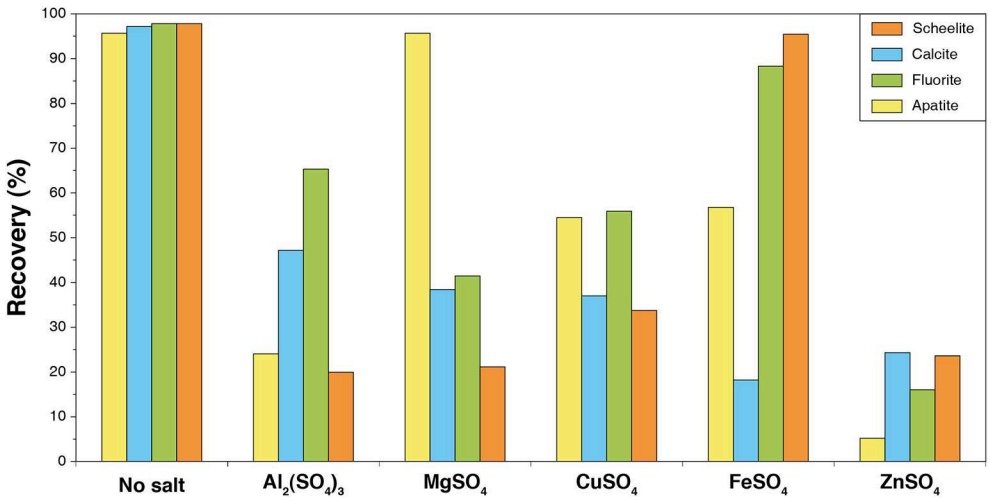

FIGURE 12 | Combined effect of polyvalent metallic cations (300 g/t) and Na_2SiO_3 (1.5 kg/t) on the flotation recovery of calcium salts. Reproduced from Hanna and Somasundaran (1976) with permission of SME. Tests were performed with 2 kg/t Na_2CO_3 and 100 g/t oleic acid at pH 9.1–9.5.

however, contradictory results (Kupka and Rudolph, 2018a). Indeed, some authors successfully used phosphate derivatives to depress calcite and fluorite in scheelite flotation (Changgen and Yongxin, 1983; Yongxin and Changgen, 1983), while other researchers employed them to depress apatite in fluorite flotation (Bulatovic, 2015) or in scheelite flotation (Bel'kova et al., 1993). Phosphate derivatives are known to chelate Ca^{2+} ions in solution leading to a surface depletion in terms of calcium ions faster for fluorite and calcite than for scheelite (Changgen and Yongxin, 1983). However, Gao et al. (2018) rather suggested a chemisorption of phosphate derivatives onto surface calcium atoms (Gao et al., 2018), which exhibit a higher density and activity for calcite than for scheelite.

TABLE 2 | Calculated calcic site densities and surface Ca–Ca distance on the main cleavage planes for each studied mineral.

Mineral	Cleavage planes (according to literature)	Ca–Ca distance (Å)	$d(Ca^{2+})$ ($Ca/Å^2$)
Scheelite	(112) (Hu et al., 2012; Gao et al., 2013)	3.87	4.01×10^{-2}
	(001) (Hu et al., 2012; Gao et al., 2013)	5.22	3.67×10^{-2}
Fluorite	(111) (Parks and Barker, 1977)	3.86	7.75×10^{-2}
Apatite	(001) (Chang et al., 1996)	3.96	4.58×10^{-2}
Calcite	(101) (Chang et al., 1996)	4.05	3.38×10^{-2}
	(104) (Chang et al., 1996)	4.05	4.58×10^{-2}

THE SELECTIVE SEPARATION OF SCHEELITE: A UTOPIA?

A Low Separation Contrast in Flotation

Nowadays, a few routes exist for efficient industrial-scale scheelite flotation in the presence of gangue calcium salts and silicates. Though amine collectors demonstrated acceptable performances, they are known to float silicates due to their physisorption on negatively charged surfaces. Since silicates represent most of the gangue minerals in tungsten skarns, the use of amines is unsuited to attain acceptable WO_3 grades. Another method consists of the utilization of hydroxamic acids, mainly benzohydroxamic acid, in combination with lead cations. Nevertheless, in the EU, benzene-based compounds are forbidden, and the industrial use of lead is strictly restricted, making this method impossible to apply. The last proofed and widely used route is the flotation with fatty acids as collectors, especially sodium oleate, which are very efficient, cheap, and environment friendly. Their high efficiency is attributed to the chemisorption of the carboxylate group onto surface calcium atoms (Hanumantha Rao and Forssberg, 1991; Foucaud et al., 2018b). However, tungsten skarns commonly display high amounts of calcium-bearing minerals, either calcium silicates or calcium semi-soluble salts (fluorite, apatite, calcite, and scheelite), these latter exhibiting similar surface properties (**Table 2**). The flotation separation of scheelite from fluorite, apatite, and calcite has been intensively investigated over the past decades and remains, in the twenty first century, one of the most challenging problems in the froth flotation field.

The Petrov Process

In the early 1940s, the tungsten demand was considerable for its wide range of military applications. Hence, the exploitation of tungsten skarns appeared crucial for the economic independence of the largest powers, including the USSR. Even then, the processing of tungsten skarns was difficult due to complex gangues comprising minerals with similar surface properties to those of scheelite. To face this issue, a method, developed by Petrov, allowed to increase significantly the selectivity (Petrov, 1940) and, therefore, the WO_3 grade of the concentrates. It is

based on the heating of the pulp to 80–100°C in the presence of considerable concentrations of Na_2SiO_3 (2–4%) after a roughing stage conducted with a classical process, i.e., sodium carbonate to control the pH, sodium silicate to depress the gangue minerals, and sodium oleate to collect scheelite. In this scheme, the rougher flotation concentrate comprises significant amounts of scheelite along with calcite, fluorite, and apatite. After heating, a cleaning stage is performed and usually allows increasing significantly the WO_3 grade of the flotation concentrate, to attain WO_3 grades that can be processed by hydrometallurgy. The surface physico-chemical phenomena at play during the Petrov process have never been understood and are still poorly known. Nonetheless, this process remains one of the most used processes for scheelite processing worldwide since it provides satisfactory selectivity after the roughing stage. The rejection of calcite, fluorite, and apatite from the flotation cleaning concentrates can be very high, affording acceptable WO_3 grades for hydrometallurgy. Recently, some authors tried to substitute this process, which can be described as energy consuming considering the high temperatures that are required, by "greener" methods. This substitution is based on two main approaches: the development of specific depressants for gangue minerals, mostly the calcium salts, and the development of more specific collectors for scheelite. However, this substitution is very difficult since very few reagent formulations (depressants/collectors) exhibit satisfactory performances for all the gangue minerals, including the calcium salts (calcite, fluorite, apatite). Hence, avoiding the Petrov process depends on the product requirements existing on the scheelite concentrates for the hydrometallurgy subsequent stage and also on the contained gangue minerals. Nowadays, most Chinese and Russian mines still use the Petrov process for the industrial beneficiation of scheelite (Bernhart, 2015; Han et al., 2017) since it represents one of the only viable ways to attain the 60–65% WO_3 required for the scheelite concentrates. Without this process, the common WO_3 grades displayed, even after several cleaning stages, are as low as 30% WO_3 with, moreover, unacceptable recoveries.

Green Methods at Development

Flotation separation of calcium minerals with fatty acids is difficult: their chemisorption onto the surface calcium atoms along with the similar surface properties between the minerals generally (**Table 2**) induce a non-selective flotation. Nonetheless, different solutions can be undertaken to improve the elimination of calcium-bearing minerals during the mineral processing stage while maintaining a high level of environment friendliness:

(1) The minerals commonly contained in tungsten skarns exhibit a large range of specific gravities: 2.7 for calcite, 3.2 for fluorite and apatite, and 6.1 for scheelite, while silicates have specific gravities between 2.6 and 3.7, depending on the geological context. Hence, it allows one to perform a gravity separation to eliminate the minerals that are problematic in flotation with fatty acids, mostly the calcium-bearing semi-soluble salts (calcite, apatite, and fluorite). Nevertheless, the fine liberation size makes it difficult to process these ores by classical gravity separation methods, e.g., shaking tables, jigs, or spirals (Wells, 1991; Blazy and Joussemet, 2011; Das and Sarkar, 2018). Recently, Falcon concentrators, specifically designed for fine particle gravity processing, have been used successfully to achieve an efficient gravity separation on skarn ores (Foucaud et al., 2019b,e). Consistently, they afford a good elimination of the calcium salts that are problematic in flotation as well as fine particles (Dehaine et al., 2019), improving significantly the subsequent flotation stage.

(2) Additionally, skarns commonly contain iron, which is found within the ferromagnesian silicates of the protolith. After the thermometamorphism stage, iron is often included in the newly formed dense silicates such as vesuvianite, epidote, and garnets. Owing to the iron they contain, these silicates, which are denser compared to the non-ferromagnesian silicates, exhibit a significant magnetic susceptibility, ranking them in the paramagnetic mineral class. Hence, a high intensity magnetic separation is possible to eliminate these minerals that can represent high amounts in the tungsten skarns. It can allow reducing the amount of dense minerals going to the flotation stage after the Falcon gravity separation.

(3) In flotation, depressants can be added to enhance the separation differential between scheelite and the troublemaking minerals. Nevertheless, although silicates are quite easily depressed, very few depressants afford a satisfactory selectivity between scheelite and fluorite, apatite, and calcite. If some of them depress efficiently a specific gangue mineral, none can depress most gangue minerals without impacting significantly scheelite. In particular, the flotation separation between scheelite and fluorite has remained an industrial and a scientific challenge that has not been yet issued by the use of specific depressants. Hence, intensive developments should be done to find efficient and environmental friendly depressing conditions as well as to gain understanding in the adsorption mechanisms of the selected depressants onto calcium minerals. In most studies, the best depressing conditions are afforded by the use of the combination between sodium carbonate and sodium silicate.

(4) Considering the similar surface properties between scheelite and the other calcium minerals, the modulation of flotation collectors appears very difficult to separate scheelite from the other calcium minerals. According to recent developments, the flotation selectivity regarding the above-mentioned gangue minerals can be enhanced using collector mixtures (anionic/anionic or anionic/non-ionic), which exhibited satisfactory results in terms of flotation selectivity. Therefore, these collector mixtures should be intensively investigated to modulate the flotation selectivity in favor of scheelite and to gain understanding in the synergistic effects that they can exhibit.

The four above mentioned points should be thoroughly investigated to develop an efficient, adaptable, integrated, and environmental friendly process for a tungsten skarn. Besides, the froth flotation process is led by the adsorption of various reagents, organic or mineral, at the liquid/solid interface, with the objective of selectively rendering the target mineral(s) hydrophobic to recover it in the froth phase. Collectors, which contain a polar group and a non-polar aliphatic chain, can be adapted in terms of chain length, unsaturation, and ramification,

as well as functionalized polar group. Moreover, all reagents can be combined to improve the flotation performances [selectivity or target mineral(s) recovery]. All these optimizations are difficult to investigate by experimental methods, and molecular modeling has become a powerful tool to gain understanding in the adsorption mechanisms of flotation reagents at the mineral surfaces (Foucaud et al., 2019a). In particular, *ab initio* atomistic simulations can be applied in the future to study the fundamentals of fatty acid adsorptions onto calcium minerals and to unravel the synergistic effects highlighted when different reagents are combined together (either depressants or collectors).

With Helpful Perspectives Provided by Atomistic Simulations

Tungsten skarns are not the only ores displaying complex gangues. Indeed, over the past decades, the gangue complexness has been constantly increasing, which means that the gangue minerals are being more and more difficult to separate from the target mineral(s). This decrease in the separation contrast in flotation for most ores, including tungsten skarns, can, however, be overcome by increasing the flotation performances, i.e., the flotation selectivity and recovery. Those two key indexes mostly depend on the adsorption of flotation reagents (depressants and collectors) onto target(s) and gangue minerals. Therefore, it is of paramount interest to investigate thoroughly the molecular mechanisms involved in the adsorption of flotation reagents since they are still poorly described. Atomistic simulations such as quantum mechanic simulations or classical molecular dynamic simulations have been playing this role for several years (Badawi et al., 2011; Souvi et al., 2017; Hessou et al., 2018; Berro et al., 2019). The different molecular simulation methods existing nowadays in theoretical physics and chemistry, which can be applied to froth flotation, have been critically reviewed recently (Foucaud et al., 2019a). In particular, these methods contribute to improve the comprehension of the synergistic effects that can be significantly displayed when flotation reagents are used in combination (depressants, collectors, or both). Furthermore, they are involved in the development of novel reagent formulations and/or combinations based on the computed adsorption energies (Chehaibou et al., 2019; Rocca et al., 2019).

When applied to tungsten skarn ores, atomistic simulations can allow to:

(1) Compare the reactivity of the surfaces of the different minerals (mostly scheelite and fluorite, the main troublemaking mineral) toward water molecules, since the froth flotation process is performed in water. In particular, the water molecules adsorb onto the surface (111) of fluorite with around -55 kJ.mol^{-1} (Foucaud et al., 2018a), which is low compared to the adsorption energies of water reported on the most exposed surfaces of scheelite (Cooper and de Leeuw, 2003; Gao et al., 2013).
(2) Investigate the adsorption mechanisms of flotation reagents onto oxide minerals. Anionic collectors are traditionally used for oxide mineral flotation and require first principle simulations such as DFT to describe accurately the chemisorption processes. Besides, these regents can also be considered under their protonated, i.e., neutral form, to avoid the problem of bond creation. In this case, classical molecular dynamic simulations can be conducted to investigate the molecular mechanisms involved in the adsorption of these reagents. For instance, the adsorption mechanisms of carboxylates onto scheelite (Cooper and de Leeuw, 2004; Zhao et al., 2013; Yin et al., 2015) and fluorite have been investigated albeit a lot still has to be done.
(3) Understand and optimize the synergistic effects between reagents of the same sort (collectors, depressants) as well as between collectors and reagents. Novel reagent formulations can be developed to increase either the flotation selectivity or the flotation recovery.

The Processes Currently Used in the Industry

At the moment, a few mines in the world process scheelite-bearing ores. Owing to the abovementioned difficulties for scheelite beneficiation, several options are currently or have recently been used in the tungsten extraction industry. First, some mines, still in operation in 2020, prefer the use of gravity separation only when it is possible. It is the case for the Nui Phao Vietnamese mine (7% of the global W production) and for the Los Santos Spanish mine (1% of the global W production): they just perform talc and/or sulfide flotation stage before or after the use of classical gravity separations such as shaking tables and spirals (Ngoc, 2016). However, these latter are rarely possible considering the scheelite liberation size. Also, they generally lead to lower overall scheelite recoveries compared to flotation, and consequently, most scheelite mines prefer nowadays the use of classical flotation schemes. It is the case of the other scheelite mines worldwide, including the Vostok-2 Russian mine (3% of the global W production), the Mittersill Austrian mine (1–2% of the global W production), the Shizhuyuan Chinese mine (20% of the global W production), and most probably the other Chinese mines, although little information is available. Since 1940, Russian mines have systematically used the Petrov process for scheelite beneficiation, as is still the case in the Vostok-2 processing plant (Bernhart, 2015). First, after the sulfide flotation stage, a rougher scheelite flotation stage is performed using sodium carbonate to control the pH, sodium silicate to depress the gangue minerals, and oleic acid as the collector (Bernhart, 2015). The bulk concentrate, comprising scheelite along with calcite, fluorite, and apatite, undergoes the Petrov process to obtain, after two additional flotation stages, a scheelite concentrate assaying 53% WO_3 with an overall WO_3 recovery of 85% (Bernhart, 2015). In Shizhuyuan operations, the selectivity between scheelite and fluorite is increased by the use of a mixture of fatty acids and benzohydroxamic acid, both combined with lead nitrate (Han et al., 2017). Consistently, high amounts of sodium silicate are used to depress the gangue minerals, including fluorite and, unfortunately, scheelite. However, this development is not enough, and the flotation concentrate has to undergo the Petrov process to meet the product requirements in terms of WO_3 grade (Han et al.,

2017). Besides, in Mittersill, the use of the Petrov process is avoided since the subsequent metallurgical stage accepts lower WO_3 grade in the scheelite concentrate. Hence, the Mittersill mine produces scheelite concentrate grade assaying only 32% WO_3(Bernhart, 2015), owing to the dilution by calcite, apatite, fluorite, and other problematic calcium gangue minerals, which are still present in the concentrate. The same reagents (sodium silicate and fatty acids), widely used for scheelite flotation, are used in Mittersill operations and are responsible for the low selectivity between scheelite and calcium gangue minerals. The use of the Petrov process was also avoided in the Cantung Canadian formerly exploited scheelite mine, where gravity pre-concentration allowed rejecting the problematic gangue minerals prior to flotation (Delaney and Bakker, 2014) as recently been suggested for other European skarns (Foucaud et al., 2019b,e).

CONCLUSION

The froth flotation of scheelite still remains, in the twenty first century, a strong scientific, industrial, and technical challenge. At the moment, very few options are suitable considering the complexness of the gangue and the fine liberation size of tungsten skarns as well as the environmental concerns. In this paper, the main collectors and depressants that can be used for scheelite flotation have been thoroughly reviewed with the global objective to attain acceptable selectivity and recovery. Although many studies exhibited interesting performance with various flotation reagents, the greenest, most efficient, and cheapest method for scheelite flotation is to use fatty acids as collectors with sodium silicate as depressant. However, this solution suffers from a crucial lack of selectivity regarding the calcium salts, namely, fluorite, calcite, and apatite, which generally represent significant amounts in tungsten skarns. Those minerals, mainly fluorite, are difficult to separate from scheelite and, therefore, dilute dramatically the scheelite concentrates. More selective reagents or fatty acid-based formulations, reviewed in the present work, can hence be used to separate fluorite from scheelite, and when this approach is limited, a combination with gravity separation can be necessary. Furthermore, the challenge of selectively floating scheelite can be issued by modulating the synergistic effects commonly observed when reagents are combined together (depressants/depressants, collectors/collectors, or depressants/collectors). Overall, the atomistic simulations can provide a significant help to gain understanding in the modulation of the flotation selectivity regarding scheelite. Their use in the flotation area is considerably increasing and will be, in the next years, a crucial tool to reach the flotation performances required for the processing of low-grade fine-grained complex ores. In particular, it can allow to unravel the synergistic effects observed empirically in flotation experiments and to gain understanding in the fundamentals of flotation reagent adsorption onto mineral surfaces.

AUTHOR CONTRIBUTIONS

YF, LF, IF, and MB designed the study and the content of this review. YF and MB drafted the paper. LV and IF supervised the work of YF. All authors contributed to manuscript corrections and approved the submitted version.

FUNDING

The research leading to these results has received funding from the European Union's Horizon 2020 research and innovation program under grant agreement No. 641650 for the FAME project. We also acknowledge the support of Labex Ressources 21 (supported by the French National Research Agency through the national program Investissements d'Avenir with reference ANR-10-LABX-21 LABEX RESSOURCES 21).

ACKNOWLEDGMENTS

This work was granted access to the HPC resources of TGCC under the allocation 2019-A0060910433 made by GENCI.

REFERENCES

Abeidu, A. M. (1973). "Selective depression of calcite from fluorite," in *Transactions of the Institution of Mining and Metallurgy, Section C,* eds Taylor and Francis 49–50.

Agar, G. E. (1984). *Scheelite Flotation Process*. Virginia, NV: US Patent. 4,488,959.

Alekseev, V. S., and Morozov, G. G. (1975). Rate of flotation of kyanite, quartz, and muscovite. *Soviet Mining Sci.* 11, 62–64. doi: 10.1007/BF02501018

Angadi, S. I., Sreenivas, T., Jeon, H.-S., Baek, S.-H., and Mishra, B. K. (2015). A review of cassiterite beneficiation fundamentals and plant practices. *Miner. Eng.* 70, 178–200. doi: 10.1016/j.mineng.2014.09.009

Arnold, R., Brownbill, E. E., and Ihle, S. W. (1978). Hallimond tube flotation of scheelite and calcite with amines. *Int. J. Mineral Proc.* 5, 143–152. doi: 10.1016/0301-7516(78)90011-X

Arnold, R., and Warren, L. J. (1974). Electrokinetic properties of scheelite. *J. Colloid Interface Sci.* 47, 134–144. doi: 10.1016/0021-9797(74)90088-5

Atademir, M. R., Kitchener, J. A., and Shergold, H. L. (1979). The surface chemistry and flotation of scheelite. I. Solubility and surface characteristics of precipitated calcium tungstate. *J. Colloid Interface Sci.* 71, 466–476. doi: 10.1016/0021-9797(79)90321-7

Atademir, M. R., Kitchener, J. A., and Shergold, H. L. (1981). The surface chemistry and flotation of scheelite, II. Flotation "collectors." *Int. J. Mineral Proc.* 8, 9–16. doi: 10.1016/0301-7516(81)90003-X

Audion, A. S., and Labbé, J. F. (2012). avec la collaboration extérieure de la Compagnie Européenne d'Intelligence Stratégique (CEIS) (2012). *Panorama Mondial 2011 du Marché du Tungsténe, Vol. 108*. Rapport Public. BRGM/RP-61341-FR, 29.

Badawi, M., Paul, J.-F., Cristol, S., and Payen, E. (2011). Guaiacol derivatives and inhibiting species adsorption over MoS2 and CoMoS catalysts under HDO conditions: a DFT study. *Catal. Commun.* 12, 901–905. doi: 10.1016/j.catcom.2011.02.010

Bahr, A., Clement, M., and Surmatz, H. (1968). "On the effect of inorganic and organic substances on the flotation of some non-sulfide minerals by using fatty-acid-type collectors,"in *VIIIth International Mineral Processing Congress* (Leningrad).

Bass, J. L., and Turner, G. L. (1997). Anion distributions in sodium silicate solutions. Characterization by 29 SI NMR and infrared spectroscopies, and

vapor phase osmometry. *J. Phys. Chem*. B 101, 10638–10644. doi: 10.1021/jp9715282

Bel'kova, O. N., Leonov, S. B., and Shcherbakova, E. V. (1993). Intensification of beneficiation of scheelite ores by flotation. *J. Mining Sci.* 28, 480–485. doi: 10.1007/BF00711134

Berlinskii, I. I. (1962). Electrokinetic analysis of the reaction of flotation reagents with certain minerals of non-sulphide ores. Tr. Tsentr. Nauchno-Issled. *Gornorazved. Inst. Isvetn*. 47, 124–133.

Bernhart, W. (2015). "Processing of tungsten bearing ores - mineral processing and metallurgy," in *The Publications of the MultiScience - XXIX. MicroCAD International Scientific Conference. Presented at the MultiScience - XXIX. Microcad International Multidisciplinary Scientific Conference, University of Miskolc*.

Berro, Y., Gueddida, S., Lebègue, S., Pasc, A., Canilho, N., Kassir, M., et al. (2019). Atomistic description of phenol, CO and H2O adsorption over crystalline and amorphous silica surfaces for hydrodeoxygenation applications. *Appl. Surf. Sci.* 494, 721–730. doi: 10.1016/j.apsusc.2019.07.216

Blazy, P., and Joussemet, R. (2011). *Concentration par Gravité - Différentes Technologies* (Saint-Denis).

Bo, F., Xianping, L., Jinqing, W., and Pengcheng, W. (2015). The flotation separation of scheelite from calcite using acidified sodium silicate as depressant. *Miner. Eng.* 80, 45–49. doi: 10.1016/j.mineng.2015.06.017

Bulatovic, S. M. (2007). *Handbook of Flotation Reagents: Chemistry, Theory and Practice*, 1st Edn. Amsterdam; Boston, MA: Elsevier.

Bulatovic, S. M. (2010). *Handbook of Flotation reagents: Chemistry, Theory and Practice*, *Vol. 2: Flotation of Gold, PGM, and Oxide Minerals*, 1 Edn. Amsterdam: Elsevier.

Bulatovic, S. M. (2015). *Handbook of Flotation Reagents: Chemistry, Theory and Practice*. Vol. 3 (Amsterdam: Elsevier).

Chang, L. L. Y., Howie, R. A., Zussman, J., Deer, W. A., and Chang, L. L. Y. (1996). *Non-Silicates: Sulphates, Carbonates, Phosphates, Halides,* 2 Edn, Rock-Forming Minerals. London: Geological Society.

Changgen, L., and Yongxin, L. (1983). Selective flotation of scheelite from calcium minerals with sodium oleate as a collector and phosphates as modifiers. II. The mechanism of the interaction between phosphate modifiers and minerals. *Int. J. Mineral Proc.* 10, 219–235. doi: 10.1016/0301-7516(83)90012-1

Chehaibou, B., Badawi, M., Bučko, T., Bazhirov, T., and Rocca, D. (2019). Computing RPA adsorption enthalpies by machine learning thermodynamic perturbation theory. *J. Chem. Theory Comput*. 15, 6333–6342. doi: 10.1021/acs.jctc.9b00782

Chen, C., Hailing, Z., Wei, S., Yuehua, H. U., Wenqing, Q., and Runqing, L. (2017). Synergetic effect of the mixed anionic/non-ionic collectors in low temperature flotation of scheelite. *Minerals* 7:87. doi: 10.3390/min7060087

Chen, C., Zhu, H., Qin, W., Chai, L., and Jia, W. (2018). Improving collecting performance of sodium oleate using a polyoxyethylene ether in scheelite flotation. *J. Cent. South Univ*. 25, 2971–2978. doi: 10.1007/s11771-018-3967-5

Chen, W., Feng, Q., Zhang, G., Yang, Q., and Zhang, C. (2017a). The effect of sodium alginate on the flotation separation of scheelite from calcite and fluorite. *Miner. Eng.* 113, 1–7. doi: 10.1016/j.mineng.2017.07.016

Chen, W., Feng, Q., Zhang, G., Yang, Q., Zhang, C., and Xu, F. (2017b). The flotation separation of scheelite from calcite and fluorite using dextran sulfate sodium as depressant. *Int. J. Mineral Proc.* 169, 53–59. doi: 10.1016/j.minpro.2017.10.005

Chen, Z., Ren, Z., Gao, H., Zheng, R., Jin, Y., and Niu, C. (2019). Flotation studies of fluorite and barite with sodium petroleum sulfonate and sodium hexametaphosphate. *J. Mater. Res. Technol.* 8, 1267–1273. doi: 10.1016/j.jmrt.2018.10.002

Cheng, Y. (2016). Petrogenesis of skarn in Shizhuyuan W-polymetallic deposit, southern Hunan, China: Constraints from petrology, mineralogy and geochemistry. *Transactions of Nonferrous Metals Society of China* 26, 1676–1687. doi: 10.1016/S1003-6326(16)64277-2

Cheng, Y. L., Kuz'kin, S. F., and Solynshkin, V. I. (1963). Infrared spectra of calcite, scheelite and apatite after treatment with flotation regulators. *Izv. Vyssh. Uchebn. Zaved. Tsvetn. Metall*. 6, 28–32.

Cooper, T. G., and de Leeuw, N. H. (2003). A combined ab initio and atomistic simulation study of the surface and interfacial structures and energies of hydrated scheelite: introducing a CaWO4 potential model. *Surf. Sci.* 531, 159–176. doi: 10.1016/S0039-6028(03)00362-5

Cooper, T. G., and de Leeuw, N. H. (2004). A computer modeling study of the competitive adsorption of water and organic surfactants at surfaces of the mineral scheelite. *Langmuir* 20, 3984–3994. doi: 10.1021/la049796w

Dai, P., Mao, J., Wu, S., Xie, G., and Luo, X. (2018). Multiple dating and tectonic setting of the Early Cretaceous Xianglushan W deposit, Jiangxi Province, South China. *Ore Geol. Rev.* 95, 1161–1178. doi: 10.1016/j.oregeorev.2017.11.017

Das, A., and Sarkar, B. (2018). Advanced gravity concentration of fine particles: a review. *Mineral Proc. Extract. Metallurgy Rev.* 39, 359–394. doi: 10.1080/08827508.2018.1433176

Dawson, K. M. (1996). Skarn tungsten. Geology of Canadian mineral deposit types, geological survey of Canada, geology of Canada. *Econ.* Geol. *Rep*. 8, 495–502.

Dean, K. C., and Schack, C. H. (1964). *Flotation of Calcareous Scheelite Ores*. Report of Investigation. U.S. Bureau of Mines (1964). p. 15.

Dehaine, Q., Foucaud, Y., Kroll-Rabotin, J.-S., and Filippov, L. O. (2019). Experimental investigation into the kinetics of Falcon UF concentration: implications for fluid dynamic-based modelling. *Sep. Purif. Technol.* 215, 590–601. doi: 10.1016/j.seppur.2019.01.048

Delaney, B., and Bakker, F. (2014). *Technical Report on the Cantung Mine, Northwest Territories. North American Tungsten Corporation Ltd. (NATCL).*

Detienne, J.-L. (1978). *Valorisation Par Flottation d'un Minerai de Scheelite Finement Exprimée*. Institut National Polytechnique de Lorraine, Nancy.

Dimas, D., Giannopoulou, I., and Panias, D. (2009). Polymerization in sodium silicate solutions: a fundamental process in geopolymerization technology. *J. Mater. Sci.* 44, 3719–3730. doi: 10.1007/s10853-009-3497-5

Dong, L., Jiao, F., Qin, W., Zhu, H., and Jia, W. (2018). Effect of acidified water glass on the flotation separation of scheelite from calcite using mixed cationic/anionic collectors. *Appl. Surf. Sci.* 444, 747–756. doi: 10.1016/j.apsusc.2018.03.097

Einaudi, M. T., and Burt, D. M. (1982). Introduction; terminology, classification, and composition of skarn deposits. *Econ. Geol.* 77, 745–754. doi: 10.2113/gsecongeo.77.4.745

Ejtemaei, M., Irannajad, M., and Gharabaghi, M. (2012). Role of dissolved mineral species in selective flotation of smithsonite from quartz using oleate as collector. *Int. J. Miner. Proc.* 114–117, 40–47. doi: 10.1016/j.minpro.2012.09.004

Engelhardt, L. G., Zeigan, D., Jancke, H., Wieker, W., and Hoebbel, D. (1975). 29Si-NMR-Spektroskopie an Silicatlösungen. II. Zur Abhängigkeit der Struktur der Silicatanionen in wäßrigen Natriumsilicatläsungen vom Na: Si-Verhältnis. *Zeitschr. Anorgan. Allgemeine Chem.* 418, 17–28. doi: 10.1002/zaac.19754180103

Feng, B., Guo, W., Peng, J., and Zhang, W. (2018). Separation of scheelite and calcite using calcium lignosulphonate as depressant. *Sep. Purif. Technol.* 199, 346–350. doi: 10.1016/j.seppur.2018.02.009

Feng, B., Guo, W., Xu, H., Peng, J., Luo, X., and Zhu, X. (2017). The combined effect of lead ion and sodium silicate in the flotation separation of scheelite from calcite. *Sep. Sci. Technol.* 52, 567–573. doi: 10.1080/01496395.2016.1260590

Filho, L. S. L., Seidl, P. R., Correia, J. C. G., and Cerqueira, L. C. K. (2000). Molecular modelling of reagents for flotation processes. *Miner. Eng.* 13, 1495–1503. doi: 10.1016/S0892-6875(00)00133-3

Filippov, L. O., Dehaine, Q., and Filippova, I. V. (2016). Rare earths (La, Ce, Nd) and rare metals (Sn, Nb, W) as by-products of kaolin production - Part 3: processing of fines using gravity and flotation. *Miner. Eng.* 95, 96–106. doi: 10.1016/j.mineng.2016.06.004

Filippov, L. O., Duverger, A., Filippova, I. V., Kasaini, H., and Thiry, J. (2012). Selective flotation of silicates and Ca-bearing minerals: the role of non-ionic reagent on cationic flotation. *Miner. Eng.* 36–38, 314–323. doi: 10.1016/j.mineng.2012.07.013

Filippov, L. O., and Filippova, I. V. (2006). "Synergistic effects in mix collector systems for non-sulfide mineral flotation," in Onal, G., et al. *Proceedings of the XXIII International Mineral Processing Congress,* (Istanbul), pp. 631–4.

Filippov, L. O., Filippova, I. V., Lafhaj, Z., and Fornasiero, D. (2019). The role of a fatty alcohol in improving calcium minerals flotation with oleate. *Colloids Surf. A* 560, 410–417. doi: 10.1016/j.colsurfa.2018.10.022

Filippov, L. O., Foucaud, Y., Filippova, I. V., and Badawi, M. (2018). New reagent formulations for selective flotation of scheelite from a skarn ore with complex calcium minerals gangue. *Miner. Eng.* 123, 85–94. doi: 10.1016/j.mineng.2018.05.001

Filippov, L. O., Severov, V. V., and Filippova, I. V. (2013). Mechanism of starch adsorption on Fe-Mg-Al-bearing amphiboles. *Int. J. Mineral Proc.* 123, 120–128. doi: 10.1016/j.minpro.2013.05.010

Filippov, L. O., Shokhin, V. N., Yenbaeva, L. I., and Ignatkina, V. A. (1993). Improvement of engineering data for flotation of scheelite using combination of sodium oleate and Exol-B. *Tsvetnye Metally* 1, 60–64.

Filippova, I. V., Filippov, L. O., Duverger, A., and Severov, V. V. (2014). Synergetic effect of a mixture of anionic and nonionic reagents: Ca mineral contrast separation by flotation at neutral pH. *Miner. Eng.* 66–68, 135–144. doi: 10.1016/j.mineng.2014.05.009

Foucaud, Y., Badawi, M., Filippov, L., Filippova, I., and Lebègue, S. (2019a). A review of atomistic simulation methods for surface physical-chemistry phenomena applied to froth flotation. *Miner. Eng.* 143:106020. doi: 10.1016/j.mineng.2019.106020

Foucaud, Y., Badawi, M., Filippov, L. O., Barres, O., Filippova, I. V., and Lebègue, S. (2019d). Synergistic adsorptions of Na 2 CO 3 and Na 2 SiO 3 on calcium minerals revealed by spectroscopic and ab initio molecular dynamics studies. *Chem. Sci.* 10, 9928–9940. doi: 10.1039/C9SC03366A

Foucaud, Y., Badawi, M., Filippov, L. O., Filippova, I. V., and Lebègue, S. (2018a). Surface properties of fluorite in presence of water: an atomistic investigation. *J. Phys. Chem. B* 122, 6829–6836. doi: 10.1021/acs.jpcb.8b02717

Foucaud, Y., Dehaine, Q., Filippov, L. O., and Filippova, I. V. (2019e). Application of falcon centrifuge as a cleaner alternative for complex tungsten ore processing. *Minerals* 9:448. doi: 10.3390/min9070448

Foucaud, Y., Filippova, I., Dehaine, Q., Hubert, P., and Filippov, L. (2019b). Integrated approach for the processing of a complex tungsten Skarn ore (Tabuaço, Portugal). *Miner. Eng.* 143:105896. doi: 10.1016/j.mineng.2019.105896

Foucaud, Y., Filippova, I. V., and Filippov, L. O. (2019c). Investigation of the depressants involved in the selective flotation of scheelite from apatite, fluorite, and calcium silicates: focus on the sodium silicate/sodium carbonate system. *Powder Technol.* 352, 501–512. doi: 10.1016/j.powtec.2019.04.071

Foucaud, Y., Lebègue, S., Filippov, L. O., Filippova, I. V., and Badawi, M. (2018b). Molecular insight into fatty acid adsorption on bare and hydrated (111) fluorite surface. *J. Phys. Chem. B* 122, 12403–12410. doi: 10.1021/acs.jpcb.8b08969

Fuerstenau, D. W., and Healy, T. W. (1972). Chapter K principles of mineral flotation. *Adsorpt. Bubble Sep. Tech.* 91–131. doi: 10.1016/B978-0-12-443350-2.50011-3

Fuerstenau, D. W., and Miller, J. D. (1967). The role of the hydrocarbon chain in anionic flotation of calcite. *Trans. AIME* 238, 153–160.

Fuerstenau, M. C., Gutierrez, G., and Elgillani, D. A. (1972). The influence of sodium silicate in non-metallic flotation systems. *Trans. AIME* 241, 348–352.

Fuerstenau, M. C., and Palmer, B. R. (1976). "Anionic flotation of oxides and silicates," *in* Flotation. A.M. Gaudin Memorial Volume, ed. M.C. Fuerstenau (New York, NY: AIME), 148–196.

Fukazawa, K. (1977). *Froth Flotation Process for Recovering Sheelite.* US Patent 4,040,519.

Gao, Y., Gao, Z., Sun, W., Yin, Z., Wang, J., and Hu, Y. (2018). Adsorption of a novel reagent scheme on scheelite and calcite causing an effective flotation separation. *J. Colloid Interface Sci.* 512, 39–46. doi: 10.1016/j.jcis.2017.10.045

Gao, Z., Bai, D., Sun, W., Cao, X., and Hu, Y. (2015a). Selective flotation of scheelite from calcite and fluorite using a collector mixture. *Miner. Eng.* 72, 23–26. doi: 10.1016/j.mineng.2014.12.025

Gao, Z., Gao, Y., Zhu, Y., Hu, Y., and Sun, W. (2016a). Selective flotation of calcite from fluorite: a novel reagent schedule. *Minerals* 6:114. doi: 10.3390/min6040114

Gao, Z., Hu, Y., Sun, W., and Drelich, J. W. (2016b). Surface-charge anisotropy of scheelite crystals. *Langmuir* 32, 6282–6288. doi: 10.1021/acs.langmuir.6b01252

Gao, Z., Sun, W., and Hu, Y. (2015b). New insights into the dodecylamine adsorption on scheelite and calcite: an adsorption model. *Miner. Eng.* 79, 54–61. doi: 10.1016/j.mineng.2015.05.011

Gao, Z., Sun, W., Hu, Y., and Liu, X. (2013). Surface energies and appearances of commonly exposed surfaces of scheelite crystal. *Trans. Nonferrous Metals Soc. China* 23, 2147–2152. doi: 10.1016/S1003-6326(13)62710-7

Gaudin, A. M., and Fuerstenau, D. W. (1956). *Minerals Beneficiation - Quartz Flotation with Anionic Collectors*. The American Institute of Mining, Metallurgical and Petroleum Engineers.

Glembotskii, V. A., and Uvarov, V. S. (1964). The mechanism of action of sodium silicate during the flotation of several on-sulphide minerals. *Dokl. Akad. Nauk., Tadzh. SSSR* 7, 29–32.

González-Martín, M. L., Bruque, J. M., González-Caballero, F., Perea-Carpio, R., and Janczuk, B. (1996). The mechanism of adsorption of sodium dodecylsulfonate on fluorite and its surface free energy. *Appl. Surf. Sci.* 103, 395–402. doi: 10.1016/S0169-4332(96)00540-5

Grosman, L. I. (1962). Separation of non-sulphide minerals in acidified medium, Tr. Vses. Nauchno Issled. *Proektno Inst. Mekh. Obrab. Polezn. Iskop.* 131, 208–218.

Grosman, L. I., and Sukhoval'skaya, S. D. (1955). Flotation separation of calcium and barium minerals, Tsvetn. *Met.* 28, 7–13. doi: 10.4144/rpsj1954.1955.3_28

Halasz, I., Agarwal, M., Li, R., and Miller, N. (2007). Vibrational spectra and dissociation of aqueous Na2SiO3 solutions. *Catal. Lett.* 117, 34–42. doi: 10.1007/s10562-007-9141-6

Han, H., Hu, Y., Sun, W., Li, X., Cao, C., Liu, R., et al. (2017). Fatty acid flotation versus BHA flotation of tungsten minerals and their performance in flotation practice. *Int. J. Mineral Proc.* 159, 22–29. doi: 10.1016/j.minpro.2016.12.006

Han, Y., Liu, W., and Chen, J. (2016). DFT simulation of the adsorption of sodium silicate species on kaolinite surfaces. *Appl. Surf. Sci.* 370, 403–409. doi: 10.1016/j.apsusc.2016.02.179

Hanna, H., and Somasundaran, P. (1976). "Flotation of salt-type minerals," in *Flotation - A. M. Gaudin Memorial* ed M.C. Fuerstenau (New York, NY: AIME), p. 197–272.

Hanumantha Rao, K., and Forssberg, K. S. E. (1991). Mechanism of fatty acid adsorption in salt-type mineral flotation. *Miner. Eng.* 4, 879–890. doi: 10.1016/0892-6875(91)90071-3

Hessou, E. P., Kanhounnon, W. G., Rocca, D., Monnier, H., Vallières, C., Lebègue, S., et al. (2018). Adsorption of NO, NO2, CO, H2O and CO2 over isolated monovalent cations in faujasite zeolite: a periodic DFT investigation. *Theor. Chem. Acc.* 137, 161. doi: 10.1007/s00214-018-2373-2

Hiçyilmaz, C., Atalayü., and Özbayoglu, G. (1993). Selective flotation of scheelite using amines. *Miner. Eng.* 6, 313–320. doi: 10.1016/0892-6875(93)90039-P

Hicyilmaz, C., and Özbayoglu, G. (1992). The effects of amine and electrolytes on the zeta-potential of scheelite from Uludag, Turkey. *Miner. Eng.* 5, 945–951. doi: 10.1016/0892-6875(92)90261-7

Hu, Y., Gao, Z., Sun, W., and Liu, X. (2012). Anisotropic surface energies and adsorption behaviors of scheelite crystal. *Colloids Surfaces A* 415, 439–448. doi: 10.1016/j.colsurfa.2012.09.038

Hu, Y., Yang, F., and Sun, W. (2011). The flotation separation of scheelite from calcite using a quaternary ammonium salt as collector. *Miner. Eng.* 24, 82–84. doi: 10.1016/j.mineng.2010.08.023

Jansson, H., Bernin, D., and Ramser, K. (2015). Silicate species of water glass and insights for alkali-activated green cement. *AIP Adv.* 5:067167. doi: 10.1063/1.4923371

Jébrak, M., Marcoux, É., and Laithier, M. (2016). *Geology of Mineral Resources,* 2nd Edn. St. John's, NL: Geological Association of Canada.

Jin, J., Long, Y., Gao, H., and Ren, Z. (2019). Flotation behavior and mechanism of andalusite and kyanite in the presence of sodium oleate. *Sep. Sci. Technol.* 54, 1803–1814. doi: 10.1080/01496395.2018.1540636

Khuwijitjaru, P., Adachi, S., and Matsuno, R. (2002). Solubility of Saturated Fatty Acids in Water at Elevated Temperatures. *Biosci. Biotechnol. Biochem.* 66, 1723–1726. doi: 10.1271/bbb.66.1723

Kupka, N., and Rudolph, M. (2018a). Froth flotation of scheelite - a review. *Int. J. Min. Sci. Technol.* 28, 373–384. doi: 10.1016/j.ijmst.2017.12.001

Kupka, N., and Rudolph, M. (2018b). Role of sodium carbonate in scheelite flotation - a multi-faceted reagent. *Miner. Eng.* 129, 120–128. doi: 10.1016/j.mineng.2018.09.005

Kupka, N. M. L., Möckel, R., and Rudolph, M. (2019). Acidified water glass in the selective flotation of scheelite from calcite, part I: performance and impact of the acid type. *Physicochem. Probl. Miner. Process.* 56, 238–251. doi: 10.37190/ppmp19101

Kwak, T. A. P. (1987). *W-Sn Skarn Deposits and Related Metamorphic Skarns and Granitoids, Developments in Economic Geology*. Amsterdam; New York: Elsevier, Distributors for the United States and Canada, Elsevier Science Pub. Co.

Lassner, E., and Schubert, W.-D. (1999). Tungsten: properties, chemistry, technology of the element, alloys, and chemical compounds. Boston, MA: Springer.

Lauri, L., Brown, T., Gunn, G., Kalvig, P., and Sievers, H. (2018). *Deliverable 3.1 of the SCRREEN H2020 European project Mercade, 1975.*

Leja, J. (1981). *Surface Chemistry of Froth Flotation*. Boston, MA: Springer.

Lentz, C. W. (1964). Silicate minerals as sources of trimethylsilyl silicates and silicate structure analysis of sodium silicate solutions. *Inorg. Chem.* 3, 574–579. doi: 10.1021/ic50014a029

Li, C., and Gao, Z. (2017). Effect of grinding media on the surface property and flotation behavior of scheelite particles. *Powder Technol.* 322, 386–392. doi: 10.1016/j.powtec.2017.08.066

Liu, C., Feng, Q., Zhang, G., Chen, W., and Chen, Y. (2016). Effect of depressants in the selective flotation of scheelite and calcite using oxidized paraffin soap as collector. *Int. J. Mineral Proc.* 157, 210–215. doi: 10.1016/j.minpro.2016.11.011

Logan, R. L. (1979). Tall oil fatty acids. *J. Am. Oil Chem. Soc.* 56, 777A−779A. doi: 10.1007/BF02667443

Lu, H.-Z., Liu, Y., Wang, C., Xu, Y., and Li, H. (2003). Mineralization and fluid inclusion study of the Shizhuyuan W-Sn-Bi-Mo-F Skarn deposit, Hunan Province, China. *Econ. Geol.* 98, 955–974. doi: 10.2113/gsecongeo.98.5.955

Marinakis, K. I. (1980). *The Action of Sodium Silicate on the Flotation of Salt-Type Minerals With Oleic Acid*. PhD thesis. Imperial College, University of London, United Kingdom.

Marinakis, K. I., and Kelsall, G. H. (1987a). The surface chemical properties of scheelite (CaWO4) I. The scheelite/water interface and CaWO4 solubility. *Colloids Surf.* 25, 369–385. doi: 10.1016/0166-6622(87)80315-3

Marinakis, K. I., and Kelsall, G. H. (1987b). The surface chemical properties of scheelite (CaWO4) II. Collector adsorption and recovery of fine scheelite particles at the iso-octane/water interface. *Colloids Surf.* 26, 243–255. doi: 10.1016/0166-6622(87)80119-1

Marinakis, K. I., and Shergold, H. L. (1985). Influence of sodium silicate addition on the adsorption of oleic acid by fluorite, calcite and barite. *Int. J. Mineral Proc.* 14, 177–193. doi: 10.1016/0301-7516(85)90002-X

Martins, J. I., and Amarante, M. M. (2013). Scheelite Flotation From Tarouca Mine Ores. *Mineral Proc. Extract. Metallurgy Rev.* 34, 367–386. doi: 10.1080/08827508.2012.657022

Masan Resources (2012). *Update on Nui Phao Project in Northern Vietnam*. ITIA (2012).

Meinert, L. D. (1992). Skarns and skarn deposits. *Geoscience* 19:145–162. doi: 10.12789/gs.v19i4.3773

Meinert, L. D., Dipple, G. M., and Nicolescu, S. (2005). *World Skarn Deposits. Economic Geology 100th Anniversary Volume*, (McLean, VA), 299-336.

Mercade, V. V. (1975). Recovery of scheelite from ores by flotation. US Patent no. 3,915,391.

Mielczarski, J., Nowak, P., and Strojek, J. W. (1983). Correlation between the adsorption of sodium dodecyl sulphate on calcium fluoride (fluorite) and its floatability - an infra-red internal reflection spectrophotometric study. *Int. J. Mineral Proc.* 11, 303–317. doi: 10.1016/0301-7516(83)90051-0

Miller, J. D., and Hiskey, J. B. (1972). Electrokinetic behavior of fluorite as influenced by surface carbonation. *J. Colloid Interface Sci.* 41, 567–573. doi: 10.1016/0021-9797(72)90378-5

Miller, J. D., and Misra, M. (1984). "The hydrophobic character of semisoluble salt minerals with oleate as collector," in *International Conference on Recent Advances in Mineral Sciences and Technologic* (Johannesburg), 259–267.

Misra, K. C. (2000). *Understanding Mineral Deposits*. Dordrecht: Springer Netherlands.

Mogilevsky, P., Parthasarathy, T. A., and Petry, M. D. (2004). Anisotropy in room temperature microhardness and fracture of CaWo4 scheelite. *Acta Mater.* 52, 5529–5537. doi: 10.1016/j.actamat.2004.08.022

Nakhaei, F., and Irannajad, M. (2018). Reagents types in flotation of iron oxide minerals: a review. *Mineral Proc. Extract. Metallurgy Rev.* 39, 89–124. doi: 10.1080/08827508.2017.1391245

Neiman, A. (1996). Cooperative transport in oxides: Diffusion and migration processes involving Mo(VI), W(VI), V(V) and Nb(V). *Solid State Ionics* 83, 263–273. doi: 10.1016/0167-2738(95)00247-2

Ngoc, B. D. (2016). *Masan Resources Nui Phao Project*. London: International Tungsten Industry Association.

Nikiforov, K. A., and Skobeev, I. K. (1968). Infrared spectroscopic study of fluorite and calcite after treatment of minerals by water glass. *Nauchn. Tr. Irkutsk. Gos. Nauchno- Issled. Inst. Redk. Tsvetn. Met.* 19:153–158.

Nordström, J., Nilsson, E., Jarvol, P., Nayeri, M., Palmqvist, A., Bergenholtz, J., et al. (2011). Concentration- and pH-dependence of highly alkaline sodium silicate solutions. *J. Colloid Interface Sci.* 356, 37–45. doi: 10.1016/j.jcis.2010.12.085

Oliveira, J. F., and Sampaio, J. A. (1988). "Development studies for the recovery of Brazilian scheelite fines by froth flotation," in *Production and Processing of Fine Particles*, eds A. J. Plumpton (Amsterdam: Elsevier), pp. 209–2017.

Ozcan, O., and Bulutcu, A. N. (1993). Electrokinetic, infrared and flotation studies of scheelite and calcite with oxine, alkyl oxine, oleoyl sarcosine and quebracho. *Int. J. Mineral Proc.* 39, 275–290. doi: 10.1016/0301-7516(93)90020-B

Ozcan, O., Bulutcu, A. N., Sayan, P., and Recepoglu, O. (1994). Scheelite flotation: a new scheme using oleoyl sarcosine as collector and alkyl oxine as modifier. *Int. J. Mineral Proc.* 42, 111–120. doi: 10.1016/0301-7516(94)90023-X

Parks, T. C., and Barker, W. W. (1977). The ordered dispersal of point defects over cubic lattices: application to fluorite-related structures. *J. Solid State Chem.* 20, 397–407. doi: 10.1016/0022-4596(77)90177-3

Pastor, H. (2000). *Métallurgie et Recyclage du Tungstène*. Procédés.

Patil, D. P., and Nayak, U. B. (1985). "Selective flotation of scheelite and calcite," in *Proceeedings of National Seminar on Mineral Processing and IX Annual Technical Convention of Indian Institute of Mineral Engineers, 11th and 12th March* Jamshedpur: National Metallurgical Laboratory (CSIR), 10.

Pearse, M. J. (2005). An overview of the use of chemical reagents in mineral processing. *Miner. Eng.* 18, 139–149. doi: 10.1016/j.mineng.2004.09.015

Petrov, I. S. (1940). *A New Method for Flotation of Poor Scheelite Ores.* Sankt-Peterburg: ONTI; Mekhanobr.

Pitfield, P., Brown, T., Gunn, G., and Rayner, D. (2011). *Tungsten Profile*. London: British Geological Survey. Available online at: https://www.bgs.ac.uk/downloads/start.cfm?id=1981

Pradip, and Fuerstenau, D.W. (1983). The adsorption of hydroxamate on semi-soluble minerals. Part I: adsorption on barite, calcite and bastnaesite. *Colloids Surf.* 8, 103–119. doi: 10.1016/0166-6622(83)80079-1

Pradip, and Fuerstenau, D.W. (1985). Adsorption of hydroxamate collectors on semisoluble minerals part II: effect of temperature on adsorption. *Colloids Surf.* 15, 137–146. doi: 10.1016/0166-6622(85)80061-5

Qi, G. W., Klauber, C., and Warren, L. J. (1993). Mechanism of action of sodium silicate in the flotation of apatite from hematite. *Int. J. Mineral Proc.* 39, 251–273. doi: 10.1016/0301-7516(93)90019-7

Raatz, S. (1992). "The influence of multivalent cations on the floatability of scheelite, fluorite and calcite," in *Innovations in Flotation Technology*, eds P. Mavros and K. A. Matis (Dordrecht: Springer), 419–425. doi: 10.1007/978-94-011-2658-8_21

Rahimi, S., Irannajad, M., and Mehdilo, A. (2017). Effects of sodium carbonate and calcium chloride on calcite depression in cationic flotation of pyrolusite. *Trans. Nonferrous Met. Soc. China* 27, 1831–1840. doi: 10.1016/S1003-6326(17)60206-1

Rao, D. S., VijayaKumar, T. V., Rao, S. S., Prabhakar, S., and Raju, G. B. (2011). Effectiveness of sodium silicate as gangue depressants in iron ore slimes flotation. *Int. J. Miner. Metallurgy Mater.* 18, 515–522. doi: 10.1007/s12613-011-0471-4

Rocca, D., Dixit, A., Badawi, M., Lebègue, S., Gould, T., and Bučko, T. (2019). Bridging molecular dynamics and correlated wave-function methods for accurate finite-temperature properties. *Phys. Rev. Materials* 3:040801. doi: 10.1103/PhysRevMaterials.3.040801

Roller, P. S., and Ervin, G. (1940). The system calcium oxide-silica-water at 30°. The association of silicate * ion in dilute alkaline solution. *J. Am. Chem. Soc.* 62, 461–471. doi: 10.1021/ja01860a001

Rutledge, J., and Anderson, C. (2015). Tannins in mineral processing and extractive metallurgy. *Metals* 5, 1520–1542. doi: 10.3390/met5031520

Schmidt, S. (2012a). *From Deposit to Concentrate: The Basics of Tungsten Mining Part 1: Project Generation and Project Development*. ITIA (2012).

Schmidt, S. (2012b). *From Deposit to Concentrate: The Basics of Tungsten Mining Part 2: Operational Pratices and Challenges*. ITIA (2012).

Schubert, H., Baldauf, H., Kramer, W., and Schoenherr, J. (1990). Further development of fluorite flotation from ores containing higher calcite contents with oleoylsarcosine as collector. *Int. J. Mineral Proc.* 30, 185–193. doi: 10.1016/0301-7516(90)90014-P

Schubert, W.-D., Lassner, E., and Walser, P. (2006). *Geology of Tungsten.* International Tungsten Industry Association (ITIA) Newsletter. Available online at: http://www.itia.info/FileLib/Newsletter_2006_12.pdf

Shergold, H. L. (1972). Infra-red study of adsorption of sodium dodecyl sulphate by CaF2. *Bull. Inst. Mining Met. Sect.* 81–148.

Sis, H., and Chander, S. (2003). Reagents used in the flotation of phosphate ores: a critical review. *Miner. Eng.* 16, 577–585. doi: 10.1016/S0892-6875(03)00131-6

Soloviev, S. G., and Krivoshchekov, N. N. (2011). Vostok-2 gold-base-metal-tungsten skarn deposit, Central Sikhote-Alin, Russia. *Geol. Ore Deposits* 53, 478–500. doi: 10.1134/S1075701511060080

Somasundaran, P. (1969). Adsorption of starch and oleate and interaction between them on calcite in aqueous solutions. *J. Colloid Interface Sci.* 31, 557–565. doi: 10.1016/0021-9797(69)90056-3

Song, S., Lopez-Valdivieso, A., Martinez-Martinez, C., and Torres-Armenta, R. (2006). Improving fluorite flotation from ores by dispersion processing. *Miner. Eng.* 19, 912–917. doi: 10.1016/j.mineng.2005.10.005

Sørensen, E. (1973). On the adsorption of some anionic collectors on fluoride minerals. *J. Colloid Interface Sci.* 45, 601–607. doi: 10.1016/0021-9797(73)90177-X

Souvi, S. M. O., Badawi, M., Virot, F., Cristol, S., Cantrel, L., and Paul, J.-F. (2017). Influence of water, dihydrogen and dioxygen on the stability of the Cr2O3 surface: a first-principles investigation. *Surf. Sci.* 666, 44–52. doi: 10.1016/j.susc.2017.08.005

Suárez Sánchez, A., Krzemien, A., Riesgo Fernández, P., Iglesias Rodríguez, F. J., Sánchez Lasheras, F., and de Cos Juez, F. J. (2015). Investment in new tungsten mining projects. *Resour. Policy* 46, 177–190. doi: 10.1016/j.resourpol.2015.10.003

Tian, M., Zhang, C., Han, H., Liu, R., Gao, Z., Chen, P., et al. (2018). Novel insights into adsorption mechanism of benzohydroxamic acid on lead (II)-activated cassiterite surface: an integrated experimental and computational study. *Miner. Eng.* 122, 327–338. doi: 10.1016/j.mineng.2018.04.012

U. S. Geological Survey (2019). Mineral Commodity Summaries (2019). *Technical Report.* Reston, VA: United States Geological Survey.

Walsh, K. A., and Vidal, E. E. (2009). *Beryllium Chemistry and Processing.* Materials Park, OH: ASM International.

Wang, J., Bai, J., Yin, W., and Liang, X. (2018a). Flotation separation of scheelite from calcite using carboxyl methyl cellulose as depressant. *Miner. Eng.* 127, 329–333. doi: 10.1016/j.mineng.2018.03.047

Wang, J., and Somasundaran, P. (2005). Adsorption and conformation of carboxymethyl cellulose at solid-liquid interfaces using spectroscopic, AFM and allied techniques. *J. Colloid Interface Sci.* 291, 75–83. doi: 10.1016/j.jcis.2005.04.095

Wang, J., Zhou, Z., Gao, Y., Sun, W., Hu, Y., and Gao, Z. (2018b). Reverse flotation separation of fluorite from calcite: a novel reagent scheme. *Minerals* 8:313. doi: 10.3390/min8080313

Wei, Z., Hu, Y., Han, H., Sun, W., Wang, R., and Wang, J. (2018). Selective flotation of scheelite from calcite using Al-Na 2 SiO 3 polymer as depressant and Pb-BHA complexes as collector. *Miner. Eng.* 120, 29–34. doi: 10.1016/j.mineng.2018.01.036

Wei, Z., Hu, Y., Han, H., Sun, W.ei, Wang, R., Sun, W.enjuan, Wang, J., Gao, Z., et al. (2019). Selective separation of scheelite from calcite by self-assembly of H2SiO3 polymer using Al3+ in Pb-BHA flotation. *Minerals* 9:43. doi: 10.3390/min9010043

Wells, A. (1991). Some experiences in the design and optimisation of fine gravity concentration circuits. *Miner. Eng.* 4, 383–398. doi: 10.1016/0892-6875(91)90143-J

Werner, A. B. T., Sinclair, W. D., and Amey, E. B. (1998). *International Strategic Mineral Issues Summary Report - Tungsten. U.S. Geological Survey Circular 930-O.* Available online at: http://pubs.usgs.gov/pdf/circular/c930-o.html

Wheeler, A. (2015). *Technical Report on the Mineral Resources and Reserves of the Los Santos Mine Project. Adam Wheeler (Mining Consultant) for Daytal Resources Spain S. L.*

Wills, B., Finch, J., and Safari, O.M.C. (2016). *Wills' Mineral Processing Technology,* 8th Edn. Available online at: https://www.sciencedirect.com/science/article/pii/B9780080970530000194

Xian-Ping, L., Bo, F., Xianwen, Z., Li-Ying, L., and Zheng-He, X. (2017). Flotation separation of wolframite from quartz using N-oleoyl sarcosine acid as collector. *Physicochem. Problems Miner. Proc.* 53, 34–41. doi: 10.5277/ppmp170103

Xu, L., Hu, Y., Tian, J., Wu, H., Yang, Y., Zeng, X., et al. (2016). Selective flotation separation of spodumene from feldspar using new mixed anionic/cationic collectors. *Miner. Eng.* 89, 84–92. doi: 10.1016/j.mineng.2016.01.013

Xu, L., Peng, T., Tian, J., Lu, Z., Hu, Y., and Sun, W. (2017a). Anisotropic surface physicochemical properties of spodumene and albite crystals: implications for flotation separation. *Appl. Surf. Sci.* 426, 1005–1022. doi: 10.1016/j.apsusc.2017.07.295

Xu, L., Tian, J., Wu, H., Deng, W., Yang, Y., Sun, W., et al. (2017b). New insights into the oleate flotation response of feldspar particles of different sizes: anisotropic adsorption model. *J. Colloid Interf. Sci.* 505, 500–508. doi: 10.1016/j.jcis.2017.06.009

Yang, F., Sun, W., Hu, Y., and Long, S. (2015). Cationic flotation of scheelite from calcite using quaternary ammonium salts as collector: adsorption behavior and mechanism. *Miner. Eng.* 81, 18–28. doi: 10.1016/j.mineng.2015.07.014

Yang, X. (2018). Beneficiation studies of tungsten ores - a review. *Miner. Eng.* 125, 111–119. doi: 10.1016/j.mineng.2018.06.001

Yang, Y., Xie, B., Wang, R., Xu, S., Wang, J., and Xu, Z. (2016). Extraction and separation of tungsten from acidic high-phosphorus solution. *Hydrometallurgy* 164, 97–102. doi: 10.1016/j.hydromet.2016.05.018

Yin, W., and Wang, J. (2014). Effects of particle size and particle interactions on scheelite flotation. *Transac. Nonferrous Metals Soc. China* 24, 3682–3687. doi: 10.1016/S1003-6326(14)63515-9

Yin, W.-Z., Wang, J.-Z., and Sun, Z.-M. (2015). Structure-activity relationship and mechanisms of reagents used in scheelite flotation. *Rare Metals* 34, 882–887. doi: 10.1007/s12598-014-0381-5

Yongxin, L., and Changgen, L. (1983). Selective flotation of scheelite from calcium minerals with sodium oleate as a collector and phosphates as modifiers. I. Selective flotation of scheelite. *Int. J. Miner. Proc.* 10, 205–218. doi: 10.1016/0301-7516(83)90011-X

Yue, T., Han, H., Hu, Y., Wei, Z., Wang, J., Wang, L., et al. (2018). Beneficiation and purification of tungsten and cassiterite minerals using pb-bha complexes flotation and centrifugal separation. *Minerals* 8:566. doi: 10.3390/min8120566

Zhang, Y., Li, Y., Chen, R., Wang, Y., Deng, J., and Luo, X. (2017). Flotation separation of scheelite from fluorite using sodium polyacrylate as inhibitor. *Minerals* 7:102. doi: 10.3390/min7060102

Zhao, G., Wang, S., and Zhong, H. (2015). Study on the activation of scheelite and wolframite by lead nitrate. *Minerals* 5, 247–258. doi: 10.3390/min5020247

Zhao, G., Zhong, H., Qiu, X., Wang, S., Gao, Y., Dai, Z., et al. (2013). The DFT study of cyclohexyl hydroxamic acid as a collector in scheelite flotation. *Miner. Eng.* 49, 54–60. doi: 10.1016/j.mineng.2013.04.025

Zheng, R., Ren, Z., Gao, H., and Qian, Y. (2018). Evaluation of sulfonate-based collectors with different hydrophobic tails for flotation of fluorite. *Minerals* 8:57. doi: 10.3390/min8020057

Zheng, X., and Smith, R. W. (1997). Dolomite depressants in the flotation of apatite and collophane from dolomite. *Miner. Eng.* 10, 537–545. doi: 10.1016/S0892-6875(97)00031-9

Zhou, W., Moreno, J., Torres, R., Valle, H., and Song, S. (2013). Flotation of fluorite from ores by using acidized water glass as depressant. *Miner. Eng.* 45, 142–145. doi: 10.1016/j.mineng.2013.02.017

Zhu, G., Wang, Y., Wang, X., Yu, F., and Miller, J. D. (2018). States of coadsorption for oleate and dodecylamine at selected spodumene surfaces. *Colloids Surf. A* 558, 313–321. doi: 10.1016/j.colsurfa.2018.08.083

Conflict of Interest: The authors declare that the research was conducted in the absence of any commercial or financial relationships that could be construed as a potential conflict of interest.

frontiers in Chemistry

ORIGINAL RESEARCH
published: 28 April 2020
doi: 10.3389/fchem.2020.00242

Effects of Sodium Alginate on the Flotation Separation of Molybdenite From Chalcopyrite Using Kerosene as Collector

Guangsheng Zeng[1], *Leming Ou*[2]*, *Wencai Zhang*[3] *and Yuteng Zhu*[2]

[1] College of Chemistry and Chemical Engineering, Central South University, Changsha, China, [2] School of Minerals Processing and Bioengineering, Central South University, Changsha, China, [3] Department of Mining and Minerals Engineering, Virginia Polytechnic and State University, Blacksburg, VA, United States

In this paper, the effect of sodium alginate (SA) on the flotation separation of molybdenite (MoS_2) from chalcopyrite using kerosene as collector was systematically investigated. The results of single-mineral micro-flotation tests indicated that SA exhibited strong depression on chalcopyrite flotation while it imposed no impact on the floatability of molybdenite. However, in the chalcopyrite–molybdenite mixed-mineral flotation system, the presence of chalcopyrite significantly increased the depressing effect of SA on molybdenite flotation, leading to a considerable reduction in the flotation selectivity. The negative impact of chalcopyrite on the performance of SA in molybdenite flotation was eliminated by adding a certain dosage of kerosene prior to SA. A concentrate containing 53.43% of molybdenum (Mo) was obtained at 76.90% of recovery using 19 mg/L kerosene and 40 mg/L SA at pH 5.4. Zeta potential measurements indicated that the adsorption of SA on chalcopyrite surfaces was stronger than that on molybdenite surfaces, which agreed with the single-mineral flotation test results. The adsorption of SA on chalcopyrite was further confirmed to be chemisorption by Fourier-transform infrared spectroscopy (FTIR) spectra analyses. When Cu^{2+} appeared in solution, the flotation of molybdenite was strongly depressed by SA. Mechanism analyses indicated that more active sites were generated on molybdenite surfaces after the addition of Cu^{2+}, thus promoting the adsorption of SA.

Keywords: molybdenite, chalcopyrite, sodium alginate, Cu^{2+}-activation, flotation

OPEN ACCESS

Edited by:
Przemyslaw B. Kowalczuk, Norwegian University of Science and Technology, Norway

Reviewed by:
Lei Xie, University of Alberta, Canada
Guangyuan Xie, China University of Mining and Technology, China

***Correspondence:**
Leming Ou
olmpaper@csu.edu.cn

Specialty section:
This article was submitted to Physical Chemistry and Chemical Physics, a section of the journal Frontiers in Chemistry

Received: *25 November 2019*
Accepted: *13 March 2020*
Published: *28 April 2020*

Citation:
Zeng G, Ou L, Zhang W and Zhu Y (2020) Effects of Sodium Alginate on the Flotation Separation of Molybdenite From Chalcopyrite Using Kerosene as Collector. Front. Chem. 8:242. doi: 10.3389/fchem.2020.00242

INTRODUCTION

Molybdenite (MoS_2) is the primary source of molybdenum (Mo), and approximately half of the Mo production is obtained from copper (Cu)–Mo sulfides, mainly porphyry Cu deposits (Ansari and Pawlik, 2007; Song et al., 2012; Hirajima et al., 2014). At present, the flotation separation of Cu minerals and Mo minerals in this type of ore is normally achieved by selectively depressing the Cu sulfide minerals using various inorganic inhibitors. Sulfide is one of the most widely used Cu sulfide inhibitors in practical flotation processes (Pearse, 2005; Yin et al., 2010; Mehrabani et al., 2011; Zhao et al., 2018). However, the characteristics of high dosage and toxicity of inorganic inhibitors adversely affect the surrounding environment. Therefore, the development and application of more environment-friendly and cost-efficient inhibitors are crucial (Yin et al., 2017; Suyantara et al., 2018; Yuan et al., 2019a,b).

Sodium alginate (SA) is a natural non-toxic anionic polysaccharide extracted from various species of brown algae comprised of 1→ 4 linked β-D-mannuronic acid (M) and its C-5 epimer α-L-guluronic acid (G) (Wang and Peng, 2014). It has been extensively applied in the fields of medical, health, biology, food, etc. (Lin et al., 2005; Pawar and Edgar, 2012; Hu et al., 2017; Su et al., 2017; Li et al., 2019). The molecular structure of SA is shown in **Figure 1**. Its molecular structure contains a large number of hydroxyl (-OH) and carboxyl (-COO-) groups, and the gelling reaction of SA with divalent cations can occur easily in solution (Zhu et al., 2003; Liu et al., 2008; Yu et al., 2017). Based on the properties of SA described above, SA was considered to be a potential alternative to conventional inorganic inhibitors. The feasibility of using SA as a flotation inhibitor has been tested for various minerals. For instance, SA was used as an inhibitor of molybdenite using amyl xanthate as collector in chalcopyrite flotation (Chen et al., 2018) and as an inhibitor of galena using ammonium dibutyl dithiophosphate as collector in chalcopyrite (Chen et al., 2019) and as an inhibitor to separate the scheelite from calcite and fluorite (Chen et al., 2017). However, the effects of SA on the flotation performances of chalcopyrite and molybdenite using kerosene as collector have not been reported yet. Therefore, in this paper, SA was utilized as a depressant to separate the molybdenite from chalcopyrite using kerosene as the collector. The adsorption behaviors of SA on the mineral surfaces were studied by adsorption measurements, zeta potential measurements, and Fourier-transform infrared spectroscopy (FTIR) spectra analyses.

MATERIALS AND METHODS

Mineral Samples and Reagents

Molybdenite and chalcopyrite samples used for this study were obtained from Tibet and Yunnan, China, respectively. High-grade mineral crystals were manually picked out and pulverized to a top size of 1 mm using a laboratory roll crusher and a ceramic ball mill. The product was dry-sieved with standard screens to acquire the −74 + 38-μm and −38-μm fractions. The former fraction was used for micro-flotation tests and adsorption measurements. A portion of the latter fraction was further ground to minus 2 μm for zeta potential measurements and FTIR analyses. Based on the X-ray diffraction (XRD) results shown in **Figure 2**, the purity of molybdenite and chalcopyrite was 95.68% and 98.23%, respectively.

SA was supplied by Enoson Biotechnology Co., Ltd., Wuhan, China. A stock solution of SA (0.04% by weight) was prepared by dispersing a required amount of SA in deionized water with high-speed stirring. Kerosene and $CuCl_2$ were both purchased from Tianjin Kermil Chemical Reagents Development Centre, Tianjin, China. Hydrochloric acid (HCl) and sodium hydroxide (NaOH) were used as pH regulators and methyl isobutyl carbinol (MIBC) was used as frother. All reagents were analytical pure except for SA which was food grade. Deionized water was used throughout this study.

Micro-Flotation Tests

All the flotation tests were conducted in an XFG-1600-type laboratory flotation machine. For single-mineral flotation tests, 2.0 g pure mineral sample was first placed in a beaker of 50-ml capacity together with 30 ml deionized water. Ultrasonic cleaning of 5 min was applied to the suspension to remove the oxidized substances on the mineral surface, after which the supernatant was decanted and the mineral particles were washed into a plexiglass flotation cell of 40-ml capacity with proper amount of deionized water. The pulp was stirred for 1 min at 1,902 rpm to ensure thorough mixing, after which the pH regulators, depressant (if needed), collector, and frother were sequentially

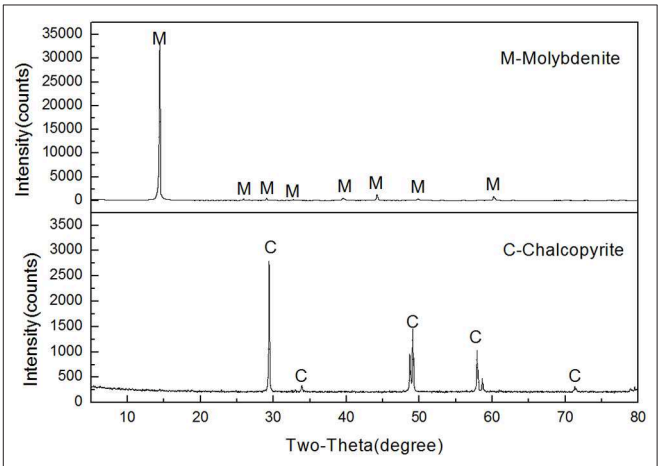

FIGURE 2 | X-ray diffraction (XRD) spectra of the chalcopyrite and molybdenite samples.

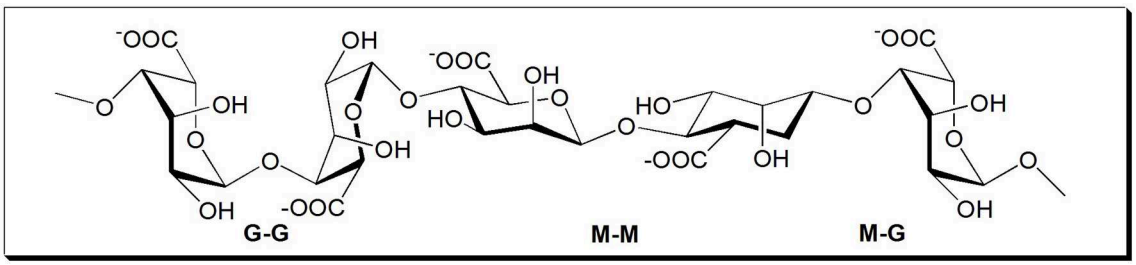

FIGURE 1 | Molecular structure of sodium alginate (SA).

added into the suspension. The pulp was conditioned for 3 min after each addition except for the frother (1 min). Flotation was conducted for a total period of 3 min for each test. After flotation, the concentrates (froth product) and tailings (in-tank product) were collected, filtered, dried and weighed. The recovery was calculated based on the weight distribution of mineral particles between the two products. Each single-mineral flotation test was repeated at least three times. The average values were reported in this study. Standard deviations were also calculated and presented as error bars.

For the mixed binary minerals flotation tests, the mass ratio of chalcopyrite and molybdenite was 2:1 (2.0 g chalcopyrite + 1.0 g molybdenite). The flotation procedures are similar to those used for the single-mineral flotation tests except that two different reagent addition sequences were tested, namely, kerosene prior to SA and SA prior to kerosene. The concentrates and tailings were assayed for Cu and Mo. The recovery of molybdenite and chalcopyrite was calculated based on the grades of Cu and Mo in the concentrates and tailings.

Adsorption Measurements

The adsorption of SA on both the original and Cu^{2+}-treated molybdenite was measured as a function of pH using a TOC-L machine supplied by Shimadzu, Kyoto, Japan. The detailed experimental procedures are as follows. First, 2.0 g of mineral samples were added to 40-ml aqueous solutions in the presence or absence of 15 mg/L Cu^{2+} followed by 30 min of conditioning. Then, the obtained suspensions were adjusted to the desired pH by adding hydrochloric acid and/or sodium hydroxide solutions, after which 40 mg/L SA was added into the suspensions followed by another 30 min of conditioning. The resultant suspensions were filtered, and subsequently the filtrate was centrifuged to remove residual particles under 9,000 rpm for 10 min. Finally, 15 ml supernatant of the centrifuged filtrate was collected for measuring the total organic carbon (TOC) concentration. The adsorption efficiency (ε) was calculated by the following equation:

$$\varepsilon = \frac{T_0 - T_1}{T_0} \times 100\%$$

where T_0 represents the TOC concentration of freshly prepared SA solution of 40 mg/L; T_1 means the TOC concentration of the supernatant obtained from the adsorption tests.

Zeta Potential Measurements

Zeta potentials of the molybdenite and chalcopyrite particles were measured using a JS94H micro electrophoresis instrument (Shanghai Zhongchen Digital Technic Apparatus Co., Shanghai, China) under the room temperature of 25°C. KNO_3 solution of 1×10^{-3} mol/L was used as a supporting electrolyte. For each measurement, 20 mg pure mineral (−2 μm) was dispersed in 40 ml of the electrolyte, and the suspension was magnetically stirred for 2 min after pH adjustment. Then, flotation reagents of desired dosages were added per the abovementioned reagent schemes. After standing for 5 min, the supernatant was collected for zeta potential measurement. The measurement under each reagent condition was conducted at least three times, and the average values were accepted as the final results.

FTIR Spectroscopy Analyses

FTIR analyses in this study were performed using a 740FT-IR instrument (Nicolet Co., MA, USA) with the diffuse reflection approach (30 scans, resolution 2 cm^{-1}) under room temperature. Spectra were collected in the absorption band range of 400 to 4,000 cm^{-1}. Tested samples were prepared by adding 1.0 g pure mineral particles (−2 μm) into 40 ml deionized water with a desired reagent scheme at pH 5.4. After conditioning for 30 min, the suspension was filtered and the filter cake was washed with deionized water of pH 5.4 for three times. Then, the filter cake was dried in a vacuum oven at 30°C. After the moisture got completely evaporated, the dry solid of 1 mg was mixed with 100 mg spectroscopic grade potassium bromide (KBr), and the mixture was used for the analysis.

RESULTS AND DISCUSSIONS

Micro-Flotation Results

Single-Mineral Flotation Experiment Results

Figure 3 shows the effect of SA dosage on the flotation performance of molybdenite and chalcopyrite when using 2 mg/L kerosene as collector at pH around 5.4. It can be seen from the figure that chalcopyrite recovery was <5% when the dosage of SA exceeded 40 mg/L. Interestingly, high recoveries (nearly 90%) of molybdenite were maintained over the investigated SA dosage, indicating that SA imposed a minimal effect on the floatability of molybdenite. Therefore, the efficient separation of molybdenite from chalcopyrite is likely to be achieved by using SA and kerosene as depressant and collector, respectively.

The flotation recoveries of molybdenite and chalcopyrite as a function of pH in the absence and presence of SA are shown in **Figure 4**. The recovery of molybdenite changed slightly at the entire pH range with the addition of 40 mg/L SA, suggesting that SA barely influenced the molybdenite floatability. However, the recovery of chalcopyrite dropped significantly at pH 3–9 when

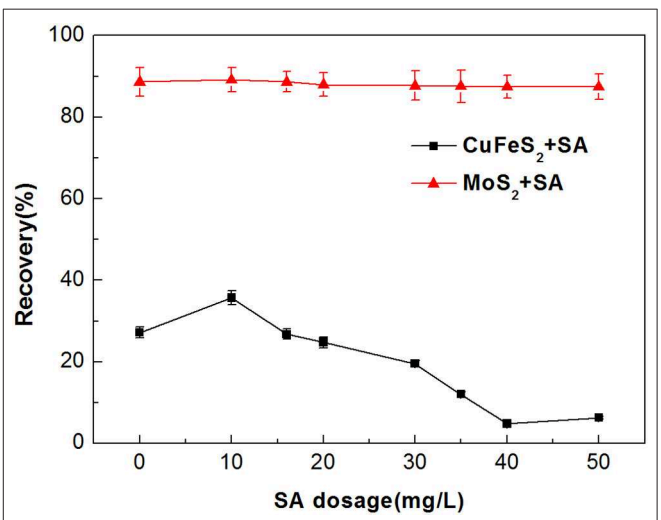

FIGURE 3 | Flotation recovery of chalcopyrite and molybdenite as a function of sodium alginate (SA) dosage (2 mg/L kerosene and pH 5.4).

40 mg/L SA was added. Therefore, the optimum pH range for the separation of molybdenite from chalcopyrite was 3–9.

Mixed-Mineral Micro-Flotation Results

The aforementioned single-mineral flotation test results indicated that the efficient separation of molybdenite from chalcopyrite could be achieved by using SA as an inhibitor in the pH range of 3–9. When different minerals simultaneously appear in a solution, surface properties of the minerals can be greatly impacted by each other, resulting in changes in their affinities toward reagents (Jin et al., 2018; Tian et al., 2018). This can potentially reduce the selectivity of flotation reagents (Liu et al., 2016; Bicak et al., 2018; Feng et al., 2018). Therefore, flotation tests of mixed minerals (chalcopyrite plus molybdenite) were conducted to further investigate the selective inhibition performance of SA. The flotation results of a mixed-mineral system (the mass ratio of chalcopyrite to molybdenite equals 2:1) in the presence of 40 mg/L SA under pH 5.4 are presented in **Table 1**.

When SA was added prior to kerosene of 2 mg/L and 19 mg/L, the concentrate Cu grades were 21.64 and 20.24%, respectively, indicating a weak selectivity of SA in the mixed-mineral system. Meanwhile, the recovery of Mo in tailing were 64.03% for 2 mg/L kerosene and 40.17% for 19 mg/L kerosene. Therefore, SA showed an inhibitory effect on molybdenite in the presence of chalcopyrite.

In order to eliminate the adverse effect of chalcopyrite on the flotation performance of SA, the effect of reagent scheme on the flotation results of chalcopyrite–molybdenite mixed systems was investigated. As shown in **Table 1**, a concentrate with Mo grade of 53.43% and recovery of 76.90% was acquired when kerosene was added before SA. This indicated that the addition of kerosene prior to SA could eliminate the adverse effect of chalcopyrite on the depressing effect of SA on molybdenite. Wie and Fuerstenau (1974) reported that adsorption of dextrin was reduced when molybdenite was coated with a layer of non-polar oil. This agrees with the findings from this study.

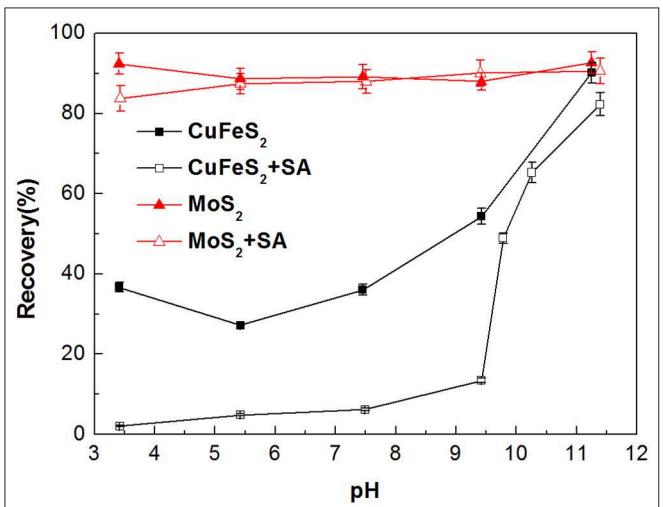

FIGURE 4 | Flotation recovery of chalcopyrite and molybdenite as a function of pH with and without sodium alginate (SA) (40 mg/L SA and 2 mg/L kerosene).

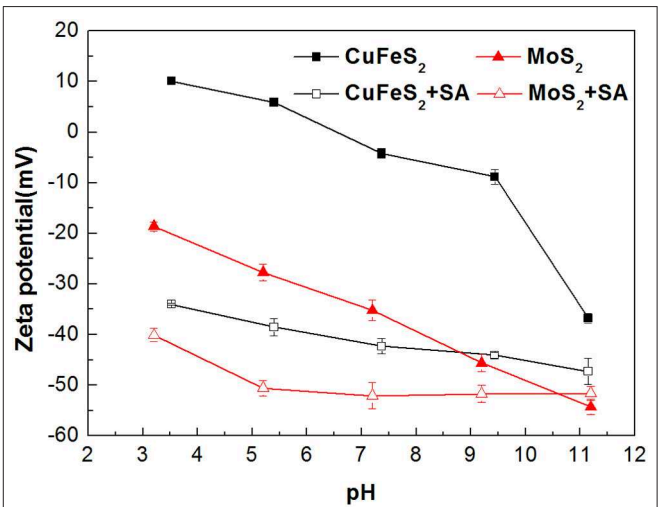

FIGURE 5 | The zeta potentials of chalcopyrite and molybdenite before and after conditioning with sodium alginate (SA) at varied pH (40 mg/L SA and 2 mg/L kerosene).

TABLE 1 | The separation of chalcopyrite and molybdenite mixture [40 mg/L sodium alginate (SA) and pH 5.4].

Test conditions		Products	Cu grade/%	Mo grade/%	Cu recovery/%	Mo recovery/%
SA prior to kerosene	Kerosene dosage: 2 mg/L	Concentrate	21.64	28.98	23.42	35.97
		Tailing	22.02	16.05	76.58	64.03
		Feed	21.93	19.12	100	100
	Kerosene dosage: 19 mg/L	Concentrate	20.24	29.13	36.52	59.83
		Tailing	23.32	12.96	63.48	40.17
		Feed	22.10	19.40	100.00	100.00
kerosene prior to SA	Kerosene dosage: 19 mg/L	Concentrate	4.55	53.43	5.78	76.90
		Tailing	29.08	6.29	94.22	23.10
		Feed	22.17	19.57	100.00	100.00

Zeta Potential Measurement Results

Zeta potentials of chalcopyrite and molybdenite as a function of pH are presented in **Figure 5**. It can be observed that remarkable negative shifts occurred in the zeta potentials of chalcopyrite and molybdenite when SA was added alone. Moreover, the shift for chalcopyrite was larger than the molybdenite, suggesting that SA adsorbed more strongly on the chalcopyrite surface relative to the molybdenite at the tested pH range. This can be explained by the fact that more negative charges occur on the molybdenite surface relative to chalcopyrite (Reyes-Bozo et al., 2015; Castro et al., 2016; Han et al., 2019; Yang et al., 2019), resulting in a stronger electrostatic repulsion between molybdenite and SA (anionic agents). Moreover, metal cations dissolved from the chalcopyrite surface could also contribute to the higher adsorption of SA (Ikumapayi et al., 2012). It is noteworthy that when pH exceeded 9.5, the zeta potential difference of raw and SA-conditioned chalcopyrite decreased, which corresponded to the steep rise of chalcopyrite recovery (**Figure 4**).

Fourier-Transform Infrared Spectra

Figure 6 presents the FTIR spectra of chalcopyrite and molybdenite before and after treatment with 40 mg/L SA at pH 5.4. The peaks at 1,609 and 1,424 cm^{-1} of the SA spectrum shown in **Figure 6A** were due to the stretching bands of -COO- (Rath et al., 2000; Chen et al., 2017, 2018), and the peak at 1,026 cm^{-1} originated from the stretching vibration of C-O-C. As shown in **Figure 6B**, after conditioning with SA, new peaks at 1,697 and 1,465 cm^{-1} occurred in the spectrum of chalcopyrite, which were shifted significantly compared to the corresponding peaks that present in the spectrum of SA (i.e., 1,609 and 1,424 cm^{-1}). This proved that SA was chemically adsorbed on chalcopyrite surfaces and probably in the form of SA–Cu chelate, which has been reported in prior studies (Zhu et al., 2003; Liu et al., 2008). It is interesting to note that the spectrum of molybdenite treated by SA was barely changed relative to the raw specimen. Therefore, the adsorption of SA on molybdenite was negligible.

Interaction Mechanisms of Chalcopyrite on the Sodium Alginate Performance in Molybdenite Flotation

The Effect of Sodium Alginate on the Flotation of Cu^{2+}-Treated Molybdenite

Metal ions dissolved from minerals may impose an adverse impact on the selectivity of flotation collector and depressant (Zhang et al., 2017; Zhang and Honaker, 2018). Dissolution of Cu^{2+} from the chalcopyrite surface is inevitable in the flotation separation of molybdenite from chalcopyrite (Zhao et al., 2018; Yang et al., 2019). Therefore, the effect of Cu^{2+} on the flotation performance of molybdenite was evaluated in the presence and absence of SA at pH around 5.4. As shown in **Figure 7**, when Cu^{2+} concentration varied from 0 to 25 mg/L, the recovery of molybdenite decreased significantly in the presence of 40 mg/L

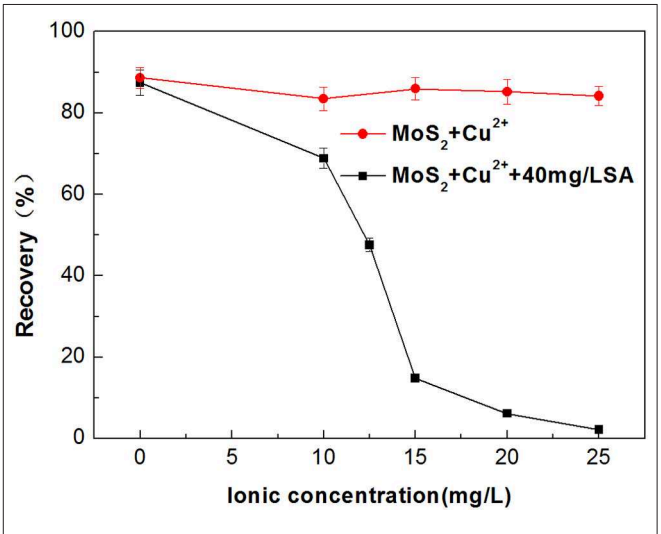

FIGURE 7 | Flotation recovery of molybdenite with and without 40 mg/L sodium alginate (SA) as a function of Cu^{2+} initial concentration at pH 5.4.

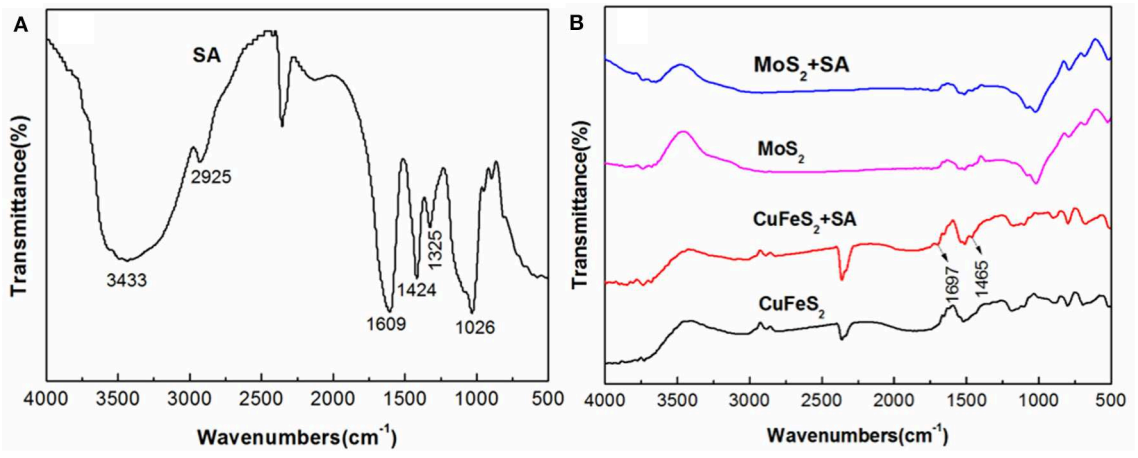

FIGURE 6 | Fourier-transform infrared spectroscopy (FTIR) spectra of **(A)** sodium alginate (SA), **(B)** chalcopyrite and molybdenite (the SA treatment was performed by conditioning with 40 mg/L SA at pH 5.4).

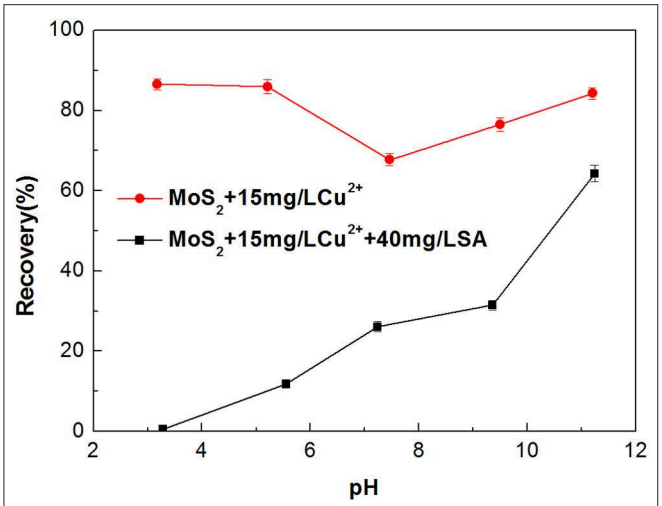

FIGURE 8 | Flotation recovery of molybdenite with and without 40 mg/L sodium alginate (SA) as a function of pH in the presence of 15 mg/L Cu^{2+}.

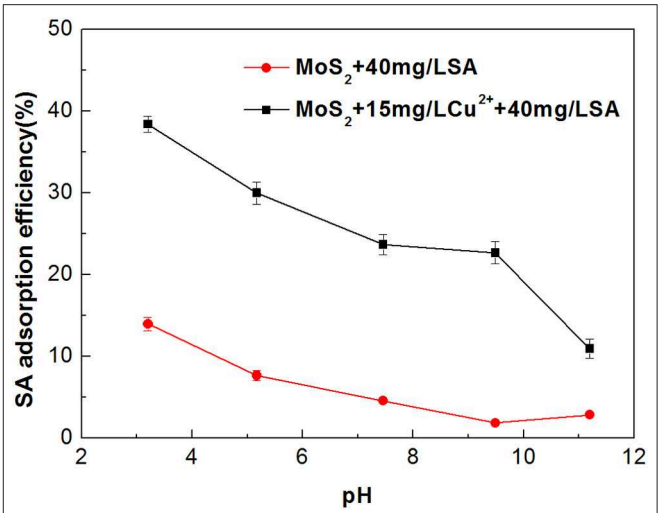

FIGURE 9 | Adsorption efficiency of sodium alginate (SA) on molybdenite surfaces with and without 15 mg/L Cu^{2+} as a function of pH.

SA. Furthermore, the depressing effect of SA on molybdenite flotation was largely dependent on pH, and stronger inhibition occurred under acidic conditions (**Figure 8**).

Adsorption Characteristics of Sodium Alginate on Cu^{2+}-Treated Molybdenite

The impact of Cu^{2+} on the adsorption characteristics of SA on the molybdenite surfaces is shown in **Figure 9**. In the absence of Cu^{2+}, much stronger adsorption occurred at relatively low pH, which can be explained by the formation of alginic acid that is insoluble under acidic conditions (Wang, 2007). When Cu^{2+} was added, the adsorption of SA on the molybdenite surface was increased significantly throughout the studied pH range. This is likely due to the increased amount of adsorption sites on the molybdenite surface provided by Cu species (Yang et al., 2019).

Zeta Potentials of Cu^{2+}-Treated Molybdenite With and Without Sodium Alginate

Zeta potentials of molybdenite in the presence and absence of Cu^{2+} with 40 mg/L SA were measured at different pH, and the results are presented in **Figure 10**. In the whole tested pH range, the raw molybdenite particles carried negative charges, and the zeta potential gradually decreased with the increase in pH, which agreed well with prior studies (Zhao et al., 2018). When the particles were dispersed in Cu^{2+} solution of 15 mg/L, the zeta potential of molybdenite increased and the trend curve was similar to that of Yang et al. (2019). According to their study, at pH lower than 5.4, the slightly positive shift of the molybdenite surface potential was due to a small amount of Cu^{2+} and $Cu(OH)^{+}$ being adsorbed on the molybdenite surface which offset the partially negative charge. The sharp rise in the range of pH 5.4 to 9.5 was due to an increased amount of cupric species adsorbed and/or precipitated on the molybdenite surface. When 40 mg/L SA together with 15 mg/L Cu^{2+} appeared in the solution, the zeta potential of molybdenite was decreased, which likely resulted from the adsorption of negatively charged alginate ions (Wang and Yang, 2014). Meanwhile, as the pH increased,

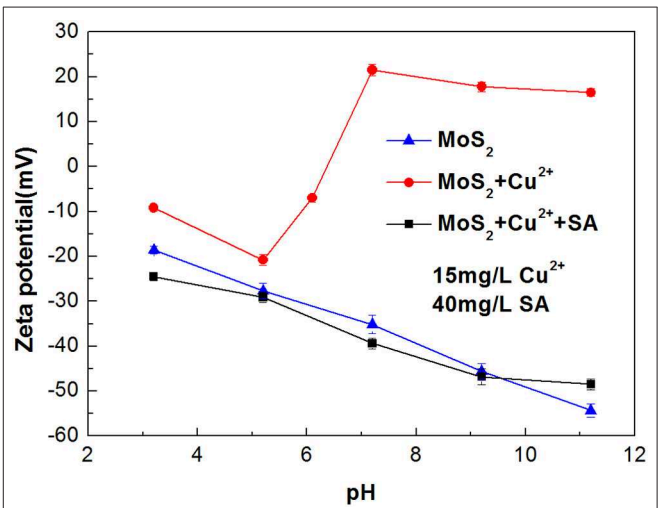

FIGURE 10 | Zeta potentials of molybdenite at varied pH.

chelation between SA and cupric species in the solution was also promoted (Zhu et al., 2003), which partially led to the reduction of SA adsorption on molybdenite surfaces (**Figure 7**). At pH higher than 9.5, $Cu(OH)_{2(s)}$ was dominant Cu species and the amount of $Cu(OH)_3^-$ and $Cu(OH)_4^{2-}$ also gradually increased. As a result, the depressing effect of SA on molybdenite was further weakened due to enhanced electrostatic repulsion.

Fourier-Transform Infrared Spectroscopy Spectra of Cu^{2+}-Treated Molybdenite With and Without Sodium Alginate

In order to further study the effect of Cu^{2+} on the depressing effect of SA on molybdenite, the IR spectra of molybdenite treated by Cu^{2+}, Cu^{2+} + SA were measured and the results are presented in **Figure 11**. For molybdenite treated by Cu^{2+} and SA, new absorption bands at 1,612, 1,562, and 1,425 cm^{-1} were observed

and the new bands corresponded to the stretching vibration of -COO- in SA, indicating the adsorption of SA on the molybdenite surface. The remarkable shift of the absorption band of -COO- from 1,609 to 1,562 cm^{-1} demonstrated that partial chemical adsorption of SA occurred on the molybdenite surface.

Based on the results of the flotation tests and mechanism studies, a possible adsorption model was proposed to explain the depressing effect of chalcopyrite on the molybdenite flotation in the presence of SA at pH 5.4 (**Figure 12**). At pH 5.4, Cu ions occurring as Cu^{2+} and $Cu(OH)^{+}$ adsorbed on the molybdenite surface. Meanwhile, SA existed in the form of alginic acid (a little) and alginate ions (dominantly), and the adsorption of SA on the molybdenite surface occurred by chelating with Cu species *via* the -COO- and -OH. The electrostatic attraction between the negative group -COO- and the Cu species also contributed to the adsorption of SA. The promotion of SA adsorption by Cu^{2+} resulted in the depression of molybdenite flotation.

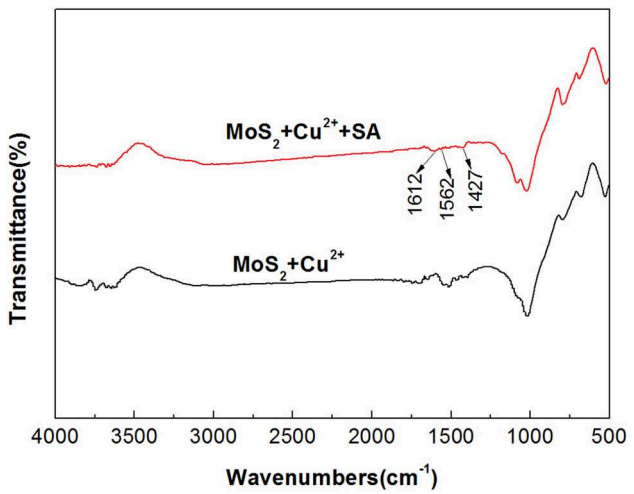

FIGURE 11 | Fourier-transform infrared spectroscopy (FTIR) spectra of molybdenite with and without treatment of 40 mg/L sodium alginate (SA) in the presence of 15 mg/L Cu^{2+} at pH 5.4.

CONCLUSIONS

In this paper, interaction mechanisms of SA in the flotation separation of molybdenite from chalcopyrite were evaluated by micro-flotation tests, adsorption measurements, zeta potential measurements, and FTIR spectrum analyses. Single-mineral flotation tests showed that selective flotation separation of chalcopyrite and molybdenite could be achieved using SA as a depressant for the chalcopyrite. However, in the chalcopyrite–molybdenite mixed-mineral flotation system, the presence of chalcopyrite significantly increased the depressing effect of SA on the molybdenite floatability, reducing the selectivity of the separation. It is interesting to note that the addition of a certain dosage of kerosene prior to SA could restore the molybdenite floatability in the mixed-mineral flotation system. Given the findings of the adsorption tests, zeta potential measurements, and FTIR analyses, it was concluded that SA chemically adsorbed on the surface of chalcopyrite, thus causing a considerable decrease in its floatability. Moreover, strong adsorption of SA on the Cu^{2+}-treated molybdenite surfaces also occurred in forms of electrostatic attraction and chelation. Therefore, the negative impact of SA on molybdenite flotation in the mixed-mineral system was due to the dissolution of Cu ions from the chalcopyrite surfaces which re-adsorbed onto the molybdenite surfaces and played as active sites for SA adsorption.

DATA AVAILABILITY STATEMENT

All datasets generated for this study are included in the article/supplementary material.

AUTHOR CONTRIBUTIONS

GZ and LO conceived the research, designed the tests, and analyzed the data. GZ, WZ, and YZ wrote and revised the manuscript.

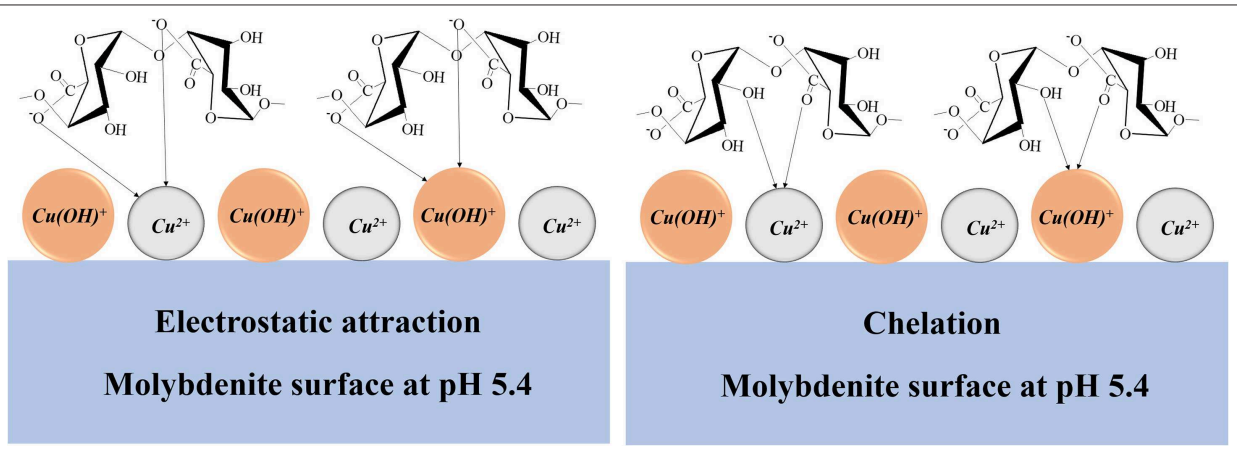

FIGURE 12 | Schematic diagram of influence mechanism of chalcopyrite on the performance of sodium alginate (SA) in molybdenite flotation at pH 5.4.

FUNDING

This work was financially supported by the Fundamental Research Funds for the Central Universities of Central South University (No. 2018zzts075) and the Key Laboratory of Hunan Province for Clean and Efficient Utilization of Strategic Calcium-containing Mineral Resources (No. 2018TP1002).

REFERENCES

Ansari, A., and Pawlik, M. (2007). Floatability of chalcopyrite and molybdenite in the presence of lignosulfonates. Part II. Hallimond tube flotation. *Miner. Eng.* 20, 609–616. doi: 10.1016/j.mineng.2006.12.008

Bicak, O., Ozturk, Y., Ozdemir, E., and Ekmekci, Z. (2018). Modelling effects of dissolved ions in process water on flotation performance. *Miner. Eng.* 128, 84–91. doi: 10.1016/j.mineng.2018.08.031

Castro, S., Lopez-Valdivieso, A., and Laskowski, J. S. (2016). Review of the flotation of molybdenite. Part I: Surface properties and floatability. *Int. J. Miner. Process.* 148, 48–58. doi: 10.1016/j.minpro.2016.01.003

Chen, W., Chen, T., Bu, X., Chen, F., Ding, Y., Zhang, C., et al. (2019). The selective flotation of chalcopyrite against galena using alginate as a depressant. *Miner. Eng.* 141:105848. doi: 10.1016/j.mineng.2019.105848

Chen, W., Feng, Q., Zhang, G., Yang, Q., and Zhang, C. (2017). The effect of sodium alginate on the flotation separation of scheelite from calcite and fluorite. *Miner. Eng.* 113, 1–7. doi: 10.1016/j.mineng.2017.07.016

Chen, Z., Gu, G., Li, S., Wang, C., and Zhu, R. (2018). The effect of seaweed glue in the separation of copper–molybdenum sulphide ore by flotation. *Minerals* 8, 1–15. doi: 10.3390/min8020041

Feng, Q., Wen, S., Zhao, W., and Chen, Y. (2018). Effect of calcium ions on adsorption of sodium oleate onto cassiterite and quartz surfaces and implications for their flotation separation. *Sep. Purif. Technol.* 200, 300–306. doi: 10.1016/j.seppur.2018.02.048

Han, G., Wen, S., Wang, H., and Feng, Q. (2019). Effect of starch on surface properties of pyrite and chalcopyrite and its response to flotation separation at low alkalinity. *Miner. Eng.* 143:106015. doi: 10.1016/j.mineng.2019.106015

Hirajima, T., Mori, M., Ichikawa, O., Sasaki, K., Miki, H., Farahat, M., et al. (2014). Selective flotation of chalcopyrite and molybdenite with plasma pre-treatment. *Miner. Eng.* 66, 102–111. doi: 10.1016/j.mineng.2014.07.011

Hu, Y., Mao, A. S., Desai, R. M., Wang, H., Weitz, D. A., and Mooney, D. J. (2017). Controlled self-assembly of alginate microgels by rapidly binding molecule pairs. *Lab Chip* 17, 2481–2490. doi: 10.1039/C7LC00500H

Ikumapayi, F., Makitalo, M., Johansson, B., and Rao, K. H. (2012). Recycling of process water in sulphide flotation: effect of calcium and sulphate ions on flotation of galena. *Miner. Eng.* 39, 77–88. doi: 10.1016/j.mineng.2012.07.016

Jin, S., Shi, Q., Li, Q., Ou, L., and Ouyang, K. (2018). Effect of calcium ionic concentrations on the adsorption of carboxymethyl cellulose onto talc surface: flotation, adsorption and AFM imaging study. *Powder Technol.* 331, 155–161. doi: 10.1016/j.powtec.2018.03.014

Li, Q., Lan, H., and Zhao, Z. (2019). Protection effect of sodium alginate against heat-induced structural changes of lactoferrin molecules at neutral pH. *Lwt* 99, 513–518. doi: 10.1016/j.lwt.2018.10.019

Lin, Y. H., Liang, H. F., Chung, C. K., Chen, M. C., and Sung, H. W. (2005). Physically crosslinked alginate/N,O-carboxymethyl chitosan hydrogels with calcium for oral delivery of protein drugs. *Biomaterials* 26, 2105–2113. doi: 10.1016/j.biomaterials.2004.06.011

Liu, C., Feng, Q., Zhang, G., Ma, W., Meng, Q., and Chen, Y. (2016). Effects of lead ions on the flotation of hemimorphite using sodium oleate. *Miner. Eng.* 89, 163–167. doi: 10.1016/j.mineng.2016.02.002

Liu, X., Yu, W., Wang, W., Xiong, Y., Ma, X., and Yuan, Q. (2008). Polyelectrolyte microcapsules prepared by alginate and chitosan for biomedical application. *Prog. Chem.* 20, 126–139.

Mehrabani, J. V., Mousavi, S. M., and Noaparast, M. (2011). Evaluation of the replacement of NaCN with Acidithiobacillus ferrooxidans in the flotation of high-pyrite, low-grade lead-zinc ore. *Sep. Purif. Technol.* 80, 202–208. doi: 10.1016/j.seppur.2011.04.006

Pawar, S. N., and Edgar, K. J. (2012). Alginate derivatization: a review of chemistry, properties and applications Siddhesh. *Biomaterials* 33, 3279–3305. doi: 10.1016/j.biomaterials.2012.01.007

Pearse, M. J. (2005). An overview of the use of chemical reagents in mineral processing. *Miner. Eng.* 18, 139–149. doi: 10.1016/j.mineng.2004.09.015

Rath, R. K., Subramanian, S., and Pradeep, T. (2000). Surface chemical studies on pyrite in the presence of polysaccharide-based flotation depressants. *J. Colloid Interface Sci.* 229, 82–91. doi: 10.1006/jcis.2000.6990

Reyes-Bozo, L., Escudey, M., Vyhmeister, E., Higueras, P., Godoy-Faúndez, A., Salazar, J. L., et al. (2015). Adsorption of biosolids and their main components on chalcopyrite, molybdenite and pyrite: Zeta potential and FTIR spectroscopy studies. *Miner. Eng.* 78, 128–135. doi: 10.1016/j.mineng.2015.04.021

Song, S., Zhang, X., Yang, B., and Lopez-Mendoza, A. (2012). Flotation of molybdenite fines as hydrophobic agglomerates. *Sep. Purif. Technol.* 98, 451–455. doi: 10.1016/j.seppur.2012.06.016

Su, C. H., Kumar, G. V., Adhikary, S., Velusamy, P., Pandian, K., and Anbu, P. (2017). Preparation of cotton fabric using sodium alginate-coated nanoparticles to protect against nosocomial pathogens. *Biochem. Eng. J.* 117, 28–35. doi: 10.1016/j.bej.2016.10.020

Suyantara, G. P. W., Hirajima, T., Miki, H., Sasaki, K., Yamane, M., Takida, E., et al. (2018). Selective flotation of chalcopyrite and molybdenite using H2O2 oxidation method with the addition of ferrous sulfate. *Miner. Eng.* 122, 312–326. doi: 10.1016/j.mineng.2018.02.005

Tian, M., Liu, R., Gao, Z., Chen, P., Han, H., Wang, L., et al. (2018). Activation mechanism of Fe (III) ions in cassiterite flotation with benzohydroxamic acid collector. *Miner. Eng.* 119, 31–37. doi: 10.1016/j.mineng.2018.01.011

Wang, B., and Peng, Y. (2014). The effect of saline water on mineral flotation - A critical review. *Miner. Eng.* 66, 13–24. doi: 10.1016/j.mineng.2014.04.017

Wang, X. (2007). Extraction and application of sodium alginate. *J. Chongqing Inst. Technol. Sci. Ed.* 21, 124–128. doi: 10.3969/j.issn.1674-8425-B.2007.05.032

Wang, Z., and Yang, H. (2014). Impact of pH values on viscosity of sodium alginate solution and hydrogen bonds in the system. *Mater. Rep.* 33, 1289–1292.

Wie, J. M., and Fuerstenau, D. W. (1974). The effect of dextrin on surface properties and the flotation of molybdenite. *Int. J. Miner. Process.* 1, 17–32. doi: 10.1016/0301-7516(74)90024-6

Yang, B., Wang, D., Wang, T., Zhang, H., Jia, F., and Song, S. (2019). Effect of Cu2+ and Fe3+ on the depression of molybdenite in flotation. *Miner. Eng.* 130, 101–109. doi: 10.1016/j.mineng.2018.10.012

Yin, W. Z., Zhang, L. R., and Xie, F. (2010). Flotation of Xinhua molybdenite using sodium sulfide as modifier. *Trans. Nonferrous Met. Soc.* 20, 702–706. doi: 10.1016/S1003-6326(09)60201-6

Yin, Z., Sun, W., Hu, Y., Zhang, C., Guan, Q., Liu, R., et al. (2017). Utilization of acetic acid-[(hydrazinylthioxomethyl)thio]-sodium as a novel selective depressant for chalcopyrite in the flotation separation of molybdenite. *Sep. Purif. Technol.* 179, 248–256. doi: 10.1016/j.seppur.2017.01.049

Yu, C., Wang, M., Dong, X., Shi, Z., Zhang, X., and Lin, Q. (2017). Removal of Cu(II) from aqueous solution using Fe3O4-alginate modified biochar microspheres. *RSC Adv.* 7, 53135–53144. doi: 10.1039/C7RA10185F

Yuan, D., Cadien, K., Liu, Q., and Zeng, H. (2019a). Selective separation of copper-molybdenum sulfides using humic acids. *Miner. Eng.* 133, 43–46. doi: 10.1016/j.mineng.2019.01.005

Yuan, D., Cadien, K., Liu, Q., and Zeng, H. (2019b). Adsorption characteristics and mechanisms of O-Carboxymethyl chitosan on chalcopyrite and molybdenite. *J. Colloid Interface Sci.* 552, 659–670. doi: 10.1016/j.jcis.2019.05.023

Zhang, W., and Honaker, R. Q. (2018). Flotation of monazite in the presence of calcite part II: Enhanced separation performance using sodium silicate and EDTA. *Miner. Eng.* 127, 318–328. doi: 10.1016/j.mineng.2018.01.042

Zhang, W., Honaker, R. Q., and Groppo, J. G. (2017). Flotation of monazite in the presence of calcite part I: Calcium ion effects on the adsorption of hydroxamic acid. *Miner. Eng.* 100, 40–48. doi: 10.1016/j.mineng.2016.09.020

Zhao, Q., Wengang, L., Wei, D., Wang, W., Cui, B., and Wenbao, L. (2018). Effect of copper ions on the flotation separation of chalcopyrite and molybdenite using sodium sulfide as a depressant. *Miner. Eng.* 115, 44–52. doi: 10.1016/j.mineng.2017.10.008

Zhu, Y., Shen, Y., Wei, D., (2003). Adsorption of sodium alginate to copper ion in disposal water. *J. Northeast. Univ. Sci.* 24, 589–592.

Conflict of Interest: The authors declare that the research was conducted in the absence of any commercial or financial relationships that could be construed as a potential conflict of interest.

frontiers in Materials

ORIGINAL RESEARCH
published: 17 June 2020
doi: 10.3389/fmats.2020.00176

Effect of Grinding Media on Grinding-Flotation Behavior of Chalcopyrite and Pyrite

Ningning Liao[1], *Caibin Wu*[1,2]*, *Jindong Xu*[1], *Bo Feng*[1,2], *Ji Wu*[1] *and Yuan Gong*[1]

[1] College of Resources and Environmental Engineering, Jiangxi University of Science and Technology, Ganzhou, China,
[2] Jiangxi Key Laboratory of Mining Engineering, Jiangxi University of Science and Technology, Ganzhou, China

Grinding media have significant influence on the flotation of chalcopyrite and pyrite. This effect is mainly related to the change in the surface properties of chalcopyrite and pyrite. This paper investigates the influence of steel ball and nano-ceramic ball grinding on the floatability of chalcopyrite and pyrite. Flotation results, as well-scanning electron microscopy (SEM), X-ray photoelectron spectroscopy (XPS), ultraviolet spectrophotometer, and zeta potential measurement results indicate that nano-ceramic ball grinding is beneficial to the flotation of chalcopyrite. Flotation results also indicate that chalcopyrite has better floatability after nano-ceramic ball grinding compared with steel ball grinding. Results of adsorption experiments show that nano-ceramic ball grinding contributes to the adsorption of isobutyl xanthate to chalcopyrite. XPS and SEM techniques demonstrated that steel ball grinding easily produces oxidation species at the surface of chalcopyrite, thereby reducing its floatability. Results from this study also confirmed that steel ball grinding is beneficial to the flotation of pyrite. Therefore, nano-ceramic media grinding produces better selective flotation in chalcopyrite than steel media grinding.

Keywords: chalcopyrite, pyrite, nano-ceramic ball, steel ball, grinding, flotation

OPEN ACCESS

Edited by:
Zhiyong Gao,
Central South University, China

Reviewed by:
Yin Wanzhong,
Northeastern University, China
Haiyun Xie,
Kunming University of Science and Technology, China

***Correspondence:**
Caibin Wu
caibin.wu@jxust.edu.cn

Specialty section:
This article was submitted to Colloidal Materials and Interfaces, a section of the journal Frontiers in Materials

Received: *23 October 2019*
Accepted: *13 May 2020*
Published: *17 June 2020*

Citation:
Liao N, Wu C, Xu J, Feng B, Wu J and Gong Y (2020) Effect of Grinding Media on Grinding-Flotation Behavior of Chalcopyrite and Pyrite. Front. Mater. 7:176. doi: 10.3389/fmats.2020.00176

INTRODUCTION

Grinding operation is an essential process in a mineral processing plant. The primary purpose of grinding is to achieve monomer dissociation between useful minerals, gangue minerals, and other minerals. Grinding also provides the right-sized raw materials for the downstream sorting process. The grinding process is affected by different factors, such as ore characteristics, grinding media, and grinding concentration. Moreover, grinding media have important effect on subsequent flotation operations by changing the grinding pulp environment (Martin et al., 1991; Palm et al., 2010, 2011; Li and Gao, 2017, 2018; Corin et al., 2018; Feng et al., 2019), particularly the pulp chemistry and surface properties of minerals in the flotation. The effect of the grinding media on flotation is mostly determined using three parameters, namely dissolved oxygen concentration, slurry potential, and galvanic interaction between the medium and the mineral (Erdemoglu and Sarikaya, 2002; Gonçalves et al., 2003; Peng and Grano, 2010a,b). The electrochemical standard potentials interaction between sulfide minerals and grinding media during the grinding processing. The grinding media act as the anode, whereas the mineral acts as the cathode (Gonçalves et al., 2003). Steel media generate hydrophilic products on mineral surfaces, reduce the natural floatability of minerals, and also affect the adsorption of collectors at the surface of mineral (Heyes and Trahar, 1979; Greet et al., 2004; Huang and Grano, 2006; Bruckard et al., 2011; Feng et al., 2020).

Studies have shown that the grinding media can affect the flotation of chalcopyrite and pyrite. Galvanic interaction between the steel media and chalcopyrite forms iron hydroxide species at the surface of the chalcopyrite, which affects the adsorption of collectors and reduces the floatability of the chalcopyrite (Forssberg et al., 1988; Rao and Natarajan, 1988). However, it has been reported that mild steel grinding is beneficial to the flotation of pyrite (Learmont and Iwasaki, 1984). A possible explanation is that the collector produced dixanthogen at the surface of the pyrite (Woods, 1976). Another reason is that galvanic interaction between the iron medium and the mineral surface generated elemental sulfur at the surface of the pyrite (Rao et al., 1976). Yuan et al. (1996) and Van Deventer et al. (1991) found that chalcopyrite separation from pyrite has no advantage in strong oxidizing stainless media grinding environment but was restored in a mild steel medium reducing environment. Peng et al. (2003a) and Peng et al. (2003b) found that chalcopyrite separation from pyrite in a chromium medium grinding environment is better than in a mild steel medium. Stainless media or inert media (ceramic media, SAG pebble) are more beneficial to chalcopyrite flotation. Inert medium grinding can improve the pulp environment and flotation recovery of chalcopyrite (Forssberg et al., 1988; Ahn and Gebhardt, 1991; Martin et al., 1991; Guo et al., 2019). As compared with steel balls used as grinding media, SAG pebble is beneficial to improve the recovery rate of copper ore (Shi and Zhou, 2019; Wu et al., 2019). The flotation performance of calcite after ceramic ball grinding is better than that that of steel ball grinding (Yao et al., 2019). Zhang et al. have also compared the flotation kinetics of pyrite with nano-ceramic balls and cast iron balls (Zhang et al., 2019). Nano-ceramic balls, which were invented and patented by Jingdezhen Betterwear New Material Co, Ltd, Jiangxi Province, China (Zhang et al., 2013). Nano-ceramic balls were made of nano-scale alumina powder and other minerals. In our past research, nano-ceramic balls as a fine grinding media can improve the grade and recovery of copper concentrate of copper sulfur ore and have achieved good industrial applications in Yinshan Mining Concentrator of Jiangxi Copper Corporation, China. Nano-ceramic balls as new grinding media have light density, good wear resistance, no iron pollution of pulp and other characteristics (Liao et al., 2019).

However, the surface of ground chalcopyrite, pyrite and the flotation products, as well as the effect of the medium on adsorption of collectors to minerals have not been clearly clarified in nano-ceramic grinding media. This study investigated the effects of nano-ceramic ball and steel ball grinding on chalcopyrite and pyrite flotation behavior, as well as the effects on the surface morphology of the ground products and flotation concentrate. Adsorption between the collector and the mineral was analyzed using adsorption tests in two grinding media.

TABLE 1 | Chemical analysis results of chalcopyrite and pyrite.

Element	Composition (%)	
	Chalcopyrite	Pyrite
Cu	31.86	0.00
Fe	27.35	44.01
S	32.31	54.62

MATERIALS AND METHODS

Materials and Reagents

The purities of chalcopyrite and pyrite are above 90% (**Table 1**). The X-ray diffraction (XRD) analysis of chalcopyrite and pyrite is shown in **Figure 1**. The grinding medium of this experiment used 15 mm nano ceramic balls (95%Al_2O_3) and 12 mm steel balls(3%C) of equal quality. The nano-ceramic balls were sourced from Jingdezhen Betterwear New Material Co. Ltd., China, whereas the steel balls were from Goldpro New Material Co. Ltd., China. Grinding media with chemical compositions, densities were selected for the tests as shown in **Table 2**.

The collector used in this study was isobutyl xanthate obtained from Shanxi Baoji Chemical Reagent Factory. Pine oil was used as a frother in flotation. Analytical grade sodium hydroxide and

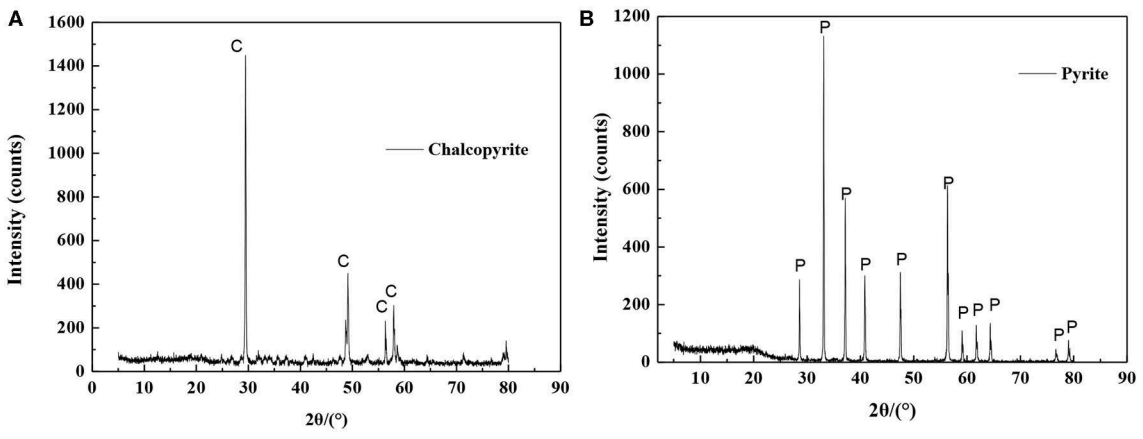

FIGURE 1 | XRD patterns of **(A)** chalcopyrite and **(B)** pyrite.

TABLE 2 | Grinding media, chemical compositions, densities.

Media type	Chemistry (wt.%)		Density (g/cm^3)
	Al_2O_3	C	
Steel ball	0.00	3.00	7.80
Nano- ceramic ball	95.00	0.00	3.70

hydrochloric acid were used as pH adjusters, which were supplied by Xilong Scientific Co. Ltd., China.

Experimental Methods

Grinding Tests

The chalcopyrite and pyrite are crushed with a small hammer to 1–2 mm, then, the samples were ground in a grinding bowl using the 15 mm nano-ceramic balls and 12 mm steel balls (of the same weight) as grinding media. Firstly, the grinding medium and appropriate amount of sample were added in the grinding bowl. Secondly, the samples were ground with a grinding rod for 3 min. Then, the grinding medium were removed from the grinding bowl and the samples were sieved using 200 mesh and 400 mesh sieves. Finally, upper 200 mesh samples were return to regrind until all samples were reached passing 200 meshes. Samples with particles size of 0.038∼0.075 mm were used for the flotation test, whereas samples with particle size of the passing 0.038 mm were used for the adsorption test. The surface morphology of the passing 0.038 mm ground samples were analyzed using an MIA650F scanning electron microscope (American FEI Company).

Micro-Flotation Tests

The flotation test was conducted in a 40 ml XFG flotation machine. The flotation machine rotational speed of the impeller was 1,992 r/min, and each flotation used 2 g of the samples. We added 2 g of the samples and distilled water into a 50 ml beaker. The suspended minerals were placed in an ultrasonic bath for 5 min. Then, the mineral added to the flotation cell was conditioned for 3 min and adjusted to the desired pH value with HCl or NaOH solutions. Isobutyl xanthate and pine oil were sequentially added into the flotation cell at a conditioning time of 3 and 1 min, respectively. The flotation concentrate was filtered and dried, and the flotation recovery rate was calculated using the mass ratios of floated and un-floated fractions. The surface morphology of the flotation concentrate product was analyzed using an MIA650F scanning electron microscope (SEM).

Adsorption Tests

The amount of adsorption at the surface of mineral was determined using the residual concentration method. The specific surface areas of pyrite and chalcopyrite were obtained using the BET test. The adsorption tests were conducted using an ultraviolet spectrophotometer. We placed 2.0 g of the passing 0.038 mm samples into a 40 mL conical flask, and adjusted the suspension to the desired pH value of 8 with dilute NaOH or HCl solutions. A given concentration of isobutyl xanthate mixed with distilled water was added into a 40 ml solution. After dispersion in a high-speed centrifuge for 15 min at a rotation speed of 1,500 r/min, the supernatant was filtered for measurement using an ultraviolet spectrophotometer. The amount of isobutyl xanthate adsorbed at the surface of chalcopyrite and pyrite was calculated as given in Equation 1 (Qu et al., 2016):

$$Q_t = \frac{V \cdot C_s}{MS} \quad (1)$$

where Q_t is the amount of adsorption of isobutyl xanthate to the surfaces of chalcopyrite or pyrite surfaces at time t (mol· m^{-2}), C_s is the adsorption concentration of isobutyl xanthate (mol·L^{-1}), V is the volume (L), S is the specific surface area of chalcopyrite or pyrite ($m^2 \cdot g^{-1}$), and M is the mass of chalcopyrite or pyrite (g).

X-ray Photoelectron Spectroscopy (XPS)

The concentration of surface species on the flotation concentrates was determined using a Thermo Scientific ESCALAB 250Xi XPS instrument (USA). This instrument used the focused beam of monochromatic Al Kα X-rays (1486.68 eV) operating at 140 W. Firstly, the survey mode was used to obtain the elements on the surfaces of flotation concentrates. Then, the high-resolution mode was used to observe the chemical bonds and oxidation states of Fe and S. The spectral data were processed using Avantage XPS and Origin software. Details of this procedure have been reported previously by Beke et al. (2009) and Rabieh et al. (2017).

Zeta Potential Measurement

The zeta potential was measured using an A80030E Zeta Probe. The mineral samples were added to distilled water to form a 0.5% mineral solution. After stirring for 5 min, the zeta potential of the solution was tested at a given pH in the presence and absence of isobutyl xanthate at a concentration of $1 \cdot 10^{-4}$ mol·L^{-1}.

Results and Discussion

Effect of Different Grinding Media on Grinding Performance

Figure 2 shows the SEM images of chalcopyrite and pyrite after dry grinding in mortar. As seen from **Figure 2A**, it appears that the surface of chalcopyrite after dry grinding using steel balls is rough and has a structure consisting of cracks. **Figure 2B** shows the smooth surface of chalcopyrite after dry grinding using nano-ceramic balls which has little cracks on. **Figures 2C,D** indicated that the surface morphology of pyrite is rough after ground with nano-ceramic balls or steel balls. The surface of the pyrite after ground with steel ball (**Figure 2C**) has more fine particles attached to the large particles than the surface after ground with nano-ceramic ball (**Figure 2D**). There are less crack on the surface of the pyrite after grinding with nano-ceramic balls as shown in (**Figure 2D**) in comparison with steel balls (**Figure 2C**). Hence, in the case of dry grinding, the effect of the grinding media on the surface morphology of the mineral is related to the type of the mineral. Moreover, the surrounding of larger particles by smaller particles and crack on the surface of mineral may be owing to the mechanical force of grinding media,

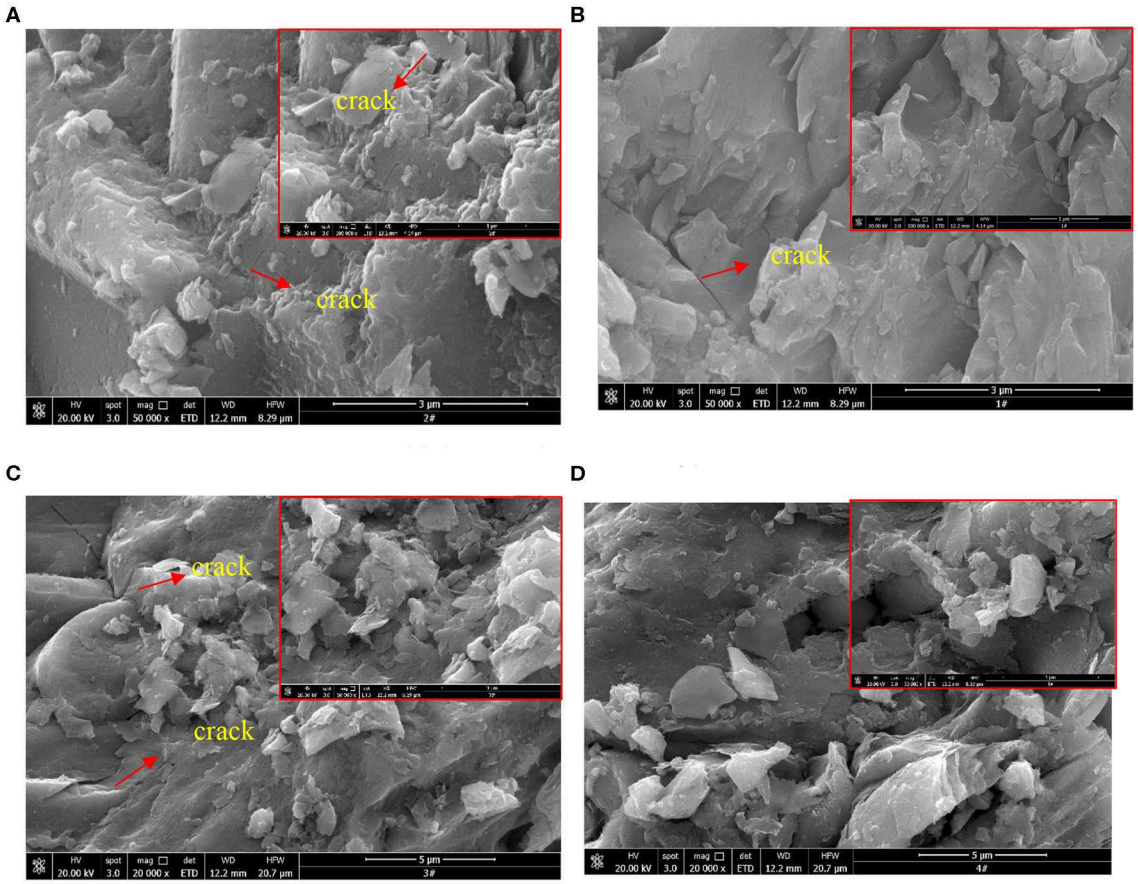

FIGURE 2 | SEM images of chalcopyrite and pyrite after dry grinding: **(A)** Chalcopyrite (steel ball); **(B)** Chalcopyrite (nano-ceramic ball); **(C)** Pyrite (steel ball); **(D)** Pyrite (nano-ceramic ball).

because the mechanical actions between the nano-ceramic balls and chalcopyrite or pyrite are small.

Effect of Different Grinding Media on Flotation

Figure 3 shows the effects of pH on the flotation recovery of chalcopyrite and pyrite after ground using nano-ceramic balls and steel balls. The recovery of chalcopyrite increased as the pH increased after ground using nano-ceramic balls and steel balls. Chalcopyrite exhibited good floatability after ground using nano-ceramic balls compared with ground using steel balls. Pyrite exhibited the opposite trend as the recovery of pyrite decreased with the increase in pH. Pyrite exhibited good floatability using steel ball grinding. This result is consistent with the result obtained in the study by Peng et al. (2003a,b).

Figure 4 shows the effects of isobutyl xanthate concentration on the flotation recovery of chalcopyrite and pyrite at pH 8.0 after ground using nano-ceramic balls and steel balls. The flotation recoveries of chalcopyrite and pyrite increased with the increase in the isobutyl xanthate concentration. The recovery of pyrite increased sharply before the initial concentration reached $1{\cdot}10^{-4}$ $mol{\cdot}L^{-1}$ and then remained stable, whereas that of chalcopyrite increased slowly before the initial concentration reached $1{\cdot}10^{-4}$ $mol{\cdot}L^{-1}$ and then remained stable. This indicates that the floatability of chalcopyrite in ceramic media and the floatability of pyrite in iron media are good.

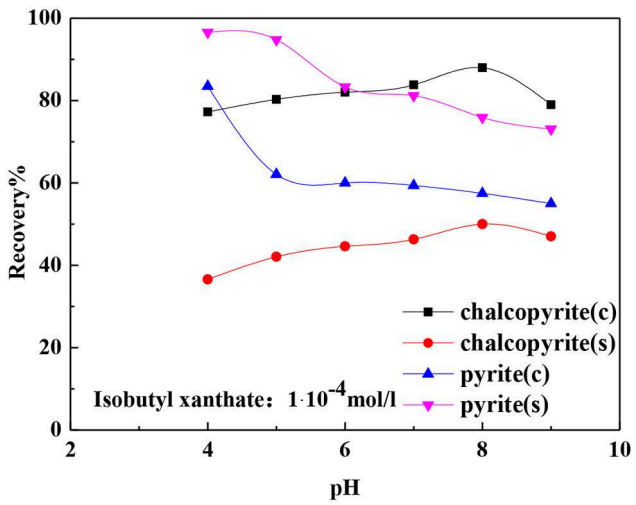

FIGURE 3 | Effect of pH on flotation recovery.

To investigate this trend, we performed scanning electron microscopy analysis of chalcopyrite and pyrite flotation concentrates at a pH of 8 and the addition of $1{\cdot}10^{-4}$ mol·L^{-1} of isobutyl xanthate concentration. **Figure 5** shows SEM images of chalcopyrite and pyrite flotation concentrates. The surface of the chalcopyrite flotation concentrate ground with nano-ceramic balls is smooth, whereas there are many flocs on the surface ground with steel balls. The flotation of chalcopyrite was affected by the hydrophilic products generated at the surfaces by the steel media grinding (Heyes and Trahar, 1979; Greet et al., 2004; Yekeler et al., 2004). The surface of the pyrite flotation concentrate has more flocs on the surface ground with steel balls than ground with nano-ceramic balls. The flotation of pyrite improved after ground with steel balls owing to the galvanic interaction between the steel media and the mineral surface, which generated elemental sulfur at the surface of the pyrite (Rao et al., 1976).

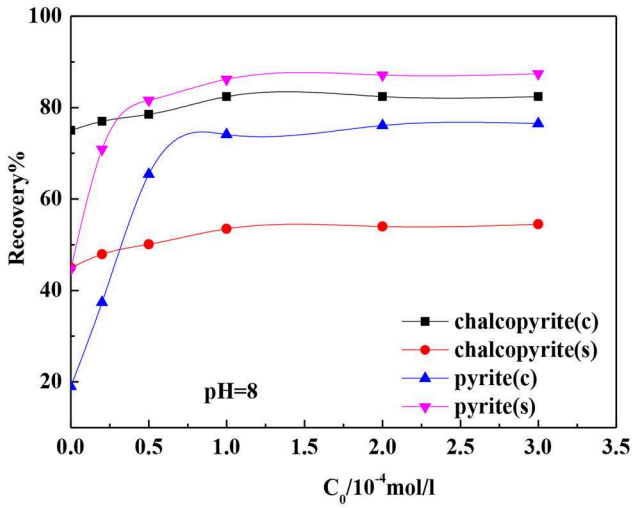

FIGURE 4 | Effect of isobutyl xanthine concentration on flotation recovery.

Effect of Different Grinding Media on Adsorption

The adsorption of chalcopyrite, pyrite, and the collector is affected by many factors such as the pH, the type of collector, and the grinding medium (Heyes and Trahar, 1979; Greet et al., 2004; Huang and Grano, 2006; Bagci et al., 2007; Qu et al., 2016; Huang X. et al., 2019). The adsorption of the collector to chalcopyrite is affected by the grinding medium mainly because the galvanic action of the iron medium results in adsorption of

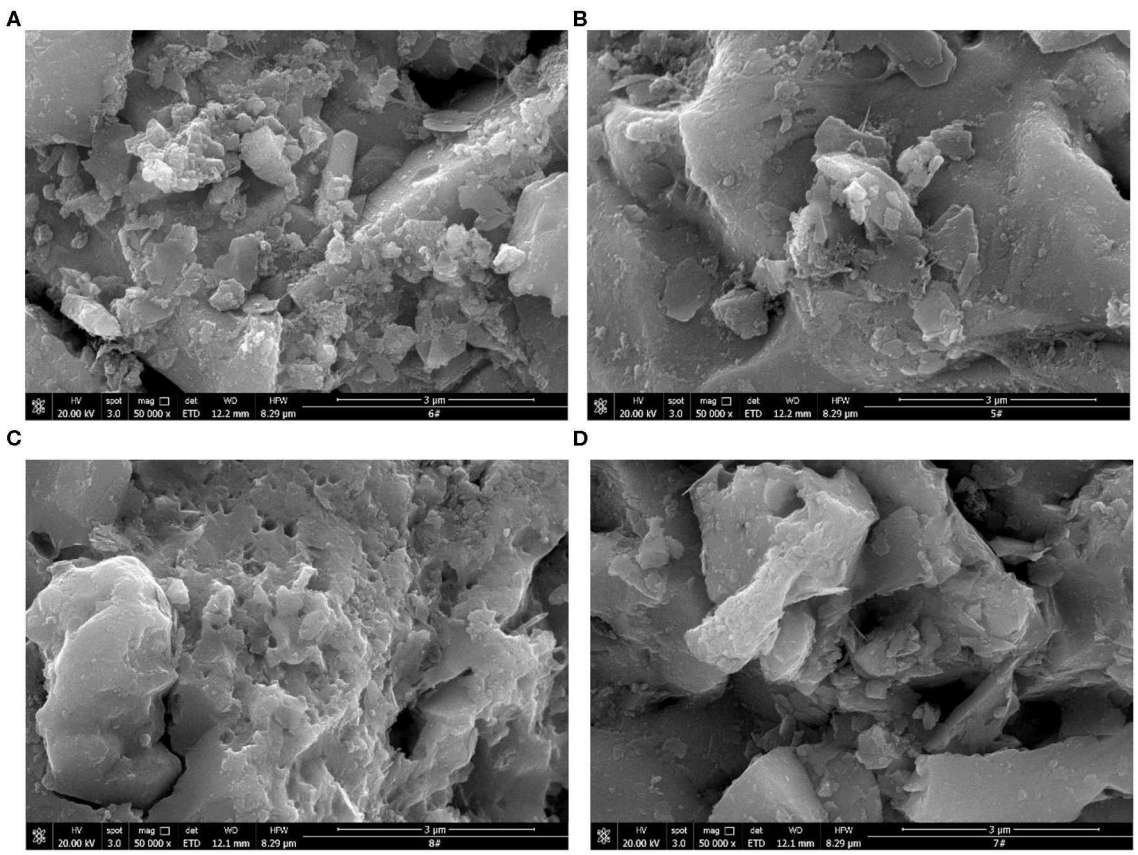

FIGURE 5 | SEM images of chalcopyrite and pyrite flotation concentrates: **(A)** Chalcopyrite (steel ball); **(B)** Chalcopyrite (nano-ceramic ball); **(C)** Pyrite (steel ball); **(D)** Pyrite (nano-ceramic ball).

the hydroxide of the iron at the mineral surface, which affects the adsorption of the agent at the surface of mineral (Heyes and Trahar, 1979; Greet et al., 2004; Huang and Grano, 2006). Qu et al. (2016) found that HATTs(3-hexyl-4-amino-1,2,4-triazole-5-thione)exhibited strong adsorption capacity for chalcopyrite at pH 4∼8. Bagci et al. (2007) found that selective and non-selective collectors can improve the amount of adsorption of the collector at the surface of chalcopyrite.

Figure 6 shows the relationship between the amount of adsorption of isobutyl xanthate at the surfaces of chalcopyrite or pyrite and the isobutyl xanthate concentration. The figure shows that with the increase in the concentration of isobutyl xanthate, the amount of adsorption at the chalcopyrite surface increases, and the amount of adsorption of isobutyl xanthate with ceramic ball grinding is larger than that of steel ball grinding. This result is consistent with the result obtained by Qu et al. (2016). The authors reported that the adsorption of the collector at the surface of mineral increases as the concentration of collector increases. Nano-ceramic balls can improve the pulp environment and contribute to the adsorption of collectors molecules at the surface of chalcopyrite, which in turn enhances the flotation of minerals (Ahn and Gebhardt, 1991; Martin et al., 1991). Pyrite exhibits the opposite trend. In iron media grinding environment, the collector produces dixanthogen at the surface of the pyrite and forms Fe–collector complexes (Woods, 1976; Nagaraj and Brinen, 2001). Therefore, the amount of adsorption of isobutyl xanthate at the surface of pyrite in iron media is higher than that of ceramic media.

Figure 7 shows the relationship between the adsorption rate and isobutyl xanthate concentration. The figure shows that with the increase in the concentration of isobutyl xanthate, the adsorption rate at the surface of chalcopyrite first increased and then stabilized, and the adsorption rate of isobutyl xanthate to chalcopyrite ground with ceramic ball grinding is higher than that of ground with steel ball grinding; pyrite exhibited the opposite trend.

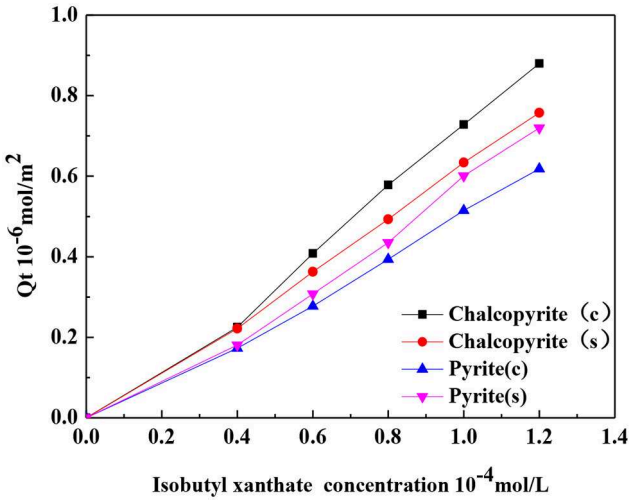

FIGURE 6 | Adsorption concentration at the surfaces of samples as a function of isobutyl xanthate concentration.

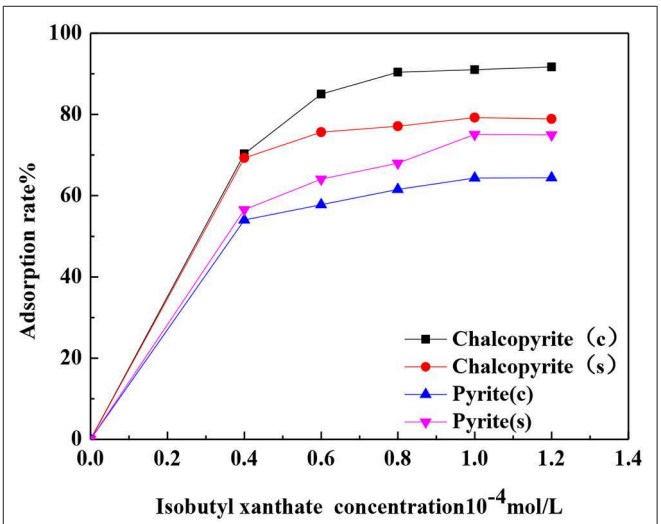

FIGURE 7 | Adsorption rates at the surfaces of samples as a function of isobutyl xanthate concentration.

XPS Analysis

The chalcopyrite and pyrite flotation concentration at pH of 8 and addition of $1{\cdot}10^{-4}$ mo$\cdot L^{-1}$ of isobutyl xanthate concentration were also analyzed using XPS. The survey spectra of chalcopyrite and pyrite were used to determine the surface element content of the samples under different grinding media. The high-resolution spectra of Fe and S provided information about the oxidation state and chemical bonding of Fe and S.

Figures 8A,B show the survey spectra of chalcopyrite and pyrite, respectively. The percentage of elements at the surface of the samples are presented in **Table 3**. Compared with chalcopyrite ground with steel balls, grinding with nano-ceramic balls decreased the iron concentration at the chalcopyrite surface from 11.02 to 10.63% and the oxygen concentration from 48.8 to 39.71%, whereas the sulfur concentration increased from 8.19 to 16.38%. The increase in sulfur concentration at the surface of chalcopyrite after the addition of isobutyl xanthate is due to the adsorption of isobutyl xanthate, whereas the decrease in oxygen concentration suggests the removal of surface oxidation species from the surface of chalcopyrite (Cao et al., 2018). This also indicates that ceramic media grinding is beneficial to the flotation of chalcopyrite, which is consistent with the flotation results of the dosage isobutyl xanthate. Compared with pyrite ground with steel balls, grinding with nano-ceramic balls decreased the iron concentration at the surface of pyrite from 7.98 to 7.71% and the sulfur concentration from 21.5 to 20.58%, whereas the oxygen concentration increased from 27.35 to 34.65%. This also indicates that steel media grinding is beneficial to the flotation of pyrite, which is consistent with the flotation results of the dosage isobutyl xanthate.

Figures 8C,D show the high-resolution spectra of Fe of chalcopyrite and pyrite, respectively, whereas **Table 4** presents the qualification of iron species based on Fe 2p XPS spectra.

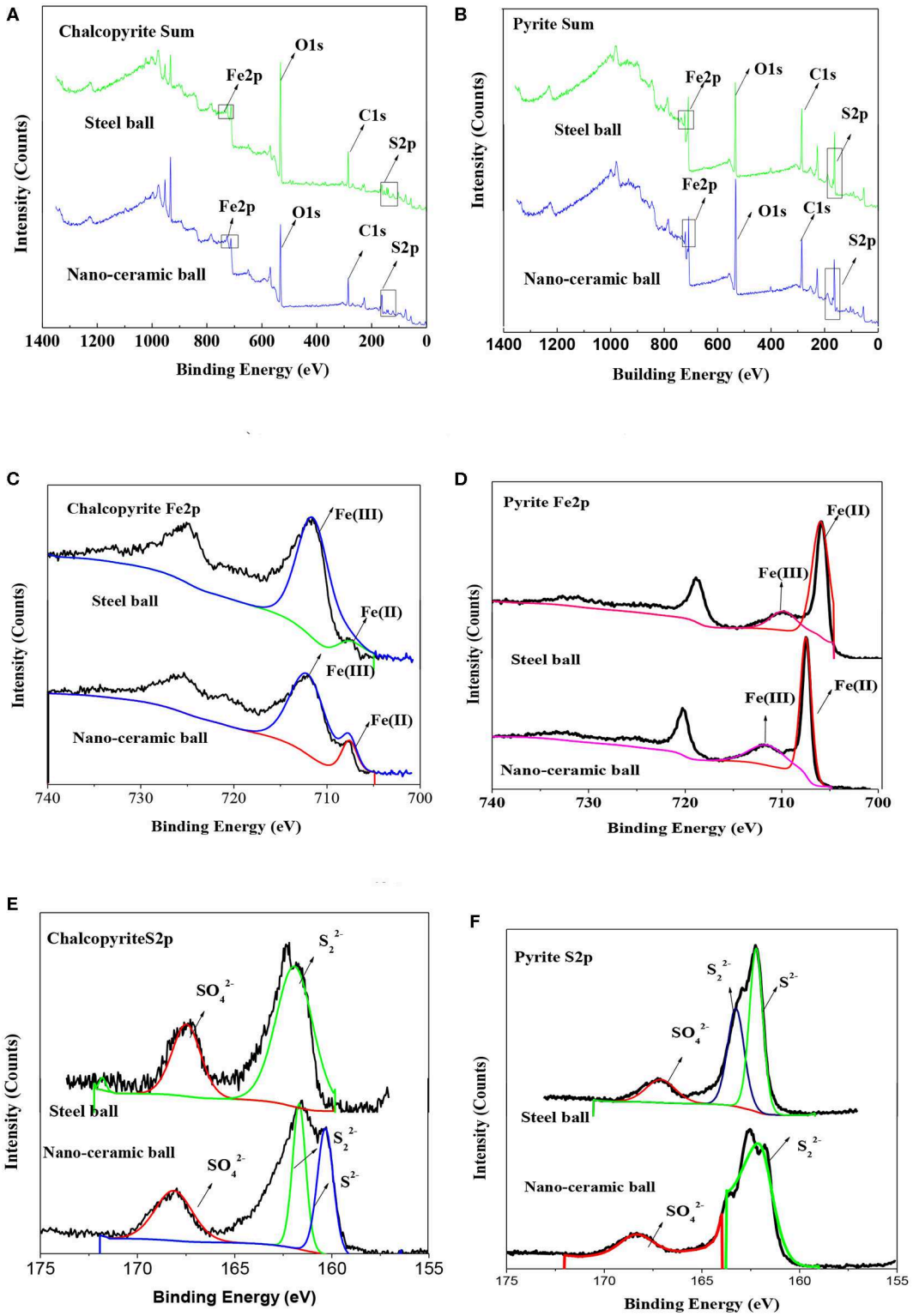

FIGURE 8 | XPS spectra of chalcopyrite and pyrite: **(A)** Chalcopyrite (survey); **(B)** Pyrite (survey); **(C)** Chalcopyrite (Fe 2p); **(D)** Pyrite (Fe 2p); **(E)** Chalcopyrite (S2p); **(F)** Pyrite (S2p).

In the Fe 2p3/2 spectra, the peaks near 711 eV for Fe(III)-O and at 708 eV for Fe(II)-S, the Fe(III)-O concentration at the surface of chalcopyrite ground using ceramic balls decreased significantly from 90.96 to 86.01% (Taheri et al., 2014; Mikhlin et al., 2016; Peng et al., 2017; Rabieh et al., 2017; Cao et al., 2018). This indicates that ceramic ball grinding can reduce the

adsorption of iron oxide on the surface of chalcopyrite and is conducive to the flotation of chalcopyrite. Cao et al. (2018) found that pyrite has a higher energy site at approximately 707.2 eV; thus, Fe(II)-S has the highest concentration in the pyrite Fe 2p spectra. The Fe(II)-S concentration at the surface of pyrite ground using ceramic balls significantly increased from 68.36 to 79.83%. Rabieh et al. (2017) also found the same regular pattern in pyrite.

Figures 8E,F show the high-resolution spectra of S of chalcopyrite and pyrite, respectively, whereas **Table 5** presents the qualification of sulfur species based on the S 2p XPS spectra. Disulfide S_2^{2-} is produced at a binding energy range of 162.4–162.7 eV and S^{2-} is produced at a lower binding energy range of 161.3–162.1 eV, whereas SO_4^{2-} is produced at higher binding energies of approximately 168 eV (Peng et al., 2003a; Moslemi and Gharabaghi, 2017; Cao et al., 2018). Peng et al. (2003a) found that a 30 wt.% chromium medium produced more sulfate at the surface of chalcopyrite than a mild steel medium. **Figure 8E** shows that ceramic balls produced more S_2^{2-} at the surface of chalcopyrite than steel balls. Rabieh et al. (2017) found that there are more SO_4^{2-} at the surface of pyrite using ceramic media grinding compared with using steel media. In this paper, we also

TABLE 3 | Atomic concentration of elements in XPS at the surfaces of samples.

Mineral	Grinding media	Atomic concentration of element (%)			
		Fe	C	O	S
Chalcopyrite	Ceramic	10.63	33.28	39.71	16.38
Chalcopyrite	Steel	11.02	31.99	48.8	8.19
Pyrite	Ceramic	7.71	37.06	34.65	20.58
Pyrite	Steel	7.98	43.17	27.35	21.5

TABLE 4 | Quantification of iron species at the surface of samples based on Fe 2p XPS spectra.

Mineral	Chalcopyrite		Chalcopyrite		Pyrite		Pyrite	
Grinding Media	Ceramic		Steel		Ceramic		Steel	
Species	B.E.	at.%	B.E.	at.%	B.E.	at.%	B.E.	at.%
Fe(II)	707.58	13.99	707.52	9.04	707.48	68.36	706.28	79.83
Fe(III)	712.08	86.01	711.48	90.96	711.48	31.64	710.08	20.17

TABLE 5 | Quantification of sulfur species at the surface of samples based on S 2p XPS spectra.

Mineral	Chalcopyrite		Chalcopyrite		Pyrite		Pyrite	
Grinding Media	Ceramic		Steel		Ceramic		Steel	
Species	B.E.	at.%	B.E.	at.%	B.E.	at.%	B.E.	at.%
S^{2-}	161.68	2.49	161.13	71.55	161.95	78.48	161.53	48.62
S_2^{2-}	162.14	80.22	-	-	-	-	162.78	36.21
SO_4^{2-}	168.78	17.29	168.08	28.45	168.36	21.52	167.83	15.18

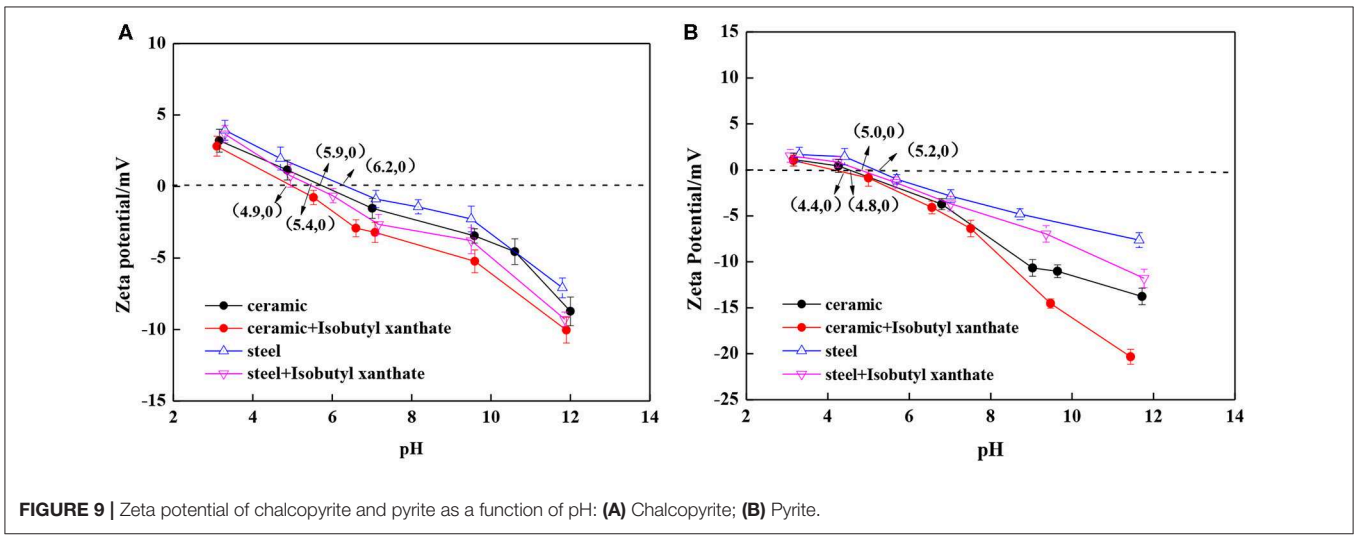

FIGURE 9 | Zeta potential of chalcopyrite and pyrite as a function of pH: **(A)** Chalcopyrite; **(B)** Pyrite.

found the same regular pattern in pyrite, as presented in **Table 5** and **Figure 8F**.

Zeta Potential Measurement

The surface potential of minerals will be affected by the adsorption of collectors, the degree of oxidation of minerals, the flotation atmosphere, and the influence of the grinding media (Peng and Grano, 2010a,b; Yin et al., 2018; Huang Z. et al., 2019; Jia et al., 2019). **Figure 9** shows the zeta potential of chalcopyrite and pyrite as a function of pH in the absence and presence of 1 10^{-4} mol L^{-1} isobutyl xanthate using two different grinding media. Peng et al. (2003a) found that steel media tend to produce lower Eh values than a 30 wt.% chromium medium when Cu^{2+} was added. Moreover, Peng and Grano (2010a,b) found that the zeta potential of pyrite is affected by the flotation atmosphere and the oxidation of sulfide minerals increased its isoelectric points. As shown in **Figure 9A**, the isoelectric point of chalcopyrite after nano-ceramic ball grinding is 5.9, whereas that of steel ball grinding is 6.2. The isoelectric point of chalcopyrite after nano-ceramic ball grinding is consistent with that in the study by Huang X. et al. (2019). The increase in the isoelectric point of chalcopyrite after steel ball grinding is related to the hydroxide formed by the wear of the iron medium (Peng and Grano, 2010a,b). After the addition of isobutyl xanthate, the isoelectric point of chalcopyrite shifted to the left because the negatively charged collector reduces the isoelectric point of chalcopyrite (Huang X. et al., 2019). As shown in **Figure 9B**, the isoelectric point of pyrite after nano-ceramic ball grinding is 4.8, whereas that of the steel ball grinding is 5.2. This value is also similar to the values reported in previous studies (Yin et al., 2018; Huang X. et al., 2019). After the addition of isobutyl xanthate, the isoelectric point of pyrite shifted to the left. Iron media grinding can cause iron media pollution. Under alkaline conditions, a stable complex of xanthogen ions and iron hydroxides is adsorbed at the surface of pyrite (Yang et al., 2018; Yin et al., 2018). This is also consistent with the results shown in **Figures 3**, **6**, **7**.

CONCLUSIONS

Grinding media has significant influence on the flotation of chalcopyrite and pyrite. This effect is mainly related to the change in the surface properties of chalcopyrite and pyrite, which in turn affects their floatability. Grinding using steel medium easily produces oxidation species at the surface of chalcopyrite, thereby reducing its floatability. Scanning electron microscopy results show that the surface of the ground product and the flotation concentrate of chalcopyrite using nano-ceramic balls grinding is smooth, whereas the surface of the product ground using steel balls is rough and the surface of chalcopyrite flotation concentrates have many flocs. The flotation recovery of chalcopyrite after nano-ceramic ball grinding is higher than that of steel ball grinding. XPS demonstrated that steel ball grinding produced more iron hydroxide species than nano-ceramic ball grinding, which is not conducive to the flotation of chalcopyrite. Adsorption experiments also show that nano-ceramic media grinding contributes to the adsorption of isobutyl xanthate to chalcopyrite. The zeta potential of chalcopyrite indicates that ceramic media grinding is beneficial to the reduction of the isoelectric point of mineral flotation. However, steel media grinding is conducive to the flotation of pyrite. XPS was used to verify the flotation recovery of pyrite and the adsorption of isobutyl xanthate at the surface of pyrite. Further research should be conducted on the effect of nano-ceramic media on the selective separation of chalcopyrite from pyrite. Therefore, the nano-ceramic ball is a good grinding medium for chalcopyrite grinding, it is beneficial to improve the recovery rate of chalcopyrite. Steel balls is better for grinding pyrite than nano-ceramic balls. For copper-sulfur ore which is chalcopyrite associated pyrite, nano-ceramic balls can be used to replace steel balls as grinding media in some ways.

DATA AVAILABILITY STATEMENT

All datasets generated for this study are included in the article/supplementary material.

AUTHOR CONTRIBUTIONS

CW initiated the research topic. NL wrote the manuscript text. BF reviewed and edited the manuscript. JX, JW, YG, and NL performed experiments. All authors reviewed the manuscript.

FUNDING

This work was financially supported by the Projects of the National Natural Science Foundation of China (51764015) and (51964016).

ACKNOWLEDGMENTS

We acknowledge the support received from the Jiangxi Key Laboratory of Mining Engineering.

REFERENCES

Ahn, J. H., and Gebhardt, J. E. (1991). Effect of grinding media-chalcopyrite interaction on the self-induced flotation of chalcopyrite. *Int. J. Miner. Process.* 33, 243–262. doi: 10.1016/0301-7516(91)90056-O

Bagci, E., Ekmekci, Z., and Bradshaw, D. (2007). Adsorption behaviour of xanthate and dithiophosphinate from their mixtures on chalcopyrite. *Miner. Eng.* 20, 1047–1053. doi: 10.1016/j.mineng.2007.04.011

Beke, S., Korösi, L., Papp, S., Oszkó, A., and Nánai, L. (2009). XRD and XPS analysis of laser treated vanadium oxide thin films. *Appl. Surf. Sci.* 255, 9779–9782. doi: 10.1016/j.apsusc.2009.04.069

Bruckard, W., Sparrow, G., and Woodcock, J. (2011). A review of the effects of the grinding environment on the flotation of copper sulphides. *Int. J. Miner. Process.* 100, 1–13. doi: 10.1016/j.minpro.2011.04.001

Cao, Z., Chen, X., and Peng, Y. (2018). The role of sodium sulfide in the flotation of pyrite depressed in chalcopyrite flotation. *Miner. Eng.* 119, 93–98. doi: 10.1016/j.mineng.2018.01.029

Corin, K. C., Song, Z. G., Wiese, J. G., and O'Connor, C. T. (2018). Effect of using different grinding media on the flotation of a base metal sulphide ore. *Miner. Eng.* 126, 24–27. doi: 10.1016/j.mineng.2018.06.019

Erdemoglu, M., and Sarikaya, M. (2002). The effect of grinding on pyrophyllite flotation. *Miner. Eng.* 15, 723–725. doi: 10.1016/S0892-6875(02)00210-8

Feng, B., Peng, J., and Guo, W. (2019). The depression behavior and mechanism of carboxymethyl chitosan on calcite flotation. *J. Mater. Res. Technol.* 8, 1036–1040. doi: 10.1016/j.jmrt.2018.07.013

Feng, B., Zhong, C., Zhang, L., Guo, Y., Wang, T., and Huang, Z. (2020). Effect of surface oxidation on the depression of sphalerite by locust bean gum. *Miner. Eng,* 146:106142. doi: 10.1016/j.mineng.2019.106142

Forssberg, E., Sundberg, S., and Hongxin, Z. (1988). Influence of different grinding methods on floatability. *Int. J. Miner. Process.* 22, 183–192. doi: 10.1016/0301-7516(88)90063-4

Gonçalves, K. L. C., Andrade, V. L. L., and Peres, A. E. C. (2003). The effect of grinding conditions on the flotation of a sulphide copper ore. *Miner. Eng.* 16, 1213–1216. doi: 10.1016/j.mineng.2003.05.006

Greet, C., Small, G., Steinier, P., and Grano, S. (2004). The magotteaux mill®: investigating the effect of grinding media on pulp chemistry and flotation performance. *Miner. Eng.*17, 891–896. doi: 10.1016/j.mineng.2004.03.003

Guo, W., Feng, B., and Peng, J. (2019). Depressant behavior of tragacanth gum and its role in the flotation separation of chalcopyrite from talc. *J. Mater. Res. Technol.* 8, 697–702. doi: 10.1016/j.jmrt.2018.05.015

Heyes, G. W., and Trahar, W. J. (1979). Oxidation–reduction effects in the flotation of chalcocite and cuprite. *Int. J. Miner. Process.* 6, 229–252. doi: 10.1016/0301-7516(79)90039-5

Huang, G., and Grano, S. (2006). Galvanic interaction between grinding media and arsenopyrite and its effect on flotation Part I. *quantifying galvanic interaction during grinding. Int. J. Miner. Process.* 78, 182–197. doi: 10.1016/j.minpro.2005.10.008

Huang, X., Huang, K., Jia, Y., Wang, S., Cao, Z., and Zhong, H. (2019). Investigating the selectivity of a xanthate derivative for the flotation separation of chalcopyrite from pyrite. *Chem. Eng. Sci.* 205, 220–229. doi: 10.1016/j.ces.2019.04.051

Huang, Z., Wang, J., Sun, W., Hu, Y., Cao, J., and Gao, Z. (2019). Selective flotation of chalcopyrite from pyrite using diphosphonic acid as collector. *Miner. Eng*, 140:105890. doi: 10.1016/j.mineng.2019.105890

Jia, Y., Huang, K., Wang, S., Cao, Z., and Zhong, H. (2019). The selective flotation behavior and adsorption mechanism of thiohexanamide to chalcopyrite. *Miner. Eng.* 137, 187–199. doi: 10.1016/j.mineng.2019.04.015

Learmont, M. E., and Iwasaki, I. (1984). Effect of grinding media on galena flotation. *Mining Met. Explor.* 1, 136–143. doi: 10.1007/BF03402566

Li, C., and Gao, Z. (2017). Effect of grinding media on the surface property and flotation behavior of scheelite particles. *Powder Technol.* 322, 386–392. doi: 10.1016/j.powtec.2017.08.066

Li, C., and Gao, Z. (2018). Tune surface physicochemical property of fluorite particles by regulating the exposure degree of crystal surfaces. *Miner. Eng.* 128, 123–132. doi: 10.1016/j.mineng.2018.08.044

Liao, N., Wu, C., Wu, Z., and Wang, X. (2019). Effect of nano ceramic ball on grinding and flotation in copper sulfur ore. *Nonferrous. Met. Eng.* 9, 70–76. doi: 10.3969/j.issn.2095-1744.2019.01.012 (In Chinese).

Martin, C. J., McIvor, R. E., Finch, J. A., and Rao, S. R. (1991). Review of the effect of grinding media on flotation of sulphide minerals. *Miner. Eng.* 4, 121–132. doi: 10.1016/0892-6875(91)90028-T

Mikhlin, Y., Karacharov, A., Tomashevich, Y., and Shchukarev, A. (2016). Cryogenic XPS study of fast-frozen sulfide minerals: flotation-related adsorption of n -butyl xanthate and beyond. *J. Electron Spectrosc.* 206, 65–73. doi: 10.1016/j.elspec.2015.12.003

Moslemi, H., and Gharabaghi, M. (2017). A review on electrochemical behavior of pyrite in the froth flotation process. *J. Ind. Eng. Chem.* 47, 1–18. doi: 10.1016/j.jiec.2016.12.012

Nagaraj, D., and Brinen, J. (2001). SIMS study of adsorption of collectors on pyrite. *Int. J. Miner. Process.* 63, 45–57. doi: 10.1016/S0301-7516(01)00043-6

Palm, N. A., Shackleton, N. J., Malysiak, V., and O'Connor, C. T. (2010). The effect of using different comminution procedures on the flotation of sphalerite. *Miner. Eng.* 23, 1053–1057. doi: 10.1016/j.mineng.2010.08.001

Palm, N. A., Shackleton, N. J., Malysiak, V., and O'Connor, C. T. (2011). The effect of using different comminution procedures on the flotation of platinum group. *Miner. Eng.* 24, 731–736. doi: 10.1016/j.mineng.2011.01.001

Peng, H., Wu, D., and Abdelmonem, M. (2017). Flotation performances and surface properties of chalcopyrite with xanthate collector added before and after grinding. *Results Phys.* 7, 3567–3573. doi: 10.1016/j.rinp.2017.09.028

Peng, Y., and Grano, S. (2010a). Effect of grinding media on the activation of pyrite flotation. *Miner. Eng.* 23, 600–605. doi: 10.1016/j.mineng.2010.02.003

Peng, Y., and Grano, S. (2010b). Effect of iron contamination from grinding media on the flotation of sulphide minerals of different particle size. *Int. J. Miner. Process.* 97, 1–6. doi: 10.1016/j.minpro.2010.07.003

Peng, Y., Grano, S., Fornasiero, D., and Ralston, J. (2003a). Control of grinding conditions in the flotation of chalcopyrite and its separation from pyrite. *Int. J. Miner. Process.* 69, 87–100. doi: 10.1016/S0301-7516(02)00119-9

Peng, Y., Grano, S., Fornasiero, D., and Ralston, J. (2003b). Control of grinding conditions in the flotation of galena and its separation from pyrite. *Int. J. Miner. Process.* 70, 67–82. doi: 10.1016/S0301-7516(02)00153-9

Qu, X., Xiao, J., Liu, G., Liu, S., and Zhang, Z. (2016). Investigation on the flotation behavior and adsorption mechanism of 3-hexyl-4-amino-1,2,4-triazole-5-thione to chalcopyrite. *Miner. Eng.* 89, 10–17. doi: 10.1016/j.mineng.2015.12.015

Rabieh, A., Albijanic, B., and Eksteen, J. J. (2017). Influence of grinding media and water quality on flotation performance of gold bearing pyrite. *Miner. Eng.* 112, 68–76. doi: 10.1016/j.mineng.2017.07.010

Rao, M. Y., and Natarajan, K. A. (1988). Influence of galvanic interaction between chalcopyrite and some metallic materials on flotation. *Miner. Eng.* 1, 281–294. doi: 10.1016/0892-6875(88)90018-0

Rao, S. R., Moon, K. S., and Leja, J. (1976). "Effect of grinding media on the surface reactions and flotation of heavy metal sulphides," in, A. M. Flotation, Gaudin Memorial. Flotation: A.M. Gaudin Memorial Vol I (New York, NY: Fuerstenau, MD, Ed., A.I.M.E), 1, 509

Shi, G. M., and Zhou, Y. C. (2019). The impact of SAG pebbles as media vs steel media on flotation performance of a copper sulphide ore. *Can. Metall. Quart.* 58, 362–366. doi: 10.1080/00084433.2019.1590038

Taheri, B., Abdollahy, M., Tonkaboni, S. Z. S., Javadian, S., and Yarahmadi, M. (2014). Dual effects of sodium sulfide on the flotation behavior of chalcopyrite: I. *effect of pulp potential. Int. J. Miner. Met. Mater.* 21, 415–422. doi: 10.1007/s12613-014-0924-7

Van Deventer, J. S. J., Ross, V. E., and Dunne, R. C. (1991). "The effect of milling environment on the selective flotation of chalcopyrite from a complex sulphide ore," in *Proceeding XVII International Mineral Proceeding Congress Dresden*, 129–140.

Woods, R. (1976). *Electrochemistry of Sulphide Flotation: Flotation*. New York, NY: AIME.

Wu, C., Lei, A., Jiang, L., Yuan, C., Yin, Q., and Shen, T. (2019). Semi-autogenous grinding mill pebbles as a vertically stirred mill medium. *Sep. Sci. Technol.* 1–10. doi: 10.1080/01496395.2019.1675697

Yang, X., Albijanic, B., Liu, G., and Zhou, Y. (2018). Structure–activity relationship of xanthates with different hydrophobic groups in the flotation of pyrite. *Miner. Eng.* 125, 155–164. doi: 10.1016/j.mineng.2018.05.032

Yao, W., Li, M., Zhang, M., Cui, R., Jiang, H., Li, Y., et al. (2019). Effects of grinding media on flotation performance of calcite. *Miner. Eng.* 132, 92–94. doi: 10.1016/j.mineng.2018.12.005

Yekeler, M., Ulusoy, U., and Hiçyilmaz, C. (2004). Effect of particle shape and roughness of talc mineral ground by different mills on the wettability and floatability. *Powder Technol.* 140, 68–78. doi: 10.1016/j.powtec.2003.12.012

Yin, W., Xue, J., Li, D., Sun, Q., Yao, J., and Huang, S. (2018). Flotation of heavily oxidized pyrite in the presence of fine digenite particles. *Miner. Eng.* 115, 142–149. doi: 10.1016/j.mineng.2017.10.016

Yuan, X.-M., Pålsson, B., and Forssberg, K. S. (1996). Flotation of a complex sulphide ore II. *influence of grinding environments on sulphide selectivity and pulp chemistry. Int. J. Miner. Process.* 46, 181–204. doi: 10.1016/0301-7516(95)00095-X

Zhang, X., Han, Y., Gao, P., Li, Y., and Sun, Y. (2019). Effects of particle size and ferric hydroxo complex produced by different grinding media on the flotation kinetics of pyrite. *Powder Technol.* 360, 1028–1036. doi: 10.1016/j.powtec.2019.11.014

Zhang, Z., Dong, L., and Wang, Z. (2013). *A Super Wear-Resistant Alumina-Ceramic Ball and Its Preparation Method*. CHN, patent, ZL201310174278.6, 2013-08-07. (In Chinese)

Conflict of Interest: The authors declare that the research was conducted in the absence of any commercial or financial relationships that could be construed as a potential conflict of interest.

Advantages of publishing in Frontiers

OPEN ACCESS
Articles are free to read for greatest visibility and readership

FAST PUBLICATION
Around 90 days from submission to decision

HIGH QUALITY PEER-REVIEW
Rigorous, collaborative, and constructive peer-review

TRANSPARENT PEER-REVIEW
Editors and reviewers acknowledged by name on published articles

Frontiers
Avenue du Tribunal-Fédéral 34
1005 Lausanne | Switzerland

Visit us: www.frontiersin.org
Contact us: info@frontiersin.org | +41 21 510 17 00

REPRODUCIBILITY OF RESEARCH
Support open data and methods to enhance research reproducibility

DIGITAL PUBLISHING
Articles designed for optimal readership across devices

FOLLOW US
@frontiersin

IMPACT METRICS
Advanced article metrics track visibility across digital media

EXTENSIVE PROMOTION
Marketing and promotion of impactful research

LOOP RESEARCH NETWORK
Our network increases your article's readership